

# Wall-crossing, Hitchin Systems, and the WKB Approximation

---

Davide Gaiotto<sup>1</sup>, Gregory W. Moore<sup>2</sup>, Andrew Neitzke<sup>3</sup>

<sup>1</sup> *School of Natural Sciences, Institute for Advanced Study,  
Princeton, NJ 08540, USA*

<sup>2</sup> *NHETC and Department of Physics and Astronomy, Rutgers University,  
Piscataway, NJ 08855-0849, USA*

<sup>3</sup> *Department of Physics, Harvard University,  
Cambridge, MA 02138, USA*

`dgaiotto@ias.edu, gmoore@physics.rutgers.edu, neitzke@physics.harvard.edu`

**ABSTRACT:** We consider BPS states in a large class of  $d = 4$ ,  $\mathcal{N} = 2$  field theories, obtained by reducing six-dimensional  $(2, 0)$  superconformal field theories on Riemann surfaces, with defect operators inserted at points of the Riemann surface. Further dimensional reduction on  $S^1$  yields sigma models, whose target spaces are moduli spaces of Higgs bundles on Riemann surfaces with ramification. In the case where the Higgs bundles have rank 2, we construct canonical Darboux coordinate systems on their moduli spaces. These coordinate systems are related to one another by Poisson transformations associated to BPS states, and have well-controlled asymptotic behavior, obtained from the WKB approximation. The existence of these coordinates implies the Kontsevich-Soibelman wall-crossing formula for the BPS spectrum. This construction provides a concrete realization of a general physical explanation of the wall-crossing formula which was proposed in [1]. It also yields a new method for computing the spectrum using the combinatorics of triangulations of the Riemann surface.

---

## Contents

<b>1. A narrative table of contents</b>	<b>4</b>
<b>2. Review</b>	<b>14</b>
2.1 Setup	14
2.2 Darboux coordinates	15
2.3 Wall-crossing	17
2.4 Riemann-Hilbert problem	18
<b>3. From brane constructions to Hitchin systems</b>	<b>19</b>
3.1 Compactifying the $(2,0)$ theory	19
3.1.1 The $(2,0)$ theory on $\mathbb{R}^{1,5}$ and its Coulomb branch	19
3.1.2 The $(2,0)$ theory on $\mathbb{R}^{1,3} \times C$ and its Coulomb branch	21
3.1.3 BPS strings on the Coulomb branch	22
3.1.4 Charge lattices	25
3.1.5 Kinetic terms	26
3.1.6 Compactifying the $(2,0)$ theory on $C \times S^1$ : Hitchin's equations	28
3.1.7 Defects and geometric Langlands	30
3.1.8 Boundary conditions from fivebrane intersections	31
3.2 Witten's construction	32
3.2.1 Type IIA	33
3.2.2 Lift to M-theory	35
3.2.3 Conformal quivers	35
3.2.4 Mapping to a Hitchin system	42
3.2.5 Linear conformal quivers with fundamental matter	43
3.2.6 Brane-bending and irregular singularities	49
3.2.7 The asymptotically free case	52
3.2.8 A surprising isomorphism	55
3.2.9 Non-Abelian flavor symmetries and punctures	55
3.3 Type IIB construction	57
<b>4. Hitchin systems</b>	<b>59</b>
4.1 Moduli space	59
4.2 Hyperkähler structure	60
4.2.1 Flat connections	61
4.2.2 Higgs bundles	61
4.3 Another viewpoint on defects	62

<b>5. Fock-Goncharov coordinates</b>	<b>63</b>
5.1 Defining the Fock-Goncharov coordinates	64
5.2 Monodromies	65
5.3 Counting the coordinates	65
5.4 Hamiltonian flows	66
5.5 Poisson bracket	66
5.6 Coordinate transformations and the groupoid of decorated triangulations	67
5.7 Transformation under flips	70
5.8 Degenerate triangulations and transformation under pops	71
5.9 Limits of triangulations and the juggle	73
<b>6. The WKB triangulation</b>	<b>76</b>
6.1 WKB curves	76
6.2 Local behavior of WKB curves	77
6.3 Global behavior of WKB curves	77
6.4 Defining the WKB triangulation	79
6.5 The WKB decoration: small flat sections	79
6.6 Jumps of the WKB triangulation	81
6.6.1 A jump from a BPS hypermultiplet	81
6.6.2 A jump when $me^{-i\vartheta} \in i\mathbb{R}$	82
6.6.3 A jump from a BPS vectormultiplet	82
6.6.4 Other degenerations are nongeneric	83
<b>7. The canonical coordinates</b>	<b>84</b>
7.1 Labeling by homology	84
7.1.1 For ordinary edges	84
7.1.2 For degenerate edges	85
7.1.3 Cycles around singular points	85
7.1.4 Lattice generated by $\{\gamma_E\}$	86
7.2 Defining the canonical coordinates	87
7.3 Some easy properties	87
7.4 Asymptotic behavior	88
7.5 From triangulations to KS symplectomorphisms	90
7.6 Jumps at special $\vartheta$	90
7.6.1 Symplectomorphism from a BPS hypermultiplet	90
7.6.2 Symplectomorphism from a BPS vectormultiplet	92
7.6.3 No symplectomorphism when $me^{-i\vartheta} \in i\mathbb{R}$	96
7.7 Quadratic refinement	97
7.8 Some comments on the full BPS spectrum	98
<b>8. Irregular singularities</b>	<b>100</b>

<b>9. Scaling limits of linear <math>SU(2)</math> quivers: the case of one irregular singular point</b>	<b>103</b>
9.1 Linear $SU(2)$ quivers and their parameter spaces	103
9.2 Scaling limit	105
9.3 Hitchin system	106
9.4 Examples	107
9.4.1 $N = 1$	107
9.4.2 $N = 2$	108
9.4.3 Intermission: $N = 2$ and periodic Taub-NUT space	109
9.4.4 $N = 3$	112
9.4.5 Intermission: Symplectomorphisms and monodromy	114
9.4.6 $N = 4$	116
9.5 General $N$ and the associahedron	120
<b>10. <math>SU(2)</math> gauge theory</b>	<b>123</b>
10.1 $N_f = 0$	123
10.2 $N_f = 1$	125
10.3 $N_f = 2$ , first realization	128
10.4 Intermission: non-abelian flavor symmetries and WKB triangulations	132
10.5 $N_f = 2$ , second realization	132
10.6 $N_f = 3$	134
10.7 $N_f = 4$ : The superconformal case	136
<b>11. The spectrum generator</b>	<b>141</b>
11.1 Deriving the transformation under an omnipop	142
11.2 $N = 3$	146
11.3 $N = 4$	148
11.4 $SU(2)$ , $N_f = 0$	149
11.5 $SU(2)$ , $N_f = 1$	149
11.6 $SU(2)$ , $N_f = 4$	150
<b>12. Categorical matters</b>	<b>152</b>
<b>13. <math>R \rightarrow \infty</math> limit</b>	<b>154</b>
13.1 A parameterization of Higgs bundles	154
13.2 Reformulating Hitchin's equations	156
13.3 The trivial solution	157
13.4 The regular solution	157
13.5 The large $R$ limit of $\mathcal{X}_\gamma$	160
13.6 The real section	160
13.7 Relation to Hitchin flows	161
<b>14. Comparison with [1]: differential equations and the Riemann-Hilbert problem</b>	<b>162</b>

<b>A. Expressing monodromy matrices in terms of Fock-Goncharov coordinates</b>	<b>164</b>
<b>B. Computing the Hamiltonian flows</b>	<b>169</b>
<b>C. WKB error analysis</b>	<b>171</b>
<b>D. Holomorphic coordinates on multi-center Taub-NUT</b>	<b>172</b>
<b>E. Configurations of integers with nonpositive second discrete derivative</b>	<b>174</b>

---

## 1. A narrative table of contents

Supersymmetric gauge theories have been a plentiful source of delightful surprises both in theoretical physics and in mathematics. A particularly rich class of theories are those with  $d = 4, \mathcal{N} = 2$  supersymmetry (henceforth referred to as  $\mathcal{N} = 2$  supersymmetry). In this context an important and distinguished subspace of the Hilbert space is the space of BPS states. These states are in “small” or “rigid” representations of the supersymmetry algebra and this rigidity leads to an amenability to analysis which is in turn the foundation for the exact results known about these theories. Although BPS representations of  $\mathcal{N} = 2$  are rigid, the BPS subspace nevertheless depends nontrivially both on the ultraviolet parameters as well as on the choice of quantum vacuum of the theory, a phenomenon known as wall-crossing.

Despite the fundamental nature of this BPS subspace, there is no algorithm for computing it given an arbitrary  $\mathcal{N} = 2$  theory with its choice of vacuum. Indeed the BPS spectrum is only known explicitly in a small set of examples where special *ad hoc* techniques can be applied. The main result of this paper is a new algorithm for determining the BPS spectrum of a certain infinite set of  $\mathcal{N} = 2$  theories. The theories to which our methods apply are described in Section 3 and the new algorithm is described in Section 11 of this paper. Our result is promising because there are indications that generalizations of the algorithm will apply to a much wider set of  $\mathcal{N} = 2$  theories.

The class of theories to which our main result applies are linear quiver gauge theories with  $SU(2)$  factor gauge groups at the nodes. These are part of a larger class of distinguished  $\mathcal{N} = 2$  gauge theories, described extensively in Section 3. This larger class of theories, which we call  $\mathcal{S}$  (for “six”), originates from compactifications of M5-branes on a punctured Riemann surface,  $C$ .<sup>1</sup> The superconformal  $(2,0)$  theories have an A-D-E classification and so we can label elements of  $\mathcal{S}$  by a simply laced “gauge group,” a Riemann surface  $C$ , and a decoration of the punctures of  $C$  by “defect operators.” Theories

---

<sup>1</sup>To be more precise, we consider the low energy  $(2,0)$  superconformal field theory resulting from the decoupling of gravity. We then compactify this theory on  $C$  with a partial twisting of the  $d = 6$   $(2,0)$  superalgebra so as to preserve  $\mathcal{N} = 2$  supersymmetry.

in class  $\mathcal{S}$  have the important property that they enjoy a close relationship with Hitchin systems. This relation, which is absolutely central to this paper, is revealed when one further compactifies to three dimensions on a circle. At low energies the three-dimensional effective theory is a  $d = 3, \mathcal{N} = 4$  sigma model with target space  $\mathcal{M}$ . This target space may be identified, as a Riemannian manifold, with the moduli space of solutions to a Hitchin system. To justify this, the essential observation is that instead of compactifying on  $C$  and then on  $S^1$ , we can — by a QFT version of the “Fubini theorem” — construct the same effective theory in three dimensions by first compactifying on  $S^1$  and then on  $C$ . The first compactification on  $S^1$  leads to a five-dimensional supersymmetric Yang-Mills theory. The subsequent compactification of the (twisted)  $d = 5$  super-Yang-Mills theory on  $C$  then leads to BPS equations which are well known to be the Hitchin equations. In particular, if we begin with  $K$  M5-branes (i.e. the superconformal  $u(K)$   $(2, 0)$  theory in six dimensions) then the Hitchin equations are equations (3.32)-(3.34) below:

$$F + R^2[\varphi, \bar{\varphi}] = 0, \tag{1.1}$$

$$\partial_{\bar{z}}\varphi + [A_{\bar{z}}, \varphi] = 0, \tag{1.2}$$

$$\partial_z\bar{\varphi} + [A_z, \bar{\varphi}] = 0, \tag{1.3}$$

where  $R$  is the radius of the circle,  $F$  is the fieldstrength of a  $u(K)$  gauge field  $A$  on  $C$  and  $\varphi$  is the  $(1, 0)$  part of a 1-form valued in the adjoint.  $z$  is a local holomorphic coordinate on  $C$ .

The description of the Hitchin system is incomplete without specifying boundary conditions on  $(A, \varphi)$  at the punctures of  $C$ . At these punctures the fields  $(A, \varphi)$  have singularities. Physically these singularities encode the somewhat mysterious “defect operators” of the six-dimensional superconformal theory (and in practice the defect operators are defined by the specified singularities of  $(A, \varphi)$ ). The simplest operators to consider – and the ones upon which we focus – arise from intersections, at the punctures of  $C$ , of the multiple  $u(K)$  M5-brane theory with “transverse” singly-wrapped M5-branes. By transverse we mean the following. In general the curve  $C$  is embedded in some hyperkahler manifold  $Q$  as a holomorphic curve. The gravitational decoupling limit allows us to replace  $Q$  by a neighborhood of the zero-section of  $T^*C$ . The transverse fivebranes fill the four-dimensional spacetime  $\mathbb{R}^{1,3}$  of the  $\mathcal{N} = 2$  theory and run along fibers of the projection  $T^*C \rightarrow C$ . In Section 3 we show how to translate this physical picture into conditions on the singularities of  $(A, \varphi)$ . The singularities are described in detail in Section 3.2.4; see (3.74), (3.75), and (3.76), for the case of regular singularities, and Section 3.2.6, equation (3.115), (3.116), as well as Section 9.3, for the case of irregular singularities.

The Hitchin system plays a central role throughout the paper and Section 4 of the paper summarizes the basic facts we need about Hitchin systems. The mathematically-oriented reader can skip Section 3 and proceed with the brief summary in Section 4, although the rules for finding BPS states might then appear somewhat unmotivated.

A particularly important set of examples of theories in the class  $\mathcal{S}$  are provided by Witten’s geometric construction of  $\mathcal{N} = 2$  theories using arrays of NS5- and D4-branes [2]. These are often summarized by figures such as Figure 5. Much of Section 3 is merely

a review of Witten’s construction and may be safely skipped by readers familiar with [3, 2]. We would note however that Sections 3.2.4, 3.2.5, and 3.2.6 contain some new points concerning how to use the physical picture to describe the boundary conditions on  $(A, \varphi)$ . In addition, Sections 3.2.8 and 3.2.9 contain some novel remarks on isomorphisms between Hitchin moduli spaces and on flavor symmetries, respectively. In particular, the isomorphisms of Section 3.2.8 should be of some mathematical interest. A similar class of isomorphisms has been independently noted recently by Philip Boalch [4].

The geometry of the Hitchin system on  $C$  beautifully encodes the key data of the low energy effective Seiberg-Witten theory of the *four-dimensional*  $\mathcal{N} = 2$  theory in  $\mathcal{S}$ . First, the Seiberg-Witten curve, which is a branched cover  $\Sigma$  of  $C$ , is nicely presented as the spectral curve of the Hitchin system. Thus  $\Sigma \subset T^*C$  and moreover the sheets of the cover may be labeled by the eigenvalues of  $\varphi$ . Quite generally, a cotangent bundle  $T^*C$  is canonically endowed with a symplectic form which is further canonically trivialized by a one-form. Restricting this one-form to  $\Sigma$  one obtains the Seiberg-Witten differential, denoted  $\lambda$ .

Since our main theme is the BPS spectrum it behooves us to understand how to describe this spectrum in the context of Hitchin systems. Given the origin of the theories from M5-branes wrapped on  $C$  one can systematically understand the BPS states in terms of strings in the six-dimensional theory, which in turn originate from open M2-branes ending on M5-branes [5]. The translation of this description of BPS states to the language of Hitchin systems is described in Sections 3.1.1 and 3.1.3. In the case  $K = 2$  we recover a well-known construction of Klemm et. al. [3]: BPS states are associated with curves on  $C$  that minimize the local tension of the strings. Expressed mathematically, near a point  $z_0$  on the curve we choose a branch of the cover and define a local coordinate by  $w = \int_{z_0}^z \lambda$ . The curve is then a straight line in the  $w$ -plane. BPS (half)-hypermultiplets are associated with curves which begin and end on branch points of the cover  $\Sigma \rightarrow C$ , while BPS vectormultiplets are associated with curves which are closed. For reasons explained below, we call either of these *finite WKB curves*. See Figures 3 and 4 for illustrations. The central charge of the corresponding BPS state is  $Z_\gamma = \pi^{-1} \oint_\gamma \lambda$ . An important point below is that the phase of this central charge is the angle  $\vartheta$  between the straight line in the  $w$  plane and the  $\text{Re}(w)$ -axis. When  $K > 2$  the analogous description of BPS states is more involved, and makes use of string webs on  $C$ .

As so often happens, our main result was in fact not the initial goal of this work. Rather, the original motivation came from a recent construction [1] of hyperkähler metrics, which in turn was motivated by the search for the physical underpinnings of the Kontsevich-Soibelman wall-crossing formula [6]. In order to make the remainder of our summary intelligible we must first recall here the most essential points of [1]. A more technical summary of [1] can be found in Section 2.

The starting point of [1] is the compactification of a general  $d = 4, \mathcal{N} = 2$  theory on a circle of radius  $R$ . As mentioned above, at low energies the theory is a three-dimensional sigma model whose target space  $\mathcal{M}$  must carry a hyperkähler metric. The space  $\mathcal{M}$  has a fibration  $\mathcal{M} \rightarrow \mathcal{B}$  where  $\mathcal{B}$  is the moduli space of vacua of the four-dimensional theory and the generic fiber is a real torus of dimension  $\dim \mathcal{B}$ . As  $R \rightarrow \infty$  the metric on  $\mathcal{M}$

becomes exponentially close to a simple and explicit metric which is hyperkähler, but has singularities in real codimension two. This metric is called the “semiflat metric” and denoted  $g^{\text{sf}}$ . It is easily derived by naive dimensional reduction along  $S^1$  of the Seiberg-Witten effective Lagrangian. Quantum corrections at finite values of  $R$  smooth out  $g^{\text{sf}}$ . Moreover, these quantum corrections depend solely on the spectrum of BPS states. Since that spectrum is itself a function of the (four-dimensional) vacuum, the smoothness of the metric implies a wall-crossing formula. In [1] it is shown that this is precisely the Kontsevich-Soibelman wall-crossing formula (KSWCF).

From the purely mathematical viewpoint one can view [1] as giving a construction of hyperkähler metrics from the following three pieces of data:

- D1: A local system of lattices  $\hat{\Gamma} \rightarrow \mathcal{B}$  with an integral antisymmetric form  $\langle, \rangle$  (possibly degenerate) on the fibers. Letting  $\Gamma$  be the local system of symplectic lattices obtained by dividing by the radical of  $\hat{\Gamma}$ , we require  $\mathcal{B}$  to have real dimension equal to the rank of  $\Gamma$ .
- D2: A central charge function  $Z \in \text{Hom}(\hat{\Gamma}, \mathbb{C})$  such that  $\langle dZ, dZ \rangle = 0$  where  $d$  is the differential along  $\mathcal{B}$ .
- D3: A piecewise constant function  $\Omega : \hat{\Gamma} \rightarrow \mathbb{Z}$  satisfying the KSWCF.

When a physical  $\mathcal{N} = 2$  theory provides the data D1, D2, D3 the moduli space  $\mathcal{M}$  of the physical problem can be identified with the total space of the fibration  $\Gamma^* \otimes \mathbb{R}/2\pi\mathbb{Z}$  over  $\mathcal{B}$ . Thus we expect that just given the data D1, D2, D3 we can construct a hyperkähler metric on  $\mathcal{M} = \Gamma^* \otimes \mathbb{R}/2\pi\mathbb{Z}$ , as indeed proves to be the case. In fact, we construct a *family* of hyperkähler metrics on  $\mathcal{M}$ . The parameters of the family are described below.

An essential part of the construction of the metrics on  $\mathcal{M}$  involves the twistor description of hyperkähler metrics. Exploiting the fact that  $\hat{\Gamma}^* \otimes \mathbb{R}/2\pi\mathbb{Z}$  has a fibration by tori one reduces the construction of suitable holomorphic data on twistor space to the construction of a certain map  $\mathcal{X}^{\text{RH}} : \mathcal{M} \times \mathbb{C}^\times \rightarrow \hat{\Gamma}^* \otimes \mathbb{C}^\times$ ,<sup>2</sup> where the factor  $\mathbb{C}^\times$  in the domain is part of the twistor sphere. It is very convenient to let  $\mathcal{X}_\gamma^{\text{RH}} : \mathcal{M} \rightarrow \mathbb{C}^\times$  be the contraction of  $\mathcal{X}^{\text{RH}}$  with  $\gamma \in \hat{\Gamma}$ . We will refer to these functions as *Darboux coordinates*.<sup>3</sup> Note that  $\mathcal{X}_\gamma^{\text{RH}} \mathcal{X}_{\gamma'}^{\text{RH}} = \mathcal{X}_{\gamma+\gamma'}^{\text{RH}}$ . The map  $\mathcal{X}^{\text{RH}}$  is subject to a list of defining properties. The full list of detailed properties is recalled in Section 2 but three crucial properties must be stated here:

- P1: First, the Poisson structure is defined by equation (2.3):

$$\{\mathcal{X}_\gamma^{\text{RH}}, \mathcal{X}_{\gamma'}^{\text{RH}}\} = \langle \gamma, \gamma' \rangle \mathcal{X}_{\gamma+\gamma'}^{\text{RH}}. \quad (1.4)$$

<sup>2</sup>In [1] this map was just called  $\mathcal{X}$ .

<sup>3</sup>There is an abuse of terminology here which we regret. Once one chooses a basis  $\{\gamma_i\}$  of  $\Gamma$  compatible with a Lagrangian decomposition together with a lifting to  $\hat{\Gamma}$  then  $\log \mathcal{X}_{\gamma_i}^{\text{RH}}$  truly provide a system of Darboux coordinates on the holomorphic symplectic manifold  $\mathcal{M}$ .



- P2: Second, the  $\mathcal{X}_\gamma^{\text{RH}}$  are asymptotic to the analogous functions  $\mathcal{X}_\gamma^{\text{sf}}$  associated with the semiflat metric  $g^{\text{sf}}$ . Let  $\zeta \in \mathbb{C}^\times$  be an element of the twistor sphere. The semiflat Darboux coordinates can be written very explicitly as

$$\mathcal{X}_\gamma^{\text{sf}} := \exp \left( \pi R \zeta^{-1} Z_\gamma + i \theta_\gamma + \pi R \zeta \bar{Z}_\gamma \right), \quad (1.5)$$

where  $\theta_\gamma : \hat{\Gamma}^* \otimes \mathbb{R}/2\pi\mathbb{Z} \rightarrow \mathbb{R}/2\pi\mathbb{Z}$  are canonically defined by contraction. We demand that  $\mathcal{X}_\gamma^{\text{RH}} \sim \mathcal{X}_\gamma^{\text{sf}}$  both for  $\zeta \rightarrow 0, \infty$  and for  $R \rightarrow \infty$ .

- P3: Third, the analytic structure of  $\mathcal{X}^{\text{RH}}$  as a function of  $\zeta$  is constrained as follows. Define the *BPS rays* to be the rays  $\ell_{\gamma,u} := \{\zeta : Z_\gamma(u)/\zeta \in \mathbb{R}_-\}$ . Then, as  $\zeta$  crosses a BPS ray  $\ell_{\gamma_0,u}$  the  $\mathcal{X}_\gamma^{\text{RH}}$  are discontinuous by a Poisson transformation  $\mathcal{K}_{\gamma_0}^{\Omega(\gamma_0;u)}$  where<sup>4</sup>

$$\mathcal{K}_{\gamma_0} : \mathcal{X}_\gamma^{\text{RH}} \rightarrow \mathcal{X}_\gamma^{\text{RH}} (1 \pm \mathcal{X}_{\gamma_0}^{\text{RH}})^{\langle \gamma, \gamma_0 \rangle}. \quad (1.6)$$

The transformations  $\mathcal{K}_{\gamma_0}$  will be referred to as *KS transformations*. For the more precise equation (in particular the choice of  $\pm$  sign) see (2.6) below. In addition  $\mathcal{X}_\gamma^{\text{RH}}$  must be *holomorphic* (without any singularities) as a function of  $\zeta$  on the complement of the set of BPS rays  $\ell_{\gamma,u}$  with  $\Omega(\gamma;u) \neq 0$ .

As explained in [1], from the functions  $\mathcal{X}_\gamma^{\text{RH}}$  one can recover the hyperkähler metric on  $\mathcal{M}$ . The resulting metric smoothes out the real codimension two singularities of  $g^{\text{sf}}$  (but some real codimension four singularities might remain).

Returning to the physical viewpoint, the functions  $\mathcal{X}_\gamma^{\text{RH}}$  have nice interpretations in terms of line operator expectation values as well as elements in a chiral ring in a three-dimensional topological field theory. We hope to describe these aspects of the  $\mathcal{X}_\gamma^{\text{RH}}$  elsewhere (we again touch on this point briefly in Remark 3 of Appendix A).

We said above that we obtain a family of hyperkähler metrics. To understand this first note that the radical of  $\hat{\Gamma}$  is, physically, a lattice of flavor charges. We have

$$0 \rightarrow \Gamma_{\text{flavor}} \rightarrow \hat{\Gamma} \rightarrow \Gamma \rightarrow 0 \quad (1.7)$$

and the symplectic lattice  $\Gamma$  is the lattice of electric and magnetic gauge charges. The manifold  $\hat{\Gamma}^* \otimes \mathbb{R}/2\pi\mathbb{Z}$  is foliated by copies of  $\mathcal{M}$ . Moreover, the  $\mathcal{X}_\gamma^{\text{RH}}$  for  $\gamma \in \Gamma_{\text{flavor}}$  take the exact form (1.5), where  $Z_\gamma$  encode hypermultiplet masses and  $\theta_\gamma$  encode flavor Wilson lines. These parameters, together with  $R$ , parameterize the family of hyperkähler metrics on  $\mathcal{M}$ .

The last aspect of [1] we must recall is the explicit construction of  $\mathcal{X}^{\text{RH}}$ . This is done by a series of maneuvers using the properties P2 and P3 to characterize  $\mathcal{X}^{\text{RH}}$  as a solution of a Riemann-Hilbert problem that is in turn equivalent to an integral equation. This integral equation, incidentally, turns out to be a version of the Thermodynamic Bethe Ansatz (TBA).<sup>5</sup> This TBA equation can then be solved by iteration *provided* the radius  $R$  is large.

<sup>4</sup>Actually, we should consider all multiples of  $\gamma_0$ , thus the correct transformation to use is  $\prod_{\gamma_0'' \parallel \gamma_0} \mathcal{K}_{\gamma_0''}^{\Omega(\gamma_0'';u)}$ . In the examples we study only a single charge will contribute to the discontinuity.

<sup>5</sup>Another relation between four-dimensional super Yang-Mills theory and the TBA has recently been discussed by Nekrasov and Shatashvili [7].

The result is an explicit series expansion in terms of multiple integrals whose integrands are small when  $\mathcal{X}_\gamma^{\text{sf}}$  is small. Hence we obtain an explicit construction of the hyperkähler metric. We must stress that  $R$  should be large in order to justify the solution of the integral equation by iteration. (An important fact used here is that  $\mathcal{X}_\gamma^{\text{sf}}$  are exponentially small on  $\ell_{\gamma,u}$  as  $R \rightarrow \infty$ .)

Having recalled the main features of [1] we can at last return to describing the original goal in writing the present paper: It is to give an alternative construction of the  $\mathcal{X}_\gamma^{\text{RH}}$  which does not rely on the integral equation and is valid for all  $R$ . In this paper we will indeed give an alternative construction of the functions  $\mathcal{X}_\gamma^{\text{RH}}$  for the theories in  $\mathcal{S}$  associated to  $SU(2)$  Hitchin systems. Our definition is indeed sensible for *all values of  $R$* . Moreover the new construction lends itself to elegant geometrical verifications of the key defining properties P1, P2, and (part of) P3.<sup>6</sup>

Before explaining the new construction we must confess at the outset that one difficulty will remain unresolved. Concerning the behavior of the Darboux coordinates at small  $R$  there is some tension between this paper and [1]. In [1] we proposed that the TBA equation would have a regular solution for all  $R$ . This would yield a  $\mathcal{X}^{\text{RH}}$  with no poles in the  $\zeta$ -plane.<sup>7</sup> The results of this paper suggest that the truth might be more complicated: we indeed find a natural candidate for  $\mathcal{X}^{\text{RH}}$ , and it is indeed defined for all  $R$ , but for small  $R$ , we are not able to show that it is pole-free. On the other hand, it is hard to envision a scenario where there are two *different*  $\mathcal{X}^{\text{RH}}$ , one with poles and one without. So we see two reasonable options. One option is that the  $\mathcal{X}_\gamma^{\text{RH}}$  of this paper actually do not have poles. They could then be identified with solutions of the integral equation of [1] for all  $R$ . The other option is that the  $\mathcal{X}_\gamma^{\text{RH}}$  of this paper do have poles. In that case they are, strictly speaking, not solutions of the integral equation of [1] for small  $R$ . The appearance of such “extra poles” as a parameter is varied is well-known in the literature on the TBA (see for example [9]), and can be dealt with in that context. Clearly, these matters deserve further attention!

Now let us summarize the new construction of the  $\mathcal{X}_\gamma^{\text{RH}}$ . The key idea begins with the fact that Hitchin’s moduli space  $\mathcal{M}$  is *also* a moduli space of flat connections with fixed monodromy<sup>8</sup> around the punctures of  $C$ . Indeed, given a solution of the Hitchin equations we can form a non-unitary connection (equation (4.8) below)

$$\mathcal{A} := \frac{R}{\zeta} \varphi + A + R\zeta \bar{\varphi}, \quad (1.8)$$

and the Hitchin equations imply this is a flat connection on  $C$  for any  $\zeta \in \mathbb{C}^\times$ . Conversely, the flatness of such a connection for all  $\zeta$  implies that  $(A, \varphi)$  solve the Hitchin equations. The next observation is that Fock and Goncharov have constructed a beautiful set of

---

<sup>6</sup>The reader experienced with the Thermodynamic Bethe Ansatz may view our results as a broad generalization of the work [8], where solutions to TBA equations (in a “conformal limit”) were basically constructed from the monodromy data of a holomorphic connection.

<sup>7</sup>More precisely,  $\mathcal{X}^{\text{RH}}$  is holomorphic in the complement of the set of BPS rays with  $\Omega \neq 0$ .

<sup>8</sup>Since the Hitchin system may have both regular and irregular singularities, the “monodromy data” includes Stokes data.

coordinates on the moduli space of flat connections, using the data of a triangulation of  $C$  [10]. (This useful set of coordinates is available only if  $C$  has at least one puncture and hence we will not attempt to extend our construction of the  $\mathcal{X}_\gamma$  beyond that case, even though the physical theory makes sense when  $C$  has no punctures.) We will use the Fock-Goncharov coordinates to construct our functions  $\mathcal{X}_\gamma$ . In outline our program is the following: First, given an angle<sup>9</sup>  $\vartheta$ , we define a distinguished triangulation which we call a *WKB triangulation*. Second, applying the Fock-Goncharov construction to that triangulation we get a set of functions  $\mathcal{X}_\gamma^\vartheta : \mathcal{M} \times \mathbb{C}^\times \rightarrow \mathbb{C}^\times$ . We then use the  $\mathcal{X}_\gamma^\vartheta$  in turn to construct  $\mathcal{X}_\gamma^{\text{RH}}$ , by specializing  $\vartheta = \arg(\zeta)$ . Third, we show that the resulting functions satisfy the defining properties outlined in Section 2 (in particular P1, P2, P3). Let us now sketch how this program is accomplished in slightly more detail.

In Section 5 we recall the construction of Fock and Goncharov [10]. We deviate from their discussion in two ways. One rather minor difference is that we prefer to use *decorated triangulations*. In the case of regular singular points (on which we mostly focus), these are ideal triangulations whose vertices are the singular points  $\mathcal{P}_i$  of the Hitchin system, but where we add an extra piece of data at each point  $\mathcal{P}_i$ . Specifically, we consider flat sections  $s$  solving  $(d + \mathcal{A})s = 0$ , and the decoration of  $\mathcal{P}_i$  consists in choosing a flat section  $s_i$ , defined up to scale, in a neighborhood of  $\mathcal{P}_i$ . Such a flat section is necessarily an eigenvector of the monodromy around  $\mathcal{P}_i$ , so equivalently, the decoration is a choice of one of the two eigenlines of that monodromy. (An analogous notion of decorated triangulation for irregular singular points is explained in Section 8.) The second, more important, deviation from the work of Fock and Goncharov is that the existence of the vectormultiplets in the BPS spectrum forces us to extend the notion of triangulation to include more elaborate objects which we call “limit triangulations.” These are described in Section 5.9. The heart of the Fock-Goncharov construction is to use “overlaps” of the (parallel transport of the) flat sections  $s_i$  to describe the monodromy of the flat connection  $\mathcal{A}$ . In Appendix A we explain how this can be done. The procedure naturally leads to the key definition of equation (5.2).

That the property P1 of the  $\mathcal{X}_\gamma^{\text{RH}}$  will emerge correctly can already be seen nicely at this stage. The Hitchin moduli space has a natural holomorphic symplectic form, given in (4.10),

$$\varpi_\zeta = \frac{1}{2} \int_C \text{Tr} \delta \mathcal{A} \wedge \delta \mathcal{A}. \quad (1.9)$$

The corresponding Poisson brackets of the Fock-Goncharov coordinates then take the simple form (5.9). To be self-contained, we give an elementary derivation of these Poisson brackets in Sections 5.4-5.5, using results from Appendix B.

A second key defining property (P2 above) of the coordinates  $\mathcal{X}_\gamma^{\text{RH}}$  is their asymptotic behavior for  $\zeta \rightarrow 0, \infty$  and  $R \rightarrow \infty$ . It is this property that motivates our definition of a WKB triangulation. As described in Section 6, we define WKB curves of phase  $\vartheta$  to satisfy  $\langle \lambda, \partial_t \rangle = e^{i\vartheta}$ . Of course, we have already met this condition above, when discussing BPS states! It is equivalent to the assertion that in the local coordinate  $w = \int_{z_0}^z \lambda$ , where  $z_0$  is a

---

<sup>9</sup>The periodicity of  $\vartheta$  can be an integer multiple of  $2\pi$ , or it might even live in the universal cover  $\mathbb{R}$ .

point on the curve, the curve is a straight line parallel to  $e^{i\vartheta}$ . These WKB curves tend to be “captured” by the singularities (as shown in the local analysis of Section 6.2) and hence the generic WKB curve begins and ends on a singularity. The WKB triangulation is then defined by choosing a suitable finite set of “topologically distinct” generic WKB curves using a procedure explained in Sections 6.3 and 6.4. Moreover, there is a canonical decoration given by choosing the flat section which becomes exponentially small along a WKB curve plummeting into a singularity. This choice of decorated triangulation is motivated by the WKB analysis (with small parameter  $\zeta, 1/\zeta$  or  $1/R$ ) of the equation  $(d + \mathcal{A})s = 0$  for the flat sections. Recall that in the WKB approximation, exponentially small wavefunctions can be computed reliably, but exponentially large wavefunctions are ambiguous by the addition of an unknown exponentially small component. For this reason we must take care when computing “overlaps” of flat sections  $s_i$  transported from the different locations  $\mathcal{P}_i$  of  $C$ : We must transport these sections along WKB curves. In summary, given an angle  $\vartheta$  and a vacuum  $u \in \mathcal{B}$  – or, better, a Seiberg-Witten differential  $\lambda$  – we have a canonically determined decorated triangulation. It will be denoted as  $T_{\text{WKB}}(\vartheta, u)$  or as  $T_{\text{WKB}}(\vartheta, \lambda^2)$ . The second notation reflects the fact that the edges are unoriented, and hence only depend on the quadratic differential  $\lambda^2$ .

Turning now to the third key property P3 we must consider how different WKB triangulations are related as we vary  $\vartheta$  at fixed  $\lambda$ . Quite generally, different decorated triangulations (not necessarily of WKB type) can be turned into each other by a series of elementary transformations which we refer to as the *flip*, *juggle*, and *pop*. We may view the decorated triangulations as objects in a groupoid, and the flips, juggles, and pops are elementary morphisms which generate all other morphisms in the groupoid. A flip is simply the standard transformation of flipping an edge within a quadrilateral formed by two triangles, as in Figure 16. The decoration is unchanged. A pop, on the other hand, leaves the triangulation unchanged but alters the choice of distinguished eigenline at a specified vertex. When  $\mathcal{A}$  has structure group  $SL(2, \mathbb{C})$  and the singularity is a regular singularity with diagonalizable monodromy the pop transformation simply exchanges the two eigenlines. The most difficult transformation, the juggle, relates different limit triangulations. See Section 5.9 for the detailed discussion and Figure 29 for an illustration. An important aspect of the Fock-Goncharov theory is that under flips the coordinates undergo *cluster transformations*. These cluster transformations turn out to be special cases of the Kontsevich-Soibelman transformations  $\mathcal{K}_{\gamma_0}$ . The transformations under pops are explicitly known, but in general are rather cumbersome. A significant point for our main result is that, nevertheless, the *omnipop*, defined to be the transformation that simultaneously pops all vertices, is a simple and computable transformation  $\mathbf{S}$ , which we call the *spectrum generator* for reasons which will be clear below. The omnipop transformation  $\mathbf{S}$  is derived in Section 11.1. The transformation under the juggle is described in Section 5.9.

Having set up all the machinery in Sections 5 and 6 we finally give the crucial definition of the functions  $\mathcal{X}_\gamma^\vartheta : \mathcal{M} \times \mathbb{C}^\times \rightarrow \mathbb{C}$  in equations (7.3) and (7.4). Since the definition is given in terms of Fock-Goncharov coordinates the Poisson brackets (property P1 above) follow naturally. Moreover, our choice of decorated triangulation  $T_{\text{WKB}}(\vartheta, \lambda^2)$  leads to a straightforward derivation of the  $\zeta \rightarrow 0, \infty$  and  $R \rightarrow \infty$  asymptotics, as indeed it was

designed to do. Now, rather beautifully, as  $\vartheta$  varies the WKB triangulations undergo flips, juggles, and pops precisely when  $\vartheta$  is the inclination of some BPS ray  $\ell_{\gamma,u}$ . Indeed, this is quite natural since, as we described above, the result of [3] simply states that BPS states are associated with nongeneric *finite* WKB curves. Recall these are closed or begin and end on branch points of the covering  $\Sigma \rightarrow C$ . The basic morphisms are illustrated in Figures 27 and 29, and in equations (7.33) and (7.56) we show that the corresponding discontinuities in  $\mathcal{X}_\gamma^\vartheta$  are precisely those associated with KS transformations, with the correct value of  $\Omega$ .

In Section 11 we use the results of Section 7 to give our algorithm for computing the BPS spectrum of theories with  $K = 2$ . Choose a half-plane  $\mathcal{H}(\vartheta, \vartheta + \pi)$  of the complex  $\zeta$  plane bounded by rays at angles  $[\vartheta, \vartheta + \pi]$  and consider evolving the triangulation  $T_{\text{WKB}}(\vartheta, \lambda^2)$  as  $e^{i\vartheta}$  rotates to  $-e^{i\vartheta}$  in this half-plane. Remarkably, it turns out that in this continuous evolution the pops always occur in special circumstances<sup>10</sup> such that the corresponding transformation of the  $\mathcal{X}_\gamma^\vartheta$  is the identity. This surprising fact is shown in Section 7.6.3. Hence the net transformation for evolving  $\vartheta \rightarrow \vartheta + \pi$  just involves a sequence of flips and juggles, and the effect on the Darboux coordinates is the transformation  $\mathbf{S} = \prod \mathcal{K}_\gamma^{\Omega(\gamma;u)}$  with the factors ordered by  $\arg Z_\gamma$ . Now, every BPS state (or its antiparticle) has a BPS ray in the chosen half-plane  $\mathcal{H}(\vartheta, \vartheta + \pi)$ , so the product captures precisely half the spectrum, while the other half are just the antiparticles. On the other hand, the initial and final triangulations  $T_{\text{WKB}}(\vartheta, \lambda^2)$  and  $T_{\text{WKB}}(\vartheta + \pi, \lambda^2)$  turn out to be simply related by an omnipop and, as we mentioned above, that transformation can be computed explicitly (Section 11). Since the product decomposition  $\mathbf{S} = \prod \mathcal{K}_\gamma^{\Omega(\gamma;u)}$  is unique, (given an ordering of BPS rays, which is in turn determined by  $u$ ), we can read off the spectrum from the aptly named spectrum generator  $\mathbf{S}$ . It is worth asking how this algorithm improves upon the prescription already given in [3] for computing the BPS spectrum of the  $A_1$  theories of class  $S$ . The latter prescription requires one to know the critical values of  $\vartheta$  for which the BPS states exist. The crucial point of the above algorithm is that one need only choose a generic value of  $\vartheta$ , and no prior knowledge of the phases of occupied BPS central charges is required.

In Sections 9 and 10 we work out a large number of examples of our formalism. In Section 9 we show how various limits of the linear  $SU(2)$  quiver theories include all the possible Argyres-Douglas (AD) superconformal theories. Already the simplest examples of AD theories provide beautiful illustrations of the KSWCF. It turns out that all the wall-crossing identities in these theories are consequences of a basic pentagon identity (9.31). In Section 10 we consider  $SU(2)$  gauge theory with  $N_f = 0, 1, 2, 3, 4$  flavors of fundamental hypermultiplets. In this case the BPS spectra are very elaborate, and the wall-crossing typically involves infinite products of KS transformations, generalizing the basic example which appears for  $N_f = 0$ , equation (10.2). It turns out that all the wall-crossing formulae in these examples — intricate though they may be — are obtained by successive use of this basic identity and the pentagon. The most elaborate and beautiful spectrum occurs in the  $N_f = 4$  case. We locate a particularly interesting strong coupling region in which the finite spectrum splits into two  $N = 4$  AD points and can therefore be described very

---

<sup>10</sup>More technically: The pop occurs at the center of a degenerate triangle such as in Figure 19.

concretely. We expect this observation to be useful in some future investigations.

Let us conclude this survey by returning to our original goal of defining the functions  $\mathcal{X}_\gamma^{\text{RH}}$  relevant to the construction of [1]. An important preliminary result is given in Section 13, where we show that in the  $R \rightarrow \infty$  limit the  $\mathcal{X}_\gamma^\vartheta$  indeed are asymptotic to the semiflat coordinates  $\mathcal{X}_\gamma^{\text{sf}}$  as long as  $\zeta$  is in the halfplane  $\mathbb{H}_\vartheta$  centered on  $e^{i\vartheta}$ . The proof uses an interesting connection to the sinh-Gordon equation (and a generalization thereof) on the Riemann surface  $C$ .<sup>11</sup> From this we are able to deduce that the only singularities of  $\mathcal{X}_\gamma^{\vartheta=\arg \zeta}$  are the essential singularities at  $\zeta = 0, \infty$  together with discontinuities across those BPS rays with  $\Omega \neq 0$ . Given the other results in Section 7 it follows that they satisfy the full set of defining properties in Section 2, and hence do indeed provide the desired alternative construction we set out to find. Maddeningly, as we have mentioned, this reasoning is valid for large enough  $R$  but might break down at some finite  $R$ , as explained in Section 14. This leaves the behavior as  $R$  decreases to zero as an important open question.

We close with a few comments and possible future directions for research:

- First, and most obviously, the generalization to higher rank theories ( $K > 2$ ) should be carried out. Since the first preprint version of this paper appeared, we have made some progress in this direction. The general story will appear in [12] and some important examples in [13].
- Our constructions raise some tantalizing possible connections to the mathematics of BPS state counting via Hall algebras (and perhaps from there to the algebras of BPS states). It seems likely that there should be a category underlying this story, a sort of Fukaya category for 1-manifolds in a Riemann surface. As we remark in Section 7.8, it is conceivable that this category is in fact equivalent to a category of quiver representations. Moreover, the geometry of the decompositions of  $C$  we consider suggests a method for realizing the Harder-Narasimhan filtration in this category. We briefly sketch these ideas in Section 12.
- One consequence of our results is a new description of the hyperkähler metrics on certain moduli spaces of Higgs bundles. Moduli spaces of Higgs bundles play a prominent role in a new approach to the geometric Langlands program initiated in [14], and indeed the way these moduli spaces appear in this paper is not unrelated to the way they appear in [14]. It is thus natural to wonder whether our results can be of any use for geometric Langlands.
- Fock and Goncharov’s construction was motivated in part by the desire to construct new infinite-dimensional modular functors (associated with Liouville theory and its higher rank “Toda” generalizations). We believe that some of the ideas of this paper, particularly the notion of “limit triangulation,” might provide some useful insights into these new modular functors.

---

<sup>11</sup>Incidentally, this relation has also recently played a useful role in the work of Alday and Maldacena [11], and that connection allowed those authors to put some of our results in this paper to good use. We discuss this connection a bit more in Section 9.4.3.



- The story of this paper applies most directly to  $\mathcal{N} = 2$  theories which are not conformal. However, there are some closely related conformal theories, discussed further in [15], which could be obtained by adjusting the eigenvalues of the monodromies at the singular points in  $C$  to zero. Now, in the closely analogous case of  $\mathcal{N} = (2, 2)$  theories in two dimensions, [16] exploited information about massive deformations to get information about the conformal points (for example, their spectrum of conformal dimensions). It is natural to wonder whether a similar trick would work here.
- Finally, as mentioned above, it would be very interesting to understand the analytic structure of the functions  $\mathcal{X}_\gamma$  constructed in this paper at small  $R$ .

## 2. Review

Let us quickly recall the setup, notation and main proposal of [1], to which we refer for more details.

### 2.1 Setup

We consider a  $d = 4$ ,  $\mathcal{N} = 2$  supersymmetric gauge theory. Call its Coulomb branch  $\mathcal{B}$ . At each point  $u \in \mathcal{B}$  the gauge group is broken to a maximal torus  $U(1)^r$ . There is a lattice  $\hat{\Gamma}_u$  of charges, equipped with an antisymmetric integer-valued pairing  $\langle, \rangle$ . The radical of this pairing is the sublattice  $(\Gamma_{\text{flavor}})_u$  of flavor charges. Dividing out by  $(\Gamma_{\text{flavor}})_u$  gives the quotient lattice  $\Gamma_u$  of gauge charges.  $\Gamma_u$  has rank  $2r$  and is equipped with a symplectic pairing.

The lattice  $\hat{\Gamma}_u$  is the fiber of a local system  $\hat{\Gamma}$ , with nontrivial monodromy around the complex-codimension-1 singular loci in  $\mathcal{B}$ , where some BPS particles become massless. There is a “central charge” homomorphism

$$Z : \hat{\Gamma}_u \rightarrow \mathbb{C} \tag{2.1}$$

varying holomorphically with  $u$ . In particular, given any local section  $\gamma$  of  $\hat{\Gamma}$ , there is a corresponding locally-defined holomorphic function  $Z_\gamma(u)$ , the central charge of a particle with charge  $\gamma$ .

We formulate the theory on  $\mathbb{R}^3 \times S^1$ , with  $S^1$  of radius  $R$ . At energies  $\ll 1/R$  this theory looks effectively three-dimensional. Its moduli space is locally a product of two hyperkähler manifolds. One factor is the Higgs branch of the  $d = 4$  theory, which we do not consider here. The other factor is the  $d = 3$  Coulomb branch  $\mathcal{M}$ . At generic, non-singular points in  $\mathcal{M}$  the Higgs branch is actually absent.  $\mathcal{M}$  is a fibration

$$\pi : \mathcal{M} \rightarrow \mathcal{B} \tag{2.2}$$

with generic fiber a  $2r$ -torus. The torus fibers appear because the gauge fields in  $d = 4$  give rise to scalars in  $d = 3$ , namely the holonomies of the gauge fields (both electric and magnetic) around  $S^1$ . For each  $\gamma \in \Gamma_u$  we have a corresponding circle-valued holonomy  $\theta_\gamma$ , with  $\theta_{\gamma+\gamma'} = \theta_\gamma + \theta_{\gamma'}$ .

Because of supersymmetry the metric  $g$  on  $\mathcal{M}$  is hyperkähler. A first approximation  $g^{\text{sf}}$  to  $g$  is obtained by naive dimensional reduction. To determine  $g$  exactly, one must also include instanton (and multi-instanton) effects, coming from BPS particles of the  $d = 4$  theory winding around  $S^1$ . These effects are weighted by the second helicity supertraces  $\Omega(\gamma; u)$  which count particles of charge  $\gamma$ .

## 2.2 Darboux coordinates

In [1] we proposed an exact description of  $g$ . The main idea is that to describe  $g$  it is enough to describe holomorphic Darboux coordinates for  $\mathcal{M}$  considered as a holomorphic symplectic manifold.

The construction is local over the base  $\mathcal{B}$ . Fix an open set  $U \subset \mathcal{B}$  over which  $\hat{\Gamma}$  is trivializable. Also fix a choice of quadratic refinement  $\sigma : \hat{\Gamma} \rightarrow \{\pm 1\}$  of the antisymmetric pairing mod 2. Our holomorphic Darboux coordinates are labeled by sections  $\gamma$  of  $\hat{\Gamma}$  over  $U$ . They are functions  $\mathcal{X}_\gamma$  on  $\pi^{-1}(U) \times \mathbb{C}^\times$  obeying

- a)  $\mathcal{X}_{\gamma+\gamma'} = \mathcal{X}_\gamma \mathcal{X}_{\gamma'}$ .
- b) For any fixed  $\zeta \in \mathbb{C}^\times$ ,  $\mathcal{X}_\gamma(\cdot; \zeta)$  is valued in  $\mathbb{C}^\times$ , and holomorphic in complex structure  $J^{(\zeta)}$  on  $\mathcal{M}$ . (Recall  $\mathcal{M}$  is hyperkähler and hence has a  $\mathbb{CP}^1$  of complex structures.)
- c) The holomorphic Poisson brackets of the  $\mathcal{X}_\gamma$  are given by<sup>12</sup>

$$\{\mathcal{X}_\gamma, \mathcal{X}_{\gamma'}\} = \langle \gamma, \gamma' \rangle \mathcal{X}_\gamma \mathcal{X}_{\gamma'}. \quad (2.3)$$

- d) For any fixed  $(u, \theta) \in \mathcal{M}$ ,  $\mathcal{X}_\gamma(u, \theta; \zeta)$  is holomorphic in  $\zeta$ . Here  $\theta$  is an angular coordinate on the fiber of  $\mathcal{M} \rightarrow \mathcal{B}$  above  $u$ .
- e)  $\mathcal{X}_\gamma(\cdot; \zeta) = \overline{\mathcal{X}_{-\gamma}(\cdot; -1/\bar{\zeta})}$ .

Moreover, in [1] it turned out to be particularly interesting to consider coordinate systems subject to a further asymptotic condition, namely

- f)  $\lim_{\zeta \rightarrow 0} \mathcal{X}_\gamma(u, \theta; \zeta) \exp[-\zeta^{-1} \pi R Z_\gamma(u)]$  exists.

However, there is a Stokes phenomenon in play here: for the  $\mathcal{M}$  of interest, it turns out to be impossible to construct Darboux coordinates which obey the conditions a)-f). The right thing to do is to ask for all desired properties to hold for  $\zeta$  in some half-plane, centered on a ray  $e^{i\vartheta} \mathbb{R}_+$ ,<sup>13</sup>

$$\mathbb{H}_\vartheta := \left\{ \zeta : \vartheta - \frac{\pi}{2} < \arg \zeta < \vartheta + \frac{\pi}{2} \right\}, \quad (2.4)$$

and for a single  $u_0 \in U \subset \mathcal{B}$ . So we ask for a *collection* of coordinate systems  $\mathcal{X}_\gamma^{\vartheta, u_0}$ , each defined on  $\pi^{-1}(U) \times \mathbb{H}_\vartheta$ . Each one should obey a)-c), and

- d')  $\mathcal{X}_\gamma^{\vartheta, u_0}(u, \theta; \zeta)$  is holomorphic in  $\zeta$ , for  $\zeta \in \mathbb{H}_\vartheta$ .

<sup>12</sup>For later convenience we have rescaled the Poisson bracket by a factor  $4\pi^2 R$  relative to that in [1].

<sup>13</sup>We emphasize that in some situations  $\mathcal{X}_\gamma^\vartheta$  actually depends on  $\vartheta \in \mathbb{R}$ , not just  $\vartheta \in \mathbb{R}/2\pi\mathbb{Z}$ . We will encounter this situation in Sections 8, 9, and 11 below.



$$\text{e')} \quad \mathcal{X}_\gamma^{\vartheta, u_0}(\cdot; \zeta) = \overline{\mathcal{X}_{-\gamma}^{\vartheta+\pi, u_0}(\cdot; -1/\bar{\zeta})}.$$

$$\text{f')} \quad \lim_{\zeta \rightarrow 0} \mathcal{X}_\gamma^{\vartheta, u_0}(u_0, \theta; \zeta) \exp[-\zeta^{-1} \pi R Z_\gamma(u_0)] \text{ exists, when } \zeta \text{ is restricted to } \mathbb{H}_\vartheta.$$

In this paper we will give a construction of functions  $\mathcal{X}_\gamma^{\vartheta, u_0}$  obeying these conditions, for sufficiently large  $R$ . These  $\mathcal{X}_\gamma^{\vartheta, u_0}$  really do depend on  $(\vartheta, u_0)$ : there is a real-codimension-1 subset in the space of  $(\vartheta, u_0)$  where  $\mathcal{X}_\gamma^{\vartheta, u_0}$  jumps. From **b)**, **c)** it follows that these jumps are holomorphic Poisson morphisms.

These jumps in the coordinates  $\mathcal{X}_\gamma^{\vartheta, u_0}$  are the most important part of the whole story. In particular, the jumps are determined by, and determine, the BPS degeneracies of the  $d = 4$  field theory. If we think of  $u_0$  as fixed, then the jumps occur at specific values of  $\vartheta$ , namely those  $\vartheta$  which are the phases of central charges of BPS states in the vacuum labeled by  $u_0$ . Moreover the precise jumps are determined by the gauge charges of the BPS states. We state this more precisely as follows:

$$\text{g')} \quad \mathcal{X}_\gamma^{\vartheta, u_0} \text{ is piecewise constant as a function of } (\vartheta, u_0), \text{ with discontinuities at pairs } (\vartheta, u_0) \text{ for which there is some } \gamma_{\text{BPS}} \text{ with } \arg -Z_{\gamma_{\text{BPS}}}(u_0) = \vartheta \text{ and } \Omega(\gamma_{\text{BPS}}; u_0) \neq 0.$$

$$\text{h')} \quad \text{Fix } \vartheta_0 \in \mathbb{R}/2\pi\mathbb{Z}, u_0 \in \mathcal{B}, \text{ and define}$$

$$\mathbf{S}_{\vartheta_0, u_0} := \prod_{\gamma_{\text{BPS}}: \arg -Z_{\gamma_{\text{BPS}}}(u_0) = \vartheta_0} \mathcal{K}_{\gamma_{\text{BPS}}}^{\Omega(\gamma_{\text{BPS}}; u_0)}, \quad (2.5)$$

where  $\mathcal{K}_{\gamma_{\text{BPS}}}$  is a holomorphic Poisson transformation of the  $\mathcal{X}_\gamma$  given by

$$\mathcal{K}_{\gamma_{\text{BPS}}} : \mathcal{X}_\gamma \mapsto \mathcal{X}_\gamma (1 - \sigma(\gamma_{\text{BPS}}) \mathcal{X}_{\gamma_{\text{BPS}}})^{\langle \gamma, \gamma_{\text{BPS}} \rangle}. \quad (2.6)$$

Then<sup>14</sup>

$$\left( \lim_{\vartheta \rightarrow \vartheta_0^+} \mathcal{X}_\gamma^{\vartheta, u_0} \right) = \mathbf{S}_{\vartheta_0, u_0} \left( \lim_{\vartheta \rightarrow \vartheta_0^-} \mathcal{X}_\gamma^{\vartheta, u_0} \right). \quad (2.7)$$

(A genericity assumption is made here: The charges with  $\arg -Z_{\gamma_{\text{BPS}}}(u_0) = \vartheta_0$  are all proportional, so we needn't order the product in  $\mathbf{S}_{\vartheta_0, u_0}$ .)

A final important property is

$$\text{i')} \quad \text{When } \zeta \in \mathbb{H}_\vartheta, \text{ we have the large } R \text{ asymptotics}$$

$$\mathcal{X}_\gamma \sim \mathcal{X}_\gamma^{\text{sf}} \quad (2.8)$$

and in fact the corrections are exponentially small, i.e.  $\mathcal{X}_\gamma = \mathcal{X}_\gamma^{\text{sf}} (1 + \mathcal{O}(e^{-\text{const} \cdot R}))$  in regions bounded away from the singular points of  $\mathcal{B}$ .

In the rest of this paper we will sometimes lighten the notation, writing  $\mathcal{X}_\gamma^{\vartheta, u_0}$  just as  $\mathcal{X}_\gamma^\vartheta$  when we are not trying to emphasize the  $u_0$  dependence, or even just as  $\mathcal{X}_\gamma$ . (This  $\mathcal{X}_\gamma$  must *not* be confused with the  $\mathcal{X}_\gamma$  of [1]. Those functions are denoted by  $\mathcal{X}_\gamma^{\text{RH}}$  in this paper. See Section 2.4 below.)

---

<sup>14</sup>Our convention here differs by a sign from [1].

### 2.3 Wall-crossing

As we have just reviewed, at least for large enough  $R$ , the moduli space  $\mathcal{M}$  carries a family of local coordinate systems  $\mathcal{X}_\gamma^{\vartheta, u_0}$ , obeying the conditions a)-c), d’)-f’), g)-i).

The mere existence of these coordinates has a rather strong consequence. Consider a point  $u \in \mathcal{B}$  and two different phases  $\vartheta_\pm$ , with  $\vartheta_+ - \vartheta_- < \pi$ . The coordinate systems  $\mathcal{X}_\gamma^{\vartheta_\pm, u}$  are generally not equal; to see how they are related, one must apply (2.7) to each Stokes line which lies between  $\vartheta_-$  and  $\vartheta_+$ . This gives the relation as

$$\mathcal{X}_\gamma^{\vartheta_+, u} = \mathbf{S}(\vartheta_-, \vartheta_+; u) \mathcal{X}_\gamma^{\vartheta_-, u}, \quad (2.9)$$

where

$$\mathbf{S}(\vartheta_-, \vartheta_+; u) = \prod_{\gamma_{\text{BPS}}: \vartheta_- < \arg -Z_{\gamma_{\text{BPS}}}(u) < \vartheta_+} \mathcal{K}_{\gamma_{\text{BPS}}}^{\Omega(\gamma_{\text{BPS}}; u)}, \quad (2.10)$$

with the product taken in increasing order of  $\arg -Z_{\gamma_{\text{BPS}}}(u)$ .

A key algebraic fact [6] is that product decompositions of the form (2.10) are unique: (2.10) actually *determines* the  $\Omega(\gamma_{\text{BPS}}; u)$  for  $\arg -Z_{\gamma_{\text{BPS}}}(u)$  between  $\vartheta_-$  and  $\vartheta_+$  (with the exception of  $\gamma_{\text{BPS}} \in \Gamma_{\text{flavor}}$ , which have  $\mathcal{K}_{\gamma_{\text{BPS}}} = \mathbf{1}$  and hence are invisible in  $\mathbf{S}(\vartheta_-, \vartheta_+; u)$ .) One can thus think of  $\mathbf{S}(\vartheta_-, \vartheta_+; u)$  as a kind of “generating function” for the  $\Omega(\gamma_{\text{BPS}}; u)$ .

Now suppose we deform  $u$  continuously to  $u'$ . As long as no  $\arg Z_{\gamma_{\text{BPS}}}(u)$  crosses  $\vartheta_+$  or  $\vartheta_-$  in the process, it follows from g) that  $\mathcal{X}_\gamma^{\vartheta_\pm, u} = \mathcal{X}_\gamma^{\vartheta_\pm, u'}$ , and so

$$\mathbf{S}(\vartheta_-, \vartheta_+; u) = \mathbf{S}(\vartheta_-, \vartheta_+; u'). \quad (2.11)$$

The formula (2.11) determines the  $\Omega(\gamma_{\text{BPS}}; u')$  given  $\Omega(\gamma_{\text{BPS}}; u)$  and hence gives a complete solution to the wall-crossing problem. In our context, it is a direct consequence of the existence of the functions  $\mathcal{X}_\gamma^{\vartheta, u}$ .

Since the product (2.10) is generally infinite, we should perhaps comment on how it is to be understood. One begins by finding some basis  $\{\gamma_i\}$  of  $\hat{\Gamma}$ , such that all  $\gamma_{\text{BPS}}$  which contribute to  $\mathbf{S}(\vartheta_-, \vartheta_+; u)$  are *nonnegative* linear combinations of the  $\gamma_i$ . This basis depends on  $(\vartheta_-, \vartheta_+, u)$ .<sup>15</sup> Each  $\mathcal{K}_\gamma$  defines a Poisson automorphism of the algebra  $F := \mathbb{C}[[x_{\gamma_1}, \dots, x_{\gamma_i}]]$ . (Infinite Taylor series arise because we expand denominators,  $1/(1-x) = 1+x+\dots$ .) Now how about their product? To understand that, we begin by defining a collection of finite-dimensional unipotent groups  $G_N(\vartheta_-, \vartheta_+; u)$  ( $N \geq 0$ ). We first use the basis  $\gamma_i$  to define the degree of  $\gamma = \sum n_i \gamma_i$  to be  $|\gamma| := \sum_i n_i$  and informally “truncate  $F$  to Fourier modes of order less than or equal to  $N$ .” More precisely, there is a filtration of  $F$  by ideals  $I_N \subset F$ , generated by monomials with degree greater than  $N$ . Since  $\mathcal{K}_\gamma$  maps  $I_N$  to itself, the transformations with  $\vartheta_- < -\arg Z_\gamma(u) < \vartheta_+$  generate a group  $G_N(\vartheta_-, \vartheta_+; u)$  of Poisson automorphisms of  $F_N := F/I_N$ . Moreover, again because the  $\mathcal{K}_\gamma$  preserve the filtration there is a projection map  $G_N \rightarrow G_{N-1}$  and we can use these to define a group  $G(\vartheta_-, \vartheta_+; u)$  as the inverse limit of the system of the  $G_N(\vartheta_-, \vartheta_+; u)$ . When projected

<sup>15</sup>Actually, the existence of such a basis is not obvious. In the mathematical work of [6] an additional technical condition was imposed which guarantees it, and which one hopes would hold in all physical examples. In Section 7.8 of this paper we will show that such a basis exists in the examples we consider.

to any  $G_N(\vartheta_-, \vartheta_+; u)$ , the product (2.10) involves only finitely many nontrivial factors and hence is well defined. Moreover it behaves coherently with respect to the projections  $G_N \rightarrow G_{N-1}$ . This is sufficient to define it in  $G(\vartheta_-, \vartheta_+; u)$ .

Let us also comment a bit more on the uniqueness of the product decomposition which was claimed above. We have  $\mathcal{K}_\gamma = e^{f_\gamma}$  where  $f_\gamma := \sum_{n \geq 1} \frac{\sigma(n\gamma)}{n^2} \{\mathcal{X}_{n\gamma}, \cdot\}$ . The  $f_\gamma$  with  $\vartheta_- < -\arg Z_\gamma(u) < \vartheta_+$  span the Lie algebra of  $G(\vartheta_-, \vartheta_+; u)$ . For the unipotent groups  $G_N$  the exponential map is bijective. It follows that the decomposition of a group element  $g \in G(\vartheta_-, \vartheta_+; u)$  into a product of the form (2.10) is indeed unique. From a more practical viewpoint, there is an algorithm for extracting the  $\Omega(\gamma_{\text{BPS}}; u)$  from  $\mathbf{S}(\vartheta_-, \vartheta_+; u)$ , easily implemented on a computer for any reasonably small  $\gamma_{\text{BPS}}$ . It amounts to considering inductively the projections of  $\mathbf{S}(\vartheta_-, \vartheta_+; u)$  to the successive subgroups  $G_N(\vartheta_-, \vartheta_+; u)$ . At the  $N$ -th step one can determine the  $\Omega(\gamma_{\text{BPS}}; u)$  for  $|\gamma_{\text{BPS}}| \leq N$ .

The formula (2.11) was first presented in [6] in a very general context. It generalizes the primitive and semi-primitive wall-crossing formulae, first derived in [17] using Denef's multicentered BPS black hole solutions of  $\mathcal{N} = 2$  supergravity [18]. The arguments of [17] apply both to supergravity and to its field theory limit. Unfortunately, the constructions in [1] and in this paper are restricted to field theory. Thus, an important open problem remains: Give a physical derivation of (2.11) for type II string theory on a compact Calabi-Yau.

## 2.4 Riemann-Hilbert problem

In [1] we did not introduce the functions  $\mathcal{X}_\gamma^\vartheta$  explicitly. Instead we formulated a Riemann-Hilbert problem, the solution of which would lead to a *single* Darboux coordinate system  $\mathcal{X}_\gamma^{\text{RH}}(\zeta)$ , obeying a)-f) for all  $\zeta$ , *except* that  $\mathcal{X}_\gamma^{\text{RH}}(\zeta)$  is not holomorphic in  $\zeta$ , but only piecewise holomorphic; it jumps by  $\mathcal{K}_{\gamma_{\text{BPS}}}^{\Omega(\gamma_{\text{BPS}}; u)}$  along each ray  $\zeta \in Z_{\gamma_{\text{BPS}}} \mathbb{R}_-$ . We argued moreover that a solution indeed exists for sufficiently large  $R$ .

There is a simple correspondence between such  $\mathcal{X}_\gamma^{\text{RH}}(\zeta)$  and  $\mathcal{X}_\gamma^\vartheta(\zeta)$  obeying a)-c), d')-f'). Given  $\mathcal{X}_\gamma^{\text{RH}}(\zeta)$ ,  $\mathcal{X}_\gamma^\vartheta(\zeta)$  can be obtained as the analytic continuation of  $\mathcal{X}_\gamma^{\text{RH}}(\zeta)$  in  $\zeta$  from the ray  $\zeta \in e^{i\vartheta} \mathbb{R}_+$ . Conversely, given  $\mathcal{X}_\gamma^\vartheta(\zeta)$ , we divide the  $\zeta$ -plane into slivers bounded by BPS rays, and define  $\mathcal{X}_\gamma^{\text{RH}}(\zeta)$  to agree with  $\mathcal{X}_\gamma^\vartheta(\zeta)$  on the sliver containing the ray  $\zeta \in e^{i\vartheta} \mathbb{R}_+$ .

One might naturally guess that if we apply this procedure to the  $\mathcal{X}_\gamma^\vartheta(\zeta)$  built in this paper, the  $\mathcal{X}_\gamma^{\text{RH}}(\zeta)$  so obtained will give a solution to the Riemann-Hilbert problem defined in [1], for all  $R$ . However, we do not prove that in this paper. The crucial problem is the possibility that the  $\mathcal{X}_\gamma^{\text{RH}}(\zeta)$  we get could be only piecewise *meromorphic* away from  $\zeta = 0, \infty$ . This would be incompatible with the Riemann-Hilbert problem, in which  $\mathcal{X}_\gamma^{\text{RH}}(\zeta)$  were required to be piecewise *holomorphic*. At sufficiently large  $R$  this is not a problem: the poles of the individual  $\mathcal{X}_\gamma^\vartheta$  lie outside the sector  $\mathbb{H}_\vartheta$ , and do not appear in  $\mathcal{X}_\gamma^{\text{RH}}$ . The important question is whether as we go to small  $R$  these poles can move into the sliver around  $\zeta \in e^{i\vartheta} \mathbb{R}_+$ .

Although our results on wall-crossing and BPS degeneracies are independent of this question, it is relevant for the issue of describing the hyperkähler metric using the methods of [1]. We will discuss this matter at some length in Section 14.

### 3. From brane constructions to Hitchin systems

In this section we describe a class of  $d = 4$ ,  $\mathcal{N} = 2$  field theories for which the hyperkähler manifold  $\mathcal{M}$  is a moduli space of solutions to Hitchin's equations.

In Section 3.1 we discuss these theories in terms of the six-dimensional  $(2, 0)$  theory reduced on a Riemann surface  $C$ , with some number of real codimension-2 defects at points of  $C$ , and explain why their further compactification on a circle leads to Hitchin's equations. In Section 3.2 we give a purely four-dimensional definition of a large class of the theories we consider, by making contact with the D4/D6/NS5-brane constructions described in [2]. Finally, in Section 3.3 we briefly recall an alternative Type IIB string theory construction which would lead to the same theories, involving a Calabi-Yau threefold containing  $C$  as a curve of ADE singularities.

#### 3.1 Compactifying the $(2, 0)$ theory

Starting with the famous  $(2, 0)$  superconformal field theories in  $d = 6$  and compactifying on appropriate Riemann surfaces  $C$ , one can produce a very large class of  $d = 4$ ,  $\mathcal{N} = 2$  field theories. As we will describe in Sections 3.1.1-3.1.5 below, this construction also naturally realizes the Seiberg-Witten curves in these theories as branched covers of  $C$  inside  $T^*C$ , as well as giving a direct handle on the BPS spectrum, extending a picture described in [3].

Our main interest in this paper is in what happens when we further compactify these four-dimensional theories on a circle. That is, we consider the  $(2, 0)$  theory on  $\mathbb{R}^{1,2} \times S^1 \times C$ , where  $S^1$  has radius  $R$ . Then we find, at low energies, a three-dimensional sigma model with hyperkähler target space  $\mathcal{M}$ .

What is  $\mathcal{M}$ ? To answer that question, we describe the same theory in a different way, by reversing the order in which we compactify. If we first compactify the six-dimensional  $(2, 0)$  theory on  $S^1$ , the low energy physics is described by five-dimensional supersymmetric Yang-Mills theory. We can then consider further compactification of this five-dimensional theory on  $C$ . From this viewpoint, the moduli space of 3-dimensional super-Poincaré invariant vacua is the moduli space of solutions of certain BPS equations for the gauge fields and scalars on  $C$ . These BPS equations turn out to be the Hitchin equations on  $C$ . While these two compactifications correspond to different limits, we do not expect any phase transition in the low energy physics when we exchange the relative length scales of  $C$  and  $S^1$ . The reason is that the BPS-protected quantities that we study are insensitive to the conformal scale of the metric on  $C$ , thanks to the topological twist described below. Therefore, we can identify the target space  $\mathcal{M}$  of the three-dimensional sigma model as a moduli space of solutions to Hitchin's equations on  $C$ . We explain this in Section 3.1.6.

The analysis of  $\mathcal{M}$  which we carry out in the rest of this paper can be applied only if  $C$  carries some defect operators, inserted at points  $\mathcal{P}_i$ . We make some comments about these defects in Sections 3.1.7-3.1.8.

##### 3.1.1 The $(2, 0)$ theory on $\mathbb{R}^{1,5}$ and its Coulomb branch

We begin with the  $(2, 0)$  superconformal theories in six-dimensional spacetime [19, 5, 20, 21, 22, 23]. These theories enjoy  $osp(6, 2|4)$  superconformal invariance. Modulo topological

subtleties, they are obtained as products of two types of basic building block: interacting theories, which have an ADE classification, and free theories with an abelian “gauge group.” Our main interest in this paper will be in the theories in the A series. From the point of view of M-theory, the theory with “gauge group”  $U(K)$  can be described as a decoupling limit of a system of  $K$  coincident M5-branes [5]. We use this picture frequently as a convenient shortcut for understanding properties of the theory.

Let us briefly recall some information about the chiral operators of the  $(2, 0)$  theory; more detail can be found in [24], and see also [25], especially the table on page 31. There is a basis of operators transforming in short representations of  $osp(6, 2|4)$ , labeled by the Casimir operators of the ADE group  $\mathfrak{g}$ . Label the Casimirs by  $k = 1, \dots, r$ . Within the  $k$ -th short multiplet we will focus on the subspace  $V_k$  of operators with lowest conformal weight.  $V_k$  is an irreducible representation of the  $so(5)$  R-symmetry. Its conformal weight is twice the exponent  $d_k$  of  $\mathfrak{g}$ .

The theory has a “Coulomb branch” parameterized by vacuum expectation values of these chiral operators. This branch is especially easy to understand in the  $A_{K-1}$  theory: it is just  $(\mathbb{R}^5)^K/S_K$ , parameterizing configurations in which the  $K$  M5-branes are separated in the transverse  $\mathbb{R}^5$ .

On the Coulomb branch the theory contains BPS strings, geometrically described as the boundaries of M2-branes running between the separated M5-branes. See Figure 1. Call

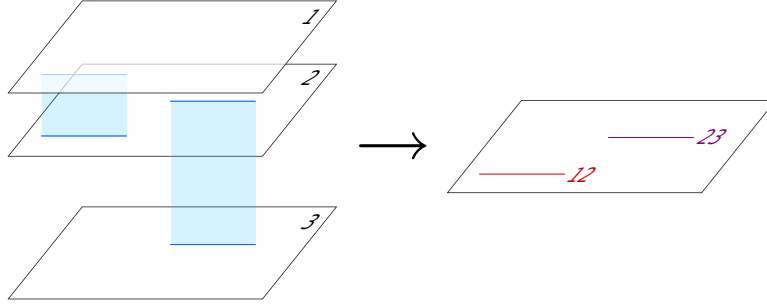


**Figure 1:** Left: three separated M5-branes, including segments of two M2-branes stretching between them. Right: the corresponding picture in the  $A_{K-1}$   $(2, 0)$  theory with  $K = 3$ . The two M2-brane segments have been projected down to string segments.

the string that comes from an M2-brane running between brane  $i$  and brane  $j$  an  $ij$ -string. These strings are oriented; reversal of orientation exchanges  $ij$ -strings with  $ji$ -strings. The BPS condition requires that the strings are straight lines in  $\mathbb{R}^{5,1}$ . The tension of a BPS  $ij$ -string can be calculated from the M2-brane picture as<sup>16</sup>

$$T_{ij} = \frac{2\pi}{\ell^3} |x_i - x_j| \quad (3.1)$$

where  $|x_i - x_j|$  is the distance in  $\mathbb{R}^5$  (with dimensions of length). From BPS non-renormalization theorems one expects that this geometric picture actually gives the exact tension, even in

<sup>16</sup>The tension of the M2-brane is  $2\pi/\ell^3$  and that of the electromagnetic dual M5-brane is  $2\pi/\ell^6$ , where  $\ell$  is the 11-dimensional Planck length.

the regime (most relevant for this paper) where the branes are separated by distances of order  $\ell$ .

One can have supersymmetric “junctions” where strings of type  $ij$ ,  $jk$ , and  $ki$  meet. The appearance of such junctions in the  $(2, 0)$  theory was noted in [26]. The supersymmetry preserved by a single  $ij$ -string depends both on the slope of the string in the worldvolume of the M5-branes, and on the direction of  $x_i - x_j$  in  $\mathbb{R}^5$ . To find the condition for a quarter-BPS junction, we can imitate the standard setup for  $(p, q)$  string junctions [27, 28, 29]: tie the relative slopes of the three strings in the plane of the junction to the relative slopes of the vectors  $(x_i - x_j)$ ,  $(x_j - x_k)$ ,  $(x_k - x_i)$  in the plane in  $\mathbb{R}^5$  defined by the three points  $x_i, x_j, x_k$ . Notice that this automatically gives mechanical equilibrium at the junction, as the tension vectors of the three string segments are then linearly related to  $(x_i - x_j)$ ,  $(x_j - x_k)$ ,  $(x_k - x_i)$ , and hence sum to zero.

### 3.1.2 The $(2, 0)$ theory on $\mathbb{R}^{1,3} \times C$ and its Coulomb branch

In order to compactify the  $(2, 0)$  theory on  $C$  without breaking four-dimensional supersymmetry, we need to consider a partial twisting. The super Poincaré subalgebra of  $osp(6, 2|4)$  has bosonic part  $so(5, 1) \oplus usp(4) \cong so(5, 1) \oplus so(5)$ . The spinor representations of  $Spin(1, 5)$  and  $Spin(5)$  are  $\mathbb{H}^2$ , where  $\mathbb{H}$  is the quaternions. Therefore the Poincaré supercharges transform in the  $(\mathbb{C}^4 \otimes \mathbb{C}^4)_+$  of  $so(5, 1) \oplus so(5)$ , where the subscript  $+$  indicates a symplectic Majorana reality constraint. Upon compactification on  $C$  we preserve the subalgebra  $so(3, 1) \oplus so(2)_C \oplus so(3) \oplus so(2)_R$ , under which the supercharges transform as

$$\left( \left( (2, 1)_{\frac{1}{2}} \oplus (1, 2)_{-\frac{1}{2}} \right) \otimes \left( 2_{\frac{1}{2}} \oplus 2_{-\frac{1}{2}} \right) \right)_+ \quad (3.2)$$

The twisting consists of identifying the diagonal  $so(2)$  of  $so(2)_C \oplus so(2)_R$  with the holonomy algebra of  $C$ , and leaves us with supercharges transforming under  $so(3, 1) \oplus so(3) \oplus so(2)'_C$  as

$$(2, 1; 2)_1 \oplus (2, 1; 2)_0 \oplus (1, 2; 2)_0 \oplus (1, 2; 2)_{-1} \quad (3.3)$$

We can introduce a corresponding basis of supercharges:

$$Q_z^{\alpha A}, Q^{\alpha A}, \bar{Q}^{\dot{\alpha} A}, \bar{Q}_{\bar{z}}^{\dot{\alpha} A} \quad (3.4)$$

where  $\alpha, \dot{\alpha}, A$  all run over  $1, 2$  and  $z$  is a local coordinate so that  $dz$  has  $so(2)'_C$  charge  $+1$ . Since the supercharges  $Q^{\alpha A}, \bar{Q}^{\dot{\alpha} A}$  of the middle two summands of (3.3) are uncharged under  $so(2)_C$  they are well-defined four dimensional supercharges, and therefore we have preserved  $\mathcal{N} = 2$  four-dimensional supersymmetry. The commutator  $\left\{ \bar{Q}^{\dot{\alpha} A}, \bar{Q}_{\bar{z}}^{\dot{\beta} B} \right\} \sim \epsilon^{\dot{\alpha} \dot{\beta}} \epsilon^{AB} \partial_{\bar{z}}$  will be quite useful below where we consider the chiral ring of the operators annihilated by  $\bar{Q}^{\dot{\alpha} A}$ .

The moduli space of the four-dimensional theory is obtained essentially by dimensional reduction from the Coulomb branch of the six-dimensional theory. More precisely, choose a Cartan subalgebra  $so(2)_R \oplus so(2)$  of the  $so(5)$   $R$ -symmetry, and let  $\mathcal{O}_k$  be the operator in  $V_k$  of weight  $(d_k, 0)$ . This operator has the largest  $so(2)_R$  charge in the multiplet and hence it must be annihilated by any supercharge, such as  $\bar{Q}^{\dot{\alpha} A}$ , with positive  $so(2)_R$  charge.

We reach the  $d = 4$  Coulomb branch by giving vacuum expectation values to these chiral operators.

After the twisting,  $\mathcal{O}_k$  is a section of the bundle  $K^{\otimes d_k}$  over  $C$ , and in particular this is true of its vacuum expectation value  $\langle \mathcal{O}_k \rangle$ . Since  $\mathcal{O}_k$  is annihilated by  $\bar{Q}^{\dot{\alpha}A}$ , and since  $\bar{Q}^{\dot{\alpha}A}$ -exact operators have vanishing vev's [30],  $\langle \mathcal{O}_k \rangle$  must be annihilated by  $\bar{\partial}$ . This is the only condition on  $\langle \mathcal{O}_k \rangle$ , so the  $d = 4$  Coulomb branch which parameterizes these vevs is simply

$$\mathcal{B} = \bigoplus_{k=1}^r H^0(C, K^{\otimes d_k}). \quad (3.5)$$

In the  $A_{K-1}$  case there is a nice geometric interpretation of  $\mathcal{B}$ . We are considering the low energy limit of a system of  $K$  M5-branes which are wrapped on a holomorphic cycle  $C$  inside a hyperkähler four-manifold  $Q$ . To go to the Coulomb branch we separate the branes so that they wrap some other cycle  $\Sigma$  inside  $Q$ .<sup>17</sup> Unlike the flat space situation, we will consider cases where the branes cannot be completely separated, so  $\Sigma$  will be a *connected* divisor inside  $Q$ . By choosing holomorphic Darboux coordinates  $(x, z)$  for  $Q$  as a holomorphic symplectic manifold we can identify a neighborhood of  $C$  with the holomorphic cotangent bundle  $T^*C$ . Picking a point of  $\mathcal{B}$  just corresponds to picking the coefficients  $u_k \in H^0(C, K^{\otimes k})$ ,  $k = 2, \dots, K$ , of the equation

$$x^K + \sum_{k=2}^K u_k(z) x^{K-k} = 0 \quad (3.6)$$

defining  $\Sigma \subset T^*C$ .

We normalize the coordinates so that the holomorphic symplectic form is

$$\Omega = \frac{\ell^3}{2\pi^2} dx \wedge dz. \quad (3.7)$$

The projection map  $T^*C \rightarrow C$  identifies  $\Sigma$  as a  $K$ -fold cover of  $C$ . The distance between the  $i$ -th and  $j$ -th sheets is a 1-form on  $C$ , which we call  $\lambda_{ij}$ .

We will see below that  $\Sigma$  should be identified with the Seiberg-Witten curve of the reduced theory. The canonical one-form

$$\lambda = x dz, \quad (3.8)$$

restricted to  $\Sigma$ , will be identified with the Seiberg-Witten differential.

### 3.1.3 BPS strings on the Coulomb branch

Our geometric picture of the Coulomb branch is a convenient way to read off the properties of the BPS strings. As in the flat space case, locally we have BPS  $ij$ -strings labeled by pairs of sheets, and BPS junctions where three such strings meet. The BPS tension of an  $ij$ -string is  $\frac{1}{\pi} |\lambda_{ij}|$ ; this tension depends on the point of  $C$ , unlike the flat space case. There

---

<sup>17</sup>One could also separate the branes in the 3 flat transverse directions; this corresponds to moving onto the  $d = 4$  Higgs branch, which will not play a role in this paper.



are also some special points on  $C$ , namely the  $ij$ -branch points where  $\lambda_{ij} = 0$ , i.e. the  $i$ -th and  $j$ -th sheets of  $\Sigma$  come together. An  $ij$ -string can end at an  $ij$ -branch point. One quick way of deriving this fact is to recall the description of these states in the M5-brane picture: the  $ij$ -string is an M2-brane foliated by segments connecting sheet  $i$  and sheet  $j$ , and can end smoothly when these segments shrink to zero size. See Figure 2.

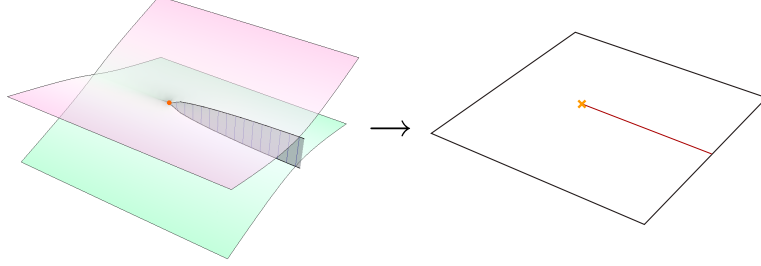


**Figure 2:** Left: a portion of an M2-brane stretching between two sheets of an M5-brane. The M2-brane is foliated by “vertical” segments, each of which lies in a single fiber of  $T^*C$ . At the branch point where the two sheets collide, the vertical segments shrink to zero length. Right: the projection of the M2-brane onto  $C$  is a string in the  $(2, 0)$  theory which ends on the branch point.

The central charge of a segment of  $ij$ -string extended along the curve  $c$  is given by

$$Z = \frac{1}{\pi} \int_c \lambda_{ij}. \quad (3.9)$$

The mass of the same segment on the other hand is just the integral of the tension,

$$M = \frac{1}{\pi} \int_c |\lambda_{ij}|. \quad (3.10)$$

So the BPS bound  $M \geq |Z|$  is saturated if and only if  $\lambda_{ij}$  has the same phase  $\vartheta$  everywhere along the curve  $c$ , i.e., if  $\partial_t$  denotes the tangent vector to  $c$ , we require

$$\lambda_{ij} \cdot \partial_t \in e^{i\vartheta} \mathbb{R}_+. \quad (3.11)$$

In this case  $Z = e^{i\vartheta} M$ .

For a multi-string junction the phase  $\vartheta$  must be the same for all strands. This condition is equivalent to the no-force condition at the junction: indeed, the vector representing the force exerted by the  $ij$ -strand on the junction can be expressed as the complex number  $e^{i\vartheta} \bar{\lambda}_{ij}$ , so since the three  $\lambda_{ij}$  sum to zero, the forces do as well.

The simplest BPS object is an  $ij$ -string stretched between two  $ij$ -branch points. In the M5-brane picture it would be represented by a disc; see Figure 3. Such an M2-brane has no moduli. Its quantization yields a single BPS hypermultiplet in four dimensions.

Similarly we can consider an  $ij$ -string stretched along a closed loop  $c$  in  $C$ . In the M5-brane picture such a string is represented by a cylindrical M2-brane; see Figure 4. Such an M2-brane has a single bosonic modulus and corresponding fermion zero mode. Its quantization yields a BPS vectormultiplet.

If  $K = 2$  these cases exhaust the possibilities; this description of the states was used in [3, 31] to study the BPS spectrum. For  $K > 2$  one should also consider string webs.



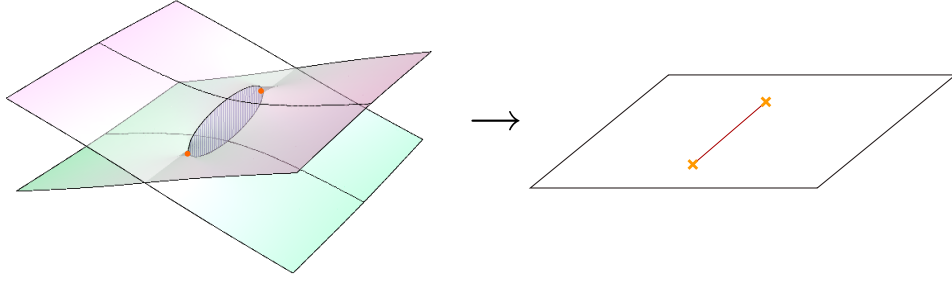


**Figure 3:** Left: An M2-brane wrapped on a disc  $D$ , stretched between two sheets of the curve  $\Sigma$  supporting the M5-brane. Right: Under the projection  $T^*C \rightarrow C$ , the disc projects to a string in the  $(2, 0)$  theory, which ends on the branch points.

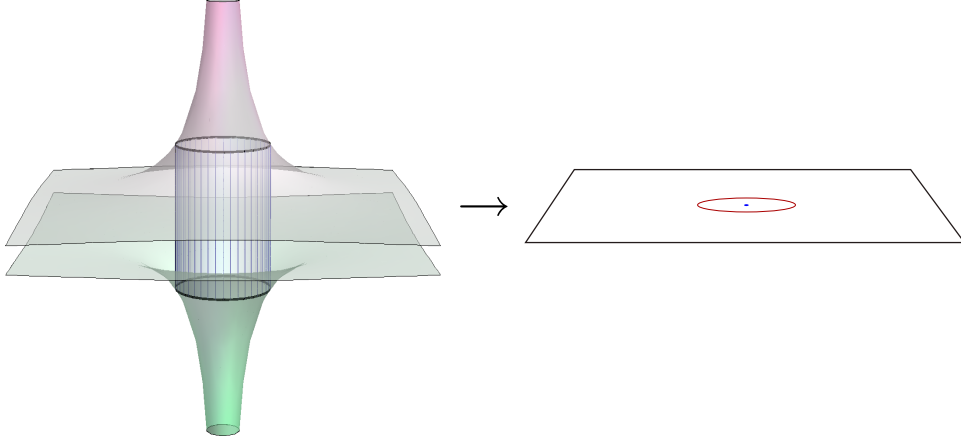


**Figure 4:** Left: An M2-brane wrapped on a cylinder, stretched between two sheets of the curve  $\Sigma$  supporting the M5-brane. Right: Under the projection  $T^*C \rightarrow C$ , the disc projects to a closed string in the  $(2, 0)$  theory.

Again lifting each strand  $c$  to  $c_i - c_j$ , the sum of all the lifts yields a closed cycle in  $\Sigma$  which gives the charge of the BPS particle. The number of bosonic moduli is equal to the number  $\ell$  of loops in  $c$ . Indeed,  $\ell = 1 + (j - b)/2$ , where  $b$  is the number of branch endpoints and  $j$  the number of three-string junctions. Each strand can be moved perpendicular to itself, except that each strand attached to a branch point loses this degree of freedom, and furthermore each junction has only two degrees of freedom and hence imposes one further constraint on the three strands ending on it. The number of strands is  $(b + 3j)/2$ , so this naive count of the bosonic moduli gives  $(j - b)/2$ . With a bit of work it is possible to see that one overall combination of the constraints at the junctions is trivial, thus giving one extra modulus, for a total of  $\ell$  (see [28], equation 23). By supersymmetry we should have  $\ell$  fermionic moduli as well. Taking into account these fermionic moduli we expect that quantization should give a multiplet of spin  $\frac{1}{2}(\ell + 1)$ .<sup>18</sup>

Finally let us consider the central charges of these BPS states. The oriented curve  $c$  on  $C$  representing a BPS  $ij$ -string can be lifted to a pair of curves  $c_i, c_j$  on  $\Sigma$ , namely, we

<sup>18</sup>As the moduli space has boundaries, depending on the precise boundary conditions multiplets of lower spin might possibly arise.

take the preimages of  $c$  on the  $i$ -th and  $j$ -th sheets, where  $c_i$  has the same orientation as  $c$  and  $c_j$  has the opposite orientation. Then (3.9) can be rewritten as

$$Z = \frac{1}{\pi} \int_c \lambda_{ij} = \frac{1}{\pi} \left( \int_{c_i} \lambda - \int_{c_j} \lambda \right). \quad (3.12)$$

For any combination of  $ij$ -strings representing a BPS state, the sum of the lifted curves is a closed cycle  $\gamma$  on  $\Sigma$ ; it is simply the boundary of the M2-brane representing the BPS state. What we have found is

$$Z = \frac{1}{\pi} \oint_{\gamma} \lambda. \quad (3.13)$$

This formula will be crucial in what follows.

Incidentally, one can also understand (3.13) as a consequence of Stokes's theorem and the fact that the BPS condition requires that the M2-brane is special Lagrangian in  $Q$ , i.e., when restricted to the M2-brane the holomorphic symplectic form  $\Omega = \frac{\ell^3}{2\pi^2} d\lambda$  is  $e^{i\vartheta}$  times the volume form. In the field theory limit, we are considering M5-branes which lie close to the zero section  $C$  in  $T^*C \subset Q$ ; in this limit the special Lagrangian M2-branes become “vertical” and reduce to the string webs (see [32] for related discussion).

### 3.1.4 Charge lattices

This is a convenient moment to pause and consider the lattice  $\hat{\Gamma}$  of all charges (flavor and gauge) in the  $d = 4$  theory. We said above that the charge of a BPS state is determined by a 1-cycle  $\gamma$  in  $\Sigma$ , the boundary of an M2-brane ending on the M5-brane. So naively one might identify the charge lattice as  $H_1(\Sigma; \mathbb{Z})$ . This is slightly wrong, for two reasons.

First, not all classes in  $H_1(\Sigma; \mathbb{Z})$  can support a BPS state. This is easiest to see in the case  $K = 2$ ; since all BPS states come from membranes which connect the two sheets, they are invariant under the operation of exchanging the two sheets and also reversing the orientation. It follows that all BPS charges lie in the sublattice of  $H_1(\Sigma; \mathbb{Z})$  which is invariant under this combined operation.

Second, some classes in  $H_1(\Sigma; \mathbb{Z})$  should be regarded as physically equivalent, because it costs zero energy to move from one to the other. This can happen for  $K > 2$  when there is some unbroken nonabelian gauge symmetry at a defect inserted somewhere on  $C$ ; then several sheets of the covering become identified near the defect, and in particular, a loop around the defect can move freely between these sheets. So to get the physical charge lattice we have to take a quotient. Assuming there are no accidental degeneracies one can describe this quotient operationally as dividing out by the kernel of  $Z$ , i.e. we identify cycles  $\gamma$  which have the same period  $Z_\gamma$ . So altogether  $\hat{\Gamma}$  is a subquotient (a quotient of a sublattice) of  $H_1(\Sigma; \mathbb{Z})$ .

The lattice  $\Gamma$  of gauge charges is simpler to describe: it is just  $H_1(\bar{\Sigma}, \mathbb{Z})$ , where  $\bar{\Sigma}$  is the compact Riemann surface obtained by filling in the punctures of  $\Sigma$ . The flavor lattice  $\Gamma_{\text{flavor}} \subset \hat{\Gamma}$  is the radical of the intersection pairing  $\langle, \rangle$  on  $H_1(\Sigma; \mathbb{Z})$ . Any element in  $\Gamma_{\text{flavor}}$  can be represented by a linear combination of small loops around the punctures.  $\hat{\Gamma}$  is an extension of  $\Gamma$  by  $\Gamma_{\text{flavor}}$ ,

$$0 \rightarrow \Gamma_{\text{flavor}} \rightarrow \hat{\Gamma} \rightarrow \Gamma \rightarrow 0. \quad (3.14)$$

As we move in the Coulomb branch  $\mathcal{B}$  the curve  $\Sigma$  varies, and in particular  $H_1(\Sigma; \mathbb{Z})$  might have monodromy around loci where  $\Sigma$  degenerates. Hence  $\hat{\Gamma}$  and  $\Gamma$  are not fixed lattices, but rather local systems of lattices varying over  $\mathcal{B}$ . In contrast  $\Gamma_{\text{flavor}}$  is monodromy invariant.

### 3.1.5 Kinetic terms

For completeness, let us discuss in a bit more detail the four-dimensional Lagrangian obtained by compactifying the  $(2, 0)$  theory on  $C$ , and verify that  $\Sigma$  is indeed the Seiberg-Witten curve and  $\lambda$  is the Seiberg-Witten differential.

We begin by calculating the kinetic terms of the vectormultiplet scalars in the IR 4d gauge theory, starting from the M5-brane picture of the Coulomb branch. The scalar part of the action of the M5-brane is just the DBI action,  $2\pi/\ell^6$  times the volume form. A vacuum of the four-dimensional theory is determined by some fixed holomorphic curve  $\Sigma_0 \subset Q$ . We consider configurations of the M5-brane which approach  $\mathbb{R}^{3,1} \times \Sigma_0$  near infinity in  $\mathbb{R}^{3,1}$ , but may fluctuate in the interior of  $\mathbb{R}^{3,1}$ . Such fluctuations (at least sufficiently mild ones, which are all we need here) are given by maps

$$f : \mathbb{R}^{3,1} \times \Sigma_0 \rightarrow Q \quad (3.15)$$

Let  $y \in \mathbb{R}^{3,1}$  and define  $f_y := f(y, \cdot) : \Sigma_0 \rightarrow Q$ . We require that as  $y \rightarrow \infty$ ,  $f_y$  approaches the identity map.

In the low energy limit, we restrict attention to maps which have zero potential energy, i.e. we require that  $\Sigma_y := f_y(\Sigma_0)$  is a volume-minimizing cycle for all  $y$ . Equivalently, we require that  $\Sigma_y$  is holomorphic in  $Q$  for all  $y$ . We can then define  $\hat{f} : y \rightarrow \Sigma_y$  as a map into the space  $\mathcal{D}$  of all holomorphic deformations of  $\Sigma$ ,

$$\hat{f} : \mathbb{R}^{3,1} \rightarrow \mathcal{D}. \quad (3.16)$$

Now we want to evaluate the kinetic energy of such a map. We work in the approximation where  $\hat{f}$  is *slowly varying* over  $\mathbb{R}^{3,1}$ , so that we may truncate to second order in the variations  $\partial_\mu \hat{f}$ . These variations are elements of the tangent space to  $\hat{f}(y) \in \mathcal{D}$ , which in turn may be identified with the space of holomorphic sections of the normal bundle  $T_{\hat{f}(y)}(\mathcal{D}) \cong H^0(N(\Sigma_y))$ . The expansion of the DBI action to quadratic order in derivatives (with the constant part subtracted) is

$$S = \frac{\pi}{\ell^6} \int_{\mathbb{R}^{1,3}} d^4x \eta^{\mu\nu} \langle \partial_\mu \hat{f}, \partial_\nu \hat{f} \rangle, \quad (3.17)$$

where  $\langle, \rangle$  is the standard Hermitian metric on the space of sections of  $N(\Sigma_y)$ , induced from the metric on  $Q$ . We are interested in fluctuations for which  $S$  is finite; to arrange this we require that  $\partial_\mu \hat{f}$  is *normalizable* for each  $\mu$ ,

$$\|\partial_\mu \hat{f}\|^2 < \infty. \quad (3.18)$$

The normalizable modes span a subspace of  $T\mathcal{D}$  and define an integrable distribution on  $\mathcal{D}$ . We let  $\mathcal{B}$  be the leaf of the distribution passing through  $\Sigma_0$ . We call  $\mathcal{B}$  the space of

“normalizable deformations” of  $\Sigma_0$ . So we are restricting attention to maps

$$\hat{f} : \mathbb{R}^{3,1} \rightarrow \mathcal{B}. \quad (3.19)$$

Let  $r$  denote the number of normalizable modes, i.e. the complex dimension of  $\mathcal{B}$ .

So far we have found that the scalar sector of our four-dimensional theory is a sigma model into  $\mathcal{B}$ . The six-dimensional tensor multiplet also contains an abelian 2-form gauge potential with self-dual field strength, and Kaluza-Klein reduction of this field leads to abelian four-dimensional gauge fields. The number of independent gauge fields is equal to  $\frac{1}{2}$  the dimension of the space of normalizable harmonic 1-forms on  $\Sigma$ , or equivalently to the dimension of the space of normalizable holomorphic 1-forms on  $\Sigma$ . In fact this is also equal to  $r$ . To see this, let us briefly consider the metric on  $Q$  in the vicinity of  $\Sigma$ . Let  $z$  be a local coordinate on  $\Sigma$ . Then we can choose a transverse coordinate  $x'$  such that  $\Sigma$  is the locus  $x' = 0$  and  $\Omega = \frac{\ell^3}{2\pi^2} dx' \wedge dz$ , and the Kähler form is of the form

$$\omega|_{\Sigma} = ig(z, \bar{z}) dz \wedge d\bar{z} + i \frac{\ell^6}{4\pi^4} g^{-1}(z, \bar{z}) Dx' \wedge D\bar{x}', \quad (3.20)$$

where  $D$  is the covariant derivative in  $N(\Sigma)$ . Now, by the adjunction formula there is an isomorphism  $N(\Sigma) \cong T^{*1,0}\Sigma$  most conveniently described by contraction with  $\Omega$ . Moreover, there are hermitian products on  $H^0(N(\Sigma))$  and  $H^0(T^{*1,0}\Sigma)$  defined by

$$\langle v_1 \frac{\partial}{\partial x'}, v_2 \frac{\partial}{\partial x'} \rangle := \int_{\Sigma} \left( v_1 \bar{v}_2 \frac{\ell^6}{4\pi^4} g^{-1}(z, \bar{z}) \right) g(z, \bar{z}) \frac{i}{2} dz d\bar{z} \quad (3.21)$$

and

$$\langle \omega_1, \omega_2 \rangle := \frac{i}{2} \int_{\Sigma} \omega_1 \bar{\omega}_2 \quad (3.22)$$

respectively. With these inner products the contraction with  $\Omega$  is an isometry:

$$\|v \partial_{x'}\|^2 = \frac{i}{2} \int_{\Sigma} (g(z, \bar{z}) dz \wedge d\bar{z}) \frac{\ell^6}{4\pi^4} g^{-1}(z, \bar{z}) |v|^2 = \frac{i}{2} \frac{\ell^6}{4\pi^4} \int_{\Sigma} |v dz|^2 = \frac{\ell^6}{4\pi^4} \|v dz\|^2. \quad (3.23)$$

So in particular,  $v dz$  is normalizable if and only if  $v \partial_{x'}$  is.

Altogether we have obtained an abelian  $\mathcal{N} = 2$  supersymmetric gauge theory in four dimensions with  $r$  vectormultiplets. (Recall that the abelian vectormultiplet contains one complex scalar and one vector field.)

We have not yet described this  $\mathcal{N} = 2$  theory in the standard way. For this, suppose that  $\Sigma$  lies close to  $C$ , and identify a neighborhood of  $C$  with  $T^*C$  as we did above. Now to obtain a good basis for the space of normalizable holomorphic 1-forms, it is convenient to remember that these are precisely the ones which extend holomorphically over  $\bar{\Sigma}$ . So choose a basis of  $A$  and  $B$  cycles  $\{A^I, B_I\}$  on  $\bar{\Sigma}$ ,  $I = 1, \dots, r$ , and let  $\{\alpha_I\}$  denote the normalizable holomorphic 1-forms dual to the  $A$  cycles,

$$\oint_{A^I} \alpha_J = \delta_J^I. \quad (3.24)$$

Then we may also define the period matrix of  $\bar{\Sigma}$  as usual by

$$\tau_{IJ} := \oint_{B_I} \alpha_J. \quad (3.25)$$

The metric on normalizable holomorphic 1-forms on  $\Sigma$  is the the same as that on holomorphic 1-forms on  $\bar{\Sigma}$ :

$$\langle \alpha_I, \alpha_J \rangle = (\text{Im } \tau)_{IJ}. \quad (3.26)$$

Further define

$$a^I := \frac{1}{\pi} \oint_{A^I} \lambda. \quad (3.27)$$

The  $a^I$  give local coordinates on  $\mathcal{B}$ . We want to describe the scalar action (3.17) in these coordinates. To do this we need to understand the isometry of  $T\mathcal{B}$  with  $H^0(N(\Sigma))_{\text{normalizable}}$  more explicitly. We claim that if  $v_J dz = \pi \alpha_J$  then  $\frac{\partial}{\partial a^J} \rightarrow v_J \frac{\partial}{\partial x^J}$ . To see this note that the action of  $v \frac{\partial}{\partial x}$  shifts the surface so that

$$\pi \left( v \frac{\partial}{\partial x^J} \right) a^I = \int_{A^{I'}} \lambda - \int_{A^I} \lambda = \int_{W^I} d\lambda = \int_{A^I} \iota(v \frac{\partial}{\partial x^J}) d\lambda = \int_{A^I} v dz \quad (3.28)$$

where  $W^I$  is an infinitesimal bit of surface given by pushing  $A^I$  along the vector field  $v \frac{\partial}{\partial x^J}$ .

Now, combining with the isometry (3.23) we have

$$\partial_\mu \hat{f} \cong \partial_\mu a^I \frac{\partial}{\partial a^I} \rightarrow \partial_\mu a^I \frac{\ell^3}{2\pi} \alpha_I \quad (3.29)$$

and therefore

$$S = \frac{1}{4\pi} \int_{\mathbb{R}^{1,3}} d^4x \eta^{\mu\nu} (\text{Im } \tau)_{IJ} \partial_\mu a^I \partial_\nu \bar{a}^J. \quad (3.30)$$

This is the standard form for the kinetic term in an abelian  $\mathcal{N} = 2$  theory, where we *identify*  $\Sigma$  with the Seiberg-Witten curve, and  $\lambda$  with the Seiberg-Witten differential.

### 3.1.6 Compactifying the (2,0) theory on $C \times S^1$ : Hitchin's equations

Now we are ready to consider the theory obtained by further dimensional reduction from  $d = 4$  to  $d = 3$  on  $S^1$ .

As we have mentioned, our approach to understanding this theory is to go back to six dimensions and consider compactifying *first* on  $S^1$  and *then* on  $C$ . So we begin by compactifying the (2,0) theory on  $S^1$  of radius  $R$ . This yields a theory which at low energies is five-dimensional supersymmetric Yang-Mills theory. We are interested in this five-dimensional theory further compactified on  $C$ , with an appropriate topological twist.

The moduli space  $\mathcal{M}$  of the resulting three-dimensional theory is just the space of BPS configurations of the five-dimensional theory, which are moreover Poincare invariant in  $\mathbb{R}^3$ . What are these configurations? Denote the adjoint scalars of the super Yang-Mills theory by  $Y^I$ ,  $I = 1, \dots, 5$ , so that

$$\varphi := \frac{1}{2}(Y^1 + iY^2) \quad (3.31)$$

has  $so(2)_R$  charge  $+1$ , and  $Y^{3,4,5}$  have charge zero. In the twisted theory,  $\varphi = \varphi_z dz$  is a  $(1,0)$  form on  $C$ . Then the BPS equations are simply the Hitchin equations for the gauge field  $A = A_z dz + A_{\bar{z}} d\bar{z}$  cotangent to  $C$  and the adjoint scalar  $\varphi$ :<sup>19</sup>

$$F + R^2[\varphi, \bar{\varphi}] = 0, \quad (3.32)$$

$$\bar{\partial}_A \varphi := d\bar{z}(\partial_{\bar{z}} \varphi + [A_{\bar{z}}, \varphi]) = 0, \quad (3.33)$$

$$\partial_A \bar{\varphi} := dz(\partial_z \bar{\varphi} + [A_z, \bar{\varphi}]) = 0. \quad (3.34)$$

We briefly digress to explain the origin of the slightly unconventional factor  $R^2$  appearing in (3.32). First note that after reducing the  $(2,0)$  theory on a circle of radius  $R$  one gets the five-dimensional SYM action in the form<sup>20</sup>

$$S = \frac{R}{8\pi^2} \int_{\mathbb{R}^{1,2} \times C} \text{Tr} \left( \frac{1}{R^2} F \wedge \star F + DY^I \wedge \star DY^I + \dots \right) \quad (3.35)$$

We could rescale  $Y^I = R^{-1} \hat{Y}^I$  to reach the standard normalization:

$$S = \frac{1}{8\pi^2 R} \int_{\mathbb{R}^{1,2} \times C} \text{Tr} \left( F \wedge \star F + D\hat{Y}^I \wedge \star D\hat{Y}^I + \dots \right) \quad (3.36)$$

It is in this frame that the BPS equations take the  $R$ -independent form  $F + [\hat{\varphi}, \bar{\hat{\varphi}}] dz d\bar{z} = 0$ . This accounts for the factor of  $R^2$  in (3.32). Our reason for preferring  $\varphi$  over the rescaled  $\hat{\varphi}$  is that the boundary conditions on the Higgs fields at the singular points are  $R$ -independent when expressed in terms of  $\varphi$ , as we will see later.

So we have found that the moduli space  $\mathcal{M}$  of the  $d = 3$  theory is the space of solutions of the Hitchin equations on  $C$ . In [34, 35, 36, 37] dualities were used to argue that the moduli space of  $SU(K)$   $d = 4$ ,  $\mathcal{N} = 2$  supersymmetric field theory compactified on a circle should be identified with a specific Hitchin system. The present section generalizes their result.<sup>21</sup> The general relation between M5-branes and Hitchin systems was already sketched by Witten in Section 2.3 of [2].

It has been observed that the Seiberg-Witten solutions of many  $\mathcal{N} = 2$  theories can be understood in terms of known complex integrable systems, as discussed e.g. in [38, 39, 40, 41]. Here we have constructed a large general class of theories for which the relevant complex integrable system is a Hitchin system.

---

<sup>19</sup>One efficient proof that the BPS equations are the Hitchin equations goes as follows. We are studying a stack of M5-branes on  $S^1 \times C \times \mathbb{R}^3$ , or equivalently a stack of D4-branes on  $C \times \mathbb{R}^3$ , and looking for BPS configurations invariant under translations along  $\mathbb{R}^3$ . It is well known that the BPS configurations on a stack of D4-branes which are invariant under translations in one direction are given by solutions of the self-dual Yang-Mills equations. The self-dual Yang-Mills equations, when evaluated on configurations which are invariant under translations in two directions, become Hitchin's equations [33].

<sup>20</sup>From the relation (3.31) between  $\varphi$  and  $Y$ , and the relation (3.13) between  $Z$  and  $\varphi$ , it follows that when  $Y^I = y^I \sigma^3$ , an open membrane stretched between the two M5-branes produces a string of tension  $\frac{1}{2\pi} y^I$ . Since the tension of the membrane is  $2\pi/\ell^3$ , it follows that the physical distance in the transverse dimension to the brane is  $\frac{\ell^3}{4\pi^2} y^I$ . A nice check on the relative normalization of the two terms in (3.35) is obtained by computing the mass of a W boson, i.e. a string running between two displaced D4-branes, which comes out to be  $R y^I$ . The overall normalization can be obtained by reducing the 6-dimensional DBI action.

<sup>21</sup>We thank Edward Witten for suggesting that the general Hitchin system could be realized in this way.

Let us say a few more words about the general structure of  $\mathcal{M}$ . On general field theory grounds [42] we expect  $\mathcal{M}$  to be hyperkähler and moreover to be a fibration over the Coulomb branch  $\mathcal{B}$  of the  $d = 4$  theory, with generic fiber a compact torus. This torus fiber is moreover expected to be a complex submanifold with respect to one “distinguished” complex structure on  $\mathcal{M}$ . How do we see this structure in our case?

The projection from  $\mathcal{M}$  to  $\mathcal{B}$  is easy to describe:  $\mathcal{B}$  is parameterized by the vacuum expectation values  $\langle \mathcal{O}_k \rangle$ , which in the five-dimensional Yang-Mills theory are identified with the independent Casimirs of  $\varphi$ , so the projection is just

$$(A, \varphi) \mapsto \{\text{Casimirs of } \varphi\}. \quad (3.37)$$

This map is well known in the mathematics literature as the “Hitchin fibration” [33]. Its fiber over a generic  $u \in \mathcal{B}$  is indeed an abelian variety, the Prym variety of the projection  $\bar{\Sigma}_u \rightarrow C$ , defined as the kernel of a corresponding map of Jacobians  $J(\bar{\Sigma}_u) \rightarrow J(C)$ . In the important special case  $C = \mathbb{CP}^1$ , where  $J(C)$  is trivial, this is simply  $J(\bar{\Sigma}_u)$ .

In the case of the  $A_{K-1}$  theory, as we noted earlier, the  $\langle \mathcal{O}_k \rangle$  determine the Seiberg-Witten curve  $\Sigma \subset T^*C$ . Since we have identified these with the Casimirs  $\text{Tr } \varphi^k$ ,  $\Sigma$  given by (3.6) is nothing but the *spectral curve* determined by  $\varphi$ ,

$$\det(x dz - \varphi) = 0. \quad (3.38)$$

In other words, the positions  $x_i$  ( $i = 1, \dots, K$ ) of the various sheets of  $\Sigma$  in the cotangent directions can be interpreted as the various *eigenvalues* of the matrix-valued 1-form field  $\varphi$ . (Thus the coefficients  $u_k(z)$  in (3.6) are elementary symmetric functions of the eigenvalues, and can be written as polynomials in the  $\langle \mathcal{O}_k \rangle$ .)

### 3.1.7 Defects and geometric Langlands

So far we have been a bit vague about exactly what  $C$  should be, and exactly what boundary conditions we should put on the fields. *A priori* one might think that the simplest possibility is just to choose  $C$  a compact Riemann surface, and require the fields to be regular everywhere. As it turns out, the BPS spectra of the resulting  $\mathcal{N} = 2$  theories are difficult to analyze using the methods of this paper. However, there is a simple modification which simplifies the story: we let  $C$  be a compact Riemann surface with *defects* inserted at finitely many points. In order to get some idea about what kind of defects should be allowed, we now take a brief detour from three dimensions down to two.

If we further compactify our three-dimensional sigma model on a circle  $\tilde{S}^1$  we obtain a two-dimensional  $\mathcal{N} = (4, 4)$  nonlinear sigma model, with the same target space  $\mathcal{M}$ . This further compactification makes contact with the work of Witten et al on the geometric Langlands program [14, 43, 44].

Indeed, altogether we have compactified the  $(2, 0)$  theory first on  $C$  and then on  $S^1 \times \tilde{S}^1$ . Suppose we do this in the opposite order. Reducing the ADE  $(2, 0)$  theory on  $S^1 \times \tilde{S}^1$  gives an ADE gauge theory with four-dimensional  $\mathcal{N} = 4$  supersymmetry. As noted in [45, 46], reduction of the  $\mathcal{N} = 4$  theory on the Riemann surface  $C$  leads to a sigma model into  $\mathcal{M}$ . This theory was the starting point for [14, 43, 44].

In the mathematics literature on the geometric Langlands program there is a well-studied class of defects (or “ramifications”) one can introduce on  $C$ . These defects are defined by specifying certain singularities for the solutions of the Hitchin equations. Physically, they can be interpreted as coming from surface operators in the four-dimensional super Yang-Mills theory. Such operators have been investigated in [43]. Within field theory they can be defined either by prescribing specific singular behavior for the fields in the path integral, or by coupling a certain two-dimensional sigma model to the four-dimensional gauge theory. Alternatively, some elementary defect operators can be defined by taking the field theory limit of intersecting-brane configurations: we intersect the stack of D3-branes which gives rise to the four-dimensional gauge theory with some extra D3-branes along a codimension-two locus.

Ultimately, these surface operators in the four-dimensional gauge theory should arise from codimension-two defects in the  $(2, 0)$  theory. However, the methods we use for defining the defect in four dimensions do not apply in six: we do not have a path integral definition of the six-dimensional  $(2, 0)$  theory, and we also do not know how to couple it to a four-dimensional theory living on a codimension-two locus. Instead we characterize the defects mainly through the singularities which they induce in the protected operators of the theory. This will be adequate for us in this paper as we concern ourselves mostly with the Hitchin system associated with the  $\mathcal{N} = 2$  field theory, and this depends only on the singularities in the protected operators.

We will assume that all the defects used in [43, 47] to produce Hitchin systems with ramification descend from defects in the six-dimensional  $(2, 0)$  theory. We can provide some partial evidence for this assumption, as follows. In Section 3.1.8 we will describe some simple defects as the field theory limit of certain M5-brane intersections. Similar defects, which induce the same type of singularities in the protected operators, appear as boundary conditions “at infinity” on a non-compact  $C$ . Given these simple defects, arbitrarily complicated ramification in the Hitchin system can be produced from their collision, and by other limiting procedures, which appear to have a simple physical meaning in the four-dimensional  $\mathcal{N} = 2$  field theory. We will consider several examples in the text.

Although it is hard to give a precise six-dimensional definition of the defect operators, it should be possible, upon compactification on  $S^1$ , to give at least a five-dimensional one. Indeed, in the infrared the five-dimensional gauge coupling goes to zero, and one should be left with some  $\mathcal{N} = 4$  three-dimensional SCFTs living at the defect, weakly coupled to the five-dimensional gauge theory. It would be interesting to identify them.

### 3.1.8 Boundary conditions from fivebrane intersections

Let us now briefly discuss one specific kind of defect which is relatively straightforward to understand. (We will encounter some more complicated defects in Section 3.2 below.)

We consider again the special case of the  $A_{K-1}$  theory, which we realized in terms of  $K$  M5-branes wrapped on  $C$ . Now consider a simple transverse intersection between  $C$  and another curve  $C_i$ , supporting a single M5-brane. Suppose that the two intersect at a point  $\mathcal{P}_i \in C$ . Then near  $C$ ,  $C_i$  is just the fiber of  $T^*C$  over  $\mathcal{P}_i$ . At a generic point on the Coulomb branch, there is a (non-normalizable) deformation of the theory which smoothes



the intersection between  $C_i$  and  $C$ . Namely, choosing a local coordinate  $z$  for which  $\mathcal{P}_i$  is at  $z = 0$ , we require that near  $\mathcal{P}_i$  one of the sheets of  $\Sigma$  looks like  $xz = \rho_i$ , for some  $\rho_i \neq 0$ . More invariantly, recalling the identification between  $x$  and an eigenvalue of  $\varphi$ , we require that  $\varphi$  is gauge equivalent near  $\mathcal{P}_i$  to

$$\varphi = \frac{1}{z} \begin{pmatrix} \rho_i & & \\ & 0 & \\ & & \ddots \\ & & & 0 \end{pmatrix} + \cdots \quad (3.39)$$

We must also choose boundary conditions on the gauge field; a natural choice compatible with the Hitchin equations is

$$A = \frac{1}{2i} \left( \frac{dz}{z} - \frac{d\bar{z}}{\bar{z}} \right) \begin{pmatrix} \alpha_i & & \\ & 0 & \\ & & \ddots \\ & & & 0 \end{pmatrix} + \cdots \quad (3.40)$$

where  $\alpha_i$  is imaginary.

As we will see in examples later,  $\rho_i$  has a natural interpretation as a mass parameter for a  $U(1)$  flavor symmetry in the four-dimensional gauge theory. Moreover, after the reduction to three dimensions, the three real parameters encoded in  $\rho_i$ ,  $\alpha_i$  can be interpreted as vevs of three scalar fields in a vectormultiplet of a  $U(1)$  flavor symmetry.

Equation (3.39) should be interpreted with care in the limit  $\rho_i \rightarrow 0$ ; we address this point further below in Section 4.3.

### 3.2 Witten's construction

An important special case of the construction we have discussed in Section 3.1 was considered by Witten some time ago in [2]. Indeed, suppose we consider an  $\mathcal{N} = 2$ ,  $d = 4$  theory defined by some conformal or asymptotically free linear quiver of unitary groups (perhaps with fundamental matter). In [2] such quivers were realized in Type IIA string theory using certain D4/D6/NS5-brane configurations. Moreover, Witten observed that upon lifting to M-theory these brane configurations are naturally described in terms of a single M5-brane.

In this section we review this construction in some detail, and argue that it can be viewed as an example of the general story of Section 3.1. In particular, upon dimensional reduction to  $d = 3$ , the moduli space  $\mathcal{M}$  of the resulting theory should be a Hitchin system. We thus give a rule for associating a specific ramified Hitchin system on  $\mathbb{CP}^1$  to any conformal or asymptotically free linear quiver of unitary groups. This Hitchin system is not the most general possible — we will see that the defect operators which arise are of a restricted sort.

Actually, by taking appropriate further scaling/decoupling limits of the quiver gauge theories, one could produce purely four-dimensional realizations of  $\mathcal{N} = 2$  field theories

associated to more general Hitchin systems on  $\mathbb{CP}^1$  or even higher genus curves  $C$ . A four-dimensional construction of the  $\mathcal{N} = 2$  field theories associated to Hitchin systems with regular singularities on a general Riemann surface has recently appeared in [15].

### 3.2.1 Type IIA

Following Witten, we begin in Type IIA string theory. We consider a system of  $n + 1$  parallel NS5-branes ( $n \geq 1$ ), labeled by  $\alpha = 0, 1, \dots, n$ . The branes are extended along the directions  $x^{1,2,3,4,5}$ , at common values of  $x^{7,8,9}$ , and separated from one another in the  $x^6$  direction. We refer to the interval

$$I_\alpha := \{x^6 : x_{\alpha-1}^6 < x^6 < x_\alpha^6\} \quad (3.41)$$

as the  $\alpha$ -th interval. Next introduce a collection of D4-branes, at fixed values of  $x^{4,5,7,8,9}$ , and extended over some intervals in  $x^6$  ending on the NS5-branes. The NS5- and D4-branes are all located at the same value of  $x^{7,8,9}$ . There are  $k_0$  semi-infinite D4-branes on the left ( $x^6 \rightarrow -\infty$ ),  $k_\alpha$  D4-branes in the interval  $I_\alpha$  for  $1 \leq \alpha \leq n$ , and  $k_{n+1}$  semi-infinite D4-branes on the right ( $x^6 \rightarrow +\infty$ ). Finally we may introduce D6-branes, extended along  $x^{1,2,3,7,8,9}$ , and at fixed values of  $x^{4,5,6}$ . An example of such a configuration is illustrated in Figure 5.

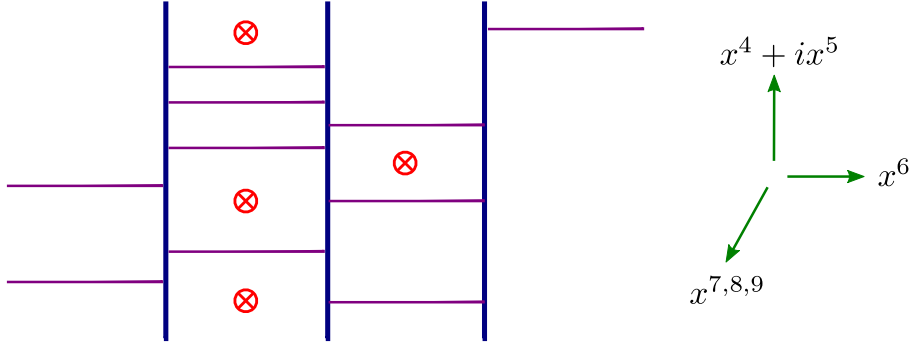


**Figure 5:** A configuration of Type IIA NS5-branes (blue), D4-branes (purple), and D6-branes (red circles with crosses). We have chosen  $n = 2$  and  $(k_0, k_1, k_2, k_3) = (2, 4, 3, 1)$ . The D6-branes are at definite values of  $x^{4,5,6}$ .

The ground state of this system preserves 8 real supercharges. On length scales much larger than the string length and the distances between the NS5-branes, the fluctuations of the branes are described by a  $d = 4, \mathcal{N} = 2$  gauge theory in the spacetime coordinatized by  $x^\mu = x^{0,1,2,3}$ . This gauge theory is a linear quiver with gauge group  $U(k_1) \times \dots \times U(k_n)$ ; see Figure 6.

The matter content of this quiver theory consists of  $d_\alpha$  matter fields transforming in the fundamental representation of each  $U(k_\alpha)$  factor. These fundamental matter fields arise in two ways. First, they can come from strings stretching between the D4- and D6-branes in the  $\alpha$ -th interval, in which case they are charged under  $U(k_\alpha)$ . Second, strings stretching between the group of semi-infinite D4-branes at either end of the  $x^6$  interval and the adjacent group of D4-branes give  $k_0$  fundamentals of  $U(k_1)$  and  $k_{n+1}$  fundamentals

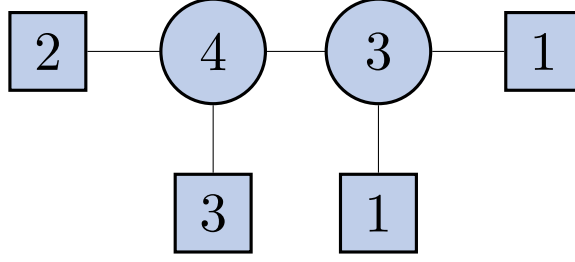


**Figure 6:** A linear quiver, corresponding to the Type IIA configuration illustrated in Figure 5. Circular nodes correspond to the  $U(k_\alpha)$  gauge groups. Links between circular nodes correspond to bifundamental matter. Links between circular and square nodes correspond to fundamental matter, with multiplicity given by the number  $d_\alpha$  in the square node.

of  $U(k_n)$ . When  $n \geq 2$ , D4-D4 strings also give hypermultiplets in the bifundamental of  $U(k_\alpha) \times U(k_{\alpha+1})$  for  $\alpha = 1, \dots, n-1$ .

As explained in [2], there is a beautiful relation between the forces exerted by the D4-branes on the NS5-branes and the beta functions of the gauge couplings of the effective four-dimensional theory. This relation shows that in order to avoid large backreaction effects we must restrict attention to asymptotically free or conformal theories. Therefore we require the beta function coefficients to be nonnegative:

$$b_\alpha := -2k_\alpha + k_{\alpha-1} + k_{\alpha+1} + d_\alpha \leq 0, \quad \alpha = 1, \dots, n. \quad (3.42)$$

The centers of the gauge groups  $U(1)_\alpha \subset U(k_\alpha)$  are not involved in the four-dimensional dynamics. The relative  $U(1)$  factors are Higgsed, so up to a quotient by a finite group, the effective gauge group is  $\prod_\alpha SU(k_\alpha) \times U(1)_d$ , where the diagonal  $U(1)_d \subset \prod_\alpha U(1)_\alpha$  represents the overall center-of-mass coordinate of the full collection of D4-branes. This diagonal  $U(1)_d$  is free and decouples.

Let us now summarize the parameters of this theory. The UV parameters are the gauge couplings or UV scales  $\tau_\alpha$  or  $\Lambda_\alpha$ , together with the bifundamental masses  $\mu_\alpha$  and the fundamental masses  $\hat{\mu}_{\alpha,j}$ ,  $1 \leq j \leq d_\alpha$  (which enter the superpotential). There are also IR “ $u$ -parameters” specifying a point of the Coulomb branch: letting  $\Phi^{(\alpha)}$  denote the adjoint scalar field in the vectormultiplet of  $SU(k_\alpha)$ , these parameters are the coefficients in the characteristic polynomials  $\langle \det(y - \Phi^{(\alpha)}) \rangle$  for each  $\alpha$ .

Finally we comment that this theory also has important flavor symmetries. Each bifundamental hypermultiplet has a  $U(1)$  flavor symmetry (enhanced to  $Sp(1) \sim SU(2)$  for bifundamentals of the gauge groups  $SU(2) \times SU(2)$ ), and each set of  $d_\alpha$  fundamental flavors has a  $U(d_\alpha)$  flavor symmetry (enhanced to  $SO(2d_\alpha)$  for fundamentals of the gauge group  $SU(2)$ ). Not all of these flavor symmetries are manifest in the brane construction. Some, like the enhancements for  $SU(2)$  gauge groups, will be visible in the six-dimensional  $(2, 0)$  theory setup, after the spurious  $U(1)$  gauge group factors have been expunged. Others emerge only after the flow to the four-dimensional gauge theory. We will see various examples throughout the paper.

### 3.2.2 Lift to M-theory

The second key element in Witten's construction is the lift of the above Type IIA configuration to M-theory. Let  $x^{10}$  denote a periodic coordinate, of period  $2\pi$ , parameterizing the M-theory circle. In the absence of D6-branes we take the 11-dimensional M-theory metric to be

$$ds^2 = \sum_{\mu=0,1,2,3} dx^\mu dx_\mu + \sum_{i=4,5,7,8,9} (dx^i)^2 + R_{11}^2 [(dx^6)^2 + (dx^{10})^2]. \quad (3.43)$$

(Note that  $x^6$  and  $x^{10}$  are dimensionless.) In the presence of D6-branes we will replace a summand in (3.43) by a multi-centered Taub-NUT manifold  $Q$ , by letting the  $x^{10}$  circle fiber nontrivially over the  $\mathbb{R}^3$  parameterized by  $x^{4,5,6}$ .

The NS5- and D4-branes both lift to M5-branes, and on the Coulomb branch of the theory they are in general unified into a single smooth M5-brane, which wraps a non-compact holomorphic curve  $\Sigma$  in  $Q$ .  $\Sigma$  is constrained by the requirement that we recover the IIA picture upon reducing along  $x^{10}$ . This leads to rules for the asymptotic shape of  $\Sigma$ , which are explained in [2] and will be recalled in the next subsection. The IR parameters of the theory are summarized in the coefficients of the polynomial equation defining the curve  $\Sigma$ . There is a fairly elaborate map from the UV parameters  $\tau_\alpha, \Lambda_\alpha, \mu_\alpha, \hat{\mu}_{\alpha,j}, \langle \det(y^i - \Phi^{(\alpha)}) \rangle$  to these IR parameters, which will be partially explained in the next section.

We will need to take a limit of the M-theory system in which the M-theory circle is large, i.e.  $R_{11}/\ell \rightarrow \infty$  where  $\ell$  is the M-theory length scale. Thus the IIA string coupling  $g_s = (R_{11}/\ell)^{3/2}$  diverges. Nevertheless, we would also like to use the low energy gauge dynamics of D-branes. This is possible because, as explained in Section 2.3 of [2], marginal and relevant parameters of the gauge theory are invariant under a simultaneous scaling of  $g_s$  and  $x^6$ . In particular, we would like to hold the four-dimensional gauge couplings fixed. Using the standard DBI action for the D4-brane, we find the four-dimensional gauge coupling  $(g_{YM}^{(\alpha)})^{-2} \sim g_s^{-1} \frac{R_{11} \Delta x^6}{\ell_s} \sim \left( \frac{\ell}{R_{11}} \right)^{1/2} (x_\alpha^6 - x_{\alpha-1}^6)$ ,  $1 \leq \alpha \leq n$ , up to numerical factors. Thus, the NS5-branes have separation  $\Delta x^6 \rightarrow \infty$ . See [2] for a detailed discussion of the regime of validity of the construction.

Our aim is to reinterpret this brane setup so that this construction can be matched to our general discussion about the  $(2,0)$  theory: indeed it is equivalent to considering an  $A_{K-1}$   $(2,0)$  theory on the cylinder, with simple defects at various finite points on the cylinder, and (possibly intricate) boundary conditions at the two ends of the cylinder. For clarity's sake, we proceed via examples of increasing complexity.

### 3.2.3 Conformal quivers

The simplest setup involves  $K$  infinite D4-branes intersecting  $n+1$  NS5-branes. That is, we take  $k_0 = k_1 = \dots = k_{n+1} = K$ . This corresponds to a linear quiver of  $n$   $SU(K)$  gauge groups, with  $K$  fundamentals for the first and final factors.

The lift to M-theory is straightforward: the  $K$  D4-branes lift to  $K$  M5-branes, wrapping the cylinder parameterized by  $s := x^6 + ix^{10}$ . This cylinder is to be identified with the Riemann surface  $C$  of Section 3.1. These  $K$  M5-branes will give rise to an  $A_{K-1}$   $(2,0)$  theory on  $C$ . The NS5-branes also lift to M5-branes, intersecting the cylinder at distinct

points  $s = s_\alpha$ ,  $\alpha = 0, \dots, n$ . Their worldvolumes fill the  $x^4$ - $x^5$  plane. They give rise to simple defects in the  $A_{K-1}$  theory on  $C$ .

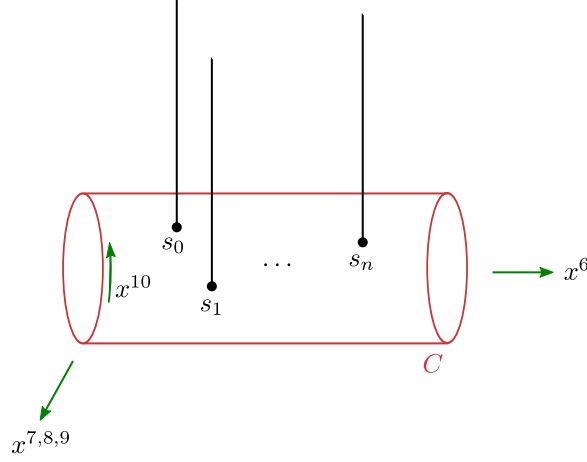


**Figure 7:**  $K$  M5-branes wrap a cylinder  $C$ . There are  $n + 1$  transverse singly-wrapped fivebranes intersecting  $C$  at points  $s_\alpha$ .

Let us introduce dimensionless coordinates  $t := e^{-s} \in \mathbb{C}^\times$  and  $v := (x^4 + ix^5)/\ell \in \mathbb{C}$ .<sup>22</sup> Figure 7 suggests that the curve  $\Sigma$  wrapped by the M5-brane is simply the locus in  $\mathbb{C}^\times \times \mathbb{C}$ ,

$$v^K \prod_{\alpha=0}^n (t - t_\alpha) = 0. \quad (3.44)$$

As we will see when describing the four-dimensional gauge theory interpretation, (3.44) actually corresponds to the conformal point, with all masses and all vevs  $\langle \text{Tr}(\Phi^\alpha)^s \rangle$  ( $1 \leq \alpha \leq n$ ,  $s = 1, \dots, k_\alpha$ ) vanishing. On the Coulomb branch, the various M5-branes of the setup join into a single smooth Riemann surface, defined by a polynomial equation in  $(t, v)$  which deforms (3.44) by terms of lower order in  $v$ :

$$F(t, v) = v^K \prod_{\alpha=0}^n (t - t_\alpha) + \sum_{i=1}^K p_i(t) v^{K-i} = 0. \quad (3.45)$$

If  $p_1(t_\alpha) \neq 0$ , then at  $t = t_\alpha$  one and only one of the roots  $v(t)$  has a pole, with residue  $\rho_\alpha := -\frac{p_1(t_\alpha)}{\prod_{\beta \neq \alpha} (t_\alpha - t_\beta)}$ . The branch of  $\Sigma$  corresponding to this divergent root at  $t = t_\alpha$  is physically identified as the M-theory lift of the  $\alpha$ -th NS5-brane in the IIA picture.

We also want to have  $K$  fivebranes going to constant values of  $v$  for very large and very small  $t$ . For very small  $t$  the  $K$  roots of (3.45) represent the asymptotic coordinates of the  $K$  D4-branes stretching to  $x^6 \rightarrow +\infty$ . If we wish also to have  $K$  distinct roots for  $v(t)$  in the limit  $t \rightarrow \infty$  then each  $p_i$  should have degree at most  $n + 1$ . Thus,  $F$  can also be written as

$$F(t, v) = \sum_{\alpha=0}^{n+1} q_\alpha(v) t^{n+1-\alpha} = 0. \quad (3.46)$$

<sup>22</sup>The algebraic relation between  $t$  and  $v$  together with the exponential relation between  $t$  and  $s$  ultimately leads to the logarithmic RG flow of couplings.

Here the  $q_\alpha(v)$  are polynomials in  $v$  of degree  $\leq K$ . Moreover,  $q_0(v)$  and  $q_{n+1}(v)$  must be of degree  $K$ . The roots of  $q_0$  and  $q_{n+1}$  are the  $k_0 = K$  and  $k_{n+1} = K$  asymptotic values of the roots  $v(t)$  for very large or very small  $t$ , respectively. We denote these by  $v_1^{(0)}, \dots, v_K^{(0)}$  and  $v_1^{(n+1)}, \dots, v_K^{(n+1)}$ , respectively.

### Weak coupling

We would like to get some intuition about the physical meaning of the coefficients of  $F(t, v)$ . This is easy if the four-dimensional gauge theories are weakly coupled. The gauge couplings of the four-dimensional  $SU(K)$  theories are determined by the dilaton, which sets the coupling of the five-dimensional gauge theory living on the D4-branes, and by the distance between NS5-branes in the  $x^6$  direction. In the lift to M-theory, this combination only depends on the coordinate  $s$  of the defects, and is independent of the overall scale  $R_{11}$  of the cylinder. The relation, including the theta angles, is

$$-i\pi\tau_\alpha = -i\pi \left( \frac{\theta_\alpha}{2\pi} + \frac{4\pi i}{g_\alpha^2} \right) = s_\alpha - s_{\alpha-1}, \quad \alpha = 1, \dots, n. \quad (3.47)$$

This relation is based on the assumption that to read off the gauge couplings, it makes sense first to descend from the  $(2, 0)$  theory on the cylinder with defects to the 5d SYM worldvolume theory on the D4-branes, and then to the four-dimensional low energy theory. This is true only in the limit where the separation between the defects is much larger than the radius of the cylinder, i.e. the gauge couplings are weak. On the other hand, at strong coupling the  $\tau_\alpha$  actually lack a precise definition: even if the theories are finite, there still is a scheme-dependent finite renormalization. The simplest choice is simply to take the  $t_\alpha$  (up to an overall rescaling) as a convenient parameterization of the space of marginal deformations of the  $\mathcal{N} = 2$  SCFT.

At weak coupling, we can take

$$\frac{|t_\alpha|}{|t_{\alpha-1}|} = \epsilon_\alpha \rightarrow 0, \quad 1 \leq \alpha \leq n, \quad (3.48)$$

so that in Type IIA language the NS5-branes are widely spaced. Next, let  $p_0(t) = \prod_{\alpha=0}^n (t - t_\alpha) = \sum_{s=0}^{n+1} c_{n+1-s} t^s$ . Then in this limit  $|c_j| = |t_0 \cdots t_{j-1}|(1 + \mathcal{O}(\epsilon_j))$ ,  $j = 1, \dots, n+1$ . Let us also set

$$q_\alpha(v) = c_\alpha \tilde{q}_\alpha(v) \quad (3.49)$$

The claim is that the roots of the monic polynomials  $\tilde{q}_\alpha(v)$  parameterize the positions of the  $\alpha$ -th group of D4-brane segments, i.e. the Coulomb branch of the  $\alpha$ -th gauge group in the quiver. Indeed we can take  $|t|$  in the range

$$|t_\beta| \ll |t| \ll |t_{\beta-1}| \quad (3.50)$$

so that, in Type IIA language, the  $x^6$  positions of D4-branes lie well inside the interval between the  $\beta^{th}$  and  $(\beta - 1)^{th}$  NS5-branes. Then

$$|t^{n+1}| \ll |t^n t_0| \ll \cdots \ll |t^{n+1-\beta} t_0 \cdots t_{\beta-1}| \quad (3.51)$$

$$|t^{n+1-\beta}t_0 \cdots t_{\beta-1}| \gg |t^{n-\beta}t_0 \cdots t_{\beta}| \gg \cdots \gg |t_0 \cdots t_{n+1}| \quad (3.52)$$

and hence in the equation  $F(t, v) = 0$  the dominant term is

$$t^{n+1-\beta}t_0 \cdots t_{\beta-1}\tilde{q}_{\beta}(v) = 0 \quad (3.53)$$

and the transverse position of the M5-branes or D4-branes is close to the roots of  $\tilde{q}_{\beta}(v)$ . Again, at strong coupling this approximate statement becomes incorrect. At the same time scheme dependent finite renormalization and operator mixing in the field theory makes it a bit meaningless to talk about “the Coulomb branch of the  $\alpha$ -th gauge group”, and try to identify the vevs  $\langle \text{Tr}(\Phi^{\alpha})^s \rangle$  of specific operators in the gauge theory.

### The Seiberg-Witten curve

A beautiful insight of [2] is that the curve (3.45) should be identified with the Seiberg-Witten curve for the four-dimensional linear quiver gauge theory. From our present perspective, this follows from the general discussion of Section 3.1. The parameters of  $F$  other than  $t_{\alpha}$ , i.e., the coefficients of the polynomials  $p_i(t)$ , encode the vevs of the adjoint scalars and the mass parameters.

The precise identification of the mass parameters is subtle, and important. The key to making this identification is the observation that the residues of the Seiberg-Witten differential encode the mass parameters. There is a simple canonical form for this differential for the problem at hand, which was only implicit in [2], and was made explicit in [48, 49, 32].

The computation is a special case of the general discussion of Section 3.1.5, but is more straightforward in this case, so we repeat it. Thus we consider a low energy configuration of the M5-brane where the embedding into  $\mathbb{R}^{1,3} \times \mathbb{C}^{\times} \times \mathbb{C}$  is given by  $(x^{\mu}, t, v(t; \xi_i(x^{\mu})))$ . Here  $\xi_i$  are a set of independent parameters of the curve, say, the coefficients of the polynomial  $F(t, v)$ .<sup>23</sup> The moduli fields  $\xi_i(x^{\mu})$  are assumed to be slowly varying as functions of the  $x^{\mu}$ . The M5-brane action has a contribution from the fluctuations of the normal bundle scalars coming from the induced worldvolume metric. Using the metric of equation (3.43),  $ds^2 = dx^{\mu}dx_{\mu} + \ell^2|dv|^2 + R_{11}^2|\frac{dt}{t}|^2 + dx_{7,8,9}^2$  we find the kinetic energy after subtracting the energy from the tension of the M5-brane in the reference configuration:

$$\frac{R_{11}^2}{\ell^2} \int_{\mathbb{R}^{1,3}} dx^{0123} \int_{\Sigma} \frac{dt d\bar{t}}{|t|^2} \frac{\partial v}{\partial \xi_i} \partial_{\mu} \xi_i \overline{\frac{\partial v}{\partial \xi_j}} \partial_{\mu} \xi_j. \quad (3.54)$$

Now, since  $\frac{\partial v}{\partial \xi_i}$  is a holomorphic function of  $t$ , we can do the integral over  $\Sigma$  as follows. First note that if the one-form  $\frac{dt}{t} \frac{\partial v}{\partial \xi_i}$  has a simple pole at any value of  $t$ , including  $t = 0, \infty$ , then the integral diverges. Thus, the *normalizable* variations of the parameters of  $F(t, v)$  are precisely those which do not alter the poles of  $\lambda = v \frac{dt}{t}$ . We label these normalizable parameters by  $u_i$ . Now, let  $\bar{\Sigma}$  be the compact Riemann surface obtained by embedding  $\Sigma$  in projective space and filling in the punctures. These punctures correspond to the noncompact branches at  $t_{\alpha}$  and the  $K$  branches above  $t = 0, \infty$ . Introduce a basis  $\gamma_a$  for

---

<sup>23</sup>Note that  $t = e^{-s}$  is *not* a time coordinate; it is the coordinate along  $C = \mathbb{C}^{\times}$ .

$H_1(\bar{\Sigma}; \mathbb{Z})$  and let  $\mathcal{I}^{ab}$  be the (dual) intersection form in this basis. Then we may compute

$$\int_{\Sigma} \frac{dt d\bar{t}}{|t|^2} \frac{\partial v}{\partial \xi_i} \frac{\overline{\partial v}}{\partial \xi_j} = \int_{\bar{\Sigma}} \frac{dt d\bar{t}}{|t|^2} \frac{\partial v}{\partial \xi_i} \frac{\overline{\partial v}}{\partial \xi_j} = \sum_{a,b} \mathcal{I}^{ab} \oint_{\gamma_a} \frac{\partial}{\partial \xi_i} \lambda \oint_{\gamma_b} \frac{\overline{\partial}}{\partial \xi_j} \lambda. \quad (3.55)$$

In this way we derive the low energy effective action for the kinetic energy of the normal bundle scalars:

$$\frac{R_{11}^2}{\ell^2} \int_{\mathbb{R}^{1,3}} dx^{0123} \mathcal{I}^{ab} \partial_{\mu} \Pi_a \partial_{\mu} \bar{\Pi}_b \quad (3.56)$$

where  $\Pi_a = \oint_{\gamma_a} v \frac{dt}{t}$ . If we choose a duality frame  $(\gamma_I, \gamma^I)$  then (3.56) becomes the standard expression  $\int \text{Im}(\tau_{IJ}) \partial_{\mu} a^I \partial_{\mu} \bar{a}^J$  that one finds in the  $\mathcal{N} = 2$  effective action. Thus we conclude that the Seiberg-Witten differential is

$$\lambda_{SW} = \lambda = v \frac{dt}{t}. \quad (3.57)$$

It is well-known that the residues of the Seiberg-Witten differential depend affine-linearly on the mass parameters of the UV Lagrangian. The differential  $v \frac{dt}{t}$  has simple poles on the  $K$  branches covering  $t = 0$  and on the  $K$  branches covering  $t = \infty$ . The residues at these poles are the asymptotic positions in the  $v$ -plane of the semi-infinite D4-branes on the left and right end of the quiver, respectively. We can verify that these depend affine-linearly on the masses as follows: Consider the Type IIA picture and suppose that  $k_1$  D4's are at a common  $v$ -position  $v_0$  in the first interval  $I_1$ . Classical string theory shows that the mass of the  $K$  fields in the fundamental representation of  $SU(k_1)$  are given by  $\ell_s^{-1} |v_i^{(0)} - v_0|$ , where  $v_i^{(0)}$  are the  $K$  roots of  $q_0(v)$ . By holomorphy we see that the complex mass parameters  $\hat{\mu}_i^{(1)}$  satisfy  $v_i^{(0)} - v_j^{(0)} \propto \hat{\mu}_{1,i} - \hat{\mu}_{1,j}$ . A similar statement holds for the fundamental fields associated with the branches stretching to  $t \rightarrow +\infty$ . Thus, the differences of mass parameters associated with the  $SU(K)$  flavor symmetry at each end are given by the differences between the roots of  $q_0(v)$  and between the roots of  $q_{n+1}(v)$ .

Finally, for generic parameters of the polynomial, as we have seen, precisely one root  $v(t)$  has a simple pole as  $t \rightarrow t_{\alpha}$ , leading to a simple pole for the Seiberg-Witten differential with residue  $\rho_{\alpha}/t_{\alpha}$ . In the weak-coupling regime described in equations (3.48) et. seq. it is not difficult to show that if we write:

$$q_{\alpha}(v) = c_{\alpha}(v^K - \mu_{\alpha} v^{K-1} - u_2^{(\alpha)} v^{K-2} - \dots - u_K^{(\alpha)}) \quad (3.58)$$

then the residues at  $t_{\alpha}$  are approximately  $(\mu_{\alpha} - \mu_{\alpha+1})$ , for  $0 \leq \alpha \leq n$ , and coincide either with the mass parameters for the bifundamental matter fields between the  $\alpha$  and  $\alpha + 1$  nodes of the quiver, or with the overall  $U(1)$  mass parameter of the fundamental matter fields at either end of the quiver for  $\alpha = 0$  or  $\alpha = n$ .

In the field theory limit the overall center of mass degree of freedom of the M5-brane system decouples. We aim to arrive at a description which involves only the degrees of freedom of the  $A_{K-1}(2,0)$  theory. A natural way ignore the shift of the overall center of mass is to eliminate the coefficient of  $v^{K-1}$  in  $F(t, s)$ . To do this, we define

$$\tilde{v} := v - p(t) \quad (3.59)$$



and make the choice  $p(t) = -\frac{p_1(t)}{K \prod_{\alpha}(t-t_{\alpha})}$ . Note that the residue at  $t = t_{\alpha}$  is  $\rho_{\alpha}/K$ .

Next, recall that all physical quantities depend on integrals of the Seiberg-Witten differential along closed paths in the Seiberg-Witten curve. In a given IR theory the Seiberg-Witten differential  $\lambda$  is not unique: it is required to satisfy (in any duality frame)

$$\tau_{IJ} = \frac{\partial}{\partial a^J} \oint_{\gamma_I} \lambda, \quad (3.60)$$

but it may be modified by the addition of a one-form which does not depend on the normalizable deformations. (Recall the notion of a normalizable deformation is defined by the finiteness of the kinetic energy (3.54)). In particular, we are free to change the definition of the Seiberg-Witten differential by the shift  $v \rightarrow v + p(t)$ , since  $p(t)$  is a single-valued rational function of  $t$ . The residues of  $p(t) \frac{dt}{t}$  are linear combinations of the mass parameters of the theory, and the first derivatives  $\lambda_{u_i}$  are unchanged, and still coincide with the holomorphic 1-forms on the Seiberg-Witten curve. The periods of  $\lambda$  are shifted by a certain linear combination of the mass parameters. In order to write a central charge as a sum of contributions from “gauge charges” and “flavor charges” we need to choose a splitting of the sequence (3.14). Once such a splitting has been made the shift of  $\lambda$  amounts to a shift of the flavor charges of BPS particles by multiples of their gauge charges, i.e. to a legal redefinition of the flavor currents. The shift of flavor charges is not simply harmless, it is actually a useful improvement. For example, in the  $K = 2$  case, we saw that the flavor symmetry groups are enhanced from  $U(1)$  to  $SU(2)$  in the field theory limit. The shift in  $\lambda$  gives a charge assignment to BPS particles which is compatible with the organization in irreps of the new  $SU(2)$ ’s (see Section 3.2.9 for more information).

The new Seiberg-Witten differential  $\tilde{v} \frac{dt}{t}$  has simple poles on the different sheets above  $t = t_{\alpha}$  whose list of residues is given by

$$(-(K-1)m_{\alpha}, m_{\alpha}, \dots, m_{\alpha}) \quad (3.61)$$

where

$$m_{\alpha} = \frac{1}{K t_{\alpha}} \frac{p_1(t_{\alpha})}{\prod_{\beta \neq \alpha} (t_{\alpha} - t_{\beta})} = -\frac{\rho_{\alpha}}{K t_{\alpha}} \quad (3.62)$$

is identified with the mass parameter of a  $U(1)$  flavor symmetry.

At  $t = 0$  (and similarly at  $t = \infty$ ) the poles on different sheets will be of the form

$$\left(-\sum m_{0,i}, m_{0,1}, \dots, m_{0,N-1}\right) \quad (3.63)$$

where  $m_{0,i}$  (and the corresponding  $m_{\infty,i}$  at  $t = \infty$ ) are linked to the relative positions of the semi-infinite D4-branes and are identified with the mass parameters of the  $SU(K)$  flavor symmetry of either group of  $K$  fundamentals. Notice that if  $K = 2$  the two types of defect are identical, and indeed the  $U(1)$ ’s are promoted to  $Sp(1) \sim SU(2)$ .

### An example

We close this section with an example. Let us consider  $n = 1$ , so that we have a simple gauge group  $SU(K)$  with  $2K$  fundamentals. The standard Seiberg-Witten curve for this

theory naively appears to be very different from the one we consider here, especially when all the mass parameters are included [50]:

$$y^2 = P(w)^2 - (1 - g^2)Q(w) \quad (3.64)$$

$$P(w) = \langle \det(w - \Phi) \rangle = w^K - u_2 w^{K-2} - \dots - u_K \quad (3.65)$$

$$Q(w) = \prod_{I=1}^{2K} (w + g\mu + \mu_I) \quad (3.66)$$

Here the parameters  $\mu, \mu_I$  determine the flavor masses by  $\mu = \frac{1}{2K} \sum_{I=1}^{2K} m_I$  and  $\mu_I = m_I - \mu$ . The parameter  $g$  is a certain modular function of the coupling  $\tau$  (see eq. (5.15) of [50]) which for weak coupling reduces to  $g = 1 + \mathcal{O}(e^{i\pi\tau})$ . The Seiberg-Witten differential is

$$\lambda^{\text{Standard}} = \frac{w + (g-1)\mu}{2\pi i} d \log \left( \frac{y - P}{y + P} \right). \quad (3.67)$$

By a transformation of variables, we can bring the curve into the form  $F(t, v) = 0$  where  $F(t, v)$  is of the form (3.45). First we introduce  $\gamma$  obeying

$$\frac{4}{(\gamma + \gamma^{-1})^2} = 1 - g^2. \quad (3.68)$$

Next, we set  $v = w + (g-1)\mu$ ; then introducing  $v_I := m_I$  we have

$$Q(w) = \prod_{j=1}^{2K} (v - v_I). \quad (3.69)$$

The symmetric group  $S_{2K}$  acts on the set of roots  $v_I$ . ( $S_{2K}$  is the Weyl group of the  $U(2K)$  flavor symmetry group which is broken to the Cartan by the masses.) We now explicitly break the symmetry to  $S_K \times S_K$  by choosing a set of  $K$  roots  $v_i, i = 1, \dots, K$ . We denote the remaining roots by  $\tilde{v}_i, i = 1, \dots, K$ . Now we set

$$t = \frac{1}{2}(\gamma + \gamma^{-1}) \frac{y - P(w)}{\prod_{i=1}^K (v - v_i)} \quad (3.70)$$

Finally we take  $\tilde{P}(v) = P(w)$ . In this way we bring the curve to the form

$$\prod_{i=1}^K (v - v_i) t^2 + (\gamma + \gamma^{-1}) \tilde{P}(v) t + \prod_{i=1}^K (v - \tilde{v}_i) = 0 \quad (3.71)$$

which is of the form (3.46). Note that if we put equation (3.71) into the form (3.45) we find that  $t_0 = \gamma, t_1 = \gamma^{-1}$ , and thus from (3.68) we confirm that  $t_0/t_1 \sim e^{i\pi\tau}$  in accord with the discussion of the weak-coupling limit. Also, note that in this presentation  $p_1(t) \neq 0$ , so we have not yet fixed the center of mass degree of freedom in the standard way.

It is worth noting that the standard Seiberg-Witten differential differs from that naturally arising from our discussion:

$$i\pi\lambda^{\text{Standard}} - \lambda^{\text{Hitchin}} = \frac{1}{2} v d \log \left( \frac{\prod_{i=1}^K (v - v_i)}{\prod_{i=1}^K (v - \tilde{v}_i)} \right) \quad (3.72)$$

The residues of the difference,  $v_i$ , are just mass parameters, so this corresponds again to a simple redefinition of the flavor charges. Before we remove the center of mass piece,  $\lambda^{\text{Hitchin}}$  has a pole on a single sheet at  $t_0 = \gamma$  or  $t_1 = \gamma^{-1}$ . It takes some work to extract the residue through all changes of variables, but the result is remarkably simple: the residue at  $t_0$  is  $\sum \tilde{v}_i$ , the overall mass parameter for the  $K$  fundamental flavors associated to the  $K$  semi-infinite branes on one side. The residue at  $t_1$  is similarly  $\sum v_i$ .

The residues of  $\lambda^{\text{Hitchin}}$  at  $t = 0, \infty$  coincide with the  $v_i$  or  $\tilde{v}_i$ , but after we remove the center of mass, the residues are modified to  $v_i - \frac{1}{K} \sum v_i$  and  $\tilde{v}_i - \frac{1}{K} \sum \tilde{v}_i$ , which are the mass parameters of the  $SU(K)$  flavor subgroups acting on each group of  $K$  fundamental flavors.

This splitting is natural: from the point of view of the  $(2,0)$  theory the  $U(2K)$  flavor symmetry is an accidental IR symmetry. The six dimensional theory only has a  $U(1)^2 \times SU(K)^2$  flavor symmetry, and each factor is somehow associated to one of the four ‘‘punctures’’ at  $t = 0, t_0, t_1, \infty$ . Notice that the punctures at  $0, \infty$  have different properties from the punctures at  $t_0, t_1$ . We will see in the next subsection how the difference manifests itself in the context of the Hitchin system.

### 3.2.4 Mapping to a Hitchin system

We are now ready to return to the Hitchin system described in Section 3.1. We interpret the  $K$  branches  $\tilde{v}(t)$  of the solutions to  $F(t, v) = 0$  as the  $K$  eigenvalues of the Higgs field  $\varphi_s$ , because these are the positions of the M5-branes. Our choice to fix the center of mass to eliminate the  $\tilde{v}^{K-1}$  term in the polynomial  $F(t, v)$  guarantees that  $\varphi_s$  is valued in  $SU(K)$  and not  $U(K)$ . The spectral curve of the Hitchin system on the cylinder is, by definition,  $\det(\tilde{v} + \varphi_s) = 0$ . We want to identify this spectral curve with the curve  $F(t, v) = 0$  wrapped by the IR M5-brane. The only important point is to remember that  $\varphi_s$  transforms as a one-form,  $\varphi_t dt = \varphi_s ds$ . Identifying the spectral curve with the curve  $F(t, v) = 0$  and making the definition  $x := \frac{\tilde{v}}{t}$ , the spectral curve in  $T^*\mathbb{C}^\times$  has the form

$$\det(x - \varphi_t) = x^K + \sum_{i=2}^K \frac{\tilde{p}_i(t)}{(t \prod_{\alpha=0}^n (t - t_\alpha))^i} x^{K-i} = 0. \quad (3.73)$$

(The  $\tilde{p}_i$  differ from the  $p_i$  which appeared in (3.45) because of the shift we made from  $v$  to  $\tilde{v}$ .) If we do not factor out the  $U(1)$  degree of freedom we identify  $x = v/t$ . In any case, this equation is to be identified with (3.38). Note that the Seiberg-Witten differential is  $x dt$ , as asserted in Section 3.1.

In order to treat the singularities in a more symmetric way it is useful to embed  $\mathbb{C}^\times \rightarrow \mathbb{CP}^1$  via  $t \rightarrow [t : 1]$ . Then we recognize that the boundary conditions at the ends of the cylinder, i.e. at  $t = 0, \infty$ , state that  $\varphi_t dt$  has a simple pole with residue given by the asymptotic values of  $v$ . Thus, we deduce the boundary conditions on the Higgs field:

$$\varphi_t dt \rightarrow \frac{dt}{t} \text{Diag}\{v_1^{(0)}, \dots, v_K^{(0)}\} \quad t \rightarrow 0 \quad (3.74)$$

$$\varphi_t dt \rightarrow \frac{dt}{t} \text{Diag}\{v_1^{(n+1)}, \dots, v_K^{(n+1)}\} \quad t \rightarrow \infty \quad (3.75)$$

There are in addition simple poles at  $t = t_\alpha$  with a residue of the form

$$\text{Diag}\{-(K-1)m_\alpha, m_\alpha, m_\alpha, \dots, m_\alpha\}, \quad \alpha = 0, \dots, n \quad (3.76)$$

if we factor out the  $U(1)$  degree of freedom, and  $\text{Diag}\{\rho_\alpha, 0, \dots, 0\}$  if we do not. Recall that  $m_\alpha$  is given in equation (3.62). Note that the residues at  $t = 0, \infty$  are generic semisimple elements of  $su(K)$  and hence correspond to regular singularities, but this is not at all true when we consider the residues at  $t = t_\alpha$ ,  $\alpha = 0, \dots, n$ , for  $K > 2$ , since then the residues are annihilated by all but the first simple root (for the standard choice of simple roots).

We stress that the conditions (3.74), (3.75) and (3.76) mean that there is a local gauge in which the fields can be put in this form.

In the main part of the paper we will focus on the case  $K = 2$ . In that case, after the center of mass  $U(1)$  is removed as described above, there is no longer any distinction between the two kinds of singularity. Thus, the Hitchin system turns out to be a general  $SU(2)$  Hitchin system on  $\mathbb{CP}^1$  with  $n + 3$  regular singularities. The equation (3.73) is equivalent to

$$\text{tr} \varphi_t^2 = \frac{1}{2} \frac{(p_1(t))^2 - 4p_2(t) \prod_{\alpha=0}^n (t - t_\alpha)}{(t \prod_{\alpha=0}^n (t - t_\alpha))^2}. \quad (3.77)$$

Note that  $\varphi_t dt$  has simple poles at  $t = 0$  and  $t = \infty$  as well as at the  $n + 1$  points  $t_\alpha$ . We will return to this formula in Section 9.

### 3.2.5 Linear conformal quivers with fundamental matter

It is straightforward to extend this analysis to a more general linear conformal quiver with fundamental matter. This is a quiver of  $SU(k_\alpha)$  gauge groups, with  $d_\alpha = 2k_\alpha - k_{\alpha-1} - k_{\alpha+1}$  fundamental fields at the  $\alpha$ -th node,  $\alpha = 1, \dots, n$ . The extra fundamental fields are represented in the brane construction by  $d_\alpha$  D6-branes at fixed values of  $x^{4,5,6}$  with the value of  $x^6$  in the interval  $I_\alpha$ . We will denote with  $K$  the maximum of the  $k_\alpha$ . When we include D6-branes the semi-infinite D4-branes on the left and right do not change the analysis in any interesting way, so in the remainder of this section we will omit them. As before, for  $\alpha = 1, \dots, n$ ,  $k_\alpha$  D4-branes are stretched between the NS5-branes along the interval  $I_\alpha$ . We assume that initially there are no D4-branes ending on D6-branes. In the weak IIA coupling limit the D4-D6 strings provide the fundamental matter. When the  $k_\alpha$  D4-branes are coincident, the mass parameter of these fundamental hypermultiplets is given by the difference of the  $v$  coordinates for the D4-brane and the D6-brane.

The lift to M-theory of the configuration we have just described is obtained by lifting the configuration of D6-branes to a multi-center Taub-NUT geometry  $Q$  and then – on the Coulomb branch of vacua – lifting the D4- and NS5-branes to a single M5-brane with worldvolume  $\mathbb{R}^{1,3} \times \tilde{\Sigma} \times \{\mathcal{P}\}$ , where  $\tilde{\Sigma} \subset Q$  is a holomorphic surface. Our goal in this section is to make contact once again with a Hitchin system on a cylinder, and show how the fundamental matter changes the boundary conditions on the Higgs field.

It turns out that there are several distinct ways to do this, as the same brane system can be subject to certain deformations which lead to the same IR four dimensional field theory, but to different intermediate six-dimensional setups. The detailed analysis is a bit intricate, so we will first anticipate the main result.

For linear conformal quivers there is a canonical choice, which still leads to a  $SU(K)$  Hitchin system on the cylinder with regular singularities. The boundary conditions at  $t = 0$  and  $t = \infty$ , (3.74) and (3.75), are modified slightly, as the  $v_i^{(0)}$  and the  $v_j^{(n+1)}$  are not generic anymore. Instead, the  $K$   $v_i^{(0)}$  are partitioned in blocks of identical values, so that each block of  $\alpha$  identical  $v_i^{(0)}$  corresponds to a fundamental flavor at the  $\alpha$ -th node of the quiver, and each block of  $\alpha$  identical  $v_i^{(n+1)}$  corresponds to a fundamental flavor at the  $(n+1-\alpha)$ -th node of the quiver. For example, if  $K = 3$  we have quivers of  $SU(3)$  gauge nodes, possibly with a single  $SU(2)$  gauge group at either or both ends. If, say,  $k_1 = 2$  and  $k_2 = k_3 = 3$ , then  $d_1 = d_2 = 1$ ,  $d_3 = 3$ , and there is a single fundamental at the first node, and another at the second node. Then the residue of the regular singularity at  $t = \infty$  will have two identical eigenvalues.

This canonical Hitchin system is characterized by the fact that the  $U(1)$  R-symmetry of the 4d theory is identified with the  $U(1)$  symmetry rotating  $v$ . Other choices lead to Hitchin systems (of rank higher than  $K$ ) on the cylinder, with no punctures away from  $t = 0, \infty$ , and with wild ramification either at  $t = 0$  or  $t = \infty$ . The  $U(1)$  R-symmetry of the 4d theory is identified with a combination of the  $U(1)$  symmetries rotating  $v$  and rotating  $t$ . It is surprising that the same 4d field theory, and hence the same hyperkähler moduli space should be described by different Hitchin systems. The matter is discussed further in Section 3.2.8.

To begin, let us recall the metric on  $Q$ . The metric on  $Q$  is determined by the positions  $\vec{r}_a = (r_{1,a}, r_{2,a}, r_{3,a}) \in \mathbb{R}^3$  where  $a$  runs over some index set. If we describe  $Q$  as a circle fibration over  $\mathbb{R}^3$ , then the metric is

$$ds_{TN}^2 = V^{-1}(d\psi + A)^2 + V d\vec{r}^2 \quad (3.78)$$

where  $\psi \sim \psi + 4\pi$ ,

$$V = 1 + \sum_a \frac{1}{|\vec{r} - \vec{r}_a|} \quad (3.79)$$

and  $dA = *dV$ . The full M-theory metric is

$$ds^2 = dx^\mu dx_\mu + \frac{R_{11}^2}{4} ds_{TN}^2 + dx_{7,8,9}^2 \quad (3.80)$$

We identify  $s = x^6 + ix^{10} = \frac{1}{2}(r_3 + i\psi)$  and  $r_1 + ir_2 = 2\frac{\ell}{R_{11}}v$ . The Taub-NUT space  $Q$  carries a hyperkähler structure, but there is a distinguished complex structure in which the coordinate  $v$  is holomorphic. In this complex structure the manifold  $Q$ , as a complex manifold, has equation

$$UW = \prod_a (v - v_a) \quad (3.81)$$

The parameters  $v_a$  are the complex structure parameters, while the  $x_a^6$  are the Kähler parameters of the hyperkahler metric on  $Q$ .

Now we turn to a description of the holomorphic curve  $\tilde{\Sigma}$  in the complex manifold (3.81). The curve can be described as a polynomial equation  $\tilde{F}(W, v) = 0$ . Alternatively, in a different chart, using  $U = W^{-1} \prod_a (v - v_a)$  this equation can be also be rearranged as

$\tilde{G}(U, v) = 0$  for a polynomial  $\tilde{G}$ . In [2] it is shown that the constraint that there are no semi-infinite D4-branes on the left or the right leads to the following structure for  $\tilde{F}(W, v)$ : To each interval  $I_\alpha := \{x^6 : \text{Re}(s_{\alpha-1}) < x^6 < \text{Re}(s_\alpha)\}$  we associate a polynomial of degree  $d_\alpha$ :

$$J_\alpha(v) := \prod_{x_a^6 \in I_\alpha} (v - v_a), \quad \alpha = 1, \dots, n. \quad (3.82)$$

Now introduce

$$A_0(v) = c_0 \quad (3.83)$$

$$A_\alpha(v) = c_\alpha g_\alpha(v) \prod_{\beta=1}^{\alpha} J_\beta^{\alpha-\beta}(v), \quad \alpha = 1, \dots, n \quad (3.84)$$

$$A_{n+1}(v) = c_{n+1} \prod_{\beta=1}^n J_\beta^{n+1-\beta}(v), \quad (3.85)$$

where  $c_\alpha$ ,  $\alpha = 0, \dots, n+1$ , are nonzero constants and  $g_\alpha(v)$  are *monic* polynomials in  $v$  of degree  $k_\alpha$ ,  $\alpha = 1, \dots, n$ . (It is also convenient to define  $g_0 = g_{n+1} = 1$ .) Then we have the curve ([2], eq. (3.23))

$$\tilde{F}(W, v) = \sum_{\alpha=0}^{n+1} A_\alpha(v) W^{n+1-\alpha} = 0 \quad (3.86)$$

or equivalently

$$\tilde{G}(U, v) = c_{n+1} U^{n+1} + c_n g_n(v) U^n + \sum_{\alpha=0}^{n-1} g_\alpha(v) \left( \prod_{\beta=\alpha+1}^n J_\beta(v)^{\beta-\alpha} \right) U^\alpha = 0 \quad (3.87)$$

Moreover, the coefficients of  $g_\alpha(v)$  are interpreted in [2] as the usual order parameters  $\langle \text{Tr}(\Phi^{(\alpha)})^s \rangle$  of the  $SU(k_\alpha)$  gauge group. The constants  $c_\alpha$  can of course be rescaled by a common nonzero factor and hence should be viewed as a point in projective space. They encode the gauge couplings. (In the weak coupling region the  $c_\alpha$  can be given in terms of the  $\alpha^{\text{th}}$  elementary symmetric function of the  $t_\alpha$ .)

Naively the Taub-NUT setup does not seem to lead to a situation where a Hitchin system is useful, as it looks quite different from our previous picture of  $T^*C$  with  $K$  fivebranes wrapping  $C$  together with transverse defects. However, as we now explain, we can take a limit of the Taub-NUT geometry in which we recover the Hitchin description.

The curve  $\tilde{\Sigma}$  will again be interpreted as the Seiberg-Witten curve. Recall that the polynomial  $\tilde{F}(W, v)$  is independent of the Kähler parameters  $x_a^6$ , as is the complex structure of  $Q$ . As we saw in Section 3.1.5 and again in (3.54) et. seq., the kinetic terms and Seiberg-Witten differential only depend on the complex structure, and hence are unaffected by changes in  $x_a^6$ : two theories which differ only by translation of the D6-branes in the  $x^6$  direction are described by the same IR fixed point. On the other hand, in the limit where the D6-branes are brought far to the left or far to the right of the NS5-brane system, the setup strongly resembles the setup without D6-branes, since evidently  $V \rightarrow 1$  if  $|x_a^6| \rightarrow \infty$  at finite values of  $\vec{r}$ .

Now, let us divide the D6-branes into two disjoint subsets  $\mathcal{L} \amalg \mathcal{R}$  and consider a limit where the D6-branes with  $a \in \mathcal{R}$  move far to the right while the D6-branes with  $a \in \mathcal{L}$  move far to the left. In Appendix D we show that, when properly normalized, the limiting value of  $W$  is

$$W \rightarrow t \prod_{a \in \mathcal{L}} (v - v_a). \quad (3.88)$$

We substitute this into (3.86) and simplify. To do this note that each polynomial  $J_\alpha(v)$  factorizes according to the D6-branes which move to the left and right respectively:  $J_\alpha(v) = J_{\alpha,L}(v)J_{\alpha,R}(v)$ . After factoring out  $\prod_\alpha J_{\alpha,L}^{n+1-\alpha}$  we are left with

$$\hat{F}(t, v) = \sum_{\alpha=0}^{n+1} \hat{g}_\alpha(v) t^{n+1-\alpha}, \quad (3.89)$$

where

$$\hat{g}_0(v) = c_0 \prod_{\beta=1}^n J_{\beta,L}^\beta \quad (3.90)$$

$$\hat{g}_\alpha(v) = c_\alpha g_\alpha(v) \prod_{\beta=1}^\alpha J_{\beta,R}^{\alpha-\beta} \prod_{\beta=\alpha+1}^n J_{\beta,L}^{\beta-\alpha} \quad \alpha = 1, \dots, n-1 \quad (3.91)$$

$$\hat{g}_n(v) = c_n g_n(v) \prod_{\beta=1}^n J_{\beta,R}^{n-\beta} \quad (3.92)$$

$$\hat{g}_{n+1}(v) = c_{n+1} \prod_{\beta=1}^n J_{\beta,R}^{n+1-\beta}. \quad (3.93)$$

There is an elegant interpretation of the factors in  $\hat{g}_\alpha(v)$  based on the Hanany-Witten effect [51]. In our context, the Hanany-Witten effect states that for each D6-brane the “linking number”

$$(L - R) - \frac{1}{2}(l - r) \quad (3.94)$$

is constant. Here  $l$ ,  $(r)$  is the number of NS5-branes to the left (right) of the D6-brane and  $L$ ,  $(R)$  is the number of D4-branes ending on the D6 from the left (right). In particular, if a D6-brane moves in the  $x^6$  direction at constant  $v$  across an NS5-brane, a D4-brane stretched between them is created. After we have moved the D6-branes with  $a \in \mathcal{R}$  far to the right, and those with  $a \in \mathcal{L}$  far to the left each interval consists of “free” and “frozen” D4-branes.<sup>24</sup> The factor  $g_\alpha(v)$  in  $\hat{g}_\alpha$  accounts for the “free” D4-branes. The coefficients of  $g_\alpha(v)$  correspond to the normalizable deformations in the usual way. The factor  $\prod_{\beta=1}^\alpha J_{R,\beta}^{\alpha-\beta}$  accounts for the “frozen” D4-branes in the interval  $I_\alpha$  which have been created by the motion of D6-branes to the right, and the factor  $\prod_{\beta=\alpha+1}^n J_{\beta,L}^{\beta-\alpha}$  accounts for the “frozen” D4-branes in the interval  $I_\alpha$  which have been created from the motion of D6-branes to the left.

---

<sup>24</sup>The adjective “frozen” refers to the so-called  $S$ -rule discussed in [51]. The D4-branes in the interval  $I_\alpha$  which are created from the horizontal motion of the D6-branes cannot move independently in the  $v$ -direction while preserving supersymmetry.



It is of some interest to compute the order  $\hat{k}_\alpha$  of the polynomials  $\hat{g}_\alpha$ . To do this note that, after a D6-brane has passed through the interval  $I_\alpha$  in either direction the net value of  $-2k_\alpha + k_{\alpha-1} + k_{\alpha+1} + d_\alpha$  remains constant. Therefore, since our initial configuration has all these values set to zero (for conformality) it follows that after all the D6-branes have been moved to the far left or far right we have  $-2\hat{k}_\alpha + \hat{k}_{\alpha+1} + \hat{k}_{\alpha-1} = 0$ ,  $1 \leq \alpha \leq n$ . Here  $\hat{k}_0$  is the number of D4-branes ending on the D6-branes on the left, i.e., the order of  $\prod J_{\beta,L}^\beta$  while similarly  $\hat{k}_{n+1}$  is the number of D4-branes ending on the D6-branes on the right, i.e. the order of  $\prod J_{\beta,R}^{n+1-\beta}$ . Using the results of Appendix E we see that  $\frac{(\hat{k}_{n+1}-\hat{k}_0)}{n+1} = r$  is a nonnegative integer and

$$\hat{k}_\alpha = \hat{k}_0 + \alpha r. \quad (3.95)$$

There are many different ways in which we can move D6-branes to the left and to the right. At one extreme, we could move them all to the right, so that  $\hat{k}_0 = 0$  and  $\hat{k}_\alpha$  increases linearly as a function of  $\alpha$ . Of course, the other extreme has all D6-branes on the left, and then  $\hat{k}_\alpha$  decreases linearly as a function of  $\alpha$ . Amongst the different ways of moving the D6-branes to the left and the right there is a canonical choice which we will refer to as the “balanced case.” To describe this choice we appeal again to Appendix E to note that the  $k_\alpha$  grow as a function of  $\alpha$  up to some maximum  $K$  attained at some  $\alpha = \alpha_-$ , then  $k_\alpha = K$  is constant up to some  $\alpha = \alpha_+ \geq \alpha_-$ , and then  $k_\alpha$  decreases monotonically for  $\alpha > \alpha_+$ . This suggests a canonical movement of the D6-branes: we bring all those in the intervals  $\alpha < \alpha_-$  to the left and all those in the intervals  $\alpha > \alpha_+$  to the right. In the interval  $I_{\alpha_-}$  we bring  $k_{\alpha_-} - k_{\alpha_- - 1}$  branes to the left and in the interval  $I_{\alpha_+}$  we bring  $k_{\alpha_+} - k_{\alpha_+ + 1}$  branes to the right. It is not difficult to show that this leads to  $\hat{k}_{\alpha_- - 1} = \hat{k}_{\alpha_-} = \dots = \hat{k}_{\alpha_+} = \hat{k}_{\alpha_+ + 1}$ . Since the  $\hat{k}_\alpha$  grow linearly it follows that  $r = 0$  and hence all  $\hat{k}_\alpha$  are equal to some common value  $\hat{K}$ .

This “balanced” motion of the D6-branes maps the system to one very similar to that of the previous section. We will consider the other possible distributions of D6-branes to the left and right in the next section, but for the remainder of this section we focus on the canonical choice. The curve (3.89) is then a special case of (3.46), where  $q_\alpha(v)$  are of the form  $\hat{g}_\alpha(v)$ . As before we can rearrange  $\hat{F}(t, v)$  to be a polynomial in  $v$  of order  $\hat{K}$ , of the form (3.45):

$$\hat{F}(t, v) = v^{\hat{K}} \prod_{\alpha=0}^n (t - t_\alpha) + \sum_{i=1}^{\hat{K}} v^{\hat{K}-i} p_i(t) \quad (3.96)$$

Dividing by  $\prod_{\alpha=0}^n (t - t_\alpha)$  we produce a monic polynomial in  $v$  with coefficients  $R_i(t) = \frac{p_i(t)}{\prod_{\alpha=0}^n (t - t_\alpha)}$  which are rational functions of  $t$ . We now interpret this as the equation for a spectral curve

$$\det(v - t\varphi_t) = v^{\hat{K}} + \sum_{i=1}^{\hat{K}} v^{\hat{K}-i} R_i(t) \quad (3.97)$$

where the Higgs field  $\varphi_t$  is in  $u(\hat{K})$ . Our goal is now to understand what the special structure of the coefficients  $\hat{g}_\alpha(v)$  implies about the boundary conditions on the Higgs field  $\varphi_t$  at the defects.

Accordingly, let us analyze the behavior of the  $\hat{K}$  roots  $v_i(t)$  of (3.89). Since there are  $n+1$  roots  $t(v)$  for  $t$  as a function of  $v$ , and since  $v$  can freely go to infinity, there must be  $(n+1)$  values  $t_\alpha$  at which  $v \rightarrow \infty$ . Generically,  $v$  will have a simple pole at  $t_\alpha$ . These simple poles imply that, (after shifting away the center of mass),  $\varphi_t$  has a first order pole with residue exactly as in (3.76). This is just the situation we had before.

On the other hand, the behavior of the roots when  $t \rightarrow 0$  or  $t \rightarrow \infty$  requires a refinement of our earlier analysis. For  $t \rightarrow 0$  the roots tend to the roots of  $\hat{g}_{n+1}(v)$  while for  $t \rightarrow \infty$  they tend to those of  $\hat{g}_0(v)$ . These roots are all at finite values of  $v$ . However, the factors of  $J_{\beta,L}$  with  $\beta > 1$  in  $\hat{g}_0$  (and those of  $J_{\beta,R}$  with  $\beta < n+1$  in  $\hat{g}_{n+1}$ ) lead to multiple roots. In general, the existence of multiple roots of the coefficient  $q_0(v)$  (or  $q_{n+1}(v)$ ) in (3.46) means that several D4-branes end on the same D6-brane. Now, there is an important distinction between the multiple roots obtained by moving several D6-branes attached to a single D4-brane to the same  $v$ -coordinate, and the multiple roots resulting from the Hanany-Witten effect. In the former case, the roots of  $q_0(v)$  are in general different from the roots of  $q_\alpha(v)$  for  $\alpha > 1$ . In the latter case, the structure of (3.90) et. seq. shows that the multiple roots from the factor  $J_{\beta,L}$  are also (multiple) roots of  $\hat{g}_\alpha$  for  $\alpha < \beta$ . Thus, in general, as  $t \rightarrow \infty$ , if  $q_0(v)$  has a root  $v_*$  of order  $\beta$ , and  $v_*$  is not a root of  $q_1(v)$ , then  $\beta$  roots  $v_i(t)$  behave like

$$v_i(t) \rightarrow v_* + \frac{\xi_i}{t^{1/\beta}} + \dots \quad (3.98)$$

as  $t \rightarrow \infty$ , where  $\xi_i$  are constants independent of  $t, v$ . On the other hand, in the case of multiple roots arising from the factors  $J_{\beta,L}$  in (3.90) the analogous set of  $\beta$  roots  $v_i(t)$  behave like

$$v_i(t) \rightarrow v_* + \frac{\xi_i}{t} + \mathcal{O}(t^{-2}) \quad (3.99)$$

Analogous statements hold for the behavior of the roots associated with D6-branes on the right, for  $t \rightarrow 0$ .

The behavior of the roots  $v(t)$  for  $t \rightarrow \infty$  we have just described have implications for the boundary conditions of the Higgs field  $\varphi_t dt$  as  $t \rightarrow \infty$ . This Higgs field will behave like

$$\varphi_t \rightarrow \frac{R}{t} + \frac{R_2}{t^2} + \dots \quad (3.100)$$

Equating  $\hat{F}(t, v) = \hat{g}_0(v)t^{n+1} + \dots$  with  $\prod_0^n (t - t_\alpha) \det(v - t\varphi_t)$ , and taking  $t \rightarrow \infty$ , we see that the characteristic polynomial of the residue  $R = t\varphi_t|_{t=\infty}$  is just  $\det(v - R) = \hat{g}_0(v)$ . Since this has multiple roots we must consider the possibility that  $R$  has nontrivial Jordan form.

We now claim that a nontrivial Jordan form leads to roots behaving like (3.98) while if  $R$  is semisimple then the roots will behave like (3.99). We may prove this as follows. For simplicity suppose that the characteristic polynomial  $\det(v - R) = v^\beta$  for some integer  $\beta > 1$ . Now consider the perturbation  $R(t) = R + C/t$  where  $t$  is large and  $C$  is *generic*. If  $R$  is semisimple, then  $R = 0$  and the eigenvalues of  $R(t)$  are  $c_i/t$  where  $c_i$  are the distinct eigenvalues of  $C$ . At the other extreme, suppose  $R$  is a Jordan block of size  $\beta$ , which we denote as  $N_\beta$ .<sup>25</sup> By a gauge transformation with  $g = \exp[\epsilon/t]$  we can bring  $R(t)$  to the

<sup>25</sup>i.e  $N_\beta = e_{1,2} + e_{2,3} + \dots + e_{\beta-1,\beta}$  in terms of matrix units.

form

$$R(t) \rightarrow N_\beta + \frac{1}{t} \left( \sum_{i=1}^{\beta} \mu_i e_{\beta,i} \right) + \mathcal{O}(1/t^2) \quad (3.101)$$

for some constants  $\mu_i$ . Here  $e_{i,j}$  is the matrix unit, that is, the matrix whose only nonzero entry is 1 in the  $i^{\text{th}}$  row and  $j^{\text{th}}$  column. On the other hand,

$$\det \left[ v - N_\beta - \frac{1}{t} \left( \sum_{i=1}^{\beta} \mu_i e_{\beta,i} \right) \right] = v^\beta + \frac{\mu_\beta}{t} v^{\beta-1} + \frac{\mu_{\beta-1}}{t} v^{\beta-2} + \dots + \frac{\mu_1}{t} \quad (3.102)$$

From the standard relation between the elementary symmetric functions and the power sum functions it follows that the roots  $v_i \sim c_i t^{-1/\beta} + \mathcal{O}(t^{-2/\beta})$ . In the intermediate cases, when  $R$  has several Jordan blocks the roots will fall off with a fractional power of  $t$  with the fractional power governed by the largest Jordan block of  $R$ .

The upshot is that the boundary condition for the Higgs field at  $t \rightarrow \infty$  has the block diagonal form:

$$\varphi_t dt \rightarrow \frac{dt}{t} \text{Diag} \{ \dots v_1^{(\beta)} 1_\beta, \dots, v_{d_{\beta,L}}^{(\beta)} 1_\beta, \dots \} + \mathcal{O}(t^{-2}) \quad (3.103)$$

where  $1_\beta$  is the diagonal matrix and  $v_1^{(\beta)}, \dots, v_{d_{\beta,L}}^{(\beta)}$  are the roots of  $J_{\beta,L}$  (assumed distinct, for simplicity). Put more simply, the boundary conditions preserve a subgroup

$$\prod_{\beta=1}^n (U(\beta))^{d_{\beta,L}} \quad (3.104)$$

of the  $U(\hat{K})$  gauge group. Entirely parallel remarks apply to the limit  $t \rightarrow 0$  and the group of branes on the right.

In conclusion, the conformal linear quivers of unitary groups give rise to Hitchin systems on  $\mathbb{CP}^1$  with two regular singularities of a generic type, labeled by two partitions of  $K$ ,  $K = \sum \beta d_{\beta,L}$  and  $K = \sum \beta d_{\beta,R}$ , and an arbitrary number of “basic” singularities, associated to the partition  $K = (1) + (K-1)$ .

### 3.2.6 Brane-bending and irregular singularities

We continue to study the conformally invariant linear quiver of the previous subsection but now consider the case where we move the D6-branes in an “unbalanced” way so that  $\hat{k}_{n+1} - \hat{k}_0$  is nonzero.

The behavior of the roots is now dramatically different. Recall that the order of  $\hat{g}_\alpha$  is  $\hat{k}_\alpha = \hat{k}_0 + \alpha r$ . For simplicity assume that  $r > 0$ , so that, by (3.95)  $\hat{g}_{n+1} = c_{n+1} v^{\hat{k}_{n+1}} + \dots$  has the highest power of  $v$ . Then, since  $\hat{g}_{n+1}$  dominates all the other coefficients  $\hat{g}_\alpha(v)$  for  $v \rightarrow \infty$  it follows that none of the roots  $v(t)$  go to infinity at finite values of  $t$ .

The fact that there are only two singular points in  $t$  can also be seen more physically by considering the  $U(1)_R$  symmetry of the theory. This symmetry rotates  $v \rightarrow e^{i\theta} v$ , and hence changes the masses  $v_a \rightarrow e^{i\theta} v_a$ . However, it must not change the coupling constants, and therefore  $c_\alpha \rightarrow c_\alpha$ . In the balanced case the curve  $\hat{F}(t, v) = 0$  is invariant under this

scaling with fixed  $t$ . On the other hand, in the unbalanced case this is not true and we must rescale  $(t, v) \rightarrow (e^{ir\theta}t, e^{i\theta}v)$ . Then, a singularity at a finite point  $t_\alpha \in \mathbb{C}^\times$  would be incompatible with the equation.

Next, let us consider the roots for  $t \rightarrow 0$ . Here  $v_i(t)$  simply approaches the  $\hat{k}_{n+1}$  roots of  $\hat{g}_{n+1}(v)$  and as we have discussed, they behave like  $v_i(t) = v_i + \xi_{i,s}t + \dots$ .

On the other hand, the behavior of the roots at  $t \rightarrow \infty$  is more complex. There are  $\hat{k}_0$  roots behaving like  $v_i(t) \rightarrow v_i + \frac{\xi_{i,a}}{t} + \mathcal{O}(1/t^2)$  where  $v_i$  are the roots of  $\hat{g}_0(v)$ . Since  $\hat{k}_{n+1} > \hat{k}_0$  this does not account for all the roots. In addition, there are  $(n+1)r$  roots where  $t, v$  both go to infinity. In this case, keeping the leading order terms in  $\hat{F}(t, v)$ , we see that the roots with  $(t, v)$  both going to infinity must asymptote to the roots of

$$0 = c_{n+1}v^{(n+1)r} + c_n tv^{nr} + \dots + c_1 t^n v^r + c_0 t^{n+1} := c_{n+1} \prod_{i=1}^{n+1} (v^r - \nu_i t). \quad (3.105)$$

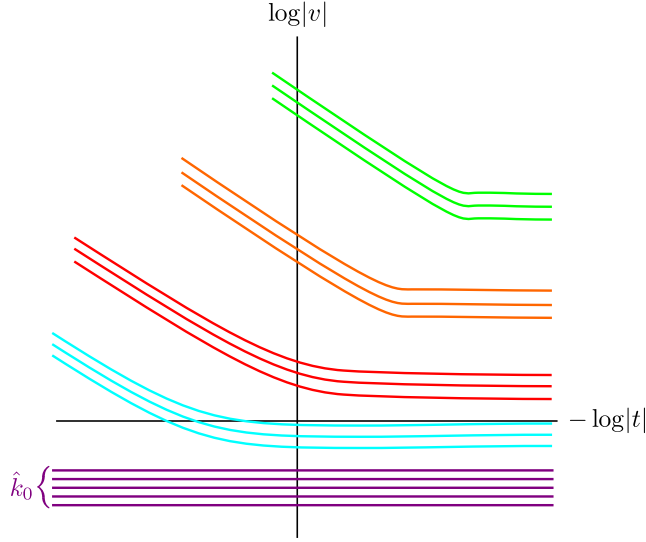


**Figure 8:** Brane bending in the conformal but unbalanced case when  $\hat{k}_{n+1} - \hat{k}_0 = (n+1)r > 0$ . Note that  $n+1$  bundles of  $r$  branes go to infinity as  $t \rightarrow \infty$ . Here  $r = 3$  and  $n+1 = 4$ . There are  $\hat{k}_{n+1} = 17$  horizontal branes at  $t \rightarrow 0$ .

Note that we have now found the phenomenon of “brane bending”: some of the roots  $v(t)$  go to infinity as  $t \rightarrow \infty$ . To picture the situation note that the projection of  $\Sigma$  into the  $(-\log|t|, \log|v|)$  plane asymptotes to the form shown in Figure 8.

Now let us consider the mapping to a Hitchin system. In this case we identify the characteristic polynomial of the Higgs field according to

$$\det(v - t\varphi_t) = \frac{1}{c_{n+1}} (\hat{g}_{n+1}(v) + t\hat{g}_n(v) + \dots + t^{n+1}\hat{g}_0(v)) \quad (3.106)$$

where  $\varphi_t \in u(\hat{k}_{n+1})$ . From our discussion of the roots above, all the singularities of the Higgs field must lie at  $t = 0$  or  $t = \infty$ . Our previous discussion applies to the roots at  $t \rightarrow 0$  and hence  $\varphi_t$  has a regular singularity at  $t \rightarrow 0$  as in (3.103).

By contrast, for  $t \rightarrow \infty$  we find that  $\varphi_t$  has a block diagonal form. There is a  $\hat{k}_0 \times \hat{k}_0$  block corresponding to a regular singularity with residues given by the roots of  $\hat{g}_0(v)$ . We interpret (3.105) to imply that in addition there are  $(n+1)$  blocks, labeled by  $i = 1, \dots, n+1$  with limiting behavior

$$\det(v - t\varphi_t) \sim v^r - \nu_i t. \quad (3.107)$$

(The matrices are understood to be restricted to the  $i^{th}$  block. We do not indicate this to avoid cluttering the notation.) Thus, in the unbalanced case, the boundary condition at  $t \rightarrow \infty$  corresponds to an *irregular singularity*, with  $(n+1)r$  eigenvalues of  $t\varphi_t$  behaving like

$$\omega^s(\nu_i t)^{\frac{1}{r}}(1 + \mathcal{O}(1/t)) \quad s = 1, \dots, r; \quad i = 1, \dots, n+1, \quad (3.108)$$

where  $\omega$  is a primitive  $r^{th}$  root of unity.

We can also consider the opposite case  $\hat{k}_0 > \hat{k}_{n+1}$ . For this case we reverse the sign of  $r$  and take  $r = (\hat{k}_0 - \hat{k}_{n+1})/(n+1) > 0$ . In this case  $t\varphi_t$  has a regular singularity at  $t \rightarrow \infty$  and an irregular one at  $t \rightarrow 0$ . The irregular singularity involves  $(n+1)$  blocks, each with eigenvalues

$$\omega^s\left(\frac{\nu_i}{t}\right)^{\frac{1}{r}}(1 + \mathcal{O}(t)) \quad s = 1, \dots, r; \quad i = 1, \dots, n+1 \quad (3.109)$$

where  $\omega$  is a primitive  $r^{th}$  root of unity.

Let us now discuss what these conditions mean for the behavior of the Higgs field  $\varphi_t$  at  $t \rightarrow 0, \infty$ . We focus on  $t \rightarrow 0$  and take  $r = (\hat{k}_0 - \hat{k}_{n+1})/(n+1) > 0$ . Using (3.102) we see that by a *complex* gauge transformation we can put  $\varphi_t$  in the form

$$\varphi_t \rightarrow \frac{1}{t} \left( \frac{\nu_i}{t} e_{r1} + N_r + \mathcal{O}(t) \right) \quad t \rightarrow 0 \quad (3.110)$$

However, to define the Hitchin system properly we must specify an actual solution to the Hitchin equations at  $t \rightarrow 0$ . We can do this block by block. For the blocks corresponding to the irregular singularity it is easy to give such a solution in the diagonal gauge,

$$\varphi_t = \frac{1}{t} \left( \frac{\nu_i}{t} \right)^{1/r} \text{Diag}\{\omega, \omega^2, \dots, \omega^r\} \quad (3.111)$$

The problem is that this is not single-valued. We can make  $\varphi_t$  single-valued by a singular gauge transformation

$$g = \eta S \eta^{-1} \quad (3.112)$$

with  $S_{ab} = \frac{1}{\sqrt{r}} e^{\frac{2\pi i}{r} ab}$  and  $\eta$  is given by

$$\eta = \left( \frac{t}{\bar{t}} \right)^{\frac{r-1}{4r}} \text{Diag}\left\{ 1, \left( \frac{\bar{t}}{t} \right)^{\frac{1}{2r}}, \left( \frac{\bar{t}}{t} \right)^{\frac{2}{2r}}, \dots, \left( \frac{\bar{t}}{t} \right)^{\frac{r-1}{2r}} \right\} \quad (3.113)$$

In order to keep the gauge field single valued we take

$$A = -d\eta \eta^{-1} \quad (3.114)$$

in diagonal gauge and the upshot is that our single-valued asymptotic solution of the Hitchin equations (for the  $i^{\text{th}}$  block) is

$$\varphi_t \rightarrow \frac{\nu_i^{1/r}}{t} \frac{1}{|t|^{1/r}} \left( \frac{\bar{t}}{|t|} e_{r1} + N_r + \mathcal{O}(t) \right) \quad (3.115)$$

with

$$A = \left( \sum_{j=1}^r \frac{2(j-1) - (r-1)}{4r} e_{jj} \right) \left( \frac{dt}{t} - \frac{d\bar{t}}{\bar{t}} \right). \quad (3.116)$$

### 3.2.7 The asymptotically free case

Let us finally turn to the general asymptotically free quiver with fundamental matter. For such a quiver the  $\beta$ -function coefficients  $b_\alpha \leq 0$ ,  $1 \leq \alpha \leq n$ , and  $b_\alpha < 0$  for at least one value of  $\alpha$ . Physically, such quiver gauge theories can be obtained by decoupling fundamental fields in a conformal linear quiver by taking the masses of some of the fundamental fields to infinity. They then decouple, leaving an asymptotically free theory.

The decoupling procedure can be elegantly carried out at the level of Seiberg-Witten curves. In each interval  $I_\alpha$  we choose a set of centers  $v_a$ ,  $a \in S_\alpha$  which we will send to infinity. We then scale  $c_\alpha \rightarrow 0$  in such a way as to leave the coefficients  $A_\alpha(v)$  in eq. (3.83) finite. However, since we are most interested here in the application to Hitchin systems we consider the decoupling limit *after* we have moved the D6-branes to large values of  $|x_a^6|$ . Therefore, we split the set  $S_\alpha = S_{\alpha,L} \amalg S_{\alpha,R}$  according to whether the D6 to be decoupled has first moved to the far left or the far right. In this limit we have

$$J_{\alpha,L}(v) \rightarrow \check{J}_{\alpha,L}(v) \prod_{a \in S_{\alpha,L}} (-v_a)(1 + \mathcal{O}(v/v_a)), \quad (3.117)$$

where  $\check{J}_{\alpha,L}(v)$  are the factors for the D6-branes not taken to infinity, and similarly for  $J_{\alpha,R}$ . Thus, we send  $c_\alpha$  to zero in such a way that

$$\check{c}_\alpha = c_\alpha \prod_{\beta=1}^{\alpha} \left( \prod_{a \in S_{\beta,R}} (-v_a) \right)^{\alpha-\beta} \prod_{\beta=\alpha+1}^n \left( \prod_{a \in S_{\beta,L}} (-v_a) \right)^{\beta-\alpha} \quad (3.118)$$

remains finite. We now have the analogs of eqs. (3.89) and (3.90):

$$\check{F}(t, v) = \sum_{\alpha=0}^{n+1} \check{g}_\alpha(v) t^{n+1-\alpha} \quad (3.119)$$

where

$$\check{g}_0(v) = \check{c}_0 \prod_{\beta=1}^n \check{J}_{\beta,L}^{\beta} \quad (3.120)$$

$$\check{g}_{\alpha}(v) = \check{c}_{\alpha} g_{\alpha}(v) \prod_{\beta=1}^{\alpha} \check{J}_{\beta,R}^{\alpha-\beta} \prod_{\beta=\alpha+1}^n \check{J}_{\beta,L}^{\beta-\alpha} \quad \alpha = 1, \dots, n-1, \quad (3.121)$$

$$\check{g}_n(v) = \check{c}_n g_n(v) \prod_{\beta=1}^n \check{J}_{\beta,R}^{\alpha-\beta}, \quad (3.122)$$

$$\check{g}_{n+1}(v) = \check{c}_{n+1} \prod_{\beta=1}^n \check{J}_{R,\beta}^{n+1-\beta}. \quad (3.123)$$

The only difference from the previous case is that now  $\check{b}_{\alpha} = -2\check{k}_{\alpha} + \check{k}_{\alpha+1} + \check{k}_{\alpha-1}$  is  $\leq 0$  for all  $1 \leq \alpha \leq n$  and can be strictly less than zero. Here  $\check{k}_{\alpha}$  is the order of  $\check{g}_{\alpha}$ .

Again referring to Appendix E the points  $(\alpha, \check{k}_{\alpha})$  define a convex polygonal curve. The  $\check{k}_{\alpha}$  are strictly increasing for  $0 \leq \alpha \leq \alpha_-$ . The maximal value  $\check{K} := \check{k}_{\alpha_-}$  is attained for  $\alpha_- \leq \alpha \leq \alpha_+$ . Thereafter the  $\check{k}_{\alpha}$  are strictly decreasing for  $\alpha \geq \alpha_+$ . If  $\check{k}_1 - \check{k}_0 = 0$  then  $\alpha_- = 0$  and if  $\check{k}_1 - \check{k}_0 < 0$  then  $\alpha_+ = 0$ . For simplicity, in what follows we will just describe the case  $\check{k}_1 - \check{k}_0 > 0$ .

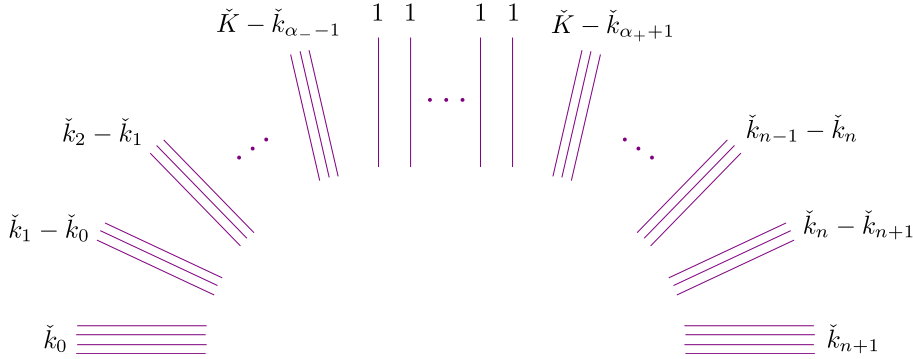


**Figure 9:** The boundary of the Newton polygon of  $\check{F}(t, v)$  dictates the asymptotic behavior of the M5-brane curve. Here it is projected on the  $(-\log|t|, \log|v|)$  plane.

Now the polygonal path can be viewed as the boundary of the Newton polytope for  $\check{F}(t, v)$ . Accordingly, we can extract the asymptotic behavior of the roots of the equation  $\check{F}(t, v) = 0$ . To do this we balance terms on the boundary faces of the polytope. Assuming, for simplicity, that a face consists of a single segment we have:

$$\check{c}_{\alpha} t^{n+1-\alpha} v^{\check{k}_{\alpha}} + \check{c}_{\alpha+1} t^{n-\alpha} v^{\check{k}_{\alpha+1}} \cong 0 \quad (3.124)$$

for  $0 \leq \alpha \leq \alpha_- - 1$  or  $\alpha_+ \leq \alpha \leq n$ . Each value of  $\alpha$  gives  $|\check{k}_{\alpha+1} - \check{k}_{\alpha}|$  roots  $v(t)$  asymptotic to

$$t \cong -\frac{\check{c}_{\alpha+1}}{\check{c}_{\alpha}} v^{(\check{k}_{\alpha+1} - \check{k}_{\alpha})} \quad (3.125)$$

For these roots  $v(t) \rightarrow \infty$  with  $t \rightarrow \infty$  for  $0 \leq \alpha \leq \alpha_- - 1$  and  $t \rightarrow 0$  for  $\alpha_+ \leq \alpha \leq n$ , respectively. The remaining roots at  $t \rightarrow \infty$  and  $t \rightarrow 0$  are the roots of  $\check{g}_0(v)$  and  $\check{g}_{n+1}(v)$ ,



respectively. These latter roots remain finite. In addition, if  $\alpha_+ > \alpha_-$  then at the roots  $t \in \mathbb{C}^\times$  of

$$\sum_{\alpha=\alpha_-}^{\alpha_+} \check{c}_\alpha t^{\alpha_+-\alpha} = 0 \quad (3.126)$$

we have  $\alpha_+ - \alpha_-$  roots  $v(t)$  going to infinity. Generically, these will be simple poles  $v(t) \sim \frac{\rho_\alpha}{t-t_\alpha}$ .<sup>26</sup> In this way the boundary of the Newton polygon dictates the asymptotic shape of the M5-branes. This is illustrated in Figure 9.

The physical interpretation of the constants  $\check{c}_\alpha$  can now be deduced from the above pictures. Consecutive branches of the M5 surface measured at the same value of  $v$  have corresponding values of  $t$  related by

$$\frac{t^{(\alpha+1)}}{t^{(\alpha)}} \simeq \frac{\check{c}_{\alpha+1}\check{c}_{\alpha-1}}{\check{c}_\alpha^2} v^{\check{b}_\alpha} \quad (3.127)$$

In the weak coupling limit we have seen that  $\log |\frac{t^{(\alpha)}}{t^{(\alpha+1)}}|$  should be interpreted as an inverse coupling constant. Thus, for  $\check{b}_\alpha < 0$  we see that it is logarithmically running with scale  $|v|$ , and moreover the UV cutoff scale is

$$\Lambda^{-\check{b}_\alpha} = \frac{\check{c}_{\alpha+1}\check{c}_{\alpha-1}}{\check{c}_\alpha^2} \quad (3.128)$$

while for  $\check{b}_\alpha = 0$  the combination  $\frac{\check{c}_{\alpha+1}\check{c}_{\alpha-1}}{\check{c}_\alpha^2}$  encodes the UV couplings, as before.

Now we are ready to describe the relevant Hitchin system. This is a  $U(\check{K})$  system with singularities at  $t = 0, \infty$ , as well as singularities at the roots of (3.126). At the latter singularities  $\varphi_t$  has a regular singularity. At  $t \rightarrow \infty$ ,  $\varphi_t$  has block diagonal form. There is a regular singular block with residues given by the roots of  $\check{g}_0(v)$ . In addition there are  $\alpha_-$  blocks of irregular singularities of the form (3.115) where we should substitute  $r = \check{k}_{\alpha+1} - \check{k}_\alpha$  and  $\nu_i = -\check{c}_\alpha/\check{c}_{\alpha+1}$ ,  $0 \leq \alpha \leq \alpha_- - 1$ . Similarly, at  $t = 0$  there is a block of regular singular points governed by the roots of  $\check{g}_{n+1}(v)$  and  $n+1-\alpha_+$  blocks of irregular singular points of the form (3.115) with  $r = \check{k}_\alpha - \check{k}_{\alpha+1}$  and  $\nu_i = -\check{c}_\alpha/\check{c}_{\alpha+1}$ ,  $\alpha_+ \leq \alpha \leq n$ .

The large mass limit leading to irregular singularities can be carried out directly at the level of the Hitchin system. For example, consider the  $\epsilon \rightarrow 0$  limit of the Higgs field:

$$\frac{1}{t} \begin{pmatrix} 0 & 1/2 \\ -\rho/\epsilon & 0 \end{pmatrix} + \frac{1}{t-\epsilon} \begin{pmatrix} 0 & 1/2 \\ \rho/\epsilon & 0 \end{pmatrix} \quad (3.129)$$

For fixed  $\epsilon$  there are two regular singular points. However, for  $\epsilon \rightarrow 0$  the Higgs field develops an irregular singular point of the type we have described.

The simplest example of the above constructions is  $n = 1$ , with  $\check{K} = 2$ . This is a  $U(2)$  theory with  $d_1 = N_f$  fundamental flavors. If  $N_f = 0$ , then  $\check{k}_0 = 0, \check{k}_1 = 2, \check{k}_2 = 0$ , so  $\check{b}_1 = -4$ . The curve (3.119) is  $\check{c}_0 t^2 + \check{c}_1 t(v^2 - u) + \check{c}_2 = 0$  and, after a rescaling of  $t$ , the curve becomes the standard  $SU(2)$  Seiberg-Witten curve

$$v^2 - u - t - \frac{\Lambda^4}{t} = 0, \quad (3.130)$$

---

<sup>26</sup>The  $U(1)_R$  symmetry forbidding these roots in the conformal case is anomalous here.

and hence  $t^2\lambda^2 = \left(u + t + \frac{\Lambda^4}{t}\right)(dt)^2$  where  $\pm\lambda$  are the eigenvalues of  $\varphi_t dt$ . The boundary conditions on the Higgs field state that, up to gauge equivalence,

$$\varphi_t dt \rightarrow \frac{\Lambda^2}{|t|^{1/2}} \begin{pmatrix} 0 & 1 \\ e^{-i\theta} & 0 \end{pmatrix} \frac{dt}{t} \quad t \rightarrow 0 \quad (3.131)$$

$$\varphi_t dt \rightarrow -|t|^{1/2} \begin{pmatrix} 0 & 1 \\ e^{i\theta} & 0 \end{pmatrix} \frac{dt}{t} \quad t \rightarrow \infty \quad (3.132)$$

where  $t = |t|e^{i\theta}$ . We will discuss this example in great detail in Section 10.

### 3.2.8 A surprising isomorphism

We can make a surprising mathematical prediction based on our physical setup. Since the IR fixed point is independent of the motion of the D6-branes, the different Hitchin moduli spaces obtained from different distributions of the D6-branes to the left and the right must be isomorphic!

Put more precisely, begin with the polynomial  $\tilde{F}(W, v)$  of equation (3.86). Then, as described in equations (3.88) et. seq., consider the different polynomials  $\hat{F}(t, v)$  arising from the different movements of the D6-branes to left and right. The resulting polynomials can be interpreted as spectral curves for a  $U(\hat{K})$  Hitchin system where  $\hat{K} = \max[\hat{k}_0, \hat{k}_{n+1}]$ , as we have explained. From these polynomials we can read off the boundary conditions for the Higgs field on  $\mathbb{C}^\times$ . Physics predicts that the resulting moduli spaces are isomorphic as hyperkähler manifolds. We will see one explicit example in Section 10. Examples of this phenomenon have very recently appeared in the mathematical literature as well [4].

Our methods offer a strategy for proving the isomorphism between these hyperkähler moduli spaces: the spectral curves of the different Hitchin systems are isomorphic (although not as fibrations  $\Sigma \rightarrow C$ ), so the semiflat limits  $g^{\text{sf}}$  of the hyperkähler metrics coincide. As soon as the BPS spectra are also found to be the same, the Riemann-Hilbert problems of [1] coincide, and hence so do the hyperkähler metrics.

### 3.2.9 Non-Abelian flavor symmetries and punctures

The relation with the linear quivers has suggested that each puncture on  $C$ , i.e. each defect in the six-dimensional  $(2, 0)$  theory, is associated with a certain flavor (sub)group of the resulting four-dimensional  $\mathcal{N} = 2$  theory. The defects which lead to the most general regular singularity for the  $SU(K)$  Hitchin system are associated to the  $K - 1$  mass parameters in the Cartan of an  $SU(K)$  flavor group. The simplest defects which break the  $SU(K)$  gauge symmetries to  $S(U(1) \times U(K - 1))$  are instead associated to the mass parameters of some  $U(1)$  flavor group (unless  $K = 2$ , in which case the two types of singularity are identical, and indeed the  $U(1)$  is enhanced to  $SU(2)$ ). We already met examples of regular singularities with a generic pattern of gauge symmetry breaking  $S(\prod U(\beta)^{d_\beta})$  labeled by a partition of  $K$ ,  $d_\beta$ , in equation (3.103). They have a single mass parameter for each  $U(\beta)$  gauge factor. It can be shown easily [15] that a non-Abelian flavor symmetry  $S(\prod U(d_\beta))$  is associated with these singularities.

In later sections of this paper we mostly focus on the  $K = 2$  case, but here we briefly digress to see how the non-Abelian  $SU(K)$  flavor symmetries manifest themselves in the spectrum of BPS string webs whenever the mass parameters at the corresponding singularity in  $C$  go to zero.

Consider first the case  $K = 2$ . Then we can take a local coordinate  $z$  near the singularity and

$$\lambda^2 \sim \left( \frac{m^2}{z^2} + \frac{u}{z} + \cdots \right) dz^2. \quad (3.133)$$

As we tune  $m \rightarrow 0$  a zero of  $\lambda^2$  must be coming close to the double pole, to reduce it to a single pole. What is the behavior of BPS strings near such a “molecule” made up of a singularity and a zero? We know that the BPS strings follow curves of constant phase  $\vartheta$  for the 1-form  $\lambda_{12} = \lambda - (-\lambda) = 2\lambda$ . For a given value of  $\vartheta$ , three such curves emanate from the branch point (this important general fact will be discussed at length in Section 6). One plunges into the singularity, while the other two wind around the singularity in opposite directions and escape together.

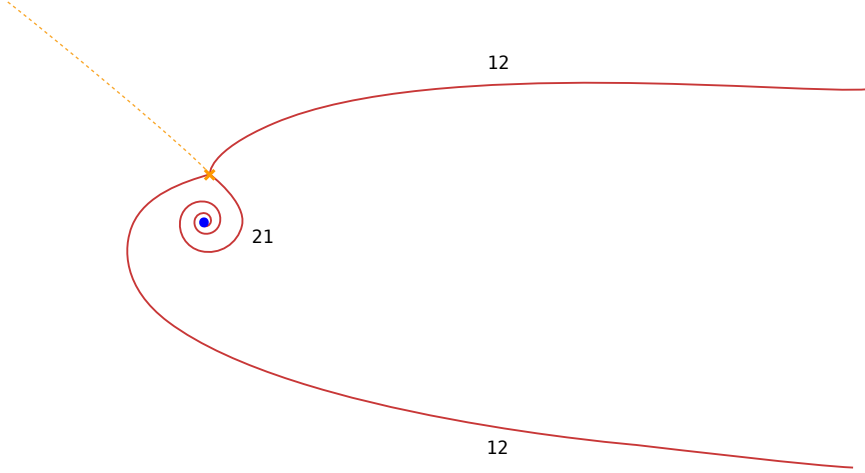


**Figure 10:** The pattern of flow lines (red) around a molecule consisting of a nearly-coincident double pole (blue dot) and zero (orange cross) of  $\lambda^2$ . Three lines emanate from the zero for each value of the phase  $\vartheta$ . If we choose the (orange dotted) branch cut in  $\lambda$  as depicted, the lines flowing from the zero correspond to BPS strings of type 12, 21, as labeled.



**Figure 11:** For two nearby values of the phase  $\vartheta$  the two flow lines which escape from the molecule may hit another turning point, giving rise to a doublet of BPS hypermultiplets.

As we vary the phase  $\vartheta$  of the central charge, this doublet of escaping lines will swipe across other zeroes of  $\lambda^2$ . This gives rise to a pair of BPS strings, which join the same two branch points, but pass on opposite sides of the singularity, as shown in Figure 11. The

central charges of the BPS particles differ by the period of  $2\lambda$  around the singularity, i.e. by  $2m$ . The fact that for small enough  $m$  BPS states always come in doublets of flavor charge  $\pm 1$  is a clear symptom of the presence of an  $SU(2)$  flavor symmetry associated to each regular singularity in the  $K = 2$  case, and predicts that the BPS states transform in doublets of these important  $SU(2)$  flavor (sub)groups. We will see in our examples of  $SU(2)$  gauge theories how the  $SU(2)$  groups are always embedded in the full flavor symmetry group in such a way that this condition is satisfied.

In the cases with  $K > 2$  it is important to consider string webs.  $K = 3$  will be sufficient to illustrate this point. Locally we have

$$\lambda^3 \sim \left( \frac{\sum m_i m_j}{z^2} + \frac{u}{z} + \dots \right) dz^2 \lambda + \left( \frac{\prod m_i}{z^3} + \frac{v}{z^2} + \dots \right) dz^3 \quad (3.134)$$

Different sheets of  $\lambda$  meet at the zeroes of the discriminant of this equation. The discriminant has a degree 6 pole, which reduces to 4 when the masses are turned off, hence we expect to see two branch points come close to the singularity. It is easy to see they must be branch points of different type, say for the sheets 12 and 13. For a given value of  $\vartheta$ , three lines emanate out of each branch point. One line emerging from each branch point flows into the singularity. A second goes around the singularity and the other branch point, and turns into a 23 line. These two 23 lines then escape together. The third pair of lines will intersect, and we can set a string junction at the intersection, from which a third 23 line escapes, close to the other two.

Again, as we vary the phase  $\vartheta$  of the central charge, this triplet of lines may swipe across a branch point of the 23 type and give rise to a triplet of BPS strings (or, more generally, may be connected through junctions to give a triplet of string webs). This triplet of states carry the same gauge charges, while their central charges differ pairwise by  $m_1 - m_2$ ,  $m_1 - m_3$ ,  $m_2 - m_3$  because they wind in different ways around the singularity. These states thus form a triplet for the  $SU(3)$  flavor symmetry associated with the singularity.

### 3.3 Type IIB construction

The M-theory realization of our theories which we use in Section 3.1 gives a convenient geometric way of understanding many properties of the theory quickly, but may be unfamiliar for the reader who is motivated by Donaldson-Thomas invariants or categories of D-branes on Calabi-Yau threefolds. In this section we briefly recall an alternative perspective on our construction.

The essential point is that the  $(2, 0)$  theory arises in Type IIB string theory on an ADE singularity [19]. Therefore, to compactify this theory on  $C$  we can consider Type IIB on a Calabi-Yau threefold which in an appropriate scaling limit develops a curve  $C$  of ADE singularities. The scaling limit decouples gravity and leaves us with the desired  $\mathcal{N} = 2$  field theory. (See [52] for a detailed construction.) The BPS states of this theory arise from D3-branes wrapping special Lagrangian cycles. In the scaling limit such cycles are obtained as fibrations of the vanishing spheres of the ADE singularity over string webs in  $C$ , which are identified with the BPS webs we considered above.

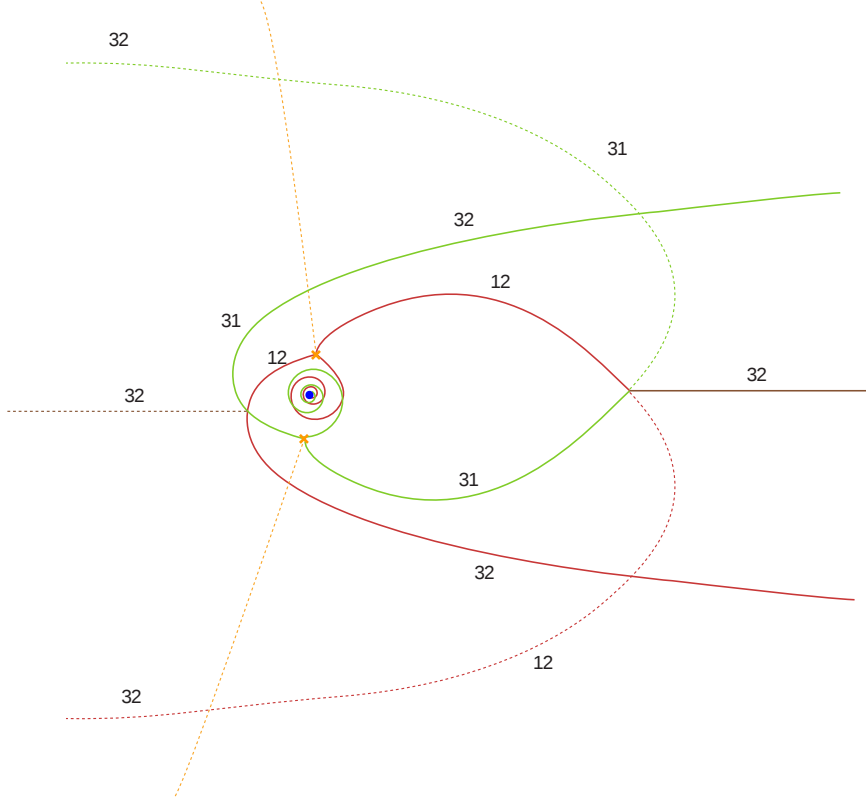


**Figure 12:** The pattern of flow lines (red, green, continuous or dotted) in a region where a singularity (blue dot) and two zeroes of the discriminant (orange dots) come close. Three lines emanate from each zero for every value of the phase  $\vartheta$ . We take the zeroes to be of the type 12 and 13. If we put the (orange dotted) cuts in  $\lambda$  as depicted, the lines flowing from the zeros correspond to BPS strings of the indicated type. When two lines of compatible type intersect, we allow for a possible web junction. All in all, for every value of  $\vartheta$ , two groups of three lines of the same type flow away from the molecule.

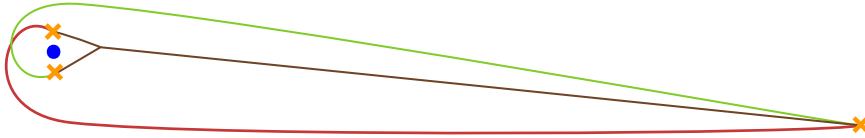


**Figure 13:** For nearby values of the phase  $\vartheta$ , a group of three flow lines escaping from the molecule may hit another turning point, giving rise to a triplet of BPS hypermultiplets.

For example, in the  $A$  case, the integral of the holomorphic three form over the  $ij$ -th vanishing sphere is identified with the differential  $\lambda_{ij}$  on  $C$ . A simple  $ij$ -string stretched between two turning points where  $\lambda_{ij} = 0$  lifts to a special Lagrangian with the topology  $S^3$ : an  $S^2$  fibered over a segment, shrinking at the endpoints. A closed  $ij$ -string wrapping a non-trivial cycle of  $C$  lifts to a special Lagrangian with the topology  $S^1 \times S^2$ .

It would be interesting to take inspiration from this correspondence, and develop a mathematical definition of some sort of Fukaya category of string webs on a Riemann surface  $C$ , with stability conditions specified by a spectral curve  $\Sigma \subset T^*C$ . This would

allow a more direct connection to the work of [6]. We make some tentative comments in this direction in Section 12.

## 4. Hitchin systems

In Section 3 we have given an extended review and discussion of the physical motivations for studying a certain class of Hitchin systems. In this section we summarize the mathematics problem motivated by this discussion, and fill in some standard facts about the hyperkähler geometry of the relevant moduli spaces.

### 4.1 Moduli space

Let  $G = U(K)$  or  $SU(K)$  for some  $K$ .<sup>27</sup> We have a complex curve  $C$  with a topologically trivial  $G$ -bundle  $V$  on it. We are considering connections  $D = \partial + A$  in  $V$ , and Higgs fields  $\varphi \in \Omega^{1,0}(\text{End } V)$ .

There are finitely many points  $\mathcal{P}_i \in C$  where the pair  $(A, \varphi)$  are required to be singular. Let us focus on a single such point, and choose a local coordinate  $z$  which vanishes there. A rigorous discussion of boundary conditions for Hitchin's equations and the construction of their hyperkähler moduli spaces has been given in [53, 54] for regular singularities, and [55] for irregular ones. Here we give a schematic account of the boundary conditions we encountered in Section 3, which will be adequate for our purposes.

Consider the regular case first. Fix simultaneously diagonalizable elements  $\alpha \in \mathfrak{g}$  (skew-Hermitian) and  $\rho \in \mathfrak{g}_{\mathbb{C}}$ , and write

$$\varphi_0 = \frac{\rho}{2} \frac{dz}{z}, \quad (4.1)$$

$$A_0 = \frac{\alpha}{2i} \left( \frac{dz}{z} - \frac{d\bar{z}}{\bar{z}} \right). \quad (4.2)$$

Near  $z = 0$  we require the pair  $(A, \varphi)$  to be close to these fiducial ones, i.e.

$$\varphi = \varphi_0 + \text{regular}, \quad (4.3)$$

$$A = A_0 + \text{regular}. \quad (4.4)$$

We let  $\mathcal{N}$  denote the space of all  $(A, \varphi)$  obeying this condition at each singularity. So  $\mathcal{N}$  depends on the data  $(\rho, \alpha)$  at each singularity, as well as on  $C$  and the points  $\mathcal{P}_i$ ; we do not write this dependence explicitly.

There is a natural action of  $G$ -valued gauge transformations on  $(A, \varphi)$ . This gives an action on  $\mathcal{N}$  as well, provided we consider only gauge transformations which preserve the singularity conditions. Roughly this means we consider gauge transformations which, at each singularity, are restricted to lie in the subgroup  $H \subset G$  commuting with the pair  $(\rho, \alpha)$ . Let  $\mathcal{G}$  denote the group of gauge transformations so restricted.

---

<sup>27</sup>One can also consider quotients of  $SU(K)$  by subgroups of its center. The different forms of the gauge group lead to Hitchin moduli spaces which are related but can differ in global structure. When the genus of  $C$  is zero these considerations lead, for example, to changes in the periodicity of  $m^{(3)}$ . When  $C$  has positive genus further issues arise which are only briefly addressed in Appendix A.

In most of our examples we also need to allow a wilder kind of singularity. The most elementary example of such a boundary condition was given in (3.115), (3.116). In those equations  $t$  denoted a local coordinate on  $C$  vanishing at the singularity; here we called that coordinate  $z$ , so those equations become

$$\varphi_0 = \frac{\nu^{1/K}}{|z|^{1/K}} \left( \frac{\bar{z}}{|z|} e_{K1} + N_K \right) \frac{dz}{z}, \quad (4.5)$$

$$A_0 = \left( \sum_{a=1}^K \frac{2(a-1) - (K-1)}{4K} e_{aa} \right) \left( \frac{dz}{z} - \frac{d\bar{z}}{\bar{z}} \right). \quad (4.6)$$

As before we require that near  $z = 0$  the pair  $(A, \varphi)$  are close to these fiducial ones.

Generally we will have some block structure at the singular points, with each block of  $(A_0, \varphi_0)$  either of the “regular” form (4.1), (4.2) or the “irregular” form (4.5), (4.6). As in the case of regular singularities, we let  $\mathcal{N}$  denote the space of all  $(A, \varphi)$  obeying our singularity conditions. Again,  $\mathcal{N}$  is acted on by an appropriate group  $\mathcal{G}$  of gauge transformations.

More general irregular singularities can also arise if we take some scaling limits of the parameters of the theory: we do not discuss this situation now, but we will meet it in Section 9.

Having specified our boundary conditions, our desired moduli space  $\mathcal{M}$  is then the subspace of  $\mathcal{N}$  consisting of solutions of Hitchin’s equations,

$$\begin{aligned} F + R^2[\varphi, \bar{\varphi}] &= 0, \\ \bar{\partial}_A \varphi &:= (\partial_{\bar{z}} \varphi_z + [A_{\bar{z}}, \varphi_z]) d\bar{z} \wedge dz = 0, \\ \partial_A \bar{\varphi} &:= (\partial_z \bar{\varphi}_{\bar{z}} + [A_z, \bar{\varphi}_{\bar{z}}]) dz \wedge d\bar{z} = 0, \end{aligned} \quad (4.7)$$

modulo gauge transformations. (Here by  $\bar{\varphi}$  we mean the Hermitian conjugate of  $\varphi$ .) The arguments of Section 3 identify this as the physically defined moduli space of an appropriate  $\mathcal{N} = 2$  field theory reduced on  $S^1$  of radius  $R$ .

## 4.2 Hyperkähler structure

As we have already emphasized,  $\mathcal{M}$  is equipped with a natural hyperkähler structure. In particular, this implies that it has a  $\mathbb{CP}^1$  worth of complex structures  $J^{(\zeta)}$ , and a complex symplectic form  $\varpi_\zeta$ , which is holomorphic at each fixed  $\zeta$ . In this subsection we explain how these complex structures arise and what can be quickly said about  $(\mathcal{M}, J^{(\zeta)})$  from the point of view of complex geometry. The most crucial point for later sections will be the identification of  $(\mathcal{M}, J^{(\zeta)})$  as a moduli space of flat connections when  $\zeta \in \mathbb{C}^\times$ .

A convenient way to think about the hyperkähler structure on  $\mathcal{M}$  begins from the observation that  $\mathcal{N}$  is an infinite-dimensional affine space, which is hyperkähler in a very simple way, basically as the cotangent bundle to the affine space of complex-valued connections. The action of the gauge group on  $\mathcal{N}$  preserves the hyperkähler structure, and moreover admits an hyperkähler moment map  $\vec{\mu}$ . The components of this moment map (in one natural basis) are precisely what appear on the left side of the Hitchin equations



(4.7). So the procedure of imposing Hitchin's equations and then dividing out by the gauge group  $\mathcal{G}$  is precisely the usual notion of hyperkähler quotient [56], i.e.  $\mathcal{M} = \mathcal{N} // \mathcal{G}$ .

There is another way to view the hyperkähler quotient, which in fact explains why it induces an hyperkähler structure on  $\mathcal{M}$ . Upon choosing a  $\zeta$ , we can divide  $\vec{\mu}$  into a real-valued moment map  $\mu_{\mathbb{R}}$  and a complex-valued moment map  $\mu_{\mathbb{C}}$ . Then instead of imposing  $\vec{\mu} = 0$  we can impose only  $\mu_{\mathbb{C}} = 0$ , and divide out by the action of a complexification  $\mathcal{G}_{\mathbb{C}}$  of the gauge group. In favorable circumstances (where each  $\mathcal{G}_{\mathbb{C}}$ -orbit is “stable,” i.e. contains a unique  $\mathcal{G}$ -orbit consisting of solutions of  $\mu_{\mathbb{R}} = 0$ ), this procedure gives exactly  $\mathcal{M}$ . Moreover  $\mu_{\mathbb{C}}$  is holomorphic on  $\mathcal{N}$ , and the complexified gauge group acts holomorphically, so this procedure induces a complex structure on  $\mathcal{M}$ , which is  $J^{(\zeta)}$ .

The way this works out for the  $\mathcal{M}$  we are considering depends drastically on whether  $\zeta \in \mathbb{C}^{\times}$  or  $\zeta \in \{0, \infty\}$ . We now describe these two cases in turn.

#### 4.2.1 Flat connections

We begin with the case  $\zeta \in \mathbb{C}^{\times}$ . Use  $A$  and  $\varphi$  to form a complex-valued connection,

$$\mathcal{A} := \frac{R}{\zeta} \varphi + A + R\zeta \bar{\varphi}. \quad (4.8)$$

At each of our marked points  $\mathcal{A}$  is singular, with leading behavior determined by the singular parts of  $\varphi$  and  $A$ . For example, in the case of a regular singularity this amounts to

$$\mathcal{A}_0 = \left( \frac{R\rho}{\zeta} + \frac{\alpha}{2i} \right) \frac{dz}{z} + \left( R\zeta \frac{\bar{\rho}}{2} - \frac{\alpha}{2i} \right) \frac{d\bar{z}}{\bar{z}}. \quad (4.9)$$

All of the holomorphic information in complex structure  $J^{(\zeta)}$  is naturally expressed in terms of  $\mathcal{A}$ . For example, the holomorphic symplectic form on  $\mathcal{N}$  is simply

$$\varpi_{\zeta} = \frac{1}{2} \int_C \text{Tr } \delta \mathcal{A} \wedge \delta \mathcal{A}. \quad (4.10)$$

Note that although  $\mathcal{A}$  is singular,  $\delta \mathcal{A}$  is regular, so the integral defining  $\varpi_{\zeta}$  is well defined. Considered as a function of  $\zeta$ ,  $\varpi_{\zeta}$  has simple poles at  $\zeta = 0$  and  $\zeta = \infty$ ; this is a standard expectation from hyperkähler geometry (sometimes expressed as the statement that  $\varpi$  is twisted by  $\mathcal{O}(2)$  over the twistor sphere).

Now the equation  $\mu_{\mathbb{C}} = 0$  simply says that  $\partial + \mathcal{A}$  is flat. Dividing out by the complexified gauge group we thus identify  $(\mathcal{M}, J^{(\zeta)})$  as a moduli space of flat,  $G_{\mathbb{C}}$ -valued connections on  $C$ . Using a theorem of [57] (for regular singularities) and [55] (more generally) we can describe this moduli space more precisely: it consists of all flat  $G_{\mathbb{C}}$ -connections with the requisite fixed boundary conditions, subject to a certain stability condition.

#### 4.2.2 Higgs bundles

At  $\zeta = 0$  or  $\zeta = \infty$  the story is rather different. Take for example  $\zeta = 0$ . In this case the equation  $\mu_{\mathbb{C}} = 0$  just says that

$$\partial_{\bar{z}} \varphi + [A_{\bar{z}}, \varphi] = 0. \quad (4.11)$$

In other words, we have a holomorphic structure on  $V$  (determined by the operator  $\bar{\partial} := (\partial_{\bar{z}} + A_{\bar{z}})d\bar{z}$ ) and a holomorphic 1-form  $\varphi$  valued in  $\text{End } V$ , with appropriate singularities at the marked points. The triplet  $(V, \varphi, \bar{\partial})$  is called a *Higgs bundle*. Dividing out by the complexified gauge transformations we thus identify  $(\mathcal{M}, J^{(\zeta=0)})$  as a moduli space of Higgs bundles, with appropriate boundary conditions on  $\varphi$  at the punctures. As above, the theorems of [57, 55] tell us that in fact we get all Higgs bundles in this way (subject to a certain stability condition which will not play much role in this paper.) Note that this space, considered as a complex manifold, is actually independent of  $R$ .

Given a Higgs bundle there is a simple way of extracting gauge invariant information: consider the characteristic polynomial of  $\varphi$ , i.e. write

$$\det(x - \varphi) = x^N + \sum_{i=1}^N p_i x^{N-i} \quad (4.12)$$

(where  $p_1 = 0$  if  $G = SU(K)$  rather than  $U(K)$ ). Since  $\varphi$  is a 1-form the coefficients  $p_i$  of its characteristic polynomial are forms of degree  $i$  on  $C$ . These forms are meromorphic, with some specific conditions on their singular behavior near the marked points, dictated by the type of singularity we have fixed. We do not write these conditions in general but just note that the space of forms  $p_i$  obeying them is an affine space  $\mathcal{B}$ , with dimension half that of  $\mathcal{M}$ . This  $\mathcal{B}$  is to be identified with the moduli space of the 4-dimensional gauge theory which we discussed in Section 3.

The map  $\mathcal{M} \rightarrow \mathcal{B}$  just discussed is sometimes called the Hitchin fibration. Its generic fiber is a compact torus, which is moreover a complex Lagrangian submanifold in complex structure  $J^{(\zeta=0)}$ . The  $p_i$  can be thought of as a maximal set of algebraically independent commuting Hamiltonians, which make  $\mathcal{M}$  into an integrable system.

### 4.3 Another viewpoint on defects

So far we have considered the singular behavior of  $(A, \varphi)$  as a fixed “boundary condition” which we introduced by hand. There is another viewpoint which is sometimes handy to keep in mind: at least for regular singularities, the poles in  $(\varphi, A)$  can be interpreted as arising from sources in the Hitchin equations (see [58] and also section 3 of [59]). In other words, we deform the equations to

$$F + R^2[\varphi, \bar{\varphi}] = 2\pi\mu_{\mathbb{R}}\delta^{(2)}(z - z_i), \quad (4.13)$$

$$\bar{\partial}_A \varphi := d\bar{z}(\partial_{\bar{z}}\varphi + [A_{\bar{z}}, \varphi]) = \pi\mu_{\mathbb{C}}\delta^{(2)}(z - z_i), \quad (4.14)$$

$$\partial_A \bar{\varphi} := dz(\partial_z\bar{\varphi} + [A_z, \bar{\varphi}]) = \pi\bar{\mu}_{\mathbb{C}}\delta^{(2)}(z - z_i). \quad (4.15)$$

The residues of  $(A, \varphi)$  obeying these deformed equations then turn out to be proportional to  $\mu_{\mathbb{R}}, \mu_{\mathbb{C}}, \bar{\mu}_{\mathbb{C}}$ . (If there are multiple singularities we will have a sum on the right-hand side.)

The usefulness of this point of view arises from interpreting the sources  $\vec{\mu}$  as moment maps for an action of  $SU(K)$  on a coadjoint orbit  $O_i$  of  $SL(K, \mathbb{C})$ . In other words, the modified equations (4.13)-(4.15) are obtained by an hyperkähler quotient  $(\mathcal{N} \times O_i) // \mathcal{G}$ ,

where a gauge transformation  $g(z)$  acts on  $\mathcal{N}$  as usual and on  $O_i$  by the coadjoint action of  $g(z_i)$ . Indeed, this is the natural supersymmetric coupling of the 5-dimensional super Yang-Mills theory to degrees of freedom living at the defects  $z = z_i$ .

The simplest example is obtained by taking  $O_i$  to be a minimal orbit. This is exactly the example we considered in Section 3.1.8. In the complex structure at  $\zeta = 0$ , the parameter  $m_i$  determines the orbit as a complex manifold, while  $m_i^{(3)}$  enters only into its metric. This viewpoint is particularly helpful for understanding how to take the limit  $m_i \rightarrow 0$ : the limit of the minimal semisimple orbit is not the zero orbit but rather the minimal nilpotent orbit. So in the holomorphic gauge the natural limiting boundary condition on  $\varphi$  is actually (up to conjugation as usual)

$$\varphi_0 = \frac{1}{z} \begin{pmatrix} 0 & 1 & & \\ & 0 & & \\ & & \ddots & \\ & & & 0 \end{pmatrix}. \quad (4.16)$$

The corresponding solution of Hitchin's equations, related to (4.16) by a complex gauge transformation, is similar to (4.5), and has a milder singularity (of order  $z^{-1/2}$ ) for  $\varphi_0$ .

The appearance of the minimal orbit can also be understood more directly. Recall that in Section 3.1.8 we were considering an M-theory setup involving a set of  $K$  M5-branes on  $C$  intersecting a single transverse M5-brane. Reducing on the  $S^1$  discussed in Section 3.1 to Type IIA so that all of these M5-branes become D4-branes one would generally expect to get a fundamental hypermultiplet of  $SU(K)$  at the intersection. The minimal semisimple orbit of  $SU(K)$  is very close to that: if we start from the  $K$  hypermultiplets coupled to  $U(K)$  and Higgs the overall  $U(1)$ , the resulting hyperkähler quotient yields the minimal orbit coupled to  $SU(K)$ .

There is a similar story for more general singularities where the residue of  $\varphi$  lies in some non-minimal semisimple orbit, i.e. it is conjugate to a diagonal matrix with a different pattern of eigenvalues. The eigenvalues still play the role of mass parameters. In the limit as the mass parameters are turned off, the semisimple orbit smoothly approaches some nilpotent orbit, so the residue of  $\varphi$  becomes a nilpotent matrix with a specific Jordan form.

## 5. Fock-Goncharov coordinates

For the next few sections we specialize to a simple case: let  $\mathcal{M}$  be the moduli space of solutions of Hitchin's equations on  $C$  with gauge group  $G = SU(2)$ , with  $l$  regular singularities with semisimple residues, at points  $\mathcal{P}_1, \dots, \mathcal{P}_l$ . We always assume  $l \geq 1$ , and if  $C$  has genus zero we assume  $l \geq 3$ .<sup>28</sup> We will remove the restriction to regular singularities in Section 8.

Fix some  $\zeta \in \mathbb{C}^\times$ . Then we can identify  $\mathcal{M}$  (considered as a holomorphic symplectic manifold, in complex structure  $J^{(\zeta)}$ ) with a moduli space of flat  $SL(2, \mathbb{C})$ -connections  $\mathcal{A}$ . In this section we will use the approach of Fock and Goncharov [10] to define a useful

---

<sup>28</sup>The case  $l = 3$ ,  $C = \mathbb{CP}^1$  is somewhat degenerate since in this case  $\mathcal{M}$  is zero-dimensional.

collection of holomorphic Darboux coordinate systems on  $\mathcal{M}$ . Each coordinate system  $\mathcal{X}^T$  will be associated to a “decorated triangulation”  $T$ , a certain combinatorial object to be defined momentarily. In the following sections we will explain how to build the desired functions  $\mathcal{X}_\gamma$  on  $\mathcal{M}$  from the coordinate systems  $\mathcal{X}^T$ .

### 5.1 Defining the Fock-Goncharov coordinates

By a *triangulation* we will always mean a triangulation of  $C$ , with all vertices at the singularities  $\mathcal{P}_i$ , and at least one edge incident on each vertex. At each  $\mathcal{P}_i$  we have the operator  $M_i$  giving the clockwise monodromy of  $\mathcal{A}$ -flat sections, which is  $SL(2, \mathbb{C})$ -valued and generically has two distinct eigenlines. We define a *decoration* at  $\mathcal{P}_i$  to be a choice of one of these two eigenlines, and a *decorated triangulation*  $T$  to be a triangulation plus a decoration at each vertex. Let  $\mu_i^T$  denote the corresponding monodromy eigenvalue.

To avoid confusion, it is useful to observe a slight difference between our setup and that of [10]. Their point of view was to include the choice of decoration in the moduli space, so they really built coordinate systems on a moduli space of “decorated flat connections.” In our situation, where the conjugacy classes of the  $M_i$  are fixed once and for all, we instead include the choice of decoration as part of the discrete datum  $T$ .

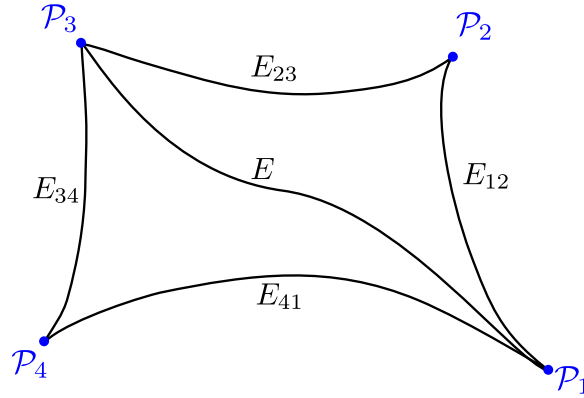


**Figure 14:** The quadrilateral  $Q_E$  associated to an edge  $E$  in the triangulation  $T$ .

Now fix a decorated triangulation  $T$ . For each edge  $E$  of  $T$ , we define a coordinate function  $\mathcal{X}_E^T$ , as follows. The two triangles bounding  $E$  make up a quadrilateral  $Q_E$ . Number its vertices  $\mathcal{P}_i$ ,  $i = 1, 2, 3, 4$ , in counterclockwise order (using the standard orientation on  $C$ ), and with  $E$  running between vertices 1 and 3. The edges are unoriented, so such a labeling is determined only up to the simultaneous exchange  $1 \leftrightarrow 3$  and  $2 \leftrightarrow 4$ . The  $\mathcal{X}_E^T$  constructed below will be independent of this ambiguity. See Figure 14.

Over  $Q_E$  we now choose four sections  $s_i$  of  $V$ , obeying the flatness equation

$$(d + \mathcal{A})s_i = 0, \tag{5.1}$$

and with each  $s_i$  an eigenvector of  $M_i$ , with eigenvalue  $\mu_i^T$ . The  $s_i$  cannot be made globally single-valued and smooth on  $C$  (the monodromy would require introducing a branch cut somewhere) but we emphasize that we do choose them to be single-valued and smooth on  $Q_E$ . Each  $s_i$  is uniquely determined up to complex rescaling.

The Fock-Goncharov coordinate is constructed from the  $s_i$ :

$$\mathcal{X}_E^T := -\frac{(s_1 \wedge s_2)(s_3 \wedge s_4)}{(s_2 \wedge s_3)(s_4 \wedge s_1)}, \quad (5.2)$$

where all  $s_i$  are evaluated at any common point  $\mathcal{P}_* \in Q_E$ . Because the connection  $\mathcal{A}$  is valued in  $sl(2, \mathbb{C})$ , this quantity is independent of  $\mathcal{P}_*$ . Moreover, the ambiguity of each  $s_i$  by a complex rescaling cancels out in  $\mathcal{X}_E^T$ .

The functions  $\mathcal{X}_E^T$  go to 0 or  $\infty$  only when  $s_i \wedge s_j = 0$  for two adjacent vertices  $\mathcal{P}_i, \mathcal{P}_j$ , which happens on a codimension-1 subvariety of  $\mathcal{M}$ . Thus the  $\mathcal{X}_E^T$  are well defined in a Zariski open patch  $\mathcal{U}_T \subset \mathcal{M}$ . In fact, the  $\mathcal{X}_E^T$  give a coordinate system on this patch [10]: in Appendix A we show how to reconstruct the connection  $\mathcal{A}$  modulo gauge equivalence (i.e. the monodromy representation of  $\mathcal{A}$ ) from the  $\mathcal{X}_E^T$ .

As an aside we note that one can think of  $\mathcal{X}_E^T$  as a cross-ratio, in the following sense. After choosing some fiducial basis in the 2-dimensional space of  $\mathcal{A}$ -flat sections of  $V$  over  $Q_E$ , the four 1-dimensional subspaces  $\{\lambda s_i : \lambda \in \mathbb{C}^\times\} \subset \mathbb{C}^2$  give four points  $x_i \in \mathbb{CP}^1$ . Then, one can show that (5.2) is just

$$\mathcal{X}_E^T = -\frac{(x_1 - x_2)(x_3 - x_4)}{(x_2 - x_3)(x_4 - x_1)}. \quad (5.3)$$

## 5.2 Monodromies

Certain combinations of the  $\mathcal{X}_E^T$  have a simple interpretation. Indeed, consider any singular point  $\mathcal{P}_i$ , and consider the product of  $\mathcal{X}_E^T$  over all edges  $E$  which meet  $\mathcal{P}_i$ . Without accounting for the monodromy of  $s_i$  one formally finds that there is a telescoping cancellation of terms in the product, leaving 1. However, in defining  $\mathcal{X}_E^T$  one must take care to define  $s_i$  to be single-valued and continuous in the whole quadrilateral  $Q_E$ . Such a choice may be made for each  $E$ , but we cannot construct a single  $s_i$  satisfying this condition everywhere; we will have to include a branch cut somewhere. If we choose our cut to run through one of the triangles meeting  $\mathcal{P}_i$ , then precisely two quadrilaterals are affected. They are each multiplied by a factor of  $\mu^T$ , so we find that

$$\prod_{E \text{ meeting } \mathcal{P}_i} \mathcal{X}_E^T = (\mu_i^T)^2. \quad (5.4)$$

(We have assumed implicitly that  $\mathcal{P}_i$  meets at least two edges; it is actually possible that it meets only one, but (5.4) will continue to hold in that case, for which see Section 5.8 below.)

## 5.3 Counting the coordinates

As we have remarked, the functions  $\mathcal{X}_E^T$  give a local coordinate system on  $\mathcal{M}$ . As a simple check we show that the dimension counting works out correctly.

The dimension of  $\mathcal{M}$  can be obtained by considering the monodromy data. Let  $g$  be the genus of  $C$ , and recall that our local system has  $l$  regular singularities  $\mathcal{P}_i$  on  $C$ . There are  $3(l + 2g)$  degrees of freedom in the  $SL(2, \mathbb{C})$ -valued monodromy matrices  $M_i, A_j, B_j$  (around the singularities,  $A$  and  $B$  cycles respectively), minus 3 for the usual constraint

$\prod M_i = \prod A_j B_j A_j^{-1} B_j^{-1}$ , minus another 3 for the  $SL(2, \mathbb{C})$  gauge symmetry, minus  $l$  because the monodromy eigenvalues are fixed. Altogether this gives

$$\dim \mathcal{M} = 2l + 6g - 6. \quad (5.5)$$

How many coordinates  $\mathcal{X}_E^T$  do we get? Using Euler's formula

$$l + (\#F) - (\#E) = 2 - 2g \quad (5.6)$$

and the fact that all of our faces are triangles

$$2(\#E) = 3(\#F) \quad (5.7)$$

we obtain

$$\#E = 3l + 6g - 6, \quad \#F = 2l + 4g - 4. \quad (5.8)$$

As we argued above,  $l$  combinations of the  $\mathcal{X}_E^T$  give the monodromy eigenvalues  $(\mu_i^T)^2$ , which are fixed up to a discrete choice; the other  $2l + 6g - 6$  are just enough to give coordinates on  $\mathcal{M}$  as desired.

#### 5.4 Hamiltonian flows

As we noted in Section 4,  $\mathcal{M}$  has a natural holomorphic symplectic form. We now describe the Hamiltonian flow generated by  $\log \mathcal{X}_E^T$ . This flow turns out to be very simple.

Given a connection  $\mathcal{A} \in \mathcal{M}$ , we may describe its image  $\mathcal{A}^t$  under the time- $t$  flow generated by  $\log \mathcal{X}_E^T$ , as follows. We consider the connection  $\mathcal{A}$  on  $C$  as divided into two pieces, namely the restrictions to the quadrilateral  $Q_E$  (“inside”) and its complement  $C \setminus Q_E$  (“outside”). On the common boundary of the two pieces we have an identification between boundary values of sections of  $V$ . Gluing the two pieces back together using this identification one would recover the original  $V$  with its connection  $\mathcal{A}$ . Now we consider gluing them together using a different identification. Namely, on edge  $E_{ij}$  (with  $i, j$  cyclically ordered) we glue  $s_i$  outside to  $e^{\pm t/2} s_i$  inside, and  $s_j$  outside to  $e^{\mp t/2} s_j$  inside, where the sign  $\pm$  is  $+$  for  $i = 2, 4$  and  $-$  for  $i = 1, 3$ . This gluing is still  $SL(2, \mathbb{C})$ -valued since it preserves  $s_i \wedge s_j$ , and preserves the flatness of the connection since we have glued flat sections to flat sections. It defines the new connection  $\mathcal{A}^t$ .

Note that the monodromy of the section  $s_i$  around  $\mathcal{P}_i$  is the same for  $\mathcal{A}^t$  as it was for  $\mathcal{A}$  (since the transformations of  $s_i$  coming from the two edges which meet  $\mathcal{P}_i$  cancel one another). It follows that  $\mathcal{A}^t$  and  $\mathcal{A}$  have the same monodromy eigenvalues, so this flow really preserves our moduli space  $\mathcal{M}$  as it should.

The derivation of this flow from the symplectic structure (4.10) is basically straightforward but notationally a bit awkward, so we have sequestered it in Appendix B.

#### 5.5 Poisson bracket

Given two edges  $E$  and  $E'$  of the triangulation  $T$ , we define  $\langle E, E' \rangle$  to be the number of faces  $E$  and  $E'$  have in common, counted with a sign  $+1$  ( $-1$ ) if  $E$  comes immediately

before  $E'$  in counterclockwise (clockwise) order going around the common face. In this section we show that the Poisson brackets of the  $\mathcal{X}_E^T$  are determined by this pairing,

$$\{\mathcal{X}_E^T, \mathcal{X}_{E'}^T\} = \langle E, E' \rangle \mathcal{X}_E^T \mathcal{X}_{E'}^T. \quad (5.9)$$

To check (5.9) we consider the action of the Hamiltonian flow generated by  $\log \mathcal{X}_E^T$  on  $\mathcal{X}_{E'}^T$ . Recall from Section 5.4 that this flow involves cutting and gluing along the sides of the quadrilateral  $Q_E$ . If  $\langle E, E' \rangle = 0$ , then one can compute  $\mathcal{X}_{E'}^T$  using only the connection  $\mathcal{A}$  outside  $Q_E$ , and hence  $\mathcal{X}_{E'}^T$  is invariant under the flow, in agreement with (5.9). Now suppose  $\langle E, E' \rangle = +1$ . The definition (5.2) of  $\mathcal{X}_{E'}^T$  requires us to transport the sections  $s_i$  from the vertices  $\mathcal{P}_{1,2,3,4}$  of  $Q_{E'}$  to a common point  $\mathcal{P}_* \in Q_{E'}$ ; let us choose that point to lie also in  $Q_E$ . See Figure 15 to fix the labeling of the vertices. The transport requires

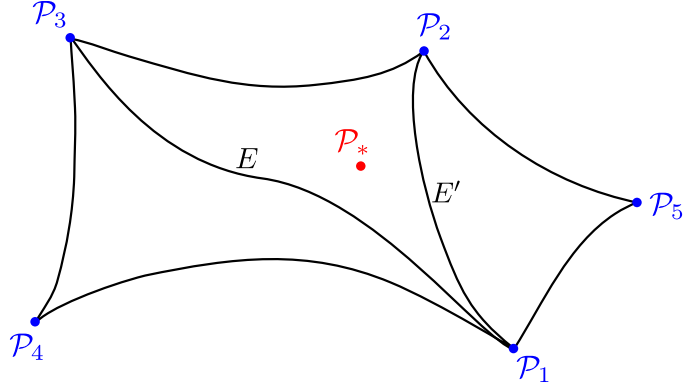


**Figure 15:** Fixing notation for calculating the effect of the flow generated by  $\log \mathcal{X}_E^T$  on the function  $\mathcal{X}_{E'}^T$ , in the case  $\langle E, E' \rangle = +1$ .

us to bring  $s_5$  from outside  $Q_E$  to inside, across the edge  $E' = E_{12}$ . It follows that the  $s_5$  appearing in the definition of  $\mathcal{X}_{E'}^T$  is transformed by the flow. Expanding  $s_5$  in the convenient basis of flat sections

$$s_5 = as_1 + bs_2 \quad (5.10)$$

the action of the flow replaces  $a \mapsto ae^{-t/2}$  and  $b \mapsto be^{t/2}$ , and hence takes

$$s_1 \wedge s_5 \rightarrow e^{t/2} s_1 \wedge s_2, \quad (5.11)$$

$$s_5 \wedge s_2 \rightarrow e^{-t/2} s_5 \wedge s_2. \quad (5.12)$$

So the flow generated by  $\log \mathcal{X}_E^T$  multiplies  $\mathcal{X}_{E'}^T$  by  $e^t$ . The desired Poisson bracket (5.9) follows directly.

It is also possible to have  $\langle E, E' \rangle = +2$ , if the two edges share two faces. In this case a similar argument shows that the flow generated by  $\log \mathcal{X}_E^T$  multiplies  $\mathcal{X}_{E'}^T$  by  $e^{2t}$ , and the desired (5.9) still holds.

## 5.6 Coordinate transformations and the groupoid of decorated triangulations

Now we come to a crucial point. The coordinate system  $\mathcal{X}^T$  depends on the choice of triangulation  $T$ . We would like to know the coordinate transformation  $S_{T,T'}$  relating  $\mathcal{X}^T$  to  $\mathcal{X}^{T'}$ .



There is a procedure to compute  $S_{T,T'}$ , which is straightforward in principle, but cumbersome in practice. The cross ratios  $\mathcal{X}_E^T$  contain enough information to parallel-transport flat sections  $s$  along paths in  $C$ , as shown in Appendix A. Therefore, if  $T$  and  $T'$  have the same decoration, one can first use the  $\mathcal{X}_E^T$  to determine  $s_i$  and  $s_j$  along the edges  $E'_{ij}$  of  $T'$ , and then use those to compute the  $\mathcal{X}_{E'_{ij}}^{T'}$ . If the decorations are different, one also needs to determine the new monodromy eigensections  $s'_i$ , by transporting reference sections around the vertices of the triangulation  $T$ . The explicit expressions for  $S_{T,T'}$  obtained in this way are generally complicated rational transformations, and will be of little use to us (except for one crucial exception, which we will meet in Section 11).

Instead, it is more useful to study the coordinate transformations corresponding to simple local changes of the triangulation  $T$ . Any two triangulations  $T, T'$  are related to one another by a sequence of such simple moves, which we call “flips at edges” and “pops at vertices”:

- Given an edge  $E$  of  $T$ , we define the flip  $\sigma_E$  as follows: the original  $T$  and the flipped  $T'$  are identical except that in the quadrilateral  $Q_E$  the edge  $E = E_{13}$  in  $T$  is replaced by an edge  $E' = E_{24}$  in  $T'$ , as illustrated in Figure 16. (We assume here that  $E$  is distinct from all edges of the quadrilateral  $Q_E$ . This can fail in the presence of degenerate triangles with two coincident edges, to be discussed below. We will not need to define a flip for such edges.)

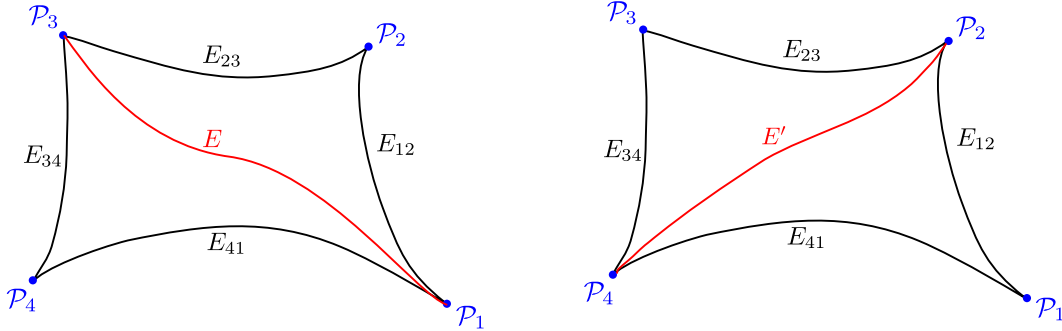


**Figure 16:** Flipping a triangulation  $T$  to  $T'$ .

- Given a vertex  $\mathcal{P}_i$ , we define the pop  $\pi_i$  as follows: the original  $T$  and the popped  $T'$  differ only by reversing the choice of monodromy eigenvalue (decoration) at  $\mathcal{P}_i$ .

The coordinate transformation  $S_{T,T'}$  is then usefully described as the composition of the coordinate transformations associated to a sequence of flips and pops which takes  $T$  to  $T'$ .

It is convenient to rephrase the above in the language of groupoids.<sup>29</sup> First we contemplate a groupoid  $\mathcal{T}$  which has as objects the various decorated triangulations, and a

<sup>29</sup>A “groupoid” is a category all of whose morphisms are invertible. In plain English this simply means we have a system of points (“objects”) and a collection of arrows between points (“morphisms”). There is an associative composition law on arrows, a unit arrow on every point, and every arrow has an inverse arrow.

unique morphism between any two decorated triangulations. (That is, the objects have no automorphisms.) It turns out that  $\mathcal{T}$  is freely generated by the flips and pops, subject to four kinds of relations:

- $\sigma_E \sigma_{E'} = \sigma_{E'} \sigma_E$  when  $\langle E, E' \rangle = 0$ .
- When  $\langle E, E' \rangle = 1$ ,  $\sigma_E \sigma_{E'} \neq \sigma_{E'} \sigma_E$ , but  $\sigma_E \sigma_{E'}$  can be rewritten as a product of *three* flips, as shown in Figure 17.<sup>30</sup>
- Each  $\pi_i$  commutes with everything else.
- $\pi_i^2 = 1$ .

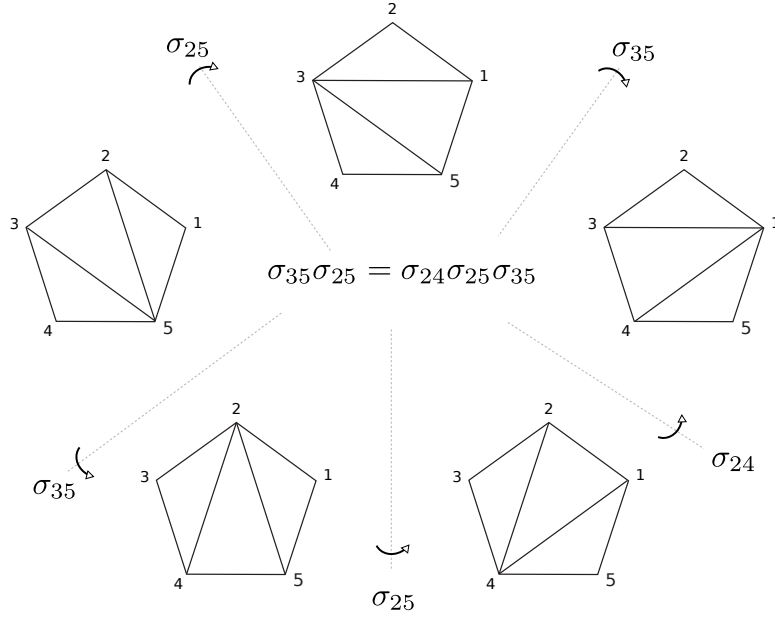


**Figure 17:** The “pentagon relation”: two different sequences of flips which relate a pair of triangulations.

Second, we define the groupoid  $\mathcal{C}$  of Darboux coordinate systems on  $\mathcal{M}$ . To define this groupoid first define a *Poisson torus* to be a space isomorphic to  $(\mathbb{C}^\times)^{\dim \mathcal{M}}$ , equipped with a Poisson structure such that the bracket of the standard coordinate functions  $x_i$  is of the form  $\{x_i, x_j\} = a_{ij} x_i x_j$ . Then a *Darboux coordinate system* is an injective Poisson map from a Zariski-open subset of  $\mathcal{M}$  to a Poisson torus. The groupoid  $\mathcal{C}$  has as objects the Darboux coordinate systems, and a unique morphism between any two objects, which may be identified with the unique Darboux coordinate transformation between them (a Poisson bijection between the two images of the overlap in  $\mathcal{M}$ ).

One can then consider (5.2) as defining a functor,

$$\mathcal{T} \rightarrow \mathcal{C} \tag{5.13}$$

$$T \mapsto \mathcal{X}^T. \tag{5.14}$$

<sup>30</sup>When  $\langle E, E' \rangle = 2$  there is no relation between  $\sigma_E$  and  $\sigma_{E'}$ , but nevertheless this case will be important in Section 5.9 below.

Under this functor the morphisms of triangulations get mapped to corresponding coordinate transformations, so relations among morphisms imply relations among coordinate transformations. As we will see momentarily, these relations can be surprising when written explicitly.

### 5.7 Transformation under flips

The effect of a flip  $\sigma_E$  on the coordinates is rather simple. First, referring to Figure 16 it is easy to see that the coordinates attached to  $E$  in  $T$  and  $E'$  in  $T'$  are trivially related,

$$\mathcal{X}_E^T = (\mathcal{X}_{E'}^{T'})^{-1}. \quad (5.15)$$

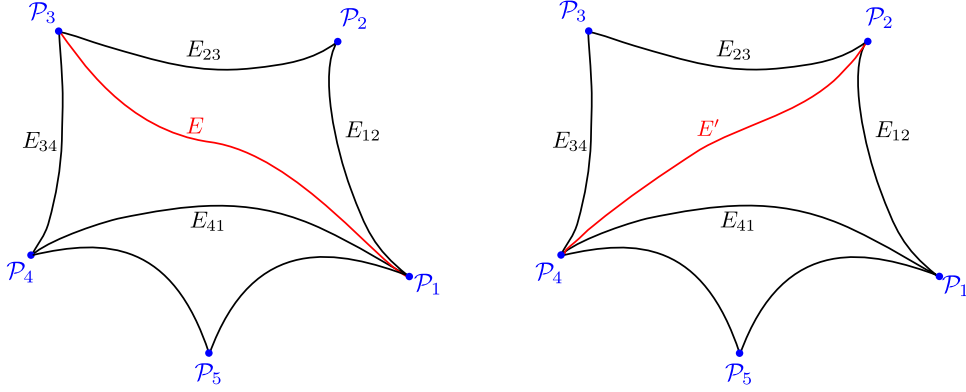


**Figure 18:** The effect of the flip on the quadrilaterals used to compute  $\mathcal{X}_{E_{41}}^T$  and  $\mathcal{X}_{E_{41}}^{T'}$ .

The flip also changes the coordinates attached to the four edges of  $Q_E$ . For example, consider the coordinate  $\mathcal{X}_{E_{41}}^T$  in Figure 18. It is the cross-ratio of  $s_1, s_3, s_4, s_5$  in that order, which we denote as  $\mathcal{X}_{E_{41}}^T = r(1, 3, 4, 5)$ . After the flip, we have instead  $\mathcal{X}_{E_{41}}^{T'} = r(1, 2, 4, 5)$ . On the other hand, we also have  $\mathcal{X}_E^T = r(1, 2, 3, 4)$ . Since any five points on  $\mathbb{CP}^1$  have only two independent cross-ratios, it follows that there must be an algebraic relation between  $\mathcal{X}_{E_{41}}^T$ ,  $\mathcal{X}_{E_{41}}^{T'}$  and  $\mathcal{X}_E^T$ . Indeed a direct computation gives this relation, and similar ones involving the other edges of  $Q_E$ :

$$\mathcal{X}_{E_{12}}^{T'} = \mathcal{X}_{E_{12}}^T (1 + \mathcal{X}_E^T), \quad (5.16)$$

$$\mathcal{X}_{E_{23}}^{T'} = \mathcal{X}_{E_{23}}^T (1 + (\mathcal{X}_E^T)^{-1})^{-1}, \quad (5.17)$$

$$\mathcal{X}_{E_{34}}^{T'} = \mathcal{X}_{E_{34}}^T (1 + \mathcal{X}_E^T), \quad (5.18)$$

$$\mathcal{X}_{E_{41}}^{T'} = \mathcal{X}_{E_{41}}^T (1 + (\mathcal{X}_E^T)^{-1})^{-1}. \quad (5.19)$$

(Above we assumed that each  $\langle E_{ij}, E \rangle = \pm 1$ , i.e. the only common face is the one appearing in the figure. If, say,  $\langle E, E_{41} \rangle = 2$  instead, then the transformation is instead  $\mathcal{X}_{E_{41}}^{T'} = \mathcal{X}_{E_{41}}^T (1 + (\mathcal{X}_E^T)^{-1})^{-2}$ , and similarly for the other edges.)

These transformations of course preserve the Poisson bracket (5.9) (in a non-trivial fashion, since the intersection matrix  $\langle E, E' \rangle$  changes under the flip.) So they define a morphism of Darboux coordinate systems. Moreover, note that this morphism strongly

resembles the KS transformations  $\mathcal{K}_\gamma$  we reviewed in Section 2. This is the first hint of the connection between the Fock-Goncharov coordinates and the Kontsevich-Soibelman wall-crossing formula. The transformation laws are still not quite the same, though. The identification will require one more important step, to be described below.

Finally we comment that the pentagon identity in the groupoid  $\mathcal{T}$  of decorated triangulations implies a corresponding pentagon identity among the morphisms in  $\mathcal{C}$ . How does it arise concretely? Consider again Figure 17, and call the two coordinate functions attached to the two interior edges of the  $n^{\text{th}}$  pentagon  $(x_n, y_n)$ , with  $n$  considered modulo 5. The flip relating adjacent pentagons gives the coordinate transformation

$$y_{n+1} = x_n^{-1}, \quad (5.20)$$

$$x_{n+1} = y_n(1 + x_n). \quad (5.21)$$

This sequence of coordinate transformations indeed has period 5. In particular, by eliminating  $y_n$  we get the beautifully simple period-5 relation  $x_{n+1}x_{n-1} = 1 + x_n$ .

### 5.8 Degenerate triangulations and transformation under pops

The effect of popping a vertex  $\mathcal{P}$  of a generic triangulation  $T$  is in general somewhat intricate. To construct the new flat section at  $\mathcal{P}$  in terms of the old one, we would need to use the parallel transport all the way around  $\mathcal{P}$ . While in principle this is determined by the  $\mathcal{X}_E^T$  for edges incident on  $\mathcal{P}$ , in practice the result is generally a complicated rational function. In this subsection we will meet a special class of triangulations with only a *single* edge incident on  $\mathcal{P}$ , for which the effect of the pop becomes very simple. These are triangulations which include degenerate faces in which two of the edges are identified, as pictured in Figure 19.

With a degenerate face included, our rules for constructing the coordinates  $\mathcal{X}_E^T$  have to be amended slightly. We “resolve” the face by passing to a covering  $\tilde{U}$  of a neighborhood  $U \subset C$ , ramified only at the center vertex. The flat connection  $\mathcal{A}$  on  $U$  pulls back to a flat connection on  $\tilde{U}$ , with regular singularities at the preimages of the singularities on  $U$ , and  $T|_U$  lifts to a triangulation  $\tilde{T}$ . We choose the covering so that  $\tilde{T}$  is not degenerate, so we can use our standard rule to define coordinates  $\mathcal{X}_{\tilde{E}}^{\tilde{T}}$ . (In order to resolve the face completely the covering should have at least three sheets, as in Figure 20.) We then define  $\mathcal{X}_E^T := \mathcal{X}_{\tilde{E}}^{\tilde{T}}$  where  $\tilde{E}$  is any preimage of  $E$ . Since the connection is pulled back, it is invariant under the automorphisms of the covering, so  $\mathcal{X}_E^T$  is independent of the choice of preimage  $\tilde{E}$ . It is similarly independent of the precise choice of covering.

For example, we compute  $\mathcal{X}_E^T$  using the quadrilateral  $Q_{\tilde{E}_1}$  as follows. Let  $s$  be the decoration at the preimage  $\tilde{\mathcal{P}}$  of  $\mathcal{P}$ , which we may choose to be the pullback of a decoration at  $\mathcal{P}$ . Let  $s'_i$  be the decorations at the various preimages  $\tilde{\mathcal{P}}'_i$  of  $\mathcal{P}'$ ; we may choose all of the  $s'_i$  to be pullbacks of a single decoration at  $\mathcal{P}'$ . Now (5.2) becomes

$$\mathcal{X}_E^T = \mathcal{X}_{\tilde{E}_1}^{\tilde{T}} = -\frac{(s'_3 \wedge s'_1)(s'_2 \wedge s)}{(s \wedge s'_3)(s'_1 \wedge s'_2)}, \quad (5.22)$$

which may be further simplified as follows. Let  $M$  denote the clockwise monodromy around  $\mathcal{P}$  in the original degenerate face. After transporting all  $s'_i$  to a common point in  $Q_{\tilde{E}_1}$  we

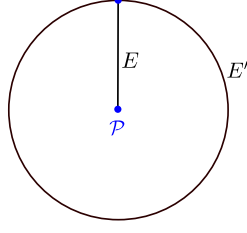


**Figure 19:** A degenerate face: it can be thought of as a triangle whose three edges are  $E'$ ,  $E$  and  $E$ .

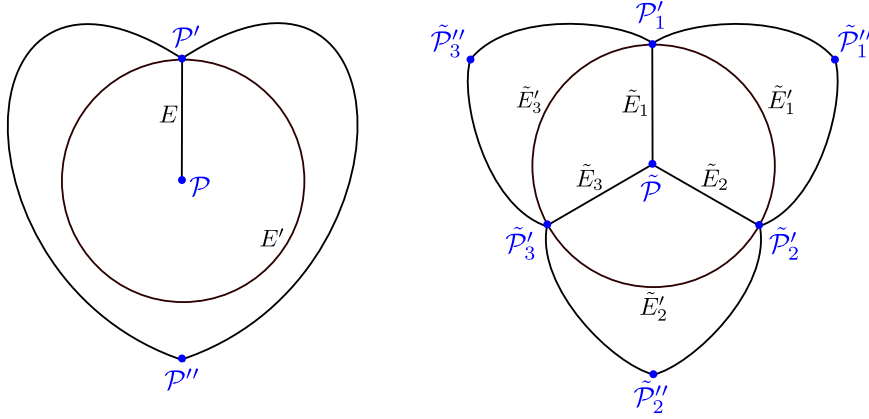


**Figure 20:** A neighborhood of a degenerate face, and its resolution by passing to a threefold cover.

will have  $s'_1 = M^{-1}s'_3 = Ms'_2$ , so

$$\mathcal{X}_E^T = -\frac{(Ms'_1 \wedge s'_1)(M^{-1}s'_1 \wedge s)}{(s \wedge Ms'_1)(s'_1 \wedge M^{-1}s'_1)} = -\frac{(Ms'_1 \wedge s'_1)(s'_1 \wedge Ms)}{(M^{-1}s \wedge s'_1)(Ms'_1 \wedge s'_1)} = (\mu^T)^2, \quad (5.23)$$

where we recall that  $\mu^T$  is the eigenvalue of  $s$  under  $M$ , and we used the fact that  $M \in SL(2, \mathbb{C})$ .

For  $\mathcal{X}_{E'}^T$  we get

$$\mathcal{X}_{E'}^T = \mathcal{X}_{\tilde{E}_3}^{\tilde{T}} = -\frac{(s \wedge s'_3)(s''_3 \wedge s'_1)}{(s'_1 \wedge s)(s'_3 \wedge s''_3)} \quad (5.24)$$

and again after transporting to a common point in  $Q_{\tilde{E}_3'}$  we have  $s'_3 = Ms'_1$ , so

$$\mathcal{X}_{E'}^T = -\frac{(s \wedge Ms'_1)(s''_3 \wedge s'_1)}{(s'_1 \wedge s)(Ms'_1 \wedge s''_3)} = -\frac{M^{-1}s \wedge s'_1}{s'_1 \wedge s} \frac{s''_3 \wedge s'_1}{Ms'_1 \wedge s''_3} = (\mu^T)^{-1} \frac{Ms'_1 \wedge s''_3}{s''_3 \wedge s'_1}. \quad (5.25)$$

Note that  $s$  enters this result only through its monodromy eigenvalue  $\mu^T$ . It follows that the only effect of a pop at the vertex  $\mathcal{P}$  is through the relation  $\mu^{T'} = (\mu^T)^{-1}$ , which gives using (5.23), (5.25) the transformation  $\pi_{\mathcal{P}}$ :

$$\mathcal{X}_{E'}^{T'} = (\mathcal{X}_E^T)^{-1}, \quad (5.26)$$

$$\mathcal{X}_{E'}^{T'} = \mathcal{X}_E^T \mathcal{X}_{E'}^T. \quad (5.27)$$

So the effect of the pop at the degenerate vertex  $\mathcal{P}$  is very simple. On the other hand, the effect of the pop at  $\mathcal{P}$  in a generic triangulation  $T$  can be determined by first flipping all edges incident on  $\mathcal{P}$  but one to reach a degenerate triangulation with a single edge incident on  $\mathcal{P}$ , then popping at  $\mathcal{P}$ , and finally flipping the edges back in the opposite order. Since pops and flips commute, this is the same as popping  $T$  at  $\mathcal{P}$ . More generally, one way to compute  $S_{T,T'}$  for a generic pair of triangulations  $T, T'$  is to decompose this morphism into a sequence of flips which change the undecorated triangulation underlying  $T$  into the one underlying  $T'$ , and which pass through degenerate triangulations where the effect of the required pops is simple.

### 5.9 Limits of triangulations and the juggle

So far we have considered the transformation of the coordinates  $\mathcal{X}_E^T$  under flips and pops. For our purposes it will actually be necessary also to consider a third, more complicated kind of transformation, which is not quite a relation between two triangulations, but rather a relation between two “infinitely twisted limits” of triangulations. In this section we introduce these limits.

We will consider triangulations  $T$  containing an annular region  $W$ , with a single vertex  $\mathcal{P}$  on the outer ring and  $\mathcal{P}'$  on the inner ring. Any such  $T$  has two interior edges on  $W$ , with both vertices in common. Suppose we hold the part of  $T$  outside  $W$  fixed, and consider varying the part on  $W$ . There are various choices of such  $T$ , differing from one another in how many times the edges wind around the annulus. See Figure 21 for some examples.

In order to parameterize the possible  $T$  we begin by choosing two fixed paths  $E_{\pm}$  from  $\mathcal{P}$  to  $\mathcal{P}'$ , such that  $E_+ - E_-$  winds once around  $W$  counterclockwise. Then we define  $T_0$  to be the triangulation with interior edges  $E_{0+} := E_+$ ,  $E_{0-} := E_-$ .

Performing a flip on  $E_{0-}$  we obtain another triangulation  $T_1$ . We label its edges as  $E_{1\pm}$ , again with  $E_{1+}$  differing from  $E_{1-}$  by one unit of counterclockwise winding: so  $E_{1+}$  is the edge created by the flip, and  $E_{1-} = E_{0+}$ . By flipping  $E_{1-}$  we obtain a new triangulation  $T_2$ . See Figure 21. Repeating this process we obtain a sequence of triangulations  $T_m$  for  $m \in \mathbb{Z}_+$ . Flipping  $E_{m-}$  takes us from  $T_m$  to  $T_{m+1}$ . Conversely, flipping  $E_{m+}$  takes us from  $T_m$  to  $T_{m-1}$ .

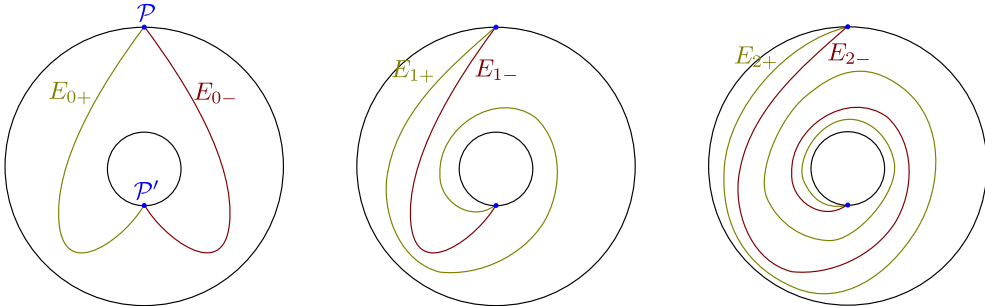


**Figure 21:** An annulus in triangulation  $T_0$ , and the triangulations  $T_1, T_2$  obtained by flipping  $E_{0-}, E_{1-}$ .

What are the Fock-Goncharov coordinates for the triangulation  $T_m$ ? To minimize confusion we pass to an infinite covering of the annulus, like the coverings we used in our discussion of degenerate triangulations, and choose specific preimages  $\tilde{E}_\pm$  of  $E_\pm$ . Define  $s, s'$  to be the decorations at the two ends  $\tilde{\mathcal{P}}, \tilde{\mathcal{P}}'$  of  $\tilde{E}_+$ , and introduce the notation

$$K = -(s \wedge Ms)(s' \wedge Ms'), \quad c_k = (s \wedge M^k s')^2. \quad (5.28)$$

The definition (5.2) becomes (see Figure 22)

$$\mathcal{X}_{E_{m+}}^{T_m} = \frac{K}{c_{1-m}}, \quad \mathcal{X}_{E_{m-}}^{T_m} = \frac{c_{-m}}{K}. \quad (5.29)$$

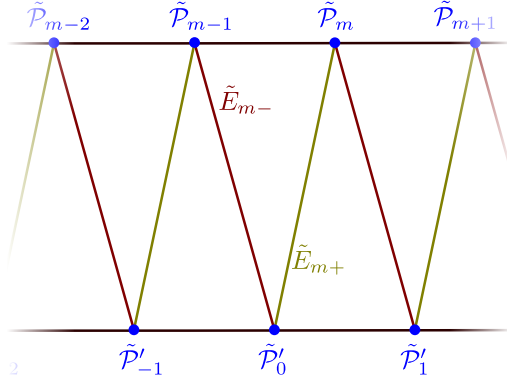


**Figure 22:** Our infinite covering of the annulus, with the triangulation  $T_m$  marked. We defined  $\tilde{\mathcal{P}}_0 := \tilde{\mathcal{P}}$  and  $\tilde{\mathcal{P}}'_0 := \tilde{\mathcal{P}}'$ , and then call their shifts  $\tilde{\mathcal{P}}_m$  and  $\tilde{\mathcal{P}}'_m$  respectively.

Our main interest here is in the  $m \rightarrow \infty$  limit. Define two “limit coordinates”  $\mathcal{X}_{A,B}^{T+\infty}$ , as follows. Denote the eigenvalues of  $M$  as  $\xi_\pm$ , where  $|\xi_+| > 1$ . (We assume that we are in the generic situation so that  $|\xi_\pm| \neq 1$ . In the physical application this corresponds to assuming generic masses for vectormultiplets.) One of our coordinates is simply

$$\mathcal{X}_A^{T+\infty} := \xi_+^2. \quad (5.30)$$

To define the other coordinate introduce the projection operators  $P_\pm$  on the two monodromy eigenspaces. Then define

$$\mathcal{X}_B^{T+\infty} := -\frac{(s \wedge P_- s')^2}{(s \wedge Ms)(s' \wedge Ms')}. \quad (5.31)$$

A direct computation shows that these are “limiting” coordinates in the sense that

$$\mathcal{X}_A^{T+\infty} = \lim_{m \rightarrow \infty} \mathcal{X}_{E_{m+}}^{T_m} \mathcal{X}_{E_{m-}}^{T_m}, \quad (5.32)$$

$$\mathcal{X}_B^{T+\infty} = \lim_{m \rightarrow \infty} (\mathcal{X}_{E_{m+}}^{T_m})^{-m} (\mathcal{X}_{E_{m-}}^{T_m})^{1-m}. \quad (5.33)$$

Letting  $E$  denote one of the boundaries of the annulus, the coordinates  $\mathcal{X}_E^{T_m}$  have well defined  $m \rightarrow \infty$  limits, which we call  $\mathcal{X}_E^{T+\infty}$ . The coordinates for all edges outside the

annulus are just  $m$ -independent, so letting  $E$  be one of these edges we simply define  $\mathcal{X}_E^{T+\infty} = \mathcal{X}_E^{T_m}$  for any  $m$ . We can then define a new coordinate system  $\mathcal{X}^{T+\infty}$  consisting of  $\mathcal{X}_A^{T+\infty}$ ,  $\mathcal{X}_B^{T+\infty}$ , and all the other  $\mathcal{X}_E^{T+\infty}$ .

The coordinate system  $\mathcal{X}^{T+\infty}$  we obtained here depended on the choice we made at the beginning, of which paths to call  $E_{\pm}$ .  $\mathcal{X}_A^{T+\infty}$  is independent of this choice, but  $\mathcal{X}_B^{T+\infty}$  for different choices differ by integral powers of  $\xi_+$ .

We can also consider the opposite kind of limit. Beginning again with  $T$  (and choosing the same paths  $E_{\pm}$ ), flipping  $E_{m+}$  repeatedly we get a sequence of triangulations  $T_m$  with  $m < 0$ , with edges winding around the annulus counterclockwise. Then define, similarly to the above,

$$\mathcal{X}_A^{T-\infty} := \xi_-^2 \quad (5.34)$$

and

$$\mathcal{X}_B^{T-\infty} := -\frac{(s \wedge P_+ s')^2}{(s \wedge M s)(s' \wedge M s')}. \quad (5.35)$$

These are also limiting coordinates, in the sense that

$$\mathcal{X}_A^{T-\infty} = \lim_{m \rightarrow -\infty} \mathcal{X}_{E_{m+}}^{T_m} \mathcal{X}_{E_{m-}}^{T_m}, \quad (5.36)$$

$$\mathcal{X}_B^{T-\infty} = \lim_{m \rightarrow -\infty} (\mathcal{X}_{E_{m+}}^{T_m})^{-m} (\mathcal{X}_{E_{m-}}^{T_m})^{1-m}. \quad (5.37)$$

From the point of view of the groupoid  $\mathcal{T}$ , we are introducing a countable family of new objects: for each of the countably many possible choices of the fiducial paths  $E_{\pm}$ , we add two “limit triangulations”  $T_{\pm\infty}$ . Relative to some fixed choice of  $E_{\pm}$  we can label the limit triangulations more concretely as  $T_{\pm\infty}^{[k]}$  for  $k \in \mathbb{Z}$ . There is a morphism from  $T_m$  to any  $T_{\pm\infty}^{[k]}$ , representing the limit of an infinite sequence of flips. There is a relatively trivial morphism which changes  $k$ : at the level of coordinate systems, it leaves  $\mathcal{X}_A$  invariant and changes  $\mathcal{X}_B$  by  $(\xi_+)^{k'-k}$ . We also introduce more interesting morphisms, which we call “juggles”: there is one juggle morphism from any  $T_{+\infty}^{[k]}$  to any  $T_{-\infty}^{[k']}$ , or vice versa. Morally speaking, introducing the juggles “closes a loop” in the groupoid of triangulations: starting from any  $T_m$  we can imagine flipping infinitely many times to reach some  $T_{+\infty}$ , then juggling to reach some  $T_{-\infty}$ , then flipping again infinitely many times to get back to  $T_m$ . We will abuse notation, using the symbol  $\mathcal{T}$  for the groupoid of decorated triangulations augmented by these limit triangulations and extra morphisms.

Now how does the juggle act on coordinate systems, i.e. what is its image under our functor  $\mathcal{T} \rightarrow \mathcal{C}$ ? For the  $A$  coordinates this is simple: from (5.30) and (5.34) we just have

$$\mathcal{X}_A^{T-\infty} = (\mathcal{X}_A^{T+\infty})^{-1}. \quad (5.38)$$

What about the  $B$  coordinates? The relation here depends on the choice of paths  $E_{\pm}$  we make in defining  $T_{+\infty}$  and  $T_{-\infty}$ . Suppose that we choose the same  $E_{\pm}$  for both. Then a simple linear algebra calculation shows that

$$\frac{(s \wedge M s)(s' \wedge M s')}{(s \wedge P_+ s')(s \wedge P_- s')} = -(\xi_+ - \xi_-)^2. \quad (5.39)$$

Combining this with the definitions (5.31), (5.35) we find

$$\mathcal{X}_B^{T-\infty} = (\mathcal{X}_B^{T+\infty})^{-1} (\xi_+ - \xi_-)^{-4}. \quad (5.40)$$



## 6. The WKB triangulation

In the last section we reviewed some basic properties of the Fock-Goncharov coordinates  $\mathcal{X}_E^T$ . Now how can these be related to the coordinates  $\mathcal{X}_\gamma^\vartheta$  we want? Upon trying to relate the two, an issue immediately presents itself:  $\mathcal{X}_E^T$  depends on the triangulation  $T$ , while  $\mathcal{X}_\gamma^\vartheta$  does not depend on any triangulation, but depends instead on the angle  $\vartheta$ . So if we want to identify the two we need a way of choosing a canonical triangulation  $T$  depending on  $\vartheta$ . We are not free to make this choice arbitrarily: ultimately we want to engineer  $\mathcal{X}_\gamma^\vartheta$  to obey the properties we listed in Section 2. In particular, we want to control the asymptotic behavior of  $\mathcal{X}_\gamma^\vartheta$  in the limit  $\zeta \rightarrow 0$ .

How can these asymptotics be determined? The basic idea is very simple. As  $\zeta \rightarrow 0$ ,  $\mathcal{A}$  becomes dominated by its leading term  $R\varphi/\zeta$ . At any point of  $C$ ,  $\varphi$  has two eigenvalues  $\pm\lambda$ , where  $\lambda$  is a multivalued one-form on  $C$ , or a single-valued one on the spectral curve  $\Sigma$ . The “WKB approximation” roughly says that, in a gauge where

$$\varphi = \begin{pmatrix} \lambda & 0 \\ 0 & -\lambda \end{pmatrix}, \quad (6.1)$$

there are two independent approximate  $\mathcal{A}$ -flat sections of the form

$$\psi^{(1)} \sim \begin{pmatrix} e^{-\frac{R}{\zeta} \int^z \lambda} \\ 0 \end{pmatrix}, \quad \psi^{(2)} \sim \begin{pmatrix} 0 \\ e^{\frac{R}{\zeta} \int^z \lambda} \end{pmatrix}. \quad (6.2)$$

So one might expect that computing the parallel transport in the  $\zeta \rightarrow 0$  limit will reduce to computing periods of the 1-form  $\lambda$  on  $\Sigma$ .

Working this idea out in detail, it turns out that not all triangulations are created equal. Indeed, if we fix the quadratic differential  $\lambda^2$  and choose an angle  $\vartheta$ , there is a unique “WKB triangulation”  $T_{\text{WKB}}(\vartheta, \lambda^2)$ , for which the WKB approximation gives the correct asymptotics when  $\zeta$  lies in the half-plane  $\mathbb{H}_\vartheta$  centered on  $e^{i\vartheta}$ . In this section we define this triangulation and describe some of its basic properties.

Throughout this section we assume  $\lambda^2$  to be held fixed and generic, meaning that it has only simple zeroes.

### 6.1 WKB curves

Fix any  $\vartheta \in \mathbb{R}/2\pi\mathbb{Z}$ . We define a *WKB curve with angle  $\vartheta$*  to be a curve in  $C$ , with tangent vector  $\partial_t$ , such that

$$\lambda \cdot \partial_t \in e^{i\vartheta} \mathbb{R}^\times \quad (6.3)$$

everywhere along the curve. ( $\lambda$  is defined on  $C$  only up to a sign, but that ambiguity is immaterial for this definition.) These curves define the *WKB foliation with angle  $\vartheta$* .

(Note that the parameter  $t$  in (6.3) has nothing to do with the coordinate  $t$  used in Sections 3 and 9. Moreover, when we speak of “exponential growth” of sections along WKB curves, we are choosing a parametrization in which  $\lambda \cdot \partial_t = \pm e^{i\vartheta}$ .)

## 6.2 Local behavior of WKB curves

Around a generic point of  $C$ , the local behavior of the WKB foliation is trivial: in terms of the local coordinate  $w = \int \lambda$ , it is just the foliation by straight lines  $\operatorname{Im} e^{-i\vartheta} w = \text{const}$ .

Now let us consider the behavior near one of the singular points  $\mathcal{P}$ . We choose coordinates so that it is at  $z = 0$ , and take  $\rho = 2m\sigma^3$ ,  $m \in \mathbb{C}$ , in (4.1). Fixing a choice of branch for  $\lambda$ , near  $z = 0$  we have approximately  $\lambda = \frac{m dz}{z}$ .

Let

$$\varepsilon(\vartheta) = \operatorname{sgn} \left( \operatorname{Re} e^{-i\vartheta} m \right) \quad (6.4)$$

(with the convention that  $\operatorname{sgn} 0 = 0$ ). If  $\varepsilon(\vartheta) = 0$  then there are no WKB curves going into the singularity (instead the WKB curves nearby are circles running around it); we assume for a while that we are not in this degenerate situation, but we will return to this point in Section 7.6.3. So long as  $\varepsilon(\vartheta) \neq 0$  the most general WKB curve is a logarithmic spiral, which we may parameterize so that

$$z(t) = z_0 e^{-\varepsilon(\vartheta) \frac{e^{i\vartheta}}{m} t}. \quad (6.5)$$

This curve goes into the singularity as  $t \rightarrow \infty$ . Note that  $-\varepsilon(\vartheta)$  is the sign of  $e^{-i\vartheta} \lambda \cdot \partial_t$ . In particular, this sign is the same for all WKB curves going into the same singularity.

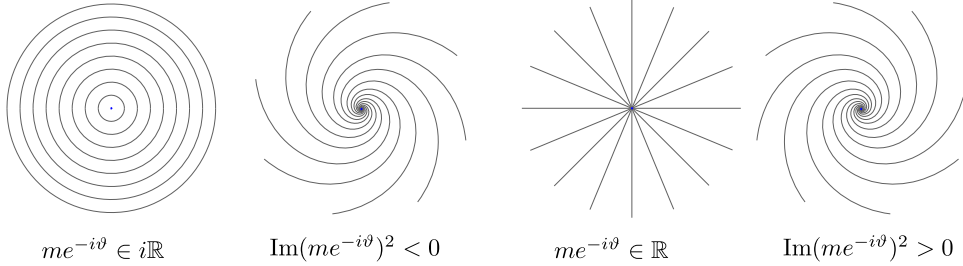


**Figure 23:** Behavior of WKB curves near a singularity.

We will also be interested in the behavior of the WKB foliation near a simple zero of  $\lambda^2$ , also known as a *turning point*. At such a point the foliation becomes singular. Three separating WKB curves emanate from the turning point, as shown in Figure 24. We will discuss these curves further below.

## 6.3 Global behavior of WKB curves

Now let us discuss the global behavior of the WKB foliation. For a general foliation of a Riemann surface, the behavior of the leaves can be quite wild. Fortunately, the WKB foliation is much easier to control. We divide up the WKB curves as follows:

- A *generic* WKB curve is asymptotic in both directions to a singular point (possibly the same one).
- A *separating* WKB curve is asymptotic in one direction to a turning point and in the other direction to a singular point.

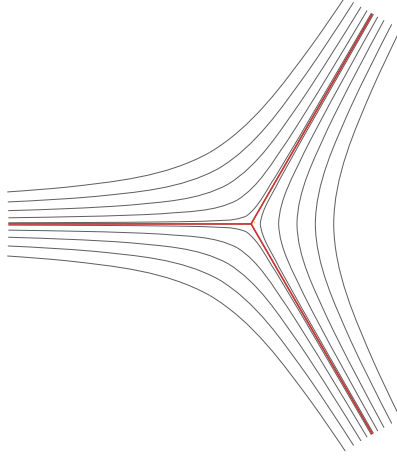


**Figure 24:** Behavior of the WKB foliation near a turning point. Generic WKB curves are shown as thin black curves, separating ones as thicker red curves.

- A *finite* WKB curve is asymptotic in both directions to a turning point (possibly the same one), or closed.
- A *divergent* WKB curve is not closed and does not approach any limit in one or both directions.

In what follows, the values of  $\vartheta$  for which a finite WKB curve exists will play a very special role. They correspond to places where a BPS state appears and the WKB triangulation jumps. So for the moment let us assume that there are no finite WKB curves. In that case, as we now show, there are also no divergent curves.

Suppose (for a contradiction) that  $\alpha$  is a divergent WKB curve. In [60] it is shown that such a curve is actually recurrent: defining  $A$  to be the closure of  $\alpha$ ,  $\alpha$  comes arbitrarily close to every point of  $A$  infinitely many times. Moreover, the interior of  $A$  is a nonempty connected domain, and the boundary of  $A$  consists of finite WKB curves. Since we have stipulated that there are no finite WKB curves, the only possibility is that the boundary of  $A$  is empty: in other words  $A$  fills up  $C$ . In particular,  $\alpha$  comes arbitrarily close to the singular points. But recall from Section 6.5 that the nearby WKB curves are logarithmic spirals going into the singular point (unless  $e^{-i\vartheta}m \in i\mathbb{R}$ , in which case they are closed BPS curves, but we have already excluded this case). So  $\alpha$  cannot pass too close to the singular point, else it would fall in. This gives the desired contradiction. (Note that this argument depends crucially on the fact that we assumed  $l \geq 1$ , i.e. we have some singular points on  $C$ . If  $\lambda^2$  were regular the WKB foliation could be considerably more complicated.<sup>31</sup>) Hence our foliation consists only of generic and separating WKB curves. The generic WKB curves fall into 1-parameter families; each family sweeps out a “cell” bounded by a union of separating WKB curves [60]. In the  $w$  coordinate such a cell just looks like a strip at angle

<sup>31</sup>This is one indication that when  $C$  has no defect operators the spectrum of BPS states is qualitatively different. Indeed, in the absence of singularities on  $C$  we would expect that there are arbitrarily long closed WKB curves. Correspondingly, when there are no defect operators we expect that there is an infinite spectrum of BPS vectormultiplets with arbitrarily large masses.

$\vartheta$ . Again using the assumption that there are no finite WKB curves, the two boundaries of this strip each can contain only a single turning point. One subtlety is that these two turning points may actually be identified. It follows that there are two possible topologies for the closure of the cell, shown in Figure 25.<sup>32</sup>

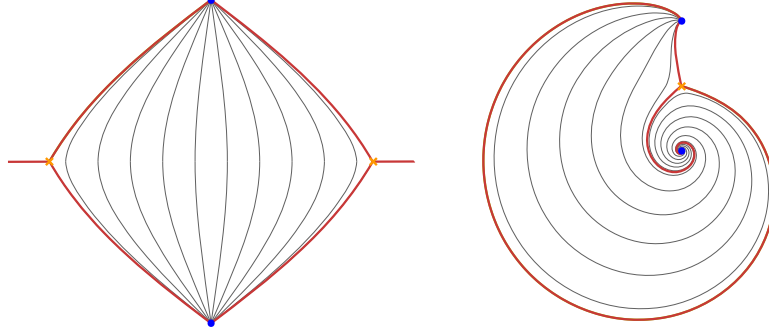


**Figure 25:** The two possible cells swept out by generic WKB curves: a diamond and a disc. The disc can be considered as a degenerate diamond, obtained by identifying the two turning points. Generic WKB curves are indicated by thin black curves, separatrices by thick red ones.

#### 6.4 Defining the WKB triangulation

Now we will define the WKB triangulation. It is roughly “dual” to the cell decomposition we have just seen.

We assume that all turning points are *simple* zeroes of  $\lambda^2$ . Choose one generic WKB curve  $E_i$  in each family. The  $E_i$  divide  $C$  into faces. Each face must contain a turning point (this follows from the fact that the edges belong to different cells and the boundary of each cell is made up of separating WKB curves.) So let us focus on a single turning point  $\mathcal{T}$ . The WKB curves running near  $\mathcal{T}$  are the edges of a face  $F$ . Looking at Figure 24, we see that  $\mathcal{T}$  is on the boundary of at most three cells. If there are exactly three then  $F$  is a triangle. It can also happen that two of the three classes of curve pictured in Figure 24 actually belong to a single cell. In this case  $F$  is a degenerate triangle.

We conclude that the  $E_i$  are the edges of a triangulation of  $C$ , with faces of two types, pictured in Figure 26. The topology of the triangulation does not depend on which generic  $E_i$  we choose within a cell, and therefore we identify two triangulations that differ by such a choice. That is, by “triangulation” we really mean an isotopy class of triangulations. With this identification understood, we have defined a triangulation of  $C$ .

#### 6.5 The WKB decoration: small flat sections

So far we have used the WKB foliation to define an undecorated triangulation. To construct  $\mathcal{X}_\gamma^\vartheta$ , we also need some canonical way of choosing a decoration.

We first consider the behavior of the flat sections around one of the singular points, which for convenience we put at  $z = 0$ . The behavior of the connection around this point

<sup>32</sup>If we had only  $l = 2$  singular points and  $C = \mathbb{CP}^1$ , there would have been a third possible kind of cell, consisting of the whole of  $C$ ; but we excluded this case by considering only  $l \geq 3$ .

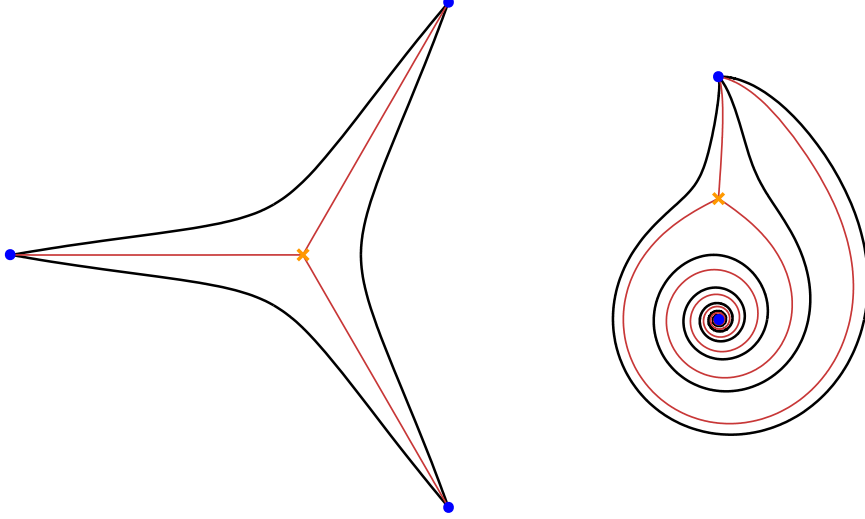


**Figure 26:** The two types of faces occurring in the WKB triangulation. On the left is an honest triangle. On the right is a degenerate triangle, with only two distinct edges and two vertices (compare Figure 19). Each face contains a single turning point. Edges of the WKB triangulation are indicated by thick black curves, separatrices by thin red ones.

is given by (4.9), determined by the residues  $\rho$  and  $\alpha$  of  $\varphi$  and  $A$  respectively. We take  $\rho = 2m\sigma^3$ , where  $m \in \mathbb{C}$ , and  $\alpha = -2im^{(3)}\sigma^3$ , where  $m^{(3)} \in \mathbb{R}$ .

Then by the standard Frobenius analysis of the behavior around a regular singular point (slightly modified here since we consider a  $C^\infty$  connection rather than a holomorphic one) there are two flat sections of the form

$$s^{(1)} = z^{-R\zeta^{-1}m+m^{(3)}} \bar{z}^{-R\zeta\bar{m}-m^{(3)}} \begin{pmatrix} 1 + O(|z|) \\ O(|z|) \end{pmatrix}, \quad (6.6)$$

$$s^{(2)} = z^{R\zeta^{-1}m-m^{(3)}} \bar{z}^{R\zeta\bar{m}+m^{(3)}} \begin{pmatrix} O(|z|) \\ 1 + O(|z|) \end{pmatrix}. \quad (6.7)$$

They have clockwise monodromy eigenvalues  $\mu^{(1)} = e^{2\pi i\nu}$ ,  $\mu^{(2)} = e^{-2\pi i\nu}$ , where

$$\nu = R\zeta^{-1}m - 2m^{(3)} - R\zeta\bar{m}. \quad (6.8)$$

Let us evaluate their behavior along a WKB curve going into the singularity. Using (6.5) we obtain

$$s^{(1)} \sim \exp \left[ \varepsilon(\vartheta) \left\{ R(e^{i\vartheta}\zeta^{-1} + e^{-i\vartheta}\zeta) + m^{(3)} \left( \frac{e^{-i\vartheta}}{\bar{m}} - \frac{e^{i\vartheta}}{m} \right) \right\} t \right] \quad (6.9)$$

where  $\varepsilon(\vartheta)$  was defined in (6.4). The piece multiplying  $m^{(3)}$  is a pure phase and does not affect the norm of  $s^{(1)}$ . Looking at the remaining piece we see that  $\|s^{(1)}\|$  is exponentially small as  $t \rightarrow \infty$  if  $\varepsilon(\vartheta) \operatorname{Re}(e^{i\vartheta}\zeta^{-1} + e^{-i\vartheta}\zeta) < 0$ . Similarly,  $\|s^{(2)}\|$  is exponentially small as  $t \rightarrow \infty$  if  $\varepsilon(\vartheta) \operatorname{Re}(e^{i\vartheta}\zeta^{-1} + e^{-i\vartheta}\zeta) > 0$ .

Thus, if  $\zeta \in \mathbb{H}_\vartheta$ , the eigensection with clockwise monodromy

$$\mu = e^{(-\varepsilon(\vartheta))2\pi i\nu} = \exp \left[ (-\varepsilon(\vartheta))2\pi i \left( R\zeta^{-1}m - 2m^{(3)} - R\zeta\bar{m} \right) \right] \quad (6.10)$$

is asymptotically smaller in norm than all other flat sections along a WKB curve going into the singularity. We call it the “small flat section.” We will see in Section 7.4 that if  $\zeta \rightarrow 0$  while remaining in  $\mathbb{H}_\vartheta$  the WKB approximation gives us good control over the evolution of this section along a WKB curve. With this motivation, we choose this small flat section as our canonical decoration at the singularity.

We have now finished defining a decorated triangulation  $T_{\text{WKB}}(\vartheta, \lambda^2)$  for each  $(\vartheta, \lambda^2)$ . We call it the *WKB triangulation*. To lighten notation we will sometimes write it as  $T_{\text{WKB}}(\vartheta)$  or even just  $T_{\text{WKB}}$ . Recalling that the quadratic differentials  $\lambda^2$  correspond to points  $u \in \mathcal{B}$  we also sometimes write  $T_{\text{WKB}}(\vartheta, u)$ .

## 6.6 Jumps of the WKB triangulation

As we vary the parameter  $\vartheta$  the WKB foliation changes, and correspondingly  $T_{\text{WKB}}(\vartheta)$  changes. For generic  $\vartheta$ ,  $T_{\text{WKB}}(\vartheta)$  just changes by a continuous homotopy of the edges, and hence the isotopy class of the triangulation is constant. However, there are some special values  $\vartheta = \vartheta_c$  at which  $T_{\text{WKB}}(\vartheta)$  jumps discontinuously.

These jumps are of crucial importance for us: they are related to the existence of BPS states. Indeed, the topology of  $T_{\text{WKB}}$  is completely determined by the behavior of the separating WKB curves, and this behavior jumps exactly when a separatrix degenerates to include a finite WKB curve.<sup>33</sup> Now comparing (3.11) with (6.3) we see that BPS strings and WKB curves obey exactly the same equation; a finite WKB curve is just the same thing as a BPS string with finite total mass. Thus, the values  $\vartheta_c$  at which the WKB foliation changes topology are the phases of BPS states.

We now examine the three kinds of topology changes of  $T_{\text{WKB}}(\vartheta)$  which can occur as  $\vartheta$  varies.

### 6.6.1 A jump from a BPS hypermultiplet

The fundamental example of a topology change occurs at  $\vartheta = \vartheta_c$  for which a WKB curve appears connecting two turning points. As we described in Section 3.1.3, this finite WKB curve represents a BPS hypermultiplet of the  $d = 4$  theory.

As  $\vartheta$  crosses  $\vartheta_c$ , the WKB foliation undergoes a topology change; see Figure 27. In particular, the generic WKB curve running from northwest to southeast is replaced by one running from northeast to southwest. Since this generic WKB curve represents one of the edges  $E$  of  $T_{\text{WKB}}$ , we see that this triangulation undergoes a flip as  $\vartheta$  crosses  $\vartheta_c$ .

---

<sup>33</sup>Consider a separating WKB curve starting from  $z_0$ . In the  $w$ -plane, where  $w = \int_{z_0}^z \lambda$  is defined in some neighborhood of the separating curve, the curve is a straight line. It varies continuously with  $\vartheta$ . This only fails when there is no open neighborhood of the separating WKB curve that does not contain another turning point. That is, it only fails when the separating WKB curve contains a finite WKB curve.

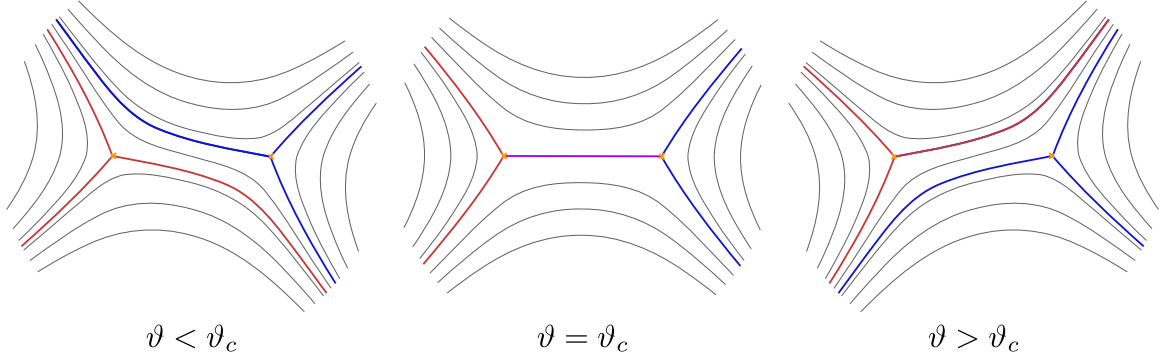


**Figure 27:** The jump of the WKB foliation as  $\vartheta$  crosses a critical  $\vartheta_c$  at which a finite WKB curve appears, corresponding to a BPS hypermultiplet.

### 6.6.2 A jump when $me^{-i\vartheta} \in i\mathbb{R}$

A more intricate jumping behavior occurs at phases  $\vartheta = \vartheta_c$  for which closed WKB curves exist. As we described in Section 3.1.3, these closed WKB curves always appear in one-parameter families.

The simplest possibility is a family of closed WKB curves surrounding a single singular point. As we already saw in Section 6.2, such a family appears whenever  $me^{-i\vartheta} \in i\mathbb{R}$ . The behavior of the WKB foliation near this value of  $\vartheta$  is shown in Figure 28.

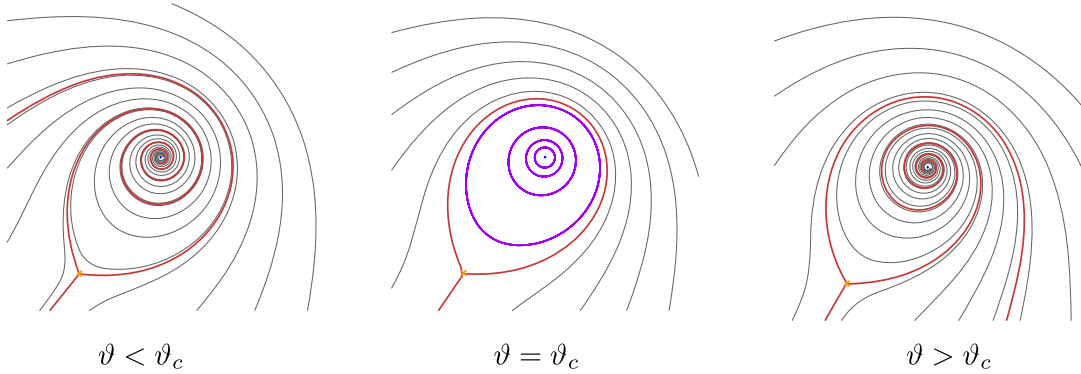


**Figure 28:** The jump of the WKB foliation as  $\vartheta$  crosses a critical  $\vartheta_c$  at which a family of closed WKB curves appears surrounding a single singular point.

In Section 6.5 we defined the decoration of the WKB triangulation, which is determined by the sign  $\varepsilon(\vartheta)$  of  $\text{Re}(e^{-i\vartheta}m)$ . This sign changes sign at  $\vartheta_c$ . It follows that at  $\vartheta_c$  the WKB triangulation undergoes a pop.

### 6.6.3 A jump from a BPS vectormultiplet

Another possibility is a family of closed WKB curves which does not contract onto a single singular point. This corresponds to a BPS vectormultiplet which carries some nonzero gauge charge.

Generically, when such a vectormultiplet appears it is accompanied by two infinite families of hypermultiplets: if we look at a narrow enough interval  $\vartheta_- < \vartheta < \vartheta_+$  containing



$\vartheta_c$ , then the WKB triangulation varies smoothly with  $\vartheta$  except in one annular region of  $C$ , and in this annular region the WKB triangulation undergoes an infinite sequence of flips. The situation is precisely the one we considered in Section 5.9. As  $\vartheta$  decreases starting from  $\vartheta_+$ ,  $T_{\text{WKB}}(\vartheta, \lambda^2)$  runs through a sequence of triangulations  $T_m$  with  $m > 0$ , and  $m \rightarrow \infty$  as  $\vartheta \rightarrow \vartheta_c^+$ . On the other hand, if we instead start from  $\vartheta_-$ , then as  $\vartheta$  increases  $T_{\text{WKB}}(\vartheta, \lambda^2)$  runs through all of the  $T_m$  with  $m < 0$ , and  $m \rightarrow -\infty$  as  $\vartheta \rightarrow \vartheta_c^-$ .

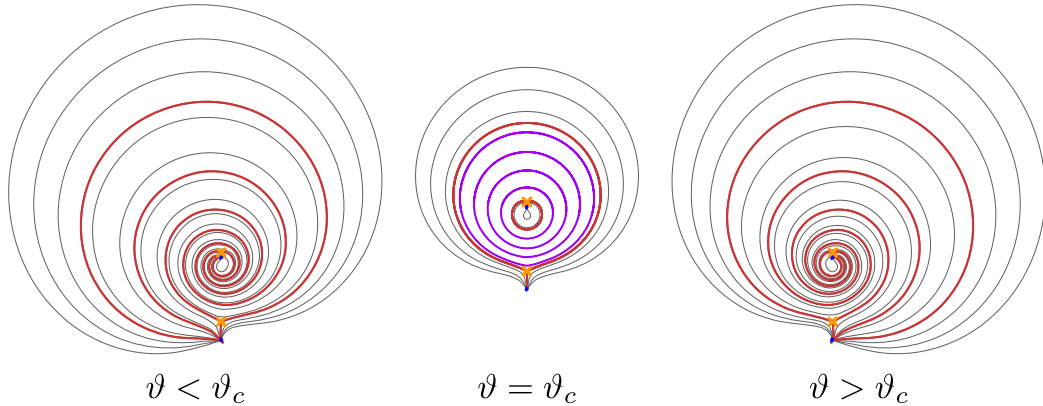


**Figure 29:** An annular region of the WKB foliation, near a critical  $\vartheta = \vartheta_c$  at which a family of closed WKB curves representing a BPS vectormultiplet appears.

Roughly speaking, after  $m$  flips a typical WKB curve runs around the annulus  $m$  times, either clockwise or counterclockwise depending whether  $\vartheta > \vartheta_c$  or  $\vartheta < \vartheta_c$ . Exactly at  $\vartheta = \vartheta_c$  the WKB curves become closed curves foliating an open region inside the annulus. See Figure 29.

#### 6.6.4 Other degenerations are nongeneric

Let us now briefly justify our claim that for *generic* quadratic differentials  $\lambda^2$  only the above three degenerations of the WKB triangulation occur as we vary  $\vartheta$ . (For non-generic moduli, other degenerations of  $T_{\text{WKB}}(\vartheta, \lambda^2)$  can and do occur. We will see an example in Section 10.2 below.)

A critical value  $\vartheta_c$  occurs when a separating WKB curve degenerates to include a finite WKB curve, which begins and ends on a turning point. There are only two possibilities: either these two turning points are the same or they are different. If the two turning points are the different, then the finite WKB curve has no moduli, and the behavior near  $\vartheta_c$  must be the hypermultiplet degeneration of Section 6.6.1. If the two turning points are the same, then the WKB curve going through an infinitesimally displaced point (in the cell of the foliation bounded locally by the finite WKB curve) must be closed. These closed WKB curves come in a one-parameter family. This family could terminate when the closed WKB curve hits a singular point, shrinks to zero size, or hits a turning point. Examining the local behavior near singular points (for generic  $m$ ) we see that the family of closed WKB curves cannot end by hitting one. If the closed WKB curves shrink to zero size then we are in the situation of Section 6.6.2. The last possibility is for the closed WKB curve to hit



another turning point. In the generic case it will hit exactly one turning point. Thus, our family describes precisely the situation encountered in the degeneration of Section 6.6.3.

## 7. The canonical coordinates

In this section, we will finally define the functions  $\mathcal{X}_\gamma$  and check that they have all of the properties we promised in Section 2.

### 7.1 Labeling by homology

As we saw in the last section, there is a canonical choice of triangulation  $T_{\text{WKB}}$  determined by the WKB foliation. We will use this triangulation. However, there is one more crucial issue to deal with before we can identify  $\mathcal{X}_\gamma$  with  $\mathcal{X}_E^{T_{\text{WKB}}}$ . The coordinates  $\mathcal{X}_E^{T_{\text{WKB}}}$  are labeled by the edges  $E$  of  $T_{\text{WKB}}$ , but we want our  $\mathcal{X}_\gamma$  to be labeled by classes  $\gamma \in \hat{\Gamma}$ . So we need to specify a map from the set of edges of  $T_{\text{WKB}}$  to  $\hat{\Gamma}$  and we will do so by defining a homology class  $\gamma_E \in H_1(\Sigma; \mathbb{Z})$  associated to each edge  $E$  of  $T_{\text{WKB}}$ .<sup>34</sup>

Since  $T_{\text{WKB}} = T_{\text{WKB}}(\vartheta)$  depends on  $\vartheta$ , we will sometimes write this map as  $E \mapsto \gamma_E^\vartheta$ . Throughout this section we assume  $\vartheta$  is generic.

#### 7.1.1 For ordinary edges

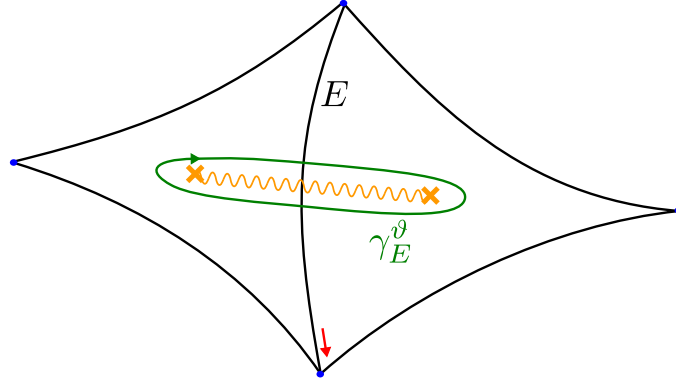


**Figure 30:** The construction of  $\gamma_E^\vartheta \in H_1(\Sigma; \mathbb{Z})$ .  $\Sigma$  is a double cover of the base  $C$ . To draw the picture we choose definite branch cuts for this double cover. Having done so, we can speak about the two sheets of the covering. We call the two sheets “upper” and “lower”, arbitrarily. A solid green line indicates a curve on the upper sheet. A red arrow next to a segment of an edge indicates the orientation of the lift of this segment to the upper sheet. (Specifying this orientation for one segment determines it for all segments.)

Given an edge  $E$  of the WKB triangulation, the quadrilateral  $Q_E$  contains two turning points. Draw a loop in  $Q_E$  which surrounds these two turning points. We aim to define a connected lift of this loop to the spectral curve to obtain a class  $\gamma_E^\vartheta \in H_1(\Sigma; \mathbb{Z})$ . There are two ambiguous choices here: the orientation of the loop and which of the two sheets we lift

<sup>34</sup>Recall from Section 3.1.4 that in the “ $K = 2$ ” case we are considering,  $\hat{\Gamma}$  is simply the sublattice (not subquotient!) of  $H_1(\Sigma; \mathbb{Z})$  which is odd under the deck transformation exchanging the two sheets.

it to. Clearly, reversing the orientation changes the sign of  $\gamma_E^\vartheta$ . Moreover, one can easily see that either connected lift of the loop is odd under the deck transformation exchanging the two sheets. So these two ambiguous choices just affect the overall sign of  $\gamma_E^\vartheta$ .

We fix this sign as follows. On  $\Sigma$ ,  $\lambda$  is a single-valued 1-form. Thus, the two possible lifts  $\hat{E}$  of any edge  $E$  of the WKB triangulation each have an orientation, defined by the condition that the positively oriented tangent vector  $\partial_t$  to  $\hat{E}$  obeys  $e^{-i\vartheta} \lambda \cdot \partial_t > 0$ . Note that  $\hat{E}$  defines a cycle in the relative homology group  $H_1(\Sigma, \{\mathcal{P}_i\}; \mathbb{Z})$ . This has a well-defined pairing with  $H_1(\Sigma; \mathbb{Z})$  and we demand that the intersection  $\langle \gamma_E^\vartheta, \hat{E} \rangle = 1$ . (This is independent of which of the two possible lifts  $\hat{E}$  we chose.) See Figure 30.<sup>35</sup>

The intersection pairing on these cycles agrees with the pairing on edges we defined above. That is, for all  $E, E'$ :

$$\langle \gamma_E^\vartheta, \gamma_{E'}^\vartheta \rangle = \langle E, E' \rangle, \quad (7.1)$$

as illustrated in Figure 31.

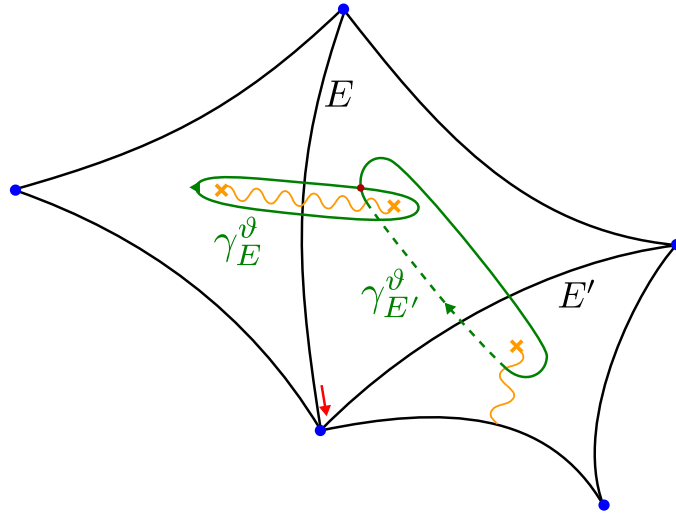


**Figure 31:** A pair of edges with  $\langle E, E' \rangle = 1$  also have  $\langle \gamma_E^\vartheta, \gamma_{E'}^\vartheta \rangle = 1$ .

### 7.1.2 For degenerate edges

We can also consider faces of the WKB triangulation which are degenerate in the sense of Section 5.8. In this case our rule for defining the cycles  $\gamma_E, \gamma_{E'}$  cannot be straightforwardly applied. To get around this difficulty we pass to a covering surface, just as we did to define the Fock-Goncharov coordinates in Section 5.8. The edges  $E, E'$  have multiple preimages on the covering surface. We choose any preimages  $\tilde{E}, \tilde{E}'$  and then construct  $\gamma_{\tilde{E}}^\vartheta$  and  $\gamma_{\tilde{E}'}^\vartheta$  as above. See Figure 32. These cycles then descend to the desired  $\gamma_E^\vartheta$  and  $\gamma_{E'}^\vartheta$ , pictured in Figure 33, which are independent of the choice of preimage.

### 7.1.3 Cycles around singular points

To every singular point  $\mathcal{P}_i$  there is a corresponding privileged cycle  $C_i$  on  $\Sigma$ , consisting of two small loops running around  $\mathcal{P}_i$  in opposite directions on the two sheets, oriented so

<sup>35</sup>Our convention is that in the standard orientation for the  $xy$  plane,  $\langle x\text{-axis}, y\text{-axis} \rangle = +1$ .

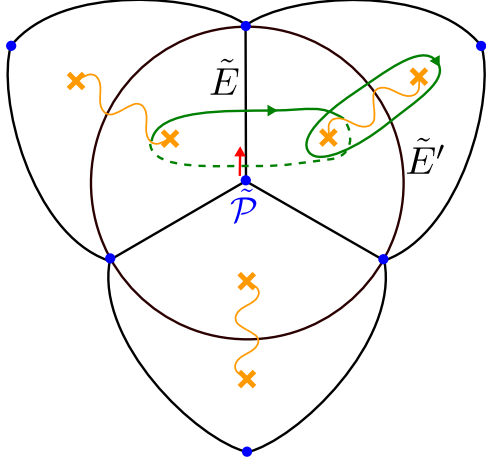


**Figure 32:** The covering surface which we use to resolve a degenerate face.

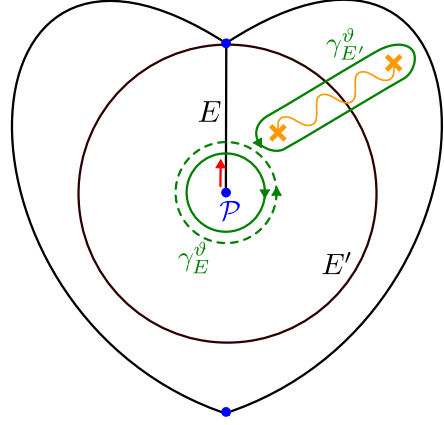


**Figure 33:** Cycles  $\gamma_{E'}^\varphi$  and  $\gamma_E^\varphi$  associated to a degenerate face.

that  $\langle C_i, \hat{E} \rangle = 1$  when  $E$  is any edge incident on  $\mathcal{P}_i$  (recall that the lifted edges  $\hat{E}$  have natural orientations). See Figure 34. The cycle  $C_i$  has a simple expression in terms of the

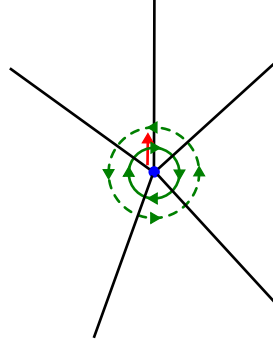


**Figure 34:** The cycle  $C_i$  associated to the puncture  $\mathcal{P}_i$ .

$\gamma_E$ :

$$C_i = \sum_{E \text{ meeting } \mathcal{P}_i} \gamma_E. \quad (7.2)$$

This fact is illustrated in Figure 35 for  $\mathcal{P}_i$  a generic vertex (with two or more edges incident on it). If  $\mathcal{P}_i$  is a degenerate vertex (with only one edge  $E$  incident on it) then Figure 33 shows directly that  $C_i = \gamma_E$ .

#### 7.1.4 Lattice generated by $\{\gamma_E\}$

The vectors  $\{\gamma_E\}$  for  $E$  running over the edges of  $T_{\text{WKB}}$  generate a sublattice of  $\hat{\Gamma}$ , and we now show that they in fact generate the entire lattice  $\hat{\Gamma}$ .

First, we show that the lattice generated by  $\{\gamma_E\}$  has the correct rank. When  $C$  has genus  $g_C$  the quadratic differential  $\lambda^2$  has  $4g_C - 4 + 2l$  zeroes. Since these are simple zeroes, by the Riemann-Hurwitz formula the genus of  $\bar{\Sigma}$  is  $g_{\bar{\Sigma}} = 4g_C + l - 3$ . Using the Lefschetz fixed point formula the rank of the anti-invariant sublattice of  $H_1(\bar{\Sigma}; \mathbb{Z})$  is  $6g_C + 2l - 6$ .

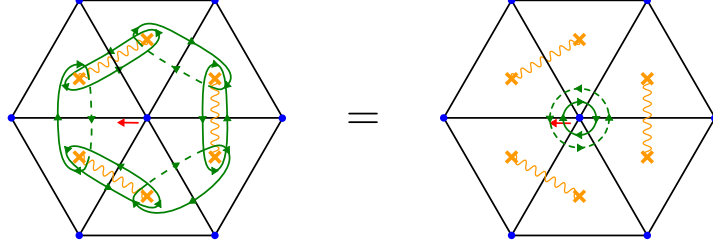


**Figure 35:** The sum of  $\gamma_E$  over all  $E$  meeting the vertex  $\mathcal{P}_i$  gives  $C_i$ .

Introducing the punctures we find that the rank of  $\hat{\Gamma}$ , the anti-invariant part of  $H_1(\Sigma; \mathbb{Z})$ , is  $6g_C + 3l - 6$ , precisely correct for the lattice generated by  $\{\gamma_E\}$ . (Recall equation (5.8).) Hence the rational vector space  $\hat{\Gamma} \otimes \mathbb{Q}$  is generated by  $\{\gamma_E\}$ . It follows that any primitive vector  $V \in \hat{\Gamma}$  can be written as  $\sum c_E \gamma_E$  with  $c_E \in \mathbb{Q}$ . Now, the relative homology  $H_1(\Sigma, \{\mathcal{P}_i\}; \mathbb{Z})$  is Poincaré dual to  $H_1(\Sigma; \mathbb{Z})$  so  $\langle V, \hat{E}' \rangle \in \mathbb{Z}$ . Recall that  $\langle \gamma_E, \hat{E}' \rangle = \delta_{E, E'}$  so we see that the coefficients  $c_E$  must in fact be integral.

## 7.2 Defining the canonical coordinates

We define  $\mathcal{X}_\gamma^{\vartheta, u_0}$  by the properties

$$\mathcal{X}_{\gamma_E^{\vartheta}}^{\vartheta, u_0} := \mathcal{X}_E^{T_{\text{WKB}}(\vartheta, u_0)} \quad (7.3)$$

for all edges  $E$  in the triangulation  $T_{\text{WKB}}(\vartheta, u_0)$  and

$$\mathcal{X}_{\gamma+\gamma'}^{\vartheta, u_0} = \mathcal{X}_\gamma^{\vartheta, u_0} \mathcal{X}_{\gamma'}^{\vartheta, u_0}. \quad (7.4)$$

for all  $\gamma, \gamma'$ . Since the  $\gamma_E^{\vartheta}$  are a basis of  $\hat{\Gamma}$ , these two properties define  $\mathcal{X}_\gamma^{\vartheta}$ .

We will mostly emphasize the  $\vartheta$ -dependence of these functions at fixed  $u_0$ , and hence we almost always denote them as  $\mathcal{X}_\gamma^{\vartheta}$ .

## 7.3 Some easy properties

Let us note a few easy properties of these canonical coordinates. First, using (5.9), (7.1), and (7.4) we see that in terms of the homology labeling the Poisson structure is simply

$$\{\mathcal{X}_\gamma^{\vartheta}, \mathcal{X}_{\gamma'}^{\vartheta}\} = \langle \gamma, \gamma' \rangle \mathcal{X}_{\gamma+\gamma'}^{\vartheta} \quad \forall \gamma, \gamma' \in \hat{\Gamma}. \quad (7.5)$$

Second, in (5.4) we noted that the product of the  $\mathcal{X}_E^T$  for all  $E$  meeting the singular point  $\mathcal{P}_i$  is  $\mu_i^2$ . On the other hand we saw in Section 7.1.3 that the sum of the  $\gamma_E^{\vartheta}$  over all these  $E$  is the cycle  $C_i$ . Combining these two statements we arrive at the simple rule that

$$\mathcal{X}_{C_i}^{\vartheta} = \mu_i^2. \quad (7.6)$$

Finally we want to establish the reality condition obeyed by the  $\mathcal{X}_\gamma^{\vartheta}$ . Note that by the definition (4.8) of  $\mathcal{A}$  we have

$$\mathcal{A}(\zeta) = -\overline{\mathcal{A}(-1/\bar{\zeta})} \quad (7.7)$$

from which it follows that, if  $s$  is a flat section for  $\mathcal{A}(\zeta)$ , then  $\bar{s}/\|s\|^2$  is a flat section for  $\mathcal{A}(-1/\bar{\zeta})$ . In particular, if  $s_i$  is the small flat section for  $\mathcal{A}(\zeta)$  at some singularity  $\mathcal{P}_i$  and at angle  $\vartheta$ , then  $\bar{s}_i/\|s_i\|^2$  is the *large* flat section at  $\mathcal{P}_i$  for  $\mathcal{A}(-1/\bar{\zeta})$  at angle  $\vartheta$ , or equivalently, it is the small flat section at  $\mathcal{P}_i$  for  $\mathcal{A}(-1/\bar{\zeta})$  at angle  $\vartheta + \pi$ . Comparing the definitions (5.2) at  $\zeta$  and  $-1/\bar{\zeta}$ , we obtain directly

$$\mathcal{X}_E^{T_{\text{WKB}}(\vartheta)}(\zeta) = \overline{\mathcal{X}_E^{T_{\text{WKB}}(\vartheta+\pi)}(-1/\bar{\zeta})}. \quad (7.8)$$

We also have as usual

$$\gamma_E^\vartheta = -\gamma_E^{\vartheta+\pi}. \quad (7.9)$$

Combining (7.8) and (7.9) gives the desired reality condition

$$\mathcal{X}_\gamma^\vartheta(\zeta) = \overline{\mathcal{X}_{-\gamma}^{\vartheta+\pi}(-1/\bar{\zeta})}. \quad (7.10)$$

#### 7.4 Asymptotic behavior

Now we come to the main motivation of our definition of the WKB triangulation and our labeling of the coordinates by cycles in  $H_1(\Sigma; \mathbb{Z})$ . We claim that, as  $\zeta \rightarrow 0$  within the half-plane  $\mathbb{H}_\vartheta$ , the asymptotics of  $\mathcal{X}_\gamma$  are simply

$$\mathcal{X}_\gamma^\vartheta \sim c_\gamma \exp(\zeta^{-1} \pi R Z_\gamma), \quad (7.11)$$

where  $c_\gamma$  is some function on  $\mathcal{M}$  which is independent of  $\zeta$ .

To obtain the asymptotics (7.11) we use directly the definition of  $\mathcal{X}_\gamma$ . Suppose  $\gamma = \gamma_E^\vartheta$  for some nondegenerate edge  $E$  as in Figure 14. Then we will apply the WKB approximation for the parallel transport of the small flat sections (decorations) along the edges. Choose a gauge along the edges such that

$$\varphi = \begin{pmatrix} \lambda & 0 \\ 0 & -\lambda \end{pmatrix}, \quad (7.12)$$

with the sign chosen so that  $e^{-i\vartheta} \lambda \cdot \partial_t < 0$  for  $\partial_t$  along  $E_{12}$  oriented away from  $z_1$ , toward  $z_2$ .

Let  $I_1(z)$  be an antiderivative of  $\lambda$ , defined on a neighborhood of the two edges  $E_{12}$  and  $E_{41}$  (here by “edge” we mean an open curve, excluding its endpoints). One would expect by the WKB approximation that one can choose the flat section  $s_1(z, \zeta)$  such that along  $E_{12}$  we have the  $\zeta \rightarrow 0$  asymptotics

$$s_1(z, \zeta) \sim c_1(z) \begin{pmatrix} e^{-\frac{R}{\zeta} I_1(z)} \\ 0 \end{pmatrix}. \quad (7.13)$$

In Appendix C we argue that this is indeed the case. The argument depends crucially on the fact that  $E_{12}$  is a WKB curve and on our choice of the WKB decoration: the point is that these choices ensure that the errors introduced in using the WKB approximation to  $s_1$  are exponentially smaller than  $s_1$  itself, and that they remain so as we evolve along  $E_{12}$ . Similarly let  $I_2(z)$  be an antiderivative of  $\lambda$ , defined on a neighborhood of the two

edges  $E_{12}$  and  $E_{23}$ . Again using Appendix C one can choose  $s_2(z, \zeta)$  such that along  $E_{12}$  we have the  $\zeta \rightarrow 0$  asymptotics

$$s_2(z, \zeta) \sim c_2(z) \begin{pmatrix} 0 \\ e^{\frac{R}{\zeta} I_2(z)} \end{pmatrix}. \quad (7.14)$$

Evaluating both at some general point  $z_{12}$  of  $E_{12}$  we get

$$s_1 \wedge s_2 \sim c_{12} \exp \left( \frac{R}{\zeta} (I_2(z_{12}) - I_1(z_{12})) \right). \quad (7.15)$$

Similar arguments with the indices 1234 permuted give

$$s_2 \wedge s_3 \sim c_{23} \exp \left( -\frac{R}{\zeta} (I_3(z_{23}) - I_2(z_{23})) \right), \quad (7.16)$$

$$s_3 \wedge s_4 \sim c_{34} \exp \left( \frac{R}{\zeta} (I_4(z_{34}) - I_3(z_{34})) \right), \quad (7.17)$$

$$s_4 \wedge s_1 \sim c_{41} \exp \left( -\frac{R}{\zeta} (I_1(z_{41}) - I_4(z_{41})) \right), \quad (7.18)$$

where we have made the obvious extensions of our notation, and we have chosen  $\lambda$  to be single-valued in a neighborhood of the union of all the edges. Combining these gives

$$\mathcal{X}_\gamma^\vartheta \sim c_\gamma \exp \left( \frac{R}{\zeta} (I_1(z_{41}) - I_1(z_{12}) + I_2(z_{12}) - I_2(z_{23}) + I_3(z_{23}) - I_3(z_{34}) + I_4(z_{34}) - I_4(z_{41})) \right). \quad (7.19)$$

If  $\lambda$  were single-valued on the whole  $Q_E$  we could have taken all  $I_i$  to be the same function, in which case they would cancel out in (7.19). Because of the two branch points in the interior of  $Q_E$  this cancellation does not occur. Instead, using  $I_i(z') - I_i(z) = \int_z^{z'} \lambda$ , (7.19) becomes

$$\mathcal{X}_\gamma^\vartheta \sim c_\gamma \exp \left( \frac{R}{\zeta} \oint_\gamma \lambda \right). \quad (7.20)$$

This is the key result: the period integral over  $\Sigma$  has emerged naturally from the WKB approximation!

If  $\gamma = \gamma_E^\vartheta$  with  $E$  a *degenerate* edge we obtain the same result in a slightly different way. In Section 7.1.2 this  $\gamma$  was defined as the sum of two loops running in opposite directions around the two lifts of the vertex. Then the period of  $\lambda$  is just determined by the residue of  $\varphi$  at the vertex, which was fixed by our boundary conditions: we obtain

$$\oint_\gamma \lambda = -4\pi i m \varepsilon(\vartheta). \quad (7.21)$$

On the other hand we know from (5.23) that  $\mathcal{X}_E^T = (\mu^T)^2$ , with  $\mu^T$  the eigenvalue of the clockwise monodromy around the degenerate vertex, in turn given by (6.10):

$$\mathcal{X}_E^T \sim \exp \left[ -\varepsilon(\vartheta) 4\pi i \left( \frac{R}{\zeta} m - 2m^{(3)} \right) \right]. \quad (7.22)$$

Comparing (7.21) and (7.22) we see that we obtained the expected (7.20) just as for non-degenerate edges. (We also got a small bonus in this case: the constant  $c_\gamma$  which gives the finite part of the asymptotics is just  $c_\gamma = e^{8\pi i \varepsilon(\vartheta)m^{(3)}}$ .)

Having established (7.20) for all  $\gamma_E^\vartheta$ , it holds for all  $\gamma \in \hat{\Gamma}$  by multiplicativity. Then finally recalling that  $Z_\gamma = \frac{1}{\pi} \oint_\gamma \lambda$ , (7.20) becomes the desired (7.11).

## 7.5 From triangulations to KS symplectomorphisms

Let us briefly take stock of where we are. We have just seen from the WKB analysis that the asymptotic properties of the coordinate systems  $\mathcal{X}^{T_{\text{WKB}}}$  are captured well by certain simple properties of the corresponding decorated triangulation  $T_{\text{WKB}}$ . To any sector  $\mathcal{V}$  around the origin in the  $\zeta$ -plane, with angular opening  $\pi$  or smaller, we can associate a nice subgroupoid  $\mathcal{T}_\mathcal{V}$  of decorated triangulations. A triangulation is in  $\mathcal{T}_\mathcal{V}$  if homotopy representatives of the edges can be picked with two basic properties: a) for all  $\zeta \in \mathcal{V}$ , the decorations are exponentially small going along the edges into the singularities, and b) along each edge,  $\lambda \cdot \partial_t$  lies in  $\mathcal{V}$  (for some choice of the sign of  $\lambda$ ). The WKB analysis tells us that the functor defined in Section 5 maps each triangulation in  $\mathcal{T}_\mathcal{V}$  to a Darboux coordinate system with “good asymptotics” in the sector  $\mathcal{V}$ : by this we mean that each function is naturally labeled by a cycle in  $\hat{\Gamma}$ , and  $\lim_{\zeta \rightarrow 0} \mathcal{X}_\gamma(\zeta) \exp[-\zeta^{-1} \pi R Z_\gamma]$  is finite if  $\zeta \in \mathcal{V}$ .

Because of this labeling, we can consider each coordinate system as a map to an abstract complex torus with a system of Fourier modes  $X_\gamma$ , and each coordinate transformation simply as a symplectomorphism of that torus. For any  $\vartheta_+, \vartheta_-$ ,  $\vartheta_+ - \vartheta_- \leq \pi$ , the transformation of coordinates relating the coordinate systems  $\mathcal{X}_\gamma^{\vartheta_\pm}$  is an interesting symplectomorphism  $\mathbf{S}(\vartheta_+, \vartheta_-; u)$ . Anticipating our results, we use the same nomenclature as in Section 2. By construction, if  $\vartheta_- < \vartheta < \vartheta_+$ , then  $\mathbf{S}(\vartheta_+, \vartheta_-; u) = \mathbf{S}(\vartheta_+, \vartheta; u) \mathbf{S}(\vartheta, \vartheta_-; u)$ .

The “Stokes factors” mentioned in Section 2 emerge in the limit where  $\vartheta_+$  and  $\vartheta_-$  approach the same value  $\vartheta_0 = \arg Z_{-\gamma_0}$  from the left or from the right. Then  $\mathbf{S}(\vartheta_+, \vartheta_-; u) \rightarrow \mathbf{S}_{\vartheta_0, u}$ . Clearly, these Stokes factors are captured by the comparison between the WKB triangulations  $T_{\text{WKB}}(\vartheta_+)$  and  $T_{\text{WKB}}(\vartheta_-)$ . Unless the triangulation jumps at  $\vartheta_0 = \arg Z_{-\gamma_0}$  the Stokes factor will be the identity. If the triangulation jumps, we can compute the corresponding symplectomorphism. We will do that in the next few subsections.

What we expect based on the comparison to Section 2 — but what is far from obvious at this stage — is that  $\mathbf{S}_{\vartheta_0, u}$  involves only symplectomorphisms generated by functions of  $X_{\gamma_0}$ . As we will see momentarily, this is indeed the case:  $\mathbf{S}_{\vartheta_0, u}$  is a product of KS factors  $\mathcal{K}_{n\gamma_0}$ , with the expected multiplicities  $\Omega(n\gamma_0)$ . The wall-crossing formula, which was written in Section 2 as the invariance of  $S(\vartheta_+, \vartheta_-; u)$  under small changes of  $\lambda$ , thus follows directly from the invariance of the decorated triangulations  $T_{\text{WKB}}(\vartheta_+, \lambda^2)$  and  $T_{\text{WKB}}(\vartheta_-, \lambda^2)$ .

## 7.6 Jumps at special $\vartheta$

### 7.6.1 Symplectomorphism from a BPS hypermultiplet

We have seen that when  $\vartheta$  crosses a critical value  $\vartheta_c$  corresponding to a BPS hypermultiplet the WKB triangulation jumps. Now we would like to know how  $\mathcal{X}_\gamma^\vartheta$  jumps at this  $\vartheta_c$ .

Let us state the problem a bit more precisely. For  $\vartheta$  in a small interval  $\vartheta_- \leq \vartheta < \vartheta_c$ , the homotopy class of the WKB triangulation is constant; call it  $T_-$ . Similarly, considering  $\vartheta$  in a small interval  $\vartheta_c < \vartheta \leq \vartheta_+$ , we have a triangulation  $T_+$ . We want to compare  $\mathcal{X}_\gamma^{\vartheta_-}$  and  $\mathcal{X}_\gamma^{\vartheta_+}$ . To lighten the notation we will sometimes replace  $\vartheta_\pm$  by simply  $\pm$  below.

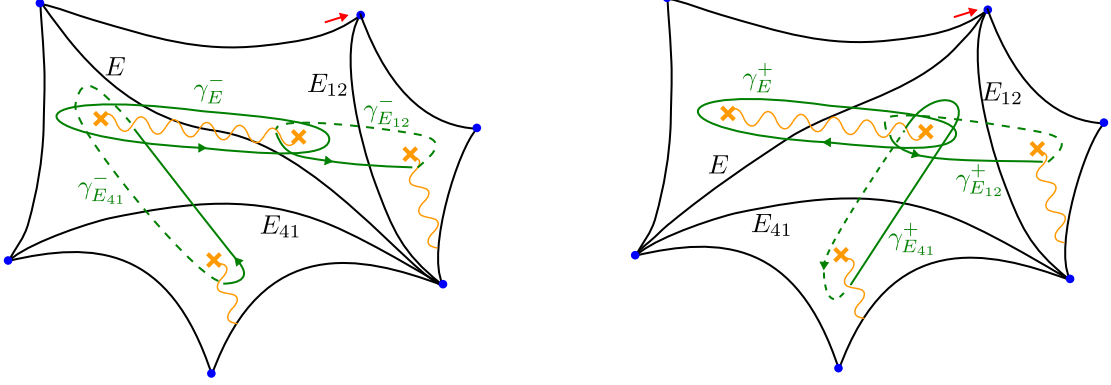


**Figure 36:** The cycles attached to the triangulations  $T_{\text{WKB}}(\vartheta_\pm)$ .

In Figure 36 we depict some of the cycles  $\gamma_E^\pm$ . From this figure we can read off the relations among them:

$$\gamma_E^- = -\gamma_E^+, \quad (7.23)$$

$$\gamma_{E_{12}}^- = \gamma_{E_{12}}^+, \quad (7.24)$$

$$\gamma_{E_{41}}^- = \gamma_{E_{41}}^+ - \gamma_E^-. \quad (7.25)$$

The last two equations can be neatly summarized as the transformation  $\gamma_{E_i}^+ = \gamma_{E_i}^- + \langle \gamma_{E_i}^-, \gamma_E^- \rangle_+ \gamma_E^-$ , where the subscript  $+$  on the intersection means we only take the positive part.

Now we can describe the relations between  $\mathcal{X}_\gamma$  before and after the flip. First, from (5.15) we see that

$$\mathcal{X}_E^+ = 1/\mathcal{X}_E^-. \quad (7.26)$$

Combining this with (7.23), and using freely the definition of  $\mathcal{X}_\gamma$  from the  $\mathcal{X}_E$ , gives

$$\mathcal{X}_{\gamma_E^+}^+ = (\mathcal{X}_{\gamma_E^-}^-)^{-1} = \mathcal{X}_{\gamma_E^+}^-. \quad (7.27)$$

In other words,  $\mathcal{X}_{\gamma_E^+}$  is continuous across the ray  $\vartheta = \vartheta_c$ .

Next let us consider the edge  $E_{12}$ . From (5.16) we have

$$\mathcal{X}_{E_{12}}^+ = \mathcal{X}_{E_{12}}^-(1 + \mathcal{X}_E^-). \quad (7.28)$$

Combining this with (7.24) gives

$$\mathcal{X}_{\gamma_{E_{12}}^+}^+ = \mathcal{X}_{\gamma_{E_{12}}^+}^- (1 + \mathcal{X}_E^-). \quad (7.29)$$

The same holds for  $\mathcal{X}_{\gamma_{E_{34}}^\pm}$ , just by replacing  $1 \rightarrow 3$  and  $2 \rightarrow 4$  above.



The story for  $E_{41}$  is slightly more complicated. From (5.19) we have

$$\mathcal{X}_{E_{41}}^+ = \mathcal{X}_{E_{41}}^- (1 + (\mathcal{X}_E^-)^{-1})^{-1}. \quad (7.30)$$

Combining this with (7.25) we have

$$\mathcal{X}_{\gamma_{E_{41}}}^+ = \mathcal{X}_{\gamma_{E_{41}}}^- (1 + (\mathcal{X}_E^-)^{-1})^{-1} = \mathcal{X}_{\gamma_{E_{41}}}^- (\mathcal{X}_E^-)^{-1} (1 + (\mathcal{X}_E^-)^{-1})^{-1} = \mathcal{X}_{\gamma_{E_{41}}}^- (1 + \mathcal{X}_E^-)^{-1}. \quad (7.31)$$

The same holds for  $\mathcal{X}_{\gamma_{E_{23}}}^\pm$ , just by replacing  $4 \rightarrow 2$  and  $1 \rightarrow 3$ .

To summarize our results, let us define

$$\gamma_{\text{hyper}} := \gamma_E^-. \quad (7.32)$$

This is the charge of the BPS hypermultiplet represented by the finite WKB curve. What we have found is

$$\mathcal{X}_\gamma^+ = \mathcal{X}_\gamma^- (1 + \mathcal{X}_{\gamma_{\text{hyper}}}^-)^{\langle \gamma, \gamma_{\text{hyper}} \rangle}. \quad (7.33)$$

This is exactly the expected transformation property (2.7), if we put  $\Omega(\gamma_{\text{hyper}}) = 1$  — precisely agreeing with the fact that the finite WKB curve represents a single BPS hypermultiplet of charge  $\gamma_{\text{hyper}}$  — and also put  $\sigma(\gamma_{\text{hyper}}) = -1$ , and all  $\Omega(n\gamma_{\text{hyper}}) = 0$  for  $n > 1$ .

### 7.6.2 Symplectomorphism from a BPS vectormultiplet

Let us now consider what happens at  $\vartheta_c$  corresponding to a vectormultiplet. Then as we discussed in Section 6.6.3, the WKB triangulation near  $\vartheta_c$  contains an annulus  $W$ , triangulated by edges which undergo an infinite sequence of flips as  $\vartheta \rightarrow \vartheta_c$  from either direction, while exactly at  $\vartheta_c$  we have an annulus foliated by closed WKB curves.

In what follows we will use some statements about the WKB foliation which were determined by computer experimentation. We believe that the picture we describe is correct at least in the case when  $C$  has genus zero; however, after the first preprint version of this paper appeared, Ivan Smith pointed out to us that the picture may be more complicated if  $C$  has genus  $g > 0$  and the annulus  $W$  cuts off a component which contains a handle and contains no punctures. In [12] we will give a different way of studying that situation. We will find that the main outcome of our analysis, (7.56) below, continues to hold even in that case.

First, to rigidify the picture it is convenient to consider some auxiliary objects, namely WKB curves with phase  $\vartheta + \frac{\pi}{2}$  instead of  $\vartheta$ ; call these *anti-WKB curves*. Generically when there is a BPS state with phase  $\vartheta_c$  there is no BPS state with phase  $\vartheta_c + \frac{\pi}{2}$ , so the anti-WKB curves vary smoothly near  $\vartheta = \vartheta_c$ , in contrast to the WKB curves which are undergoing violent changes there. In particular, for  $\vartheta$  on either side of  $\vartheta_c$ , the anti-separatrices give a convenient division of a region containing the annulus into simply connected cells. Let  $\alpha$  and  $\beta$  denote two anti-WKB curves belonging to two of these cells, as shown in Figure 37, and  $\hat{\alpha}$  and  $\hat{\beta}$  lifts to  $\Sigma$  (with the anti-WKB orientation). Using this division we can also give a canonical choice of the fiducial paths  $E_\pm$ , also shown in Figure 37.

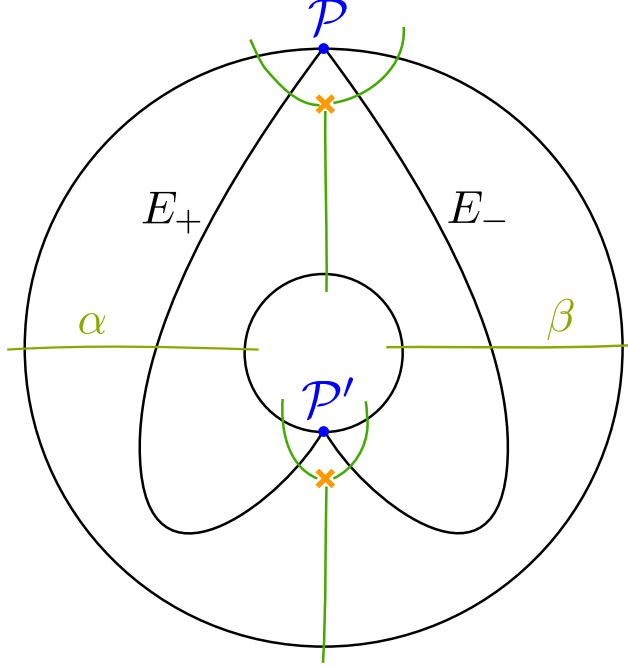


**Figure 37:** Topology of the annulus, with anti-WKB curves marked in green, and two fiducial paths  $E_{\pm}$ .

As in Section 5.9, we can label the various possible triangulations of the annulus as  $T_m$ , for  $m \in \mathbb{Z}$ . As  $\vartheta \rightarrow \vartheta_c$  from above, the WKB triangulation runs through an infinite sequence of triangulations. These triangulations can be identified as the  $T_m$  for  $m = m_+, m_+ + 1, \dots$ , with some  $m_+$ . Similarly, as  $\vartheta \rightarrow \vartheta_c$  from below the WKB triangulation runs through a different sequence of triangulations  $T_m$ , with  $m = m_-, m_- - 1, \dots$ . So the  $T_m$  for sufficiently large or sufficiently small  $m$  all occur as WKB triangulations, but the  $T_m$  for intermediate values of  $m$  need not. For notational convenience below, we look at a narrow range of  $\vartheta$  so that  $m_+ > m_-$  (so each  $T_m$  occurs at most once) and for each  $T_m$  that does occur, choose a  $\vartheta_m$  for which  $T_{\text{WKB}}(\vartheta_m) = T_m$ .

For  $m > m_+$ ,  $E_{m+}$  emerges from the singularity  $\mathcal{P}'$ , passes on the right of a turning point, turns right and winds clockwise around the annulus crossing  $2m$  anti-separatrices, then passes near a second turning point before reaching  $\mathcal{P}$ .  $E_{m-}$  is similar but crosses only  $2m - 2$  anti-separatrices. See Figure 38 for the case  $m = 1$ . From this it follows that the corresponding cycles have

$$\langle \gamma_{E_{m+}}^{\vartheta_m}, \hat{\alpha} \rangle = 1 - m, \quad (7.34)$$

$$\langle \gamma_{E_{m+}}^{\vartheta_m}, \hat{\beta} \rangle = 2 - m, \quad (7.35)$$

$$\langle \gamma_{E_{m-}}^{\vartheta_m}, \hat{\alpha} \rangle = m, \quad (7.36)$$

$$\langle \gamma_{E_{m-}}^{\vartheta_m}, \hat{\beta} \rangle = m - 1. \quad (7.37)$$

For  $m < m_-$ , the situation is very similar to the above, with the crucial difference that the word “right” is replaced by “left” at several points. So  $E_{m+}$  emerges from  $\mathcal{P}'$ , passes

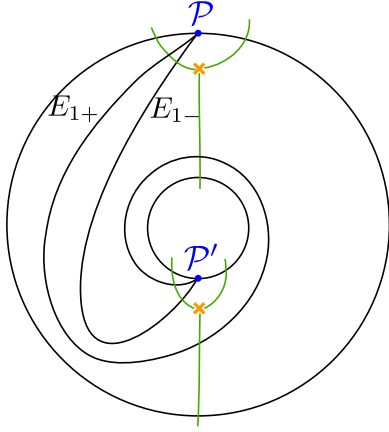


**Figure 38:** The topology of  $T_1 = T_{\text{WKB}}(\vartheta_1)$  on the annulus.

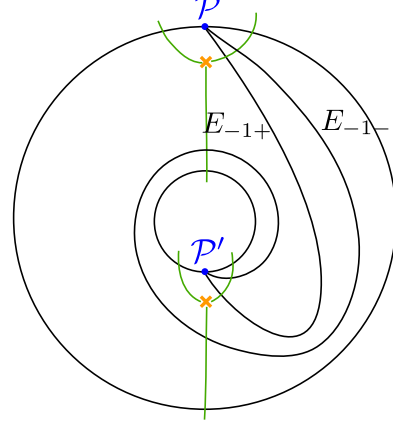


**Figure 39:** The topology of  $T_{-1} = T_{\text{WKB}}(\vartheta_{-1})$  on the annulus.

on the left of a turning point, turns left and winds counterclockwise around the annulus crossing  $-2m-2$  anti-separatrices, then passes near a second turning point before reaching  $\mathcal{P}$ .  $E_{m-}$  is similar but crosses  $-2m$  anti-separatrices. See Figure 39 for the case  $m = -1$ . The relations (7.34)-(7.37) in this case are replaced by

$$\langle \gamma_{E_{m+}}^{\vartheta_m}, \hat{\alpha} \rangle = 1 + m, \quad (7.38)$$

$$\langle \gamma_{E_{m+}}^{\vartheta_m}, \hat{\beta} \rangle = m, \quad (7.39)$$

$$\langle \gamma_{E_{m-}}^{\vartheta_m}, \hat{\alpha} \rangle = -2 - m, \quad (7.40)$$

$$\langle \gamma_{E_{m-}}^{\vartheta_m}, \hat{\beta} \rangle = -1 - m. \quad (7.41)$$

We now define four cycles  $\gamma_{A,B}^{\pm}$ , shown in Figure 40, with

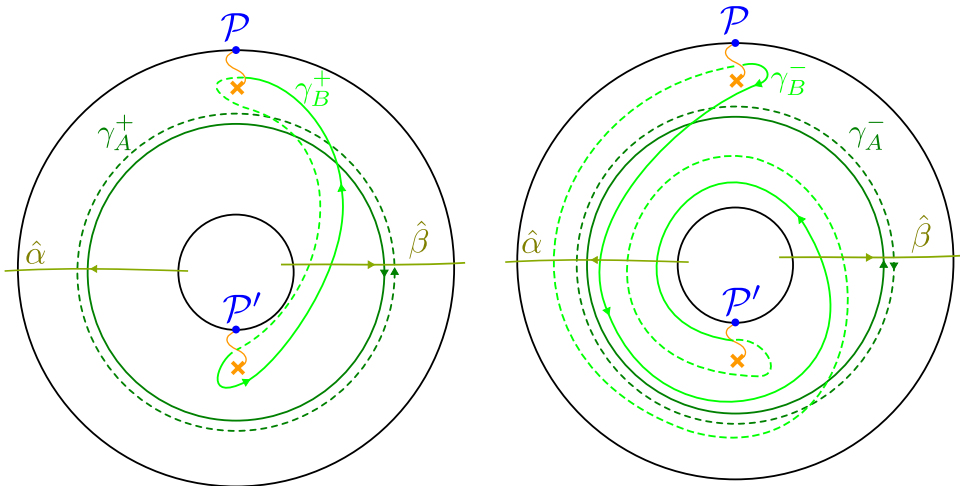


**Figure 40:** Two bases  $\gamma_{A,B}^+$  and  $\gamma_{A,B}^-$  for the part of  $\hat{\Gamma}$  supported over the annulus.

$$\langle \gamma_A^+, \hat{\alpha} \rangle = 1, \quad \langle \gamma_A^-, \hat{\alpha} \rangle = -1, \quad (7.42)$$

$$\langle \gamma_A^+, \hat{\beta} \rangle = 1, \quad \langle \gamma_A^-, \hat{\beta} \rangle = -1, \quad (7.43)$$

$$\langle \gamma_B^+, \hat{\alpha} \rangle = 0, \quad \langle \gamma_B^-, \hat{\alpha} \rangle = -2, \quad (7.44)$$

$$\langle \gamma_B^+, \hat{\beta} \rangle = -1, \quad \langle \gamma_B^-, \hat{\beta} \rangle = -1. \quad (7.45)$$

Note that it follows that

$$\gamma_A^- = -\gamma_A^+, \quad (7.46)$$

$$\gamma_B^- = -\gamma_B^+ + 2\gamma_A^-. \quad (7.47)$$

On the other hand, comparing the intersection numbers we see that these cycles are related to the ones attached to the nearby WKB triangulations by the uniform formula

$$\gamma_A^\pm = \gamma_{E_{m-}}^{\vartheta_m} + \gamma_{E_{m+}}^{\vartheta_m}, \quad (7.48)$$

$$\gamma_B^\pm = (1 - m)\gamma_{E_{m-}}^{\vartheta_m} - m\gamma_{E_{m+}}^{\vartheta_m}. \quad (7.49)$$

where on the left we choose the sign  $+$  when  $m > m_+$  and  $-$  when  $m < m_-$ .

In Section 5.9 we defined a “limit coordinate system”  $\mathcal{X}^{T+\infty}$ . Now, in the present case where  $T_{+\infty}$  arises as  $T_{\text{WKB}}(\vartheta_c)$ , we can define a corresponding labeling by homology: namely we define  $\mathcal{X}_\gamma^+$  by our usual rule (7.3), where  $E$  can denote either an edge of  $T_{+\infty}$  away from the annulus, or one of the special symbols  $A, B$ . Using (5.32), (5.33), (7.48), (7.49) we see that these coordinates indeed deserve to be called limit coordinates:

$$\lim_{\vartheta \rightarrow \vartheta_c^+} \mathcal{X}_\gamma^\vartheta = \mathcal{X}_\gamma^+. \quad (7.50)$$

We may similarly define  $\mathcal{X}_\gamma^-$ , and using (5.36), (5.37), (7.48), (7.49) we see that these similarly obey

$$\lim_{\vartheta \rightarrow \vartheta_c^-} \mathcal{X}_\gamma^\vartheta = \mathcal{X}_\gamma^-. \quad (7.51)$$

We are finally ready to compare  $\mathcal{X}_\gamma^+$  to  $\mathcal{X}_\gamma^-$ . For the  $A$  cycles this is fairly straightforward: using (7.46) and (5.38) we have

$$\mathcal{X}_{\gamma_A^+}^+ = (\mathcal{X}_{\gamma_A^-}^-)^{-1} = \mathcal{X}_{\gamma_A^+}^-. \quad (7.52)$$

For the  $B$  cycles it is a bit more complicated. From (7.47) and (5.40) we find that

$$\mathcal{X}_{\gamma_B^+}^+ = (\mathcal{X}_{\gamma_B^-}^-)^{-1}(\xi_+ - \xi_-)^{-4} = \mathcal{X}_{\gamma_B^+}^- (\mathcal{X}_{\gamma_A^-}^-)^{-2}(\xi_+ - \xi_-)^{-4} = \mathcal{X}_{\gamma_B^+}^- \xi_-^{-4}(\xi_+ - \xi_-)^{-4} \quad (7.53)$$

so finally

$$\mathcal{X}_{\gamma_B^+}^+ = \mathcal{X}_{\gamma_B^+}^- (1 - \xi_-^2)^{-4}. \quad (7.54)$$

Define

$$\gamma_{\text{vector}} := -\gamma_A^+. \quad (7.55)$$

This is the charge of the BPS vectormultiplet represented by the closed WKB curves. Combining our results (7.52), (7.54) gives the simple transformation law

$$\mathcal{X}_\gamma^+ = \mathcal{X}_\gamma^- (1 - \mathcal{X}_{\gamma_{\text{vector}}}^-)^{-2\langle \gamma, \gamma_{\text{vector}} \rangle}. \quad (7.56)$$

Note that we can read off  $\langle \gamma_B^+, \gamma_A^+ \rangle = -2$  from Figure 40.

Altogether we see that the two coordinate systems  $\mathcal{X}_\gamma^\pm$  are related by the symplectomorphism  $\mathcal{K}_{\gamma_{\text{vector}}}^{-2}$ . So again, we obtain exactly the expected transformation property (2.7) for  $\mathcal{X}_\gamma(\zeta)$ , if we put  $\Omega(\gamma_{\text{vector}}) = -2$  — precisely agreeing with the fact that the closed WKB curves represent a single BPS vectormultiplet of charge  $\gamma_{\text{vector}}$  — and also put  $\sigma(\gamma_{\text{vector}}) = +1$ , and all  $\Omega(n\gamma_{\text{vector}}) = 0$  for  $n > 1$ .

### 7.6.3 No symplectomorphism when $me^{-i\vartheta} \in i\mathbb{R}$

Now we dispose of a tricky point. Recall that at each singularity  $\mathcal{P}_i$  we have a parameter  $m_i \in \mathbb{C}$  which controls the residue of  $\varphi$ . What happens at the angles  $\vartheta = \vartheta_c$  where some  $m_i e^{-i\vartheta_c} \in i\mathbb{R}$ ?

As we described in Section 6.6.2, the triangulation  $T_{\text{WKB}}(\vartheta)$  jumps rather violently near the singular point  $\mathcal{P}_i$  as  $\vartheta$  crosses  $\vartheta_c$ , and at the same time we have a pop which changes the flat section  $s_i$ . On the other hand, the family of closed WKB curves which appear at this  $\vartheta$  do not correspond to a charged BPS state: if they are a BPS state at all, it is one carrying only flavor charge (the one associated to the puncture  $\mathcal{P}_i$ , of course). Said differently, if we define  $\gamma_{\text{BPS}}$  by lifting these closed WKB curves in our usual way, while it is indeed true that  $Z(\gamma_{\text{BPS}}) \in e^{i\vartheta_c}\mathbb{R}$ , this charge  $\gamma_{\text{BPS}}$  is in the radical of  $\langle, \rangle$ . So the symplectomorphism  $\mathcal{K}_{\gamma_{\text{BPS}}}$  is actually trivial. Hence it seems that to be consistent with (2.7) we should expect that the  $\mathcal{X}_\gamma^\vartheta$  do *not* jump at  $\vartheta = \vartheta_c$ , despite the jump of  $T_{\text{WKB}}$ . In this section we verify that this is indeed the case.

First, let us consider the coordinate  $\mathcal{X}_{C^+}$ . Recall from (7.6) that

$$\mathcal{X}_{C^\pm}^\pm = \mu_\pm^2. \quad (7.57)$$

On the other hand, we have

$$C^+ = -C^- \quad (7.58)$$

and

$$\mu_+ = 1/\mu_-. \quad (7.59)$$

Hence

$$\mathcal{X}_{C^+}^+ = (\mu_+)^2 = (\mu_-)^{-2} = (\mathcal{X}_{C^-}^-)^{-1} = \mathcal{X}_{C^+}^-. \quad (7.60)$$

There is one other  $\mathcal{X}_\gamma$  we have to worry about. Let  $E'$  be the “loop” of the degenerate face and define

$$\gamma := \gamma_{E'}^-. \quad (7.61)$$

The equality  $\mathcal{X}_\gamma^+ = \mathcal{X}_\gamma^-$  is a consequence of two different effects which cancel one another. As we showed in (5.25),

$$\mathcal{X}_{\gamma_{E'}}^\pm = (\mu_\pm)^{-1} S, \quad (7.62)$$

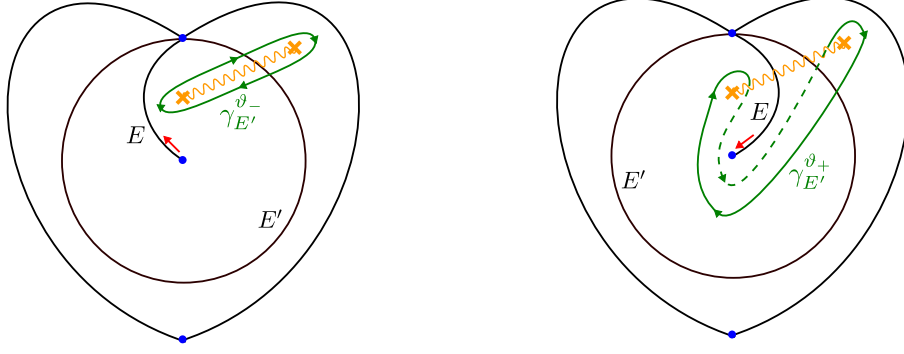


**Figure 41:** An unwinding of Figure 28, with the homology cycles corresponding to edges marked.

where  $S$  is continuous across the critical locus (in particular it does not involve the section  $s$ ). Unwinding Figure 28 to see its topological content more easily, we arrive at Figure 41, from which we see that

$$\gamma_{E'}^- = \gamma_{E'}^+ + C^+. \quad (7.63)$$

Combining all this we get

$$\mathcal{X}_{\gamma_{E'}^-}^+ = \mathcal{X}_{\gamma_{E'}^+}^+ \mathcal{X}_{C^+}^+ = (\mu_+)^{-1} S \mu_+^2 = (\mu_-)^{-1} S = \mathcal{X}_{\gamma_{E'}^-}^- \quad (7.64)$$

as desired.

So indeed the  $\mathcal{X}_\gamma^\vartheta$  are continuous across this  $\vartheta = \vartheta_c$ .

## 7.7 Quadratic refinement

Now we come to another pesky detail: the sign  $\sigma(\gamma)$  which occurs in the transformation (2.6). In the general story described in [1] one expects that  $\sigma : \hat{\Gamma} \rightarrow \mathbb{Z}_2$  is a quadratic refinement of the mod 2 intersection pairing  $\langle, \rangle$  on  $\hat{\Gamma}$ . By definition this means that

$$\sigma(\gamma)\sigma(\gamma') = \sigma(\gamma + \gamma')\sigma(0)(-1)^{\langle \gamma, \gamma' \rangle}. \quad (7.65)$$

In general, one would not expect such a quadratic refinement to exist globally over  $\mathcal{B}$ ; instead one would have to pick different refinements in different local patches, and in gluing the patches together one would have to keep track of some sign changes in  $\mathcal{X}_\gamma^\vartheta$ , coming from the fact that the refinements are not the same.

On the other hand, in this this paper we seemed to find a simpler story. The gluing laws for our functions  $\mathcal{X}_\gamma^\vartheta$  do not involve any tricky signs. Moreover, the transformations we found for the  $\mathcal{X}_\gamma^\vartheta$  agree with (2.6), provided that we have

$$\sigma(\gamma_{\text{hyper}}) = -1, \quad (7.66)$$

$$\sigma(\gamma_{\text{vector}}) = +1. \quad (7.67)$$

How can this be consistent? It would be consistent if there exists a *single* quadratic refinement  $\sigma$  which obeys (7.66), (7.67) for all hypermultiplets and vectormultiplets which appear in the spectrum at any  $u \in \mathcal{B}$ .

We can easily construct such a  $\sigma$  for any fixed  $(\vartheta, u)$ : it is determined by requiring  $\sigma(0) = +1$ ,  $\sigma(\gamma_E) = -1$  for all nondegenerate edges  $E$  of  $T_{\text{WKB}}(\vartheta, u)$ , and  $\sigma(\gamma_E) = +1$  for degenerate edges. From this definition it is straightforward to see that  $\sigma(\gamma_{\text{hyper}}) = -1$  and  $\sigma(\gamma_{\text{vector}}) = +1$  for any BPS states which have phase  $\vartheta$ . So from this perspective the trouble is to show that the  $\sigma$  so defined is actually independent of  $(\vartheta, u)$ . This amounts to checking that this formula for  $\sigma$  is consistent with the transformations of the  $\gamma_E$  when the triangulation  $T_{\text{WKB}}$  jumps. Fortunately this is indeed the case.

Indeed, as we have discussed, as we vary  $(\vartheta, u)$  the WKB triangulation undergoes three types of transformation. The first type (hypermultiplet) is given by (7.23)-(7.25) and one checks directly that it is consistent with our proposal for  $\sigma$ . The second type (vectormultiplet) is given in terms of the auxiliary cycles  $\gamma_{A,B}$  defined by (7.48), (7.49). Using those equations and our proposal for  $\sigma$  gives  $\sigma(\gamma_A) = +1$  and  $\sigma(\gamma_B) = -1$ . This  $\sigma$  is indeed consistent with the transformations (7.46), (7.47). Finally, the transformation of cycles from the third type of jump ( $m/e^{i\vartheta} \in i\mathbb{R}$ ) is given by (7.58) and (7.63), once again consistent with  $\sigma$  (recalling that  $C_+$  corresponds to a degenerate edge and so  $\sigma(C_+) = +1$ .)

There is another, more intrinsic, way of describing this quadratic refinement. Given any homology class  $\gamma \in H_1(\Sigma; \mathbb{Z})$  we first represent  $\gamma$  by a disjoint union of oriented closed curves which avoid the zeroes of  $\lambda$ . On each of these closed curves we have the *phase function* defined as the phase of  $\lambda \cdot \partial_t$ . Letting  $n_w$  denote the number of times this phase winds around the circle as we go around the curve,  $\sigma(\gamma)$  is the product of  $(-1)^{n_w+1}$  over all components of our representative for  $\gamma$ . It is straightforward to check that this is indeed well defined as a function on homology, and that it gives a quadratic refinement. Moreover, from the fact that  $\gamma_{\text{hyper}}$  is represented by a single closed constant phase curve, and  $\gamma_{\text{vector}}$  is represented by a disjoint union of two such curves, one easily sees that  $\sigma$  has the desired properties (7.66), (7.67).

## 7.8 Some comments on the full BPS spectrum

At this point we have constructed the functions  $\mathcal{X}_\gamma^\vartheta$  and verified that they jump by KS transformations as we vary  $\vartheta$ , in the class of examples related to  $SU(2)$  Hitchin systems with regular singularities. As we explained above and in Section 2, these functions are the key ingredient in our explanation of the wall-crossing formula. But that is not all: we have also learned a strategy for determining the BPS spectrum. Indeed, if we pick two phases  $\vartheta_\pm$  and compute the WKB triangulations  $T_{\text{WKB}}(\vartheta_\pm, u)$ , we can then reconstruct the coordinate transformation  $\mathbf{S}(\vartheta_+, \vartheta_-; u)$ , decompose it uniquely into a product of properly ordered KS transformations as described in Section 2.3, and read off the spectrum of BPS states with phases in the sector  $[\vartheta_-, \vartheta_+]$ .

This strategy is particularly potent if we choose  $\vartheta_+ = \vartheta_- + \pi$ .<sup>36</sup> In that case the sector is a whole half-plane, and thus big enough to determine the whole BPS spectrum (as the BPS states with phase outside this half-plane are the antiparticles of ones inside it). We therefore call  $\mathbf{S}(\vartheta, \vartheta + \pi; u)$  the “spectrum generator.” Luckily, it turns out that, unlike a random  $\mathbf{S}(\vartheta_+, \vartheta_-; u)$ , this spectrum generator is actually computable! The essential reason

<sup>36</sup>To be precise, we include only one of the two boundary rays in the sector.

for this computability is that  $T_{\text{WKB}}(\vartheta)$  and  $T_{\text{WKB}}(\vartheta + \pi)$  only differ in the decoration: to go from one to the other we just have to pop at all of the singularities. We defer the computation of the spectrum generator to Section 11, but we note now that the result is quite simple, and only depends on the combinatorial data of  $T_{\text{WKB}}(\vartheta, u)$ .

It would be very interesting to understand physically *why*  $T_{\text{WKB}}(\vartheta, u)$  can capture the whole BPS spectrum. At least one part of this story is easy to understand: for each edge  $E$  of  $T_{\text{WKB}}(\vartheta, u)$ , there is a BPS hypermultiplet of charge  $\gamma_E$  in the vacuum  $u$ . Indeed, the corresponding cell of the WKB foliation is mapped to a strip by the coordinate transformation  $z \mapsto w = \int^z \lambda$ , with the two turning points at opposite boundaries of the strip, and the preimage in the  $z$ -plane of a straight segment running between the two turning points in the  $w$ -plane yields a BPS string of charge  $\gamma_E$ .<sup>37</sup>

The charges  $\gamma_E$  of these BPS particles form a basis of the charge lattice, as shown in Section 7.1.4. In fact, more is true: this basis has an important positivity property, reminiscent of the relation between roots and simple roots in a simple Lie algebra. Recall that a BPS state corresponds to a finite WKB curve, giving a straight line segment in the  $w$ -plane. The slope of this segment is the phase of the central charge of the BPS state. In particular, if this phase lies between  $\vartheta$  and  $\vartheta + \pi$ , then the BPS string has *positive* intersection with the WKB curves of phase  $\vartheta$ . On the other hand, by the definition of the homology labeling given in Section 7.1,  $\langle \gamma_E^\vartheta, \hat{E}' \rangle = \delta_{E, E'}$ . It follows that, if a homology cycle  $\gamma_{\text{BPS}}$  supports a BPS state with phase between  $\vartheta$  and  $\vartheta + \pi$ , we have

$$\gamma_{\text{BPS}} = \sum_E c_E \gamma_E^\vartheta \quad (7.68)$$

with all  $c_E \geq 0$ .

The above facts suggest some natural speculations. First, the positive decomposition is a hint that all BPS states can be viewed as bound states of a set of “simple” BPS states, which are in correspondence with the edges  $E$  of  $T_{\text{WKB}}(\vartheta, u)$ . Further evidence for this conjecture comes from the fact that the spectrum generator  $\mathbf{S}$  can be computed purely from the combinatorial data of  $T_{\text{WKB}}$ .

Note that even for a fixed vacuum  $u$ , one can obtain various bases of simple BPS states by changing  $\vartheta$ . This is reminiscent of the oft-employed description of BPS states in terms of quiver quantum mechanics; in that story one sometimes describes the same quantum mechanics using various different quivers, corresponding to different “exceptional collections”, which are related by mutations. Indeed, in our context there is a natural quiver around, with nodes labeled by the edges  $E_i$  of the triangulation, and the number of arrows determined by  $\langle E_i, E_j \rangle$ . It is possible that with appropriate FI terms and superpotentials the BPS states of the quiver quantum mechanics would be in 1-1 correspondence with the full BPS spectrum of the theory with phases in the sector  $[\theta, \theta + \pi]$ . Relations between mutations of quivers and “cluster transformations,” closely related to the KS transformations

---

<sup>37</sup>Similar statements hold for limit triangulations: in that case each annulus foliated by WKB curves gives a family of closed BPS strings (a vectormultiplet), along with an infinite tower of hypermultiplets, namely the inverse images of straight paths in the  $w$  coordinate between the turning points, with various windings on the annulus.



we encounter in this paper, have been considered extensively in the mathematics literature (see e.g. [61]). (For further developments in this direction see e.g. [62, 63, 64].)

## 8. Irregular singularities

While we have focused on the case of regular singular points in the past three sections, the constructions can also be adapted to the case of irregular singularities. The story is quite similar to the regular case, with the following modifications:

1. We begin by defining the appropriate notion of triangulation when irregular singularities are included. Suppose that  $\mathcal{P}_*$  is an irregular singular point where  $\lambda^2$  has a pole of order  $L + 2$ , with  $L \geq 1$  integral. (The boundary conditions of Section 3 for rank two Hitchin systems involve irregular singular points with  $L = 1$ , while in Section 9 we will meet singular points with  $L = N + 2$ ,  $N \geq 0$ .) We draw a circle  $S^1(\mathcal{P}_*)$  around  $\mathcal{P}_*$ , bounding a disc  $D(\mathcal{P}_*)$ , to be considered as infinitesimally small. On this circle we mark  $L$  points  $Q_i$ ,  $i = 1, \dots, L$ . These points are cyclically ordered by saying that  $\dots, Q_i, Q_{i+1}, \dots$  are going clockwise around  $\mathcal{P}_*$ . Then our triangulations are really triangulations of the surface  $C'$  obtained by cutting all the discs  $D(\mathcal{P}_*)$ . The vertices are the marked points  $Q_i$  around all of the irregular singularities, as well as all of the regular singularities  $\mathcal{P}_i$ . The edges necessarily include the segments on the circles  $S^1(\mathcal{P}_*)$  joining consecutive points  $Q_i$ . We call these segments *boundary edges*; they will have a special status below.
2. In order to define a *decorated* triangulation, we need to choose a flat section for the connection  $\mathcal{A}$  (up to scale) near each vertex. For irregular singularities this means choosing a flat section near each point  $Q_i$  on  $S^1(\mathcal{P}_*)$ . As in the regular case we would like to narrow this down to a discrete choice. To this end we observe that in the case of an irregular singular point, in addition to a possible monodromy there is also Stokes phenomenon.<sup>38</sup> There are  $L$  rays (“Stokes rays”) emerging from  $\mathcal{P}_*$ , bounding sectors of opening angle  $2\pi/L$ . A flat section which is asymptotically exponentially small as  $z \rightarrow \mathcal{P}_*$  along a ray going into  $\mathcal{P}_*$  on one side of a Stokes ray becomes exponentially large on the other side of the Stokes ray.<sup>39</sup> We define a decoration to be a choice of flat section near  $Q_i$  (modulo overall rescaling) which, after analytic continuation around  $\mathcal{P}_*$ , is exponentially small as  $z \rightarrow \mathcal{P}_*$  in *some* sector bounded by Stokes rays.

---

<sup>38</sup>In what follows we are assuming that the standard Stokes theory for *meromorphic* connections on a complex curve can be extended in the most obvious way to apply to the connection  $\mathcal{A}$ , which is flat but not meromorphic. We have not found any literature on this precise situation, although somewhat related constructions appear in [65].

<sup>39</sup>In the literature on Stokes phenomenon there are two kinds of rays, named *Stokes* and *anti-Stokes*, each of which plays an important role in the systematic development of the theory. Regrettably, the terminology is not consistently applied by various authors on the subject. In our convention, the standard Airy function,  $Ai(x)$ , which has real exponential decay along the positive real axis and power law decay with an oscillating envelope along the negative real axis, has Stokes rays along the negative real axis and along  $|\arg(x)| = \pi/3$ .

3. We can define an infinite sequence of such sections (up to rescaling),

$$\cdots, s_{-3}, s_{-2}, s_{-1}, s_0, s_1, s_2, s_3, \dots \quad (8.1)$$

where the ordering is determined by saying that if  $s_n$  is the small solution in sector  $\mathcal{S}$ , then  $s_{n+1}$  is the small solution in the next sector in the clockwise direction. (If the monodromy is trivial, we can choose the scales of the  $s_n$  so that the sequence will have period  $L$ .) Moreover, we further restrict our choice of decoration so that if we choose, say  $s_n$  at point  $Q_i$  then at point  $Q_{i+1}$  we must also choose  $s_{n+1}$ , and so on. Thus, the choice of decoration at an irregular singularity boils down to a *single* choice of flat section at one marked point, rather than an independent choice at each point. The set of possible choices of decoration near an irregular singular point thus forms a  $\mathbb{Z}$ -torsor. If the monodromy is trivial, it can be reduced to a  $\mathbb{Z}_L$ -torsor.

4. The definition of the Fock-Goncharov coordinates  $\mathcal{X}_E^T$  can now be given just as before, with the important caveat that we define  $\mathcal{X}_E^T = 0$  if  $E$  is a boundary edge.
5. The local behavior of the WKB foliation around an irregular singularity is rather different from that around a regular singularity. Rather than spiraling isotropically into the singularity, each WKB curve is asymptotically tangent to one of  $L$  rays. These rays, which we will call *WKB rays* (with phase  $\vartheta$ ), determine points  $Q_i$ ,  $i = 1, \dots, L$ , on an infinitesimal circle  $S^1(\mathcal{P}_*)$  around  $\mathcal{P}_*$ ; these are the marked points we will use in defining  $T_{\text{WKB}}$ . If  $\vartheta = \arg \zeta$ , then the WKB rays with phase  $\vartheta$  are the same as the anti-Stokes rays for the connection  $\mathcal{A}$ .

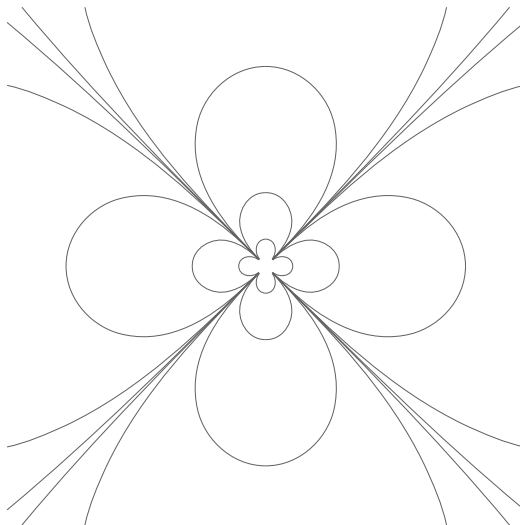


**Figure 42:** Behavior of the WKB foliation near an irregular singular point with  $L = 4$ . The WKB curves cluster onto the 4 WKB rays, separated from one another by arcs of  $\pi/2$  radians. WKB curves in a small neighborhood of the singularity look like flower petals which connect adjacent WKB rays.

6. The definition of  $T_{\text{WKB}}$  proceeds essentially as before. If a WKB curve asymptotes to a WKB ray ending on an irregular singularity  $\mathcal{P}_*$ , we regard it as ending on

the corresponding point  $Q_i$  on  $S^1(\mathcal{P}_*)$ . Then as usual, the separating WKB curves divide  $C'$  into cells foliated by generic WKB curves, and the edges of  $T_{\text{WKB}}$  consist of one generic WKB curve from each cell. Note that there are generic WKB curves which sit entirely in an arbitrarily small neighborhood of the irregular singularity, and connect adjacent WKB rays, as shown in Figure 42. Among the edges of  $T_{\text{WKB}}$  there are  $L$  such curves, to be identified with the boundary edges mentioned above which connect adjacent  $Q_i$ . Each such edge bounds a petal-shaped region touching  $\mathcal{P}_*$ ; the disc  $D(\mathcal{P}_*)$  is identified with the union of these  $L$  petals.

7. The decoration of  $T_{\text{WKB}}$  at a vertex  $Q_j$  is obtained by choosing the flat section which becomes exponentially small when following the WKB ray through  $Q_j$  going into  $\mathcal{P}_*$ . Let us describe this section a bit more precisely. Put  $\mathcal{P}_*$  at  $z = \infty$  and suppose  $\lambda^2 \sim z^{L-2} dz^2$  there. The  $L$  WKB rays are located at

$$r_j := \left\{ \arg(z) = \frac{2}{L}\vartheta + \frac{2\pi j}{L} \right\}, \quad j = 1, \dots, L. \quad (8.2)$$

The formal asymptotics of flat sections are of the form

$$\exp \left[ \pm \frac{2}{L} \frac{R}{\zeta} z^{\frac{1}{2}L} + \dots \right] s_{\text{const}} \quad (8.3)$$

as  $z \rightarrow \infty$ . In particular their norm is controlled by the sign of the real part of the exponential, which changes across the Stokes rays

$$\arg(z) = \frac{2}{L}\vartheta_\zeta + \frac{(2j+1)\pi}{L}, \quad j = 0, \dots, L-1, \quad (8.4)$$

where we defined  $\vartheta_\zeta = \arg \zeta$ . So long as  $e^{i\vartheta} \neq -e^{i\vartheta_\zeta}$ , each of the sectors bounded by these Stokes rays contains a unique WKB ray  $r_j$ . Along this WKB ray the norm of a general flat section is asymptotic to

$$\exp \left[ \pm \frac{2R}{L} \frac{|z|^{L/2}}{|\zeta|} \operatorname{Re} \left( e^{i(\vartheta + \pi j - \vartheta_\zeta)} \right) + \dots \right]. \quad (8.5)$$

If we choose the  $\pm$  sign in (8.5) opposite to the sign of  $\operatorname{Re} (e^{i(\vartheta + \pi j - \vartheta_\zeta)})$ , then this norm is exponentially small as  $z \rightarrow \infty$  along  $r_j$ , for any  $\zeta \in \mathbb{H}_\vartheta$ . So far we have just discussed the formal asymptotics, but it is an important principle that there exists a unique flat section (called the “small section”) whose norm indeed has this exponentially small asymptotic behavior along  $r_j$ , for  $\zeta \in \mathbb{H}_\vartheta$ . We choose this small section to be the decoration of  $T_{\text{WKB}}(\vartheta)$  at the WKB ray  $r_j$ . It is canonically determined by  $\vartheta$  and  $j$ . A subtle point is that this small section generally has nontrivial monodromy as  $\zeta$  goes around 0; it follows that it really depends on  $\vartheta \in \mathbb{R}$ , not just  $\vartheta \in \mathbb{R}/2\pi\mathbb{Z}$ .

8. The definitions of  $\gamma_E^\vartheta$  and  $\mathcal{X}_\gamma^\vartheta$  proceed precisely as for the case with only regular singular points. We do not define this cycle when  $E$  is a boundary edge.

9. We define a pop at an irregular singular point  $\mathcal{P}_*$  to be the action by 1 on the  $\mathbb{Z}$ -torsor of decorations at  $\mathcal{P}_*$ . To fix conventions, if  $\dots, Q_j, Q_{j+1}, \dots$  are ordered clockwise and the decoration associates to them the sections  $\dots, s_n, s_{n+1}, \dots$  then after the pop we associate to them the sections  $\dots, s_{n-1}, s_n, \dots$ . If we replace  $\vartheta \rightarrow \vartheta + \pi$ , then the decoration of  $T_{\text{WKB}}(\vartheta)$  at each irregular singular point undergoes a pop.
10. It can happen that a sequence of flips produces a new triangulation which differs from the original one only by a rotation of one of the boundary circles by  $2\pi/L$ , or, equivalently, a cyclic permutation of the  $Q_i$ . This is identical to the effect of a single pop at the irregular vertex. This reflects a relation among morphisms in the groupoid of decorated triangulations.

## 9. Scaling limits of linear $SU(2)$ quivers: the case of one irregular singular point

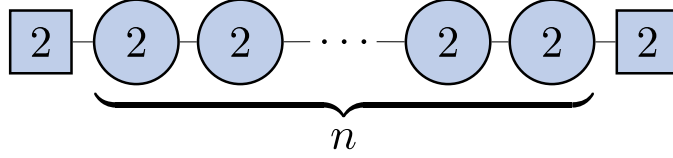


**Figure 43:** Linear quiver for the theories considered in Section 9.

In this section we illustrate some of the considerations of Sections 5-8 for some particularly simple theories. These theories are obtained as certain scaling limits of linear quivers of  $n$   $SU(2)$  gauge groups, with two fundamental hypermultiplets for each of the first and last gauge groups, as shown in Figure 43. The corresponding Hitchin systems have gauge group  $SU(2)$  and (after the scaling limit) only one singularity, an irregular one, on  $C = \mathbb{CP}^1$ .

### 9.1 Linear $SU(2)$ quivers and their parameter spaces

This theory has  $3n+3$  physical parameters: the UV Lagrangian involves  $n$  gauge couplings,  $n-1$  bifundamental masses and 4 fundamental masses, while the Coulomb branch is parameterized by  $n$  vevs  $\langle \text{Tr}(\Phi^{(\alpha)})^2 \rangle$ .

Recall from Section 3 that the corresponding Seiberg-Witten curve is  $F(t, v) = 0$ , where

$$F(t, v) = \sum_{\alpha=0}^{n+1} q_{\alpha}(v) t^{n+1-\alpha} = p_0(t) v^2 + p_1(t) v + p_2(t) \quad (9.1)$$

Moreover, we saw that one can parameterize (with some redundancy)

$$q_{\alpha}(v) = c_{\alpha}(v^2 - \mu_{\alpha} v - u_{\alpha}). \quad (9.2)$$

In the weak-coupling regime the couplings are determined from the  $c_{\alpha}$  and the masses from  $\mu_{\alpha}$  and  $u_{\alpha}$ , while the Coulomb branch is parameterized by the  $u_{\alpha}$ . Finally, as we saw in

(3.77), after factoring out the center-of-mass degree of freedom the Seiberg-Witten curve becomes the spectral curve for an  $SU(2)$  Hitchin system with

$$\lambda^2 = \frac{1}{2} \frac{p_1(t)^2 - 4p_2(t)p_0(t)}{(tp_0(t))^2} dt^2. \quad (9.3)$$

This quadratic differential has double poles at  $t = 0$  and  $t = \infty$  as well as at the  $n + 1$  zeroes of  $p_0(t)$ .

The above description somewhat obscures the S-duality properties of the problem [2, 15]. The physical gauge couplings really only depend on a point in the moduli space of spheres with  $n + 3$  marked points. Moreover, there is no S-duality invariant distinction between the bifundamental and fundamental mass parameters. These facts suggest that we should treat the  $n + 3$  singularities and mass parameters more democratically. This can be achieved by introducing some redundancy into the description, making a general fractional linear transformation from  $[t : 1] \in \mathbb{CP}^1$  to a new coordinate  $z$ . After making such a transformation we have (subscripts on polynomials indicate their degree)

$$\lambda^2 = \frac{Q_{2n+2}(z)}{(D_{n+3}(z))^2} (dz)^2. \quad (9.4)$$

After subtracting out 3 parameters for the  $SL(2, \mathbb{C})$  action and 1 parameter for simultaneous rescaling of  $Q$  and  $D$ , there are still  $3n + 7 - 4 = 3n + 3$  physical parameters.

As we have mentioned, the physical parameters are not on an equal footing. The couplings and masses specify the UV theory while the Coulomb branch parameters specify the vacuum. To bring out this distinction it is useful to parameterize  $\lambda^2$  in a slightly different way.

The  $n + 3$  mass parameters can be characterized as the residues of the  $n + 3$  poles in  $\lambda^2$ . (We will not consider the possibility that some of these poles collide, corresponding to a strong coupling singularity of the physical theory.) If the poles are located at  $z_a$  for  $a = 1, \dots, n + 3$ , and we assume all  $z_a \neq \infty$ , we can write  $\lambda^2$  in the form

$$\lambda^2 = \sum_{a=1}^{n+3} \left( \frac{m_a^2}{(z - z_a)^2} + \frac{c_a}{z - z_a} \right) dz^2. \quad (9.5)$$

Requiring that  $\lambda^2$  is regular at  $z = \infty$  gives three conditions on the  $c_a$ ,

$$\begin{aligned} \sum_{a=1}^{n+3} c_a &= 0, \\ \sum_{a=1}^{n+3} z_a c_a &= - \sum_{a=1}^{n+3} m_a^2, \\ \sum_{a=1}^{n+3} z_a^2 c_a &= -2 \sum_{a=1}^{n+3} m_a^2 z_a. \end{aligned} \quad (9.6)$$

The Coulomb branch  $\mathcal{B}$  is the space of  $c_a$  solving (9.6). Because (9.6) is an inhomogeneous linear equation for the  $c_a$ , it is an affine space of dimension  $n$ .

(Another viewpoint is that, once we have specified the couplings through  $z_a$ , the space of theories with arbitrary masses and vacua is a linear space — the space of polynomials  $Q_{2n+2}(z)$  — which can also be thought of as  $H^0(\mathbb{CP}^1, K^{\otimes 2} \otimes \mathcal{O}(2\mathcal{P}_1 + \dots + 2\mathcal{P}_{n+3}))$ . Fixing the masses then fixes an affine subspace of this space.)

## 9.2 Scaling limit

The singularities of the Coulomb branch for generic masses occur when two or more roots of  $Q_{2n+2}(z)$  coincide. At these points the metric on the Coulomb branch is singular and fluctuations around this locus have infinite action. The reason is, of course, that at least one BPS state becomes massless on this locus. The zeroes of  $Q_{2n+2}(z)$  occur on the discriminant locus  $\mathcal{D}$ , which has strata  $\mathcal{D}_k$  where precisely  $k$  zeroes coincide. We will now focus on a stratum  $\mathcal{D}_N$ . Near this locus some number of BPS states become light, and we would like to focus on the low-energy physics of these states.

Accordingly, we consider the following scaling limit. Choose a point  $\mathcal{P} \in C$  and a local coordinate  $z$  with  $z(\mathcal{P}) = 0$ . The relevant neighborhood in the space of  $Q$ 's can be parameterized by  $Q_{2n+2}(z) = \prod_{i=1}^N (z - \epsilon \theta_i) \tilde{Q}_{2n+2-N}(z)$ , with  $\tilde{Q}_{2n+2-N}(0) \neq 0$ . At  $\epsilon \rightarrow 0$ ,  $N$  zeroes of  $Q$  collide at  $z = 0$ . The mass of a typical BPS state associated with a string connecting two of these colliding zeroes is of order  $\epsilon^{(N+2)/2}$ . We thus consider physics at energies of this scale and below. We also define a scaling region of the Riemann surface  $C$  (i.e. a scaling region on the M5 worldvolume) by  $z = \epsilon \tilde{z}$ . We will only be considering fluctuations localized in this region. After a suitable rescaling of the Seiberg-Witten differential  $\lambda$  and  $\tilde{z}$ , we are therefore considering a theory with

$$\lambda^2 = P_N(z) dz^2, \quad (9.7)$$

where  $P_N$  is monic of order  $N$ , and our scaling patch of the M5-brane worldvolume has been blown up to the entire complex plane.

Many of the deformations of the original theory become non-normalizable in the scaling limit; however, some deformations remain normalizable. These are the polynomial deformations  $P_N \rightarrow P_N + \delta P_N$  such that

$$\int_{\mathbb{C}} |\delta \lambda|^2 = \int_{\mathbb{C}} \left| \frac{\delta P_N(z)}{2\sqrt{P_N(z)}} \right|^2 d^2 z < \infty. \quad (9.8)$$

Since the zeroes of  $P_N(z)$  are simple, a divergence could only come from  $z \rightarrow \infty$ , and hence the normalizability condition is

$$\delta P_N = \sum_{i < \frac{1}{2}(N-2)} \delta p_i z^i. \quad (9.9)$$

There is another useful point of view on this normalizability condition, namely, we fix the singular part of the expansion of  $\sqrt{P_N(z)}$  around  $z = \infty$ :

$$\sqrt{P_N(z)} = \Delta(z) + o(z^{-1}) \quad (9.10)$$

for some fixed  $\Delta(z)$  (determined by the UV theory which we have mostly discarded).

There is an important difference between even and odd  $N$ . When  $N$  is even,  $\Delta(z)$  is an expansion in integer powers, ending with a simple pole; we denote its residue by  $m$ . Varying  $m$  is a “log-normalizable” deformation, with  $i = \frac{1}{2}(N-2)$ . As we will see presently when we pass from Hitchin systems to flat connections,  $m$  specifies the formal monodromy at  $\infty$ . In the case of  $N$  odd there is no such log-normalizable deformation.

After the scaling limit there are still singular loci on the Coulomb branch where some  $\theta_i = \theta_j$ , i.e. where  $P_N(z)$  has multiple zeroes. These loci are intersections between higher-dimensional strata of  $\mathcal{D}$  and the scaling region around  $\mathcal{D}_N$ . At these loci some BPS states become massless. Moreover, in some cases the BPS states which become massless are mutually nonlocal ones, leading to the kinds of theories studied in [66, 67].

To reach the most extreme case, we could tune the nonnormalizable parameters so that we are considering normalizable deformations of  $\lambda^2 = z^N(dz)^2$ . The deep IR physics at this point in moduli space is described by a superconformal field theory [66, 67], and one can define a UV complete quantum field theory with a finite BPS spectrum by perturbing away from this theory with the normalizable deformations identified above. We are then studying the Seiberg-Witten curves and BPS states of those theories. From the point of view of the original UV theory specified by the linear quiver, we are focusing on a low-energy subsector in a region of moduli space where a number of BPS states are becoming parameterically light. As we will see below, the number of such states is bounded by  $\frac{1}{2}N(N-1)$  [68].

### 9.3 Hitchin system

In the previous subsection we have described a degeneration of the spectral curve of our Hitchin system. To complete the discussion we now explain the corresponding degeneration of the Hitchin system. The new Hitchin system is defined on  $\mathbb{CP}^1$  and has a single irregular singularity at  $z = \infty$ . To be specific, when  $N$  is even we have

$$A_0 = \begin{pmatrix} -m^{(3)} & 0 \\ 0 & m^{(3)} \end{pmatrix} \left( \frac{dz}{z} - \frac{d\bar{z}}{\bar{z}} \right) \quad (9.11)$$

and

$$\varphi_0 = \begin{pmatrix} \Delta(z) & 0 \\ 0 & -\Delta(z) \end{pmatrix}, \quad (9.12)$$

with  $\Delta(z)$  as defined in (9.10). Since  $\Delta(z) \sim z^{N/2} + \dots + \frac{m}{z}$ , the formal monodromy under counterclockwise rotation is

$$\exp \left( 2\pi i \left[ \frac{mR}{\zeta} - 2m^{(3)} - \bar{m}R\zeta \right] \sigma^3 \right). \quad (9.13)$$

We will denote its eigenvalues as  $\mu^{\pm 1}$ .

When  $N$  is odd there is no analog of the mass parameters  $m, m^{(3)}, \bar{m}$ . Instead, we have a generalization of (3.115),

$$\varphi_0 = \Delta(z) \begin{pmatrix} 0 & (\bar{z}/z)^{1/4} \\ (z/\bar{z})^{1/4} & 0 \end{pmatrix}, \quad (9.14)$$

$$A_0 = \frac{1}{8} \sigma^3 \left( \frac{dz}{z} - \frac{d\bar{z}}{\bar{z}} \right). \quad (9.15)$$

## 9.4 Examples

We now illustrate various aspects of our formalism in the cases where  $P(z)$  is a polynomial of degree  $N = 1, 2, 3, 4$ . Along the way we will encounter nice “real-world” examples of wall-crossing formulae involving finite collections of BPS states.

Because we have an irregular singularity at  $z = \infty$ , to define the WKB triangulation we will have to use the modified rules of Section 8. Applying these rules to the present case, we will obtain a triangulation of a surface  $C'$  which is  $\mathbb{CP}^1$  with a disc cut out around  $z = \infty$ , with vertices at marked points on that disc, corresponding to the loci where WKB curves run off to  $z = \infty$ . As we have explained in general in Section 6, for special values of  $\vartheta$  finite WKB curves will appear, corresponding to the BPS states of our field theory, and causing  $T_{\text{WKB}}(\vartheta)$  to jump.

### 9.4.1 $N = 1$

We begin with  $N = 1$ , so

$$P(z) = z. \quad (9.16)$$

There are no deformations — normalizable or otherwise — so  $\mathcal{B}$  is just a single point. Moreover there is a corresponding unique solution to the Hitchin equations, so  $\mathcal{M}$  is also just a single point. This solution can be written explicitly:

$$\varphi = \begin{pmatrix} 0 & |z|^{1/2} e^h \\ \frac{z}{|z|^{1/2}} e^{-h} & 0 \end{pmatrix}, \quad (9.17)$$

$$A = \left( \frac{1}{8} + \frac{1}{4} |z| \frac{d}{d|z|} h \right) \sigma^3 \left( \frac{dz}{z} - \frac{d\bar{z}}{\bar{z}} \right). \quad (9.18)$$

Here  $h(|z|)$  is a Painleve III transcendent: writing  $r := \frac{8R}{3} |z|^{3/2}$ , it obeys

$$\left( \frac{d^2}{dr^2} + \frac{1}{r} \frac{d}{dr} \right) h = \frac{1}{2} \sinh(2h), \quad (9.19)$$

with boundary condition  $h(r) \rightarrow -\frac{1}{3} \log r + \text{const}$  for  $r \rightarrow 0$ . It can be shown [69] that  $h(r) \rightarrow \pi^{-1} K_0(r)$  for  $r \rightarrow \infty$ . We will return to this solution in Section 13 below.

There are  $N+2 = 3$  WKB rays around  $z = \infty$ , given by (8.2), and a single turning point at  $z = 0$ . The  $\mathcal{A}$ -flatness equation somewhat resembles the Airy equation: in particular there is a small flat section  $s_k$  along each of the three rays  $r_k$ . The WKB triangulation  $T_{\text{WKB}}(\vartheta)$  consists of a single triangle, which rotates in the  $z$ -plane as  $\vartheta$  varies. There are no flips and correspondingly no BPS states. There are no Fock-Goncharov coordinates, since the triangulation has no internal edges.



### 9.4.2 $N = 2$

Next consider the case  $N = 2$ . We write

$$P(z) = z^2 + 2m, \quad (9.20)$$

and hence  $\Delta(z) = z + \frac{m}{z}$ . The parameter  $m$  is log-normalizable. The Coulomb branch  $\mathcal{B}$  is a single point and there is no  $U(1)$  gauge field. The moduli space  $\mathcal{M}$  is also a single point.

The spectral curve  $\Sigma$  has genus zero and two punctures lying over  $z = \infty$ . In this case  $H_1(\Sigma; \mathbb{Z})$  is one-dimensional and odd under the exchange of the sheets, so  $\hat{\Gamma} = H_1(\Sigma; \mathbb{Z}) \simeq \mathbb{Z}$ . This one-dimensional lattice is generated by a single flavor charge, with  $m$  the corresponding mass parameter.

In this case we do not know explicit solutions to the Hitchin equations. Nevertheless, following the general recipe of the previous sections, let us examine the WKB triangulation. There are  $N + 2 = 4$  WKB rays, and  $N = 2$  turning points. The generic behavior of the WKB triangulation is as shown in Figure 44. Combinatorially the four boundary edges make up a square, and the single internal edge gives a triangulation of that square.

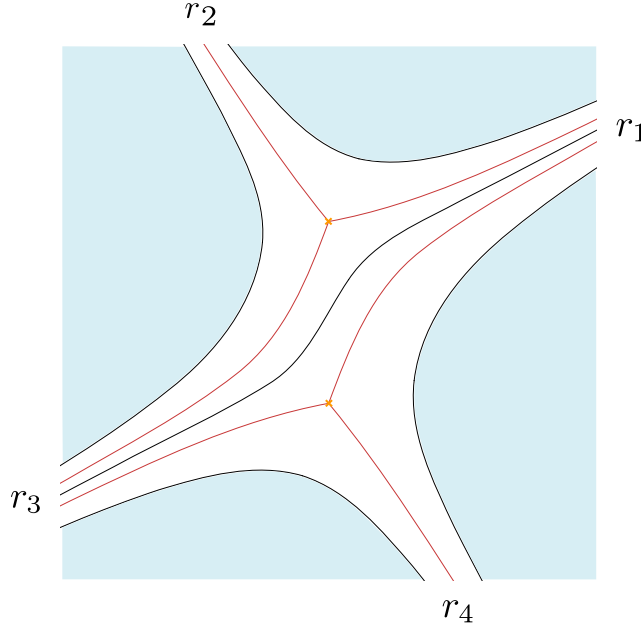


**Figure 44:** A generic WKB triangulation for  $N = 2$ . Separating WKB curves are shown in red, while the generic WKB curves chosen for the edges of the triangulation are black. The shaded region is the union of the four “petals” which we cut out around the irregular singularity at  $z = \infty$ .

Since  $\hat{\Gamma}$  is one-dimensional, there is only one independent Darboux coordinate  $\mathcal{X}_\gamma$ . In fact we claim that it is equal to  $\mu$  given in (9.13). (Indeed this is the only reasonable function of  $m, m^{(3)}$  which carries one unit of flavor charge.) To show this we use the asymptotics of  $s_i$ . Since two WKB rays are separated by a Stokes ray, in an angular sector around  $r_2$ ,  $s_1$  and  $s_3$  are exponentially growing and hence (if normalized appropriately) differ by a multiple of the small solution  $s_2$ ,

$$s_1 = s_3 + as_2 \quad (9.21)$$

for some constant  $a$ . Similarly, around  $r_4$ ,  $s_1$  and  $s_3$  are exponentially large, and hence (after taking into account the formal monodromy, i.e. the monodromy of the asymptotics)

$$s_1 = \mu s_3 + b s_4 \quad (9.22)$$

for some constant  $b$ . Since  $s_1, \dots, s_4$  are single-valued these relations hold throughout the plane, and can be used to simplify the Fock-Goncharov coordinate to

$$\mathcal{X}_E = -\frac{(s_1 \wedge s_2)(s_3 \wedge s_4)}{(s_2 \wedge s_3)(s_4 \wedge s_1)} = -\mu^{-1}. \quad (9.23)$$

As  $\vartheta$  traverses an arc of length  $\pi$ , we encounter one critical value  $\vartheta = \vartheta_c$  where a finite WKB curve appears connecting the two turning points. The WKB triangulation  $T_{\text{WKB}}(\vartheta)$  experiences a flip at this  $\vartheta$ . See Figure 45. The flip transforms the single Fock-Goncharov coordinate by  $\mathcal{X}_E^T = 1/\mathcal{X}_E^{T'}$  (where in both cases  $E$  denotes the single internal edge). On the other hand  $\mathcal{X}_\gamma^\vartheta$  is unchanged and equal to  $-\mu^{-1}$ .

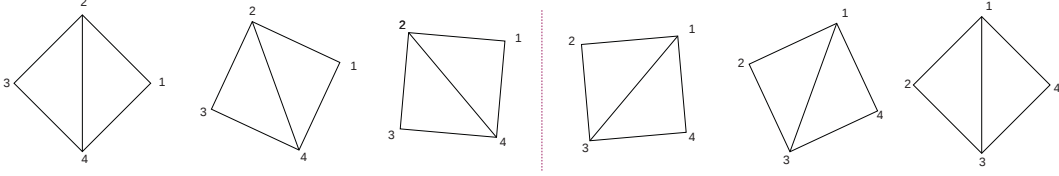


**Figure 45:** As the phase  $\vartheta$  varies from 0 to  $\pi$ , the WKB triangulation evolves simply, with a single flip (dotted line). Notice that the initial and final triangulation are identical, but for a relabeling of the WKB rays.

What is the meaning of this single flip? It means that in the scaling limit discussed above we keep a single BPS particle, of flavor charge 1. Based on this local model, we can make a more general prediction: near the simplest singularities in the Coulomb branch where two turning points collide, a single BPS particle becomes light, corresponding to a BPS string stretched between the two turning points.

#### 9.4.3 Intermission: $N = 2$ and periodic Taub-NUT space

At this point we can make contact with the most fundamental example of a quantum-corrected Coulomb branch considered in our previous paper [1]. This will provide a result which has recently been of use in the computation of gluon scattering amplitudes [11].

The fact that in the  $N = 2$  example we encountered only a log-normalizable deformation parameter, and correspondingly  $\mathcal{M}$  is trivial, might initially be a bit disappointing. One might have expected to glean some information about the behavior of the exact metric on the three-dimensional Coulomb branch near a singularity of the four-dimensional theory.

Physically, we know what to expect. In the original full theory, the flavor symmetry of the single light BPS particle is actually gauged. If we simply ignore the effect of the massive BPS particles, the Coulomb branch of a  $U(1)$  gauge theory on  $\mathbb{R}^3 \times S^1$  coupled to a single light hypermultiplet is well known as the “periodic Taub-NUT” metric [70, 71],

and played a central role in the analysis of [1]. It is not a complete hyperkähler metric; rather, it is well defined up to an arbitrary mass scale  $\Lambda$ .

In [1] the periodic Taub-NUT metric was described in terms of a pair of holomorphic Darboux coordinates  $(\mathcal{X}_e, \mathcal{X}_m)$ .  $\mathcal{X}_e$  coincides with the  $\mathcal{X}_\gamma$  discussed here. The more interesting coordinate is  $\mathcal{X}_m$ , which experiences Stokes phenomena, with Stokes factors  $\mathcal{K}_\gamma$ ,  $\mathcal{K}_{-\gamma}$  corresponding to the single massive hypermultiplet and its CPT conjugate.

Can we find a role for  $\mathcal{X}_m$  in the present context? At the level of the moduli space of flat connections, it is natural to consider letting the monodromy parameters  $\mu_a$  at the singularities vary. Indeed,  $\mu_a$  can be interpreted as the complex moment map for the residual gauge transformation at the  $a$ -th singularity. We can let  $\mu_a$  vary and at the same time restrict the gauge transformations to approach the identity at the singularities. This defines an enlarged symplectic manifold, with two extra complex coordinates for each singularity [65]. In our present context that means enlarging  $\mathcal{M}$  from complex dimension 0 to complex dimension 2. As we will now see,  $\mathcal{X}_e$  and  $\mathcal{X}_m$  will be realized as functions on this extended  $\mathcal{M}$ .

Once the gauge transformations at the singularity have been restricted to the identity, it makes gauge-invariant sense to pick a specific choice of overall normalization for the small solutions, for example by prescribing exactly the asymptotic behavior at the singularity:

$$s_i(z, \zeta) \exp \left[ \frac{R}{\zeta} \left( \frac{z^2}{2} + m \log z \right) - m^{(3)} (\log z - \log \bar{z}) + R\zeta \left( \frac{\bar{z}^2}{2} + \bar{m} \log \bar{z} \right) \right] = \begin{pmatrix} 1 \\ 0 \end{pmatrix} + O(1/z) \quad (9.24)$$

or

$$s_i(z, \zeta) \exp \left[ -\frac{R}{\zeta} \left( \frac{z^2}{2} + m \log z \right) + m^{(3)} (\log z - \log \bar{z}) - R\zeta \left( \frac{\bar{z}^2}{2} + \bar{m} \log \bar{z} \right) \right] = \begin{pmatrix} 0 \\ 1 \end{pmatrix} + O(1/z). \quad (9.25)$$

In the example we are now considering, this allows us to make gauge-invariant sense of individual elements of the Stokes matrices, for example the  $a$  in  $s_1 = s_3 + as_2$ . (Notice that this relation can be consistent with (9.24), (9.25) only if we make a proper choice of branch cut in  $\log z$ ; we place the cut slightly below  $r_3$ .) We think of  $a$  as a “ratio” (as opposed to “cross-ratio”),

$$a = \frac{s_1 \wedge s_3}{s_2 \wedge s_3}. \quad (9.26)$$

If the value of  $\arg \zeta$  falls in the half plane  $\mathbb{H}_\vartheta$  around a  $\vartheta$  for which there is an edge between  $r_1$  and  $r_3$ , we can compute the asymptotics of  $a$  for small  $\zeta$  with the WKB method. The calculation is straightforward, and gives our usual exponential form  $a \sim c \exp(\pi R \zeta^{-1} Z_{\tilde{\gamma}})$ , where  $Z_{\tilde{\gamma}}$  is a regularized period of  $\pi^{-1} \lambda$ , on a cycle  $\tilde{\gamma}$  which goes from infinity along  $r_1$  to infinity along  $r_2$ , winding around the turning point in the triangle 123:

$$Z_{\tilde{\gamma}} = 2 \int_{z=\sqrt{-2m}}^L \sqrt{z^2 + 2m} - L^2 - 2m \log L = -m \log \frac{m}{-2e} + \mathcal{O}\left(\frac{1}{L}\right). \quad (9.27)$$

This path intersects  $\gamma$  once. Motivated by these asymptotics we define  $\mathcal{X}_{\tilde{\gamma}}^\vartheta = a$  for this value of  $\vartheta$ .

As we increase the phase  $\vartheta$ , beyond the critical value  $\vartheta_c$  where the triangulation flips, we should consider instead an  $a'$  defined by  $s_4 = s_2 + a's_1$ , or

$$a' = \frac{s_4 \wedge s_2}{s_1 \wedge s_2}. \quad (9.28)$$

The WKB computation of  $a'$  is identical to that for  $a$ , but for a crucial overall sign, so here the asymptotics suggest that we should define  $\mathcal{X}_{\tilde{\gamma}}^{\vartheta}$  in terms of  $1/a'$ . Recall the relations  $s_1 = s_3 + as_2$  and  $s_1 = \mu s_3 + bs_4$ . With our choice of cut for  $\log z$ , if we continue these relations all the way to  $r_1$ , we see that  $bs_4 = (1 - \mu)s_1 + a\mu s_2$ . Comparing with  $s_4 = s_2 + a's_1$  we see that  $b = a\mu$  and  $a' = -a^{-1}(1 - \mu^{-1})$ . Then, if  $\text{Re}(im/\zeta) > 0$ , the asymptotic behavior of  $\mathcal{X}_{\tilde{\gamma}}$  remains consistent if we define  $\mathcal{X}_{\tilde{\gamma}}^{\vartheta} = -\frac{1}{a'}$  for this  $\vartheta$ .

Now we have defined our coordinates  $\mathcal{X}_{\gamma}^{\vartheta}$  and  $\mathcal{X}_{\tilde{\gamma}}^{\vartheta}$ , for  $\vartheta$  on both sides of the flip associated to the BPS state of charge  $\gamma$ . From the explicit formulas above for these coordinates, it quickly follows that the coordinate transformation across the flip coincides with  $\mathcal{K}_{\gamma}$ ! Similarly, the coordinate transformation induced by the BPS state of charge  $-\gamma$  turns out to be  $\mathcal{K}_{-\gamma}$ . With the identification  $a^{PT} = -2im$  between the coordinate  $a^{PT}$  on the base of periodic Taub-NUT and our mass parameter, we see that  $\mathcal{X}_{\gamma}, \mathcal{X}_{\tilde{\gamma}}$  have the same asymptotic behavior as  $\mathcal{X}_e, \mathcal{X}_m$  (after an appropriate choice of cutoff) and also transform in the same way as  $\vartheta$  crosses the BPS rays. The uniqueness of the solution of the Riemann-Hilbert problem in [1] then guarantees that  $\mathcal{X}_{\gamma}, \mathcal{X}_{\tilde{\gamma}}$  coincide with  $\mathcal{X}_e, \mathcal{X}_m$ . In particular, it follows that the formulas of [1] can be used to compute  $\mathcal{X}_{\tilde{\gamma}}$ .

We have seen that the Stokes data for the auxiliary flatness equations associated to this Hitchin system can be computed exactly in terms of the function  $\mathcal{X}_m(\zeta)$ , even though we cannot compute the solution to the Hitchin equations!

So far we have explained how the functions  $\mathcal{X}_e$  and  $\mathcal{X}_m$  arise in this example, by considering them as functions on an extension of the moduli space of flat connections, obtained by introducing some extra parameters associated to the singularity. But we have not considered this moduli space as a hyperkähler manifold, and hence we have not found a precise role for the periodic Taub-NUT metric in the context of Hitchin systems. To do so, we could try letting the three mass parameters  $m, m^{(3)}, \bar{m}$  at the singularity vary, and then adding one more circle-valued parameter by considering only gauge transformations which reduce to the identity at the singularity. However, it is not clear that we can define an hyperkähler metric on the resulting extended moduli space; the metric and hyperkähler forms diverge when evaluated on variations of the masses. One could try to regularize the divergence by removing a small disk around each singularity. The metric would depend logarithmically on the cutoff radius, exactly as in the case of the periodic Taub-NUT metric, and possibly be incomplete. As our twistor construction of the hyperkähler metric is completely local over the base, this potential incompleteness is not an obstacle: the metric can be computed from the coordinates  $\mathcal{X}_{\gamma}, \mathcal{X}_{\tilde{\gamma}}$  in our standard way, and because these coincide with  $\mathcal{X}_e, \mathcal{X}_m$ , the metric will coincide with the periodic Taub-NUT metric!

This approach could be extended to more complicated Hitchin systems, but we will not pursue it further in this paper.

#### 9.4.4 $N = 3$

We now come to the case  $N = 3$ , where we will first encounter a wall-crossing formula. We write

$$P(z) = z^3 - 3\Lambda^2 z + u, \quad (9.29)$$

where  $\Lambda$  is a non-normalizable parameter defining the theory, and  $u$  is a normalizable modulus parameterizing the Coulomb branch  $\mathcal{B}$ . The discriminant of  $P(z)$  is  $27((2\Lambda^3)^2 - u^2)$ , so there are two singular points on  $\mathcal{B}$  at  $u = \pm 2\Lambda^3$ , where two zeroes of  $P(z)$  collide. (We take  $\Lambda \neq 0$ , so that there is no  $u$  for which all three zeroes collide.)

As usual, there is a local system of lattices  $\hat{\Gamma}$  over  $\mathcal{B}$ , given by the odd part of the homology of the family of punctured elliptic curves  $\Sigma_u$ . In this case  $\hat{\Gamma}$  has rank 2. Altogether  $\mathcal{B}$  strongly resembles the well-known  $u$ -plane of the  $SU(2)$  Seiberg-Witten theory with  $N_f = 0$  (to be considered below in Section 10.1.)

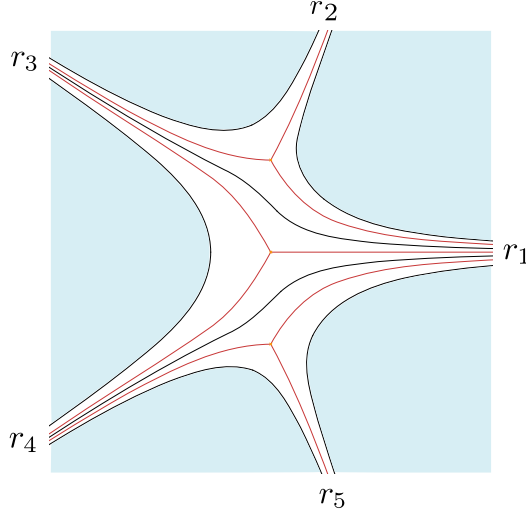


**Figure 46:** A sample WKB triangulation in the  $N = 3$  example, at generic  $\vartheta$ .

Now let us consider the WKB triangulation. There are five WKB rays (and correspondingly five Stokes rays) at  $z = \infty$  and three turning points. A generic  $T_{\text{WKB}}(\vartheta, u)$  is a triangulation of a pentagon, as depicted in Figure 46. We can get an integral basis of  $\hat{\Gamma}_u$  by taking the  $\gamma_E^\vartheta$  associated to the two internal edges  $E_{1,2}$  of this triangulation. To be concrete, let us define  $\{\gamma_1, \gamma_2\}$  to be the basis so obtained from  $T_{\text{WKB}}(\vartheta = 0, u = 0)$  with  $\langle \gamma_1, \gamma_2 \rangle = 1$ .

As we vary  $\vartheta$  from 0 to  $2\pi$  holding  $u$  fixed,  $T_{\text{WKB}}(\vartheta, u)$  jumps by a flip 4 times, at the phases of the periods  $\pm Z_{\gamma_1}$  and  $\pm Z_{\gamma_2}$ . If we vary  $\vartheta$  over a range of  $\pi$  then  $T_{\text{WKB}}(\vartheta, u)$  flips twice. These two flips are generated by two independent finite WKB curves, representing two BPS particles (the other two flips correspond to their antiparticles). See the upper strip of Figure 47. At each of the singularities in  $\mathcal{B}$ , one of these BPS states becomes massless. (As we remarked above, these singularities arise when a pair of turning points collides; the massless BPS state then corresponds to a finite WKB curve connecting this pair of turning points.)

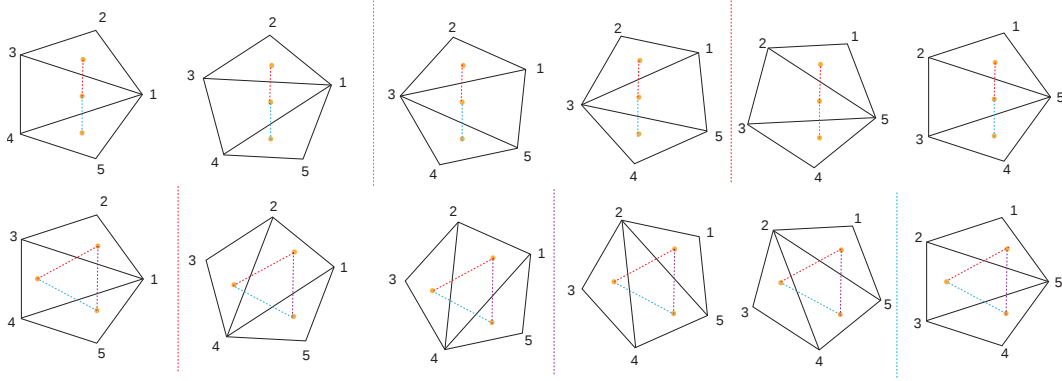


**Figure 47:** Upper strip: at  $u = 0$ , as the phase  $\vartheta$  varies from 0 to  $\pi$ ,  $T_{\text{WKB}}(\vartheta, u)$  evolves simply, with two flips (dotted lines). Lower strip: for  $u$  beyond the walls of marginal stability,  $T_{\text{WKB}}$  evolves in a different manner, involving three flips (dotted lines). Notice that  $T_{\text{WKB}}(\vartheta) = T_{\text{WKB}}(\vartheta + \pi)$  except for a relabeling of the WKB rays, which is equivalent to a pop transformation.

In  $\mathcal{B}$  there is a single closed wall of marginal stability which divides the  $u$ -plane into two connected components (again, much as in the  $SU(2)$  Seiberg-Witten theory). So far we have discussed  $u = 0$ , which lies inside the wall. If we consider some  $u$  which lies outside the wall the behavior of  $T_{\text{WKB}}(\vartheta, u)$  is different: there are three flips, induced by three finite WKB curves, corresponding to three BPS states. See the lower strip of Figure 47. (This is most easily seen by taking  $u$  to be large.)

To be more precise, the two singular points  $u = \pm 2\Lambda^3$  divide the wall of marginal stability into two segments. Along one segment the phases of  $Z_{\gamma_{1,2}}$  align. After crossing this segment from inside to outside we find three BPS states, of charges  $\gamma_1, \gamma_2, \gamma_1 + \gamma_2$ . If we cross the other segment of the wall, where  $Z_{\gamma_1}$  and  $Z_{-\gamma_2}$  align, we find instead BPS states of charges  $\gamma_1, \gamma_2, \gamma_1 - \gamma_2$ . To see that these two results are compatible we recall that  $\hat{\Gamma}$  has the standard Lefschetz monodromy around the two points  $u = \pm 2\Lambda^3$  where two zeroes of  $P(z)$  collide. Generators of the clockwise monodromy around the two singular points can be taken to be:

$$\begin{aligned} M_1 &= (\gamma_1, \gamma_2) \rightarrow (\gamma_1, \gamma_2 - \gamma_1), \\ M_2 &= (\gamma_1, \gamma_2) \rightarrow (\gamma_1 + \gamma_2, \gamma_2). \end{aligned} \tag{9.30}$$

These three finite WKB curves persist in the spectrum as we go to arbitrarily large  $|u|$  (indeed there are no other walls of marginal stability where they could disappear). We infer from this that in a more general theory, near a singularity in the Coulomb branch where three turning points are coalescing, three light BPS particles will typically be present, realized as BPS strings joining these three turning points.

### The wall-crossing formula

Now we are ready to see a wall-crossing formula emerge. Let  $u_-$  denote a point inside the wall and  $u_+$  a point outside, and fix some  $\vartheta$ . We have two coordinate systems  $\mathcal{X}_\gamma^{\vartheta, u_-}$  and  $\mathcal{X}_\gamma^{\vartheta + \pi, u_+}$  on  $\mathcal{M}$ , which are related by some symplectomorphism. To evaluate this

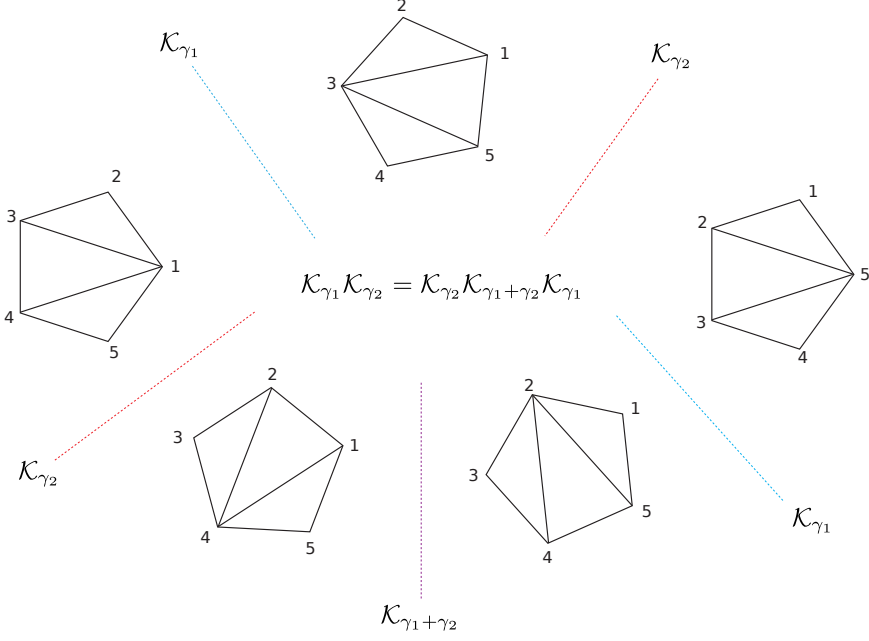


**Figure 48:** The two different ways to go from the triangulation at  $\vartheta = 0$  to the triangulation at  $\vartheta = \pi$  on the two sides of the wall must correspond to the same symplectomorphism. The pentagon identity follows.

symplectomorphism, we consider the evolution of the triangulation  $T_{\text{WKB}}(\vartheta, u)$  along a path from  $(\vartheta, u_-)$  to  $(\vartheta + \pi, u_+)$ .

One possibility is to vary first  $\vartheta$  to  $\vartheta + \pi$  and then deform from  $u_-$  to  $u_+$ . As we vary  $\vartheta$  the triangulation undergoes two flips corresponding to the two BPS states inside the wall. As we vary  $u$ , the triangulation does not jump at all, so long as no  $\arg Z_\gamma(u)$  crosses  $\vartheta$  (which we can always arrange by choosing  $u_\pm$  close enough to the wall and  $\vartheta$  generic enough). So the total transformation of the triangulation involves exactly two flips.

However there is also another possibility: first deform from  $u_-$  to  $u_+$  and then vary  $\vartheta$  to  $\vartheta + \pi$ . In that case the triangulation undergoes three flips corresponding to the three BPS states outside the wall.

These two computations must give the same symplectomorphism. This corresponds to the identity

$$\mathcal{K}_{\gamma_1} \mathcal{K}_{\gamma_2} = \mathcal{K}_{\gamma_2} \mathcal{K}_{\gamma_1 + \gamma_2} \mathcal{K}_{\gamma_1} \quad (9.31)$$

for one section of the wall,

$$\mathcal{K}_{-\gamma_2} \mathcal{K}_{\gamma_1} = \mathcal{K}_{\gamma_1} \mathcal{K}_{\gamma_1 - \gamma_2} \mathcal{K}_{-\gamma_2} \quad (9.32)$$

for the other. One can check by direct computation that these relations are indeed satisfied. We will refer to either of these basic identities as “the pentagon identity.”

All the structures we have been discussing on  $\mathcal{B}$  are illustrated in Figure 49.

#### 9.4.5 Intermission: Symplectomorphisms and monodromy

There is an interesting relation between the symplectomorphisms which we encountered

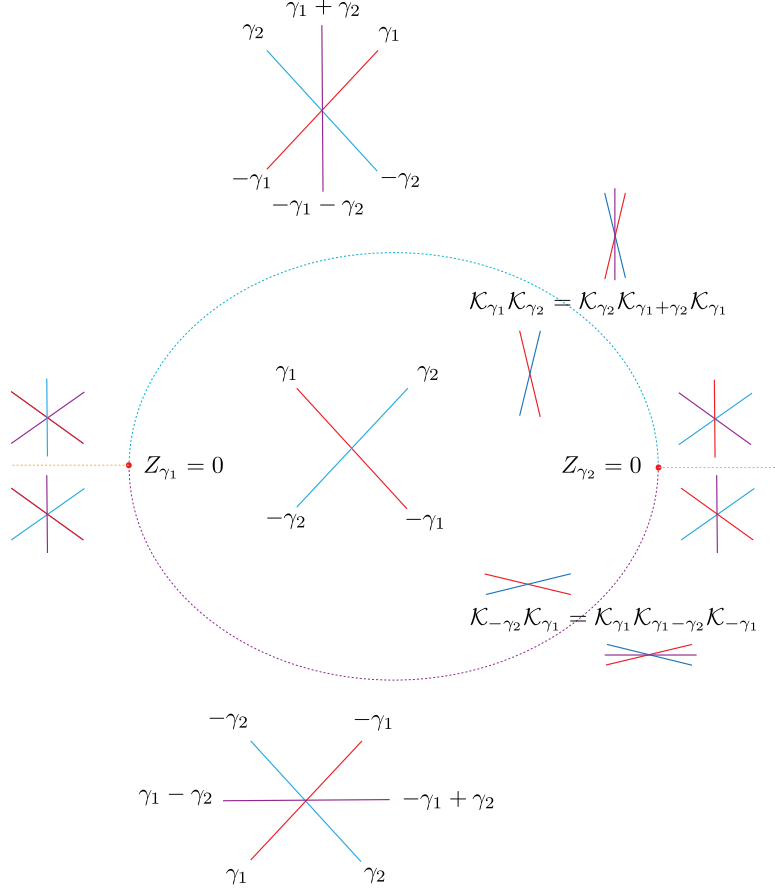


**Figure 49:** The Coulomb branch  $\mathcal{B}$  of the  $N = 3$  theory, with the walls of marginal stability where  $Z_{\pm\gamma_1}$  align with  $Z_{\gamma_2}$  marked. Note that  $\hat{\Gamma}$  has monodromy, so in order to define the basis  $\{\gamma_1, \gamma_2\}$  globally we have to introduce branch cuts, denoted here in orange. In each region we show the BPS spectrum and the cyclic ordering of the BPS rays. Along the walls we show the wall-crossing formulae.

above and the monodromy transformations which arise when we go around a singularity in  $\mathcal{B}$ .

Consider the behavior of the BPS rays as  $u$  is carried around the simplest type of singularity, where some  $Z_{\gamma_0}(u)$  has a simple zero. This is the kind of singularity we were zooming in on in our  $N = 2$  example above. The phase of  $Z_{\gamma_0}(u)$  rotates by  $2\pi$  as  $u$  goes around the singularity. Hence the BPS ray  $\ell_{\gamma_0}$  passes across all the other BPS rays, followed by the ray  $-\ell_{\gamma_0}$ . In other words, as we go around the singularity we cross a series of walls of marginal stability.

It is easy to check that  $\mathcal{K}_{\gamma_0} \mathcal{K}_{-\gamma_0}$  is the transformation

$$\mathcal{X}_\gamma \rightarrow (-\sigma(\gamma_0))^{\langle \gamma, \gamma_0 \rangle} \mathcal{X}_{\gamma + \langle \gamma, \gamma_0 \rangle \gamma_0}. \quad (9.33)$$

It follows that as the BPS rays  $\ell_{\gamma_0}$  and  $\ell_{-\gamma_0}$  sweep across the spectrum, the associated Kontsevich-Soibelman transformations implement the expected monodromy transformations of the charges. (Note that it is convenient to choose the quadratic refinement  $\sigma$  to



obey  $\sigma(\gamma_0) = -1$  whenever  $\gamma_0$  is the charge of a BPS hypermultiplet; such a quadratic refinement is invariant under this monodromy, which thus acts only on the charge label of  $\mathcal{X}_\gamma$ .)

Now how about a singularity where three turning points are coalescing, like we studied in the  $N = 3$  case? As we noted above, near such a singularity three light BPS particles will typically be present, realized as BPS strings joining the turning points. The projections of their charges to the 2-dimensional lattice of gauge charges relevant for the scaling limit are of the form  $\gamma_1, \gamma_1 + \gamma_2, \gamma_2$ . Naively, as we wind around the singularity, one might expect that each BPS line will be swept by the BPS lines of the three light particles, and then the three light antiparticles. This is actually incorrect as we can learn by a simple manipulation of KS transformations. Indeed, we have

$$\begin{aligned} \mathcal{K}_{\gamma_2} \mathcal{K}_{\gamma_1+\gamma_2} \mathcal{K}_{\gamma_1} \mathcal{K}_{-\gamma_2} \mathcal{K}_{-\gamma_1-\gamma_2} \mathcal{K}_{-\gamma_1} &= \mathcal{K}_{\gamma_1} \mathcal{K}_{\gamma_2} \mathcal{K}_{-\gamma_1} \mathcal{K}_{-\gamma_2} \\ &= (\mathcal{K}_{\gamma_1} \mathcal{K}_{-\gamma_1}) \mathcal{K}_{-\gamma_1+\gamma_2} (\mathcal{K}_{\gamma_2} \mathcal{K}_{-\gamma_2}) = (\mathcal{K}_{\gamma_1} \mathcal{K}_{-\gamma_1}) (\mathcal{K}_{\gamma_2} \mathcal{K}_{-\gamma_2}) \mathcal{K}_{-\gamma_1}. \end{aligned} \quad (9.34)$$

This is not quite the expected monodromy action — that would have been implemented just by  $(\mathcal{K}_{\gamma_1} \mathcal{K}_{-\gamma_1}) (\mathcal{K}_{\gamma_2} \mathcal{K}_{-\gamma_2})$ . To resolve this difficulty one should look more closely at the precise dependence of the small central charges on  $u$ . For simplicity take  $\Lambda \rightarrow 0$ . Then one can see from (9.29) that the central charges of the six light BPS particles behave like the six roots  $u^{5/6}$ . It follows that a loop around  $u = 0$  rotates the central charges only by  $\exp \frac{5\pi i}{3}$ . Thus on traveling around this loop a generic BPS ray undergoes five wall-crossings rather than six, and the relevant identity is in fact

$$\mathcal{K}_{\gamma_2} \mathcal{K}_{\gamma_1+\gamma_2} \mathcal{K}_{\gamma_1} \mathcal{K}_{-\gamma_2} \mathcal{K}_{-\gamma_1-\gamma_2} = (\mathcal{K}_{\gamma_1} \mathcal{K}_{-\gamma_1}) (\mathcal{K}_{\gamma_2} \mathcal{K}_{-\gamma_2}), \quad (9.35)$$

which indeed gives the desired monodromy.

#### 9.4.6 $N = 4$

Finally, let us consider  $N = 4$ . We parameterize

$$P(z) = z^4 + 4\Lambda^2 z^2 + 2mz + u, \quad (9.36)$$

so that

$$\lambda \sim \pm \left( z^2 + 2\Lambda^2 + \frac{m}{z} + \dots \right) dz. \quad (9.37)$$

$\Lambda$  is a non-normalizable parameter,  $m$  a mass deformation, and  $u$  parameterizes the Coulomb branch.  $\Sigma_u$  is a twice-punctured elliptic curve (the two punctures lying over  $z = \infty$ ). The local system  $\hat{\Gamma}$  has fiber  $\hat{\Gamma}_u \simeq \mathbb{Z}^3$  with a one-dimensional flavor lattice. The discriminant is cubic in  $u$  and hence there are generically three singular points in the  $u$ -plane, which thus resembles the  $u$ -plane of  $SU(2)$  theory with  $N_f = 1$ .

The WKB triangulations now give triangulations of a hexagon, as in Figures 50, 51. All possible triangulations appear somewhere in parameter space.

Let us now describe the BPS spectrum.

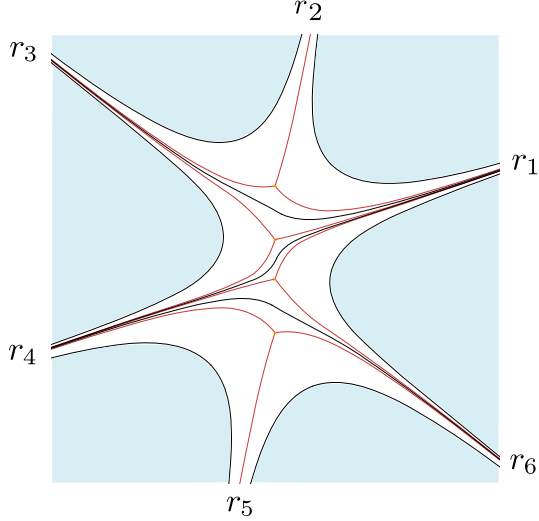


**Figure 50:** A generic WKB triangulation for  $N = 4$  with  $m = 0$ .

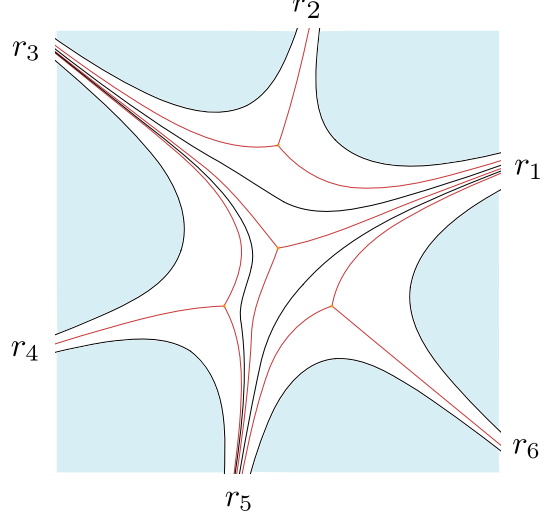


**Figure 51:** A generic WKB triangulation for  $N = 4$  with large  $m$ .

### The case $m = 0$

It is useful first to set  $m = 0$ . Then the discriminant degenerates to  $256u(u - 4\Lambda^4)^2$ , so there are two singular points in  $\mathcal{B}$ :

- At  $u = 0$ , two zeroes of  $P(z)$  coincide at  $z = 0$ , while the other two sit at  $z = \pm 2i\Lambda$ . We expect to see a single BPS particle becoming massless here.
- At  $u = 4\Lambda^4$ ,  $P(z)$  is a perfect square, and two pairs of zeroes collide, at  $z = \pm i\sqrt{2}\Lambda$ . We expect to see two distinct BPS particles becoming massless here. These two particles have the same gauge charges, as the associated cycles in  $\bar{\Sigma}$  are homologous, but they have different flavor charges. (Indeed, the difference between the two corresponding cycles on  $\Sigma$  is a cycle wrapping around  $z = \infty$ . If we took some small  $m \neq 0$ ,  $\oint \lambda$  would give the residue  $m$  of the simple pole there.)

By studying the singularity structure in  $\mathcal{B}$  we have encountered the effects of three BPS particles. Now let us explore the BPS spectrum more systematically by following the  $\vartheta$  dependence of  $T_{\text{WKB}}(\vartheta, u)$ . Begin by fixing any  $0 < u < 4\Lambda^4$ . In this case the four turning points are collinear in the  $z$ -plane, and we will encounter BPS states associated with strings between consecutive turning points. Denote the charge of the BPS string joining the two middle turning points as  $\gamma_1$ . The charges of the other two BPS strings will be denoted as  $\gamma_2, \gamma_3$ , so that  $\gamma_2 + \gamma_3$  is a pure flavor charge (and in particular, at  $m = 0$ ,  $Z_{\gamma_2} + Z_{\gamma_3} = 0$ .) We pick our conventions such that

$$\langle \gamma_3, \gamma_1 \rangle = \langle \gamma_1, \gamma_2 \rangle = 1, \quad \langle \gamma_2, \gamma_3 \rangle = 0. \quad (9.38)$$

Note that  $\mathcal{K}_{\gamma_2}$  and  $\mathcal{K}_{\gamma_3}$  commute, a fact which will be used repeatedly below. There is a wall of marginal stability in  $\mathcal{B}$ , which passes through the two singularities, and encircles

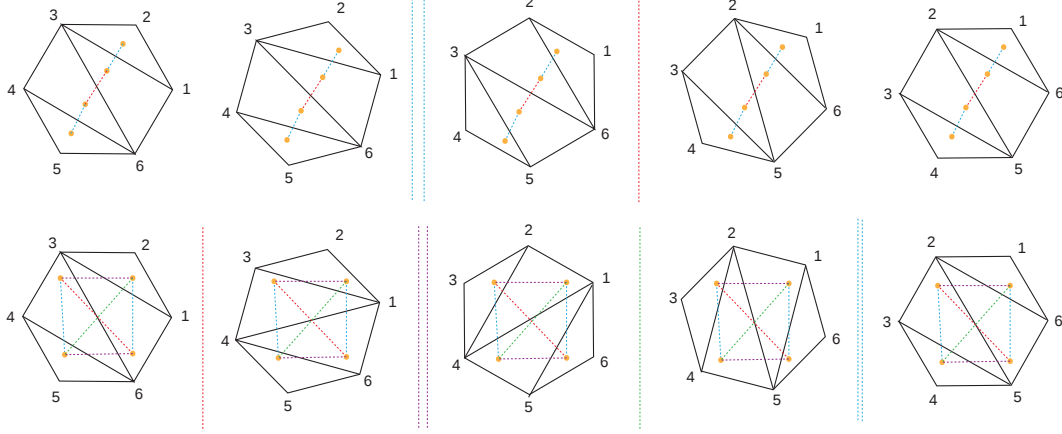


**Figure 52:** WKB triangulations at  $m = 0$ . Upper strip: at  $u = 0$ , as  $\vartheta$  varies from 0 to  $\pi$ ,  $T_{\text{WKB}}$  evolves simply, with three flips: A pair of commuting flips at the first, blue dotted line and a third flip at the red line. Lower strip: for  $u$  beyond the walls of marginal stability,  $T_{\text{WKB}}$  evolves in a different way, involving six flips. Both at the second and at the fourth dotted lines, two flips occur, corresponding to two BPS particles with the same charges. Notice that  $T_{\text{WKB}}(\vartheta)$  and  $T_{\text{WKB}}(\vartheta + \pi)$  are identical, up to a relabeling of the WKB rays.

an ellipsoidal region which includes the line  $0 < u\Lambda^{-4} < 4$ . Now by direct computation (either by hand or using a computer) one can obtain the evolution of  $T_{\text{WKB}}(\vartheta)$  with  $\vartheta$ . In Figure 52 we depict the result, for two  $u$ , one inside and one outside the wall of marginal stability. At  $u = 0$  we see three flips in  $T_{\text{WKB}}$ , corresponding to the three BPS charges  $-\gamma_3, \gamma_2, \gamma_1$ . As we cross the wall of marginal stability, the phase of the central charges  $Z_{\gamma_2}, Z_{-\gamma_3}$  aligns with one of  $Z_{\pm\gamma_1}$  (the sign depending on which segment of the wall we cross). On the other side of the wall, the flips in  $T_{\text{WKB}}$  happen in a different order, and we see a total of six BPS hypermultiplets. There is a BPS string between each pair of turning points.

Following reasoning analogous to the  $N = 3$  case above, then, we must have the wall crossing identity:

$$\mathcal{K}_{\gamma_1} \mathcal{K}_{\gamma_2} \mathcal{K}_{-\gamma_3} = \mathcal{K}_{\gamma_2} \mathcal{K}_{-\gamma_3} \mathcal{K}_{\gamma_1 + \gamma_2 - \gamma_3} \mathcal{K}_{\gamma_1 + \gamma_2} \mathcal{K}_{\gamma_1 - \gamma_3} \mathcal{K}_{\gamma_1} \quad (9.39)$$

The ordering of factors in (9.39) is easily understood, just using the facts that  $Z_{\gamma_2} = Z_{-\gamma_3}$  and the ordering of the arguments of  $Z_{k_1\gamma_1 + k_2\gamma_2}$  as  $k_1, k_2$  vary is determined by the ordering of  $k_1/k_2$ . Again, one can check explicitly that (9.39) is a true identity, but we will give a simpler proof in the next paragraph.

### The case $m \neq 0$

For  $m \neq 0$  the picture is a bit more complicated. For small  $m$ , the particles of charges  $\gamma_2$  and  $\gamma_3$  become massless at slightly different points in  $\mathcal{B}$ . The wall of marginal stability also splits into several walls. The wall-crossing formula (9.39) thus “decomposes” into three

separate pentagon identities. One possible decomposition is

$$\begin{aligned}\mathcal{K}_{\gamma_1}\mathcal{K}_{\gamma_2}\mathcal{K}_{-\gamma_3} &= \mathcal{K}_{\gamma_2}\mathcal{K}_{\gamma_1+\gamma_2}\mathcal{K}_{\gamma_1}\mathcal{K}_{-\gamma_3} = \mathcal{K}_{\gamma_2}\mathcal{K}_{\gamma_1+\gamma_2}\mathcal{K}_{-\gamma_3}\mathcal{K}_{\gamma_1-\gamma_3}\mathcal{K}_{\gamma_1} \\ &= \mathcal{K}_{\gamma_2}\mathcal{K}_{-\gamma_3}\mathcal{K}_{\gamma_1+\gamma_2-\gamma_3}\mathcal{K}_{\gamma_1+\gamma_2}\mathcal{K}_{\gamma_1-\gamma_3}\mathcal{K}_{\gamma_1},\end{aligned}\quad (9.40)$$

corresponding to three separate walls of marginal stability, where  $Z_{\gamma_1}$  aligns with  $Z_{\gamma_2}$ , then  $Z_{\gamma_1}$  aligns with  $Z_{-\gamma_3}$ , then  $Z_{-\gamma_3}$  aligns with  $Z_{\gamma_1+\gamma_2}$ . A second possibility is

$$\begin{aligned}\mathcal{K}_{\gamma_1}\mathcal{K}_{\gamma_2}\mathcal{K}_{-\gamma_3} &= \mathcal{K}_{-\gamma_3}\mathcal{K}_{\gamma_1-\gamma_3}\mathcal{K}_{\gamma_1}\mathcal{K}_{\gamma_2} = \mathcal{K}_{-\gamma_3}\mathcal{K}_{\gamma_1-\gamma_3}\mathcal{K}_{\gamma_2}\mathcal{K}_{\gamma_1+\gamma_2}\mathcal{K}_{\gamma_1} \\ &= \mathcal{K}_{\gamma_2}\mathcal{K}_{-\gamma_3}\mathcal{K}_{\gamma_1+\gamma_2-\gamma_3}\mathcal{K}_{\gamma_1+\gamma_2}\mathcal{K}_{\gamma_1-\gamma_3}\mathcal{K}_{\gamma_1}.\end{aligned}\quad (9.41)$$

The corresponding sequences of WKB triangulations are shown in Figure 53.

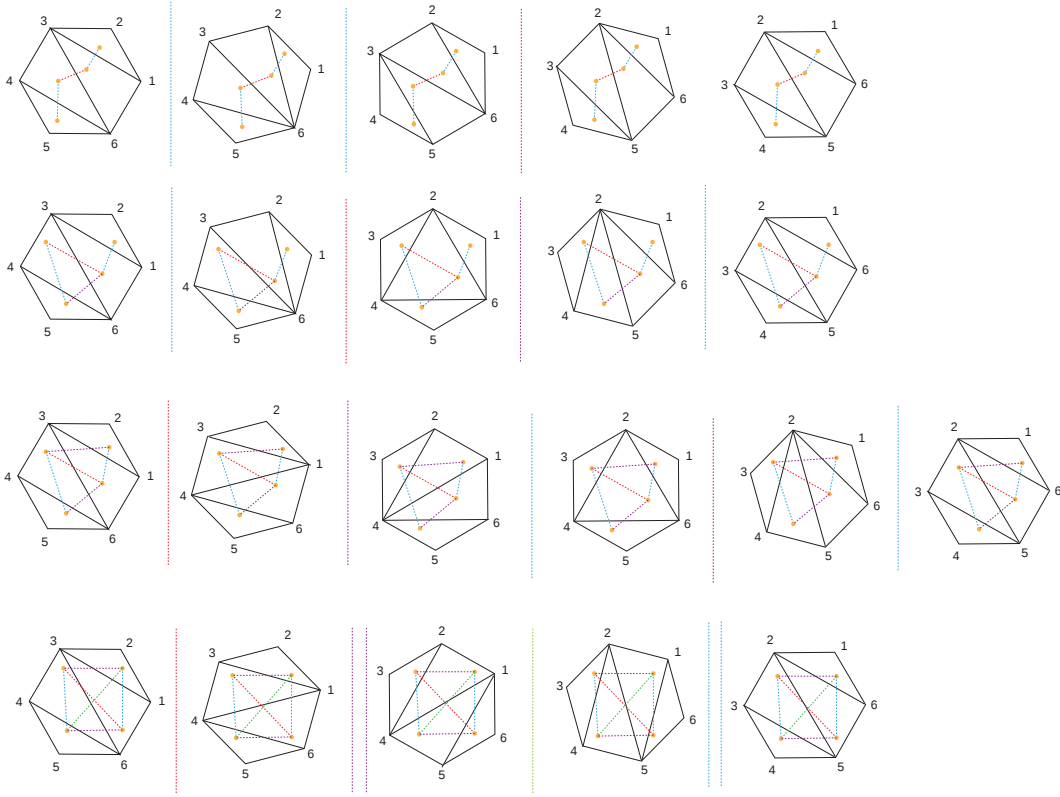


**Figure 53:** Upper strip: at  $u = 0$ ,  $T_{\text{WKB}}(\vartheta, u)$  evolves simply with  $\vartheta$ , undergoing three flips. Lower strips: as we vary  $u$  toward  $\infty$  we cross three walls. After crossing each wall, we show the new evolution of  $T_{\text{WKB}}(\vartheta, u)$  with  $\vartheta$ . In the last strip, to save space, we do not show the intermediate triangulations between pairs of BPS jumps with the same gauge charge.

In Figure 54 we show the structure of the walls in  $\mathcal{B}$  very close to the singular point where  $Z_{\gamma_1} = 0$ . The global structure of the walls is fairly intricate, and depends on the phase of  $m$ .

Notice that it is possible to go from small  $u$  to large  $u$  by a trickier path which passes between the two singularities where  $Z_{\gamma_2} = 0$  and  $Z_{\gamma_3} = 0$ . The wall-crossing formula then

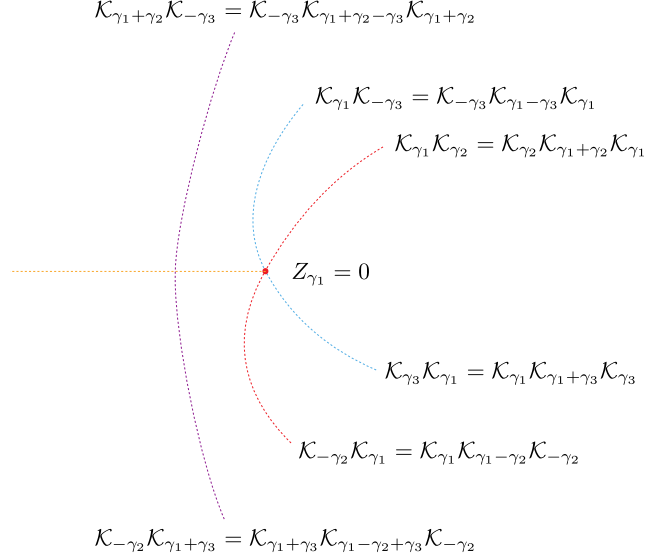


**Figure 54:** The walls of marginal stability in the  $N = 4$  theory, near a point  $u$  with  $Z_{\gamma_1}(u) = 0$ , for a certain choice of small  $m \neq 0$ . (For other phases of  $m$ ,  $\gamma_2$  and  $-\gamma_3$  may be exchanged in the figure). Note that  $\hat{\Gamma}$  has monodromy, hence the need for the orange cuts.

arranges itself in a different way, for example as

$$\begin{aligned} \mathcal{K}_{\gamma_3}\mathcal{K}_{\gamma_1}\mathcal{K}_{\gamma_2} &= \mathcal{K}_{\gamma_1}\mathcal{K}_{\gamma_1+\gamma_3}\mathcal{K}_{\gamma_3}\mathcal{K}_{\gamma_2} = \mathcal{K}_{\gamma_1}\mathcal{K}_{\gamma_2}\mathcal{K}_{\gamma_1+\gamma_2+\gamma_3}\mathcal{K}_{\gamma_1+\gamma_3}\mathcal{K}_{\gamma_3} \\ &= \mathcal{K}_{\gamma_2}\mathcal{K}_{\gamma_1+\gamma_2}\mathcal{K}_{\gamma_1}\mathcal{K}_{\gamma_1+\gamma_2+\gamma_3}\mathcal{K}_{\gamma_1+\gamma_3}\mathcal{K}_{\gamma_3}. \end{aligned} \quad (9.42)$$

(Remember that  $\mathcal{K}_{\gamma_3}$  and  $\mathcal{K}_{\gamma_2}$  commute.) It is an amusing exercise to check the self-consistency of the BPS spectra generated by crossing from the inner region to the outer region between different pairs of singular points, and the monodromies of the charge lattice around the singular points themselves. The details vary depending on the phase of  $m$ .

A judicious choice of  $m$  can bring other pairs of singularities, say  $Z_{\gamma_1} = 0$  and  $Z_{\gamma_2} = 0$ , together, and produce a scaling region in  $\mathcal{B}$  which looks like our  $N = 3$  example. In this limit we see a central region with the BPS spectrum of particles which becomes light at the composite  $N = 3$  singularity, with charges  $\gamma_2$ ,  $\gamma_1 + \gamma_2$ ,  $\gamma_1$ , together with the particle which becomes light at the remaining simple singularity, with charge  $\gamma_3$ . We show the structure of  $\mathcal{B}$  for this choice of  $m$  in Figure 55. The corresponding behavior of  $T_{\text{WKB}}$  is shown in Figure 56.

For generic  $m$ , there is a region at sufficiently large  $|u|$  where the turning points are arranged roughly into a square, with 6 BPS states associated to the sides and the diagonals. From this behavior we learn that in a generic  $\mathcal{N} = 2$  theory, near a singularity in the Coulomb branch where four turning points are coalescing, we will typically find six light BPS particles, realized as BPS strings joining any pair of turning points.

## 9.5 General $N$ and the associahedron

Finally, we make some general remarks applicable to all  $N$ . The finite WKB curves in these

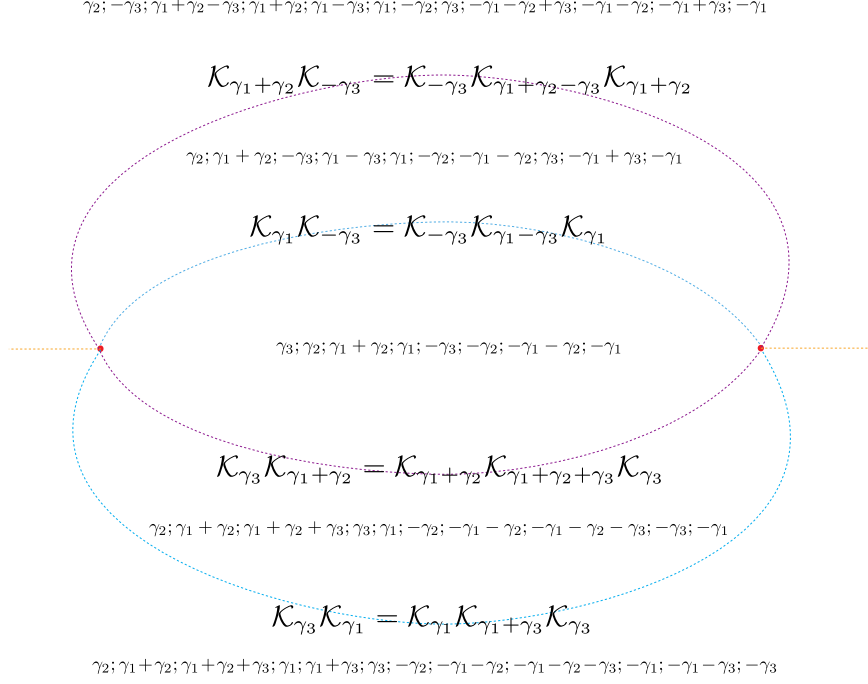


**Figure 55:** The walls of marginal stability in the  $N = 4$  theory, for the special choice of mass  $m$  where the singularities  $Z_{\gamma_1} = 0$  and  $Z_{\gamma_2} = 0$  collide. Inside each region we list the charges of all BPS hypermultiplets in the spectrum in that region, in order of their phases (up to overall cyclic permutation). On each wall we give the relevant wall-crossing formula.

theories were described by Shapere and Vafa in [68], exactly for the purpose of studying BPS states. They showed that:

- The phase  $\vartheta$  at which a finite WKB curve appears is uniquely determined by the homotopy class of the WKB curve in the punctured plane  $\mathbb{C} - \{\mathcal{T}_i\}$ .
- There is at most one finite WKB curve joining any two turning points. Hence there are only a *finite* number of BPS states.
- Any two turning points can be joined by a piecewise collection of finite WKB curves (generically with different  $\vartheta$  for each segment). Hence there are at least  $N - 1$  BPS states at any point  $u$  on the Coulomb branch.
- The minimal number of BPS states,  $N - 1$ , is attained, for example, when all the roots of  $P_N(z)$  are real. The maximal number,  $\frac{1}{2}N(N - 1)$ , is attained, for example, if  $P(z) = z^N - 1$ .
- The three separating WKB curves emanating from each of the  $N$  turning points each asymptote to a different ray at  $z = \infty$ .
- There are no closed WKB curves.

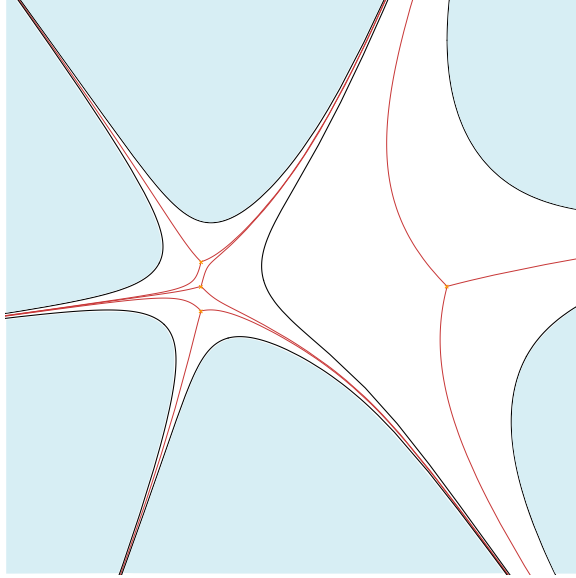


**Figure 56:** The triangulation  $T_{\text{WKB}}$  for the  $N = 4$  theory, with  $m$  and  $u$  adjusted so that three turning points are coming together. On the left, the pentagonal structure of the  $N = 3$  example emerges inside the  $N = 4$  triangulation.

The generic WKB curves thus define a triangulation of a convex polygon with  $N + 2$  vertices. (We have seen examples of this for  $N = 1, 2, 3, 4$  above.) This observation opens up a connection to a rich branch of mathematics. Triangulations of an  $(N + 2)$ -gon are dual to trivalent graphs and also correspond to rooted binary trees with  $N + 1$  terminal points, or equivalently to ways of parenthesizing a product of  $N + 1$  nonassociative variables  $x_1 \cdots x_{N+1}$ . The number of such triangulations is the Catalan number  $C_N = \frac{1}{N+1} \binom{2N}{N}$ . Moreover, the triangulations of the  $(N + 2)$ -gon can be considered as the vertices of a simplicial complex  $\mathcal{K}_{N+1}$ , with 1-simplices corresponding to the flips. This complex is the 1-skeleton of the  $N$ -th “associahedron” or Stasheff polytope [72]. (See for example [73, 74] for recent discussions.)  $\mathcal{K}_3$  is an interval, and  $\mathcal{K}_4$  is a pentagon. A basic lemma of [72] is that the faces of the associahedron are products of lower-dimensional associahedra. So in particular the 2-cells are pentagons (corresponding to the pentagon relation) and squares (corresponding to the relation that flips on disjoint edges commute). On the other hand the associahedron itself is simply connected, and hence the two-skeleton is simply connected.<sup>40</sup> In our context this implies that all the wall-crossing formulae that arise in these examples are consequences of the pentagon relation. We have seen this fact in the  $N = 3, 4$  examples above.

The appearance of the associahedron in this class of examples raises the question of whether the theory of  $A_\infty$  algebras has any interesting role to play here. Another natural question is whether there is a simple algorithm for computing the spectrum of BPS states given only the polynomial  $P(z)$ . The computation of the spectrum generator in Section 11 answers this second question in the affirmative.

<sup>40</sup>This statement is also closely related to the MacLane coherence theorem in category theory [75].

## 10. $SU(2)$ gauge theory

The examples we have just studied in Section 9 only had BPS hypermultiplets, so the WKB triangulations  $T_{\text{WKB}}(\vartheta)$  only exhibited simple flips as  $\vartheta$  varied. Next we would like to consider some examples with BPS vectormultiplets and the corresponding juggle transformations. We will look at a well-known set of theories:  $SU(2)$  gauge theories with  $N_f = 0, 1, 2, 3, 4$ . Some aspects of their spectra are well understood. See in particular [76, 77, 78] for explicit results on the BPS spectrum in various parameter ranges and [79, 80, 81, 82, 83] for an approach using  $F$ -theory. However, a complete description of their BPS spectra is not available. In this section we will make progress towards such a complete description, giving the spectra in many regions of parameter space. In fact, our methods could be used to obtain the spectrum at any point in moduli space.

### 10.1 $N_f = 0$

This is the canonical example of Seiberg-Witten theory. It can be constructed as in Section 3 from two D4-branes stretched between two NS5-branes (see equation (3.130) et. seq.) The quadratic differential is simply

$$\lambda^2 = \left( \frac{\Lambda^2}{z^3} + \frac{2u}{z^2} + \frac{\Lambda^2}{z} \right) dz^2. \quad (10.1)$$

The corresponding Hitchin system has the mildest possible irregular singularities at  $z = 0, \infty$ , with a single WKB ray emerging from each (corresponding to  $L = 1$  in the notation of Section 8). There are two turning points,  $z_{tp}^\pm = -\frac{u}{\Lambda^2} \pm \sqrt{(\frac{u}{\Lambda^2})^2 - 1}$ , which collide at  $z_{tp}^\pm = \mp 1$  when  $u = \pm \Lambda^2$ . These two values of  $u$  are singularities in  $\mathcal{B}$ . At each of the singularities a single BPS particle becomes massless. As  $u$  varies along the interval  $-\Lambda^2 < u < \Lambda^2$  the two turning points separate, move in opposite directions around  $z = 0$ , and then rejoin. The BPS spectrum anywhere on this interval, for example at  $u = 0$ , consists of two BPS hypermultiplets. They are described by strings joining the two turning points but passing on opposite sides of the singularity at  $z = 0$ . They share both endpoints, hence their charges  $\gamma_{1,2}$  satisfy  $\langle \gamma_1, \gamma_2 \rangle = 2$ .  $\gamma_{1,2}$  generate the charge lattice  $\hat{\Gamma}$ . A typical WKB triangulation  $T_{\text{WKB}}(\vartheta, u)$  for  $u$  in this interval, and its transformations as  $\vartheta$  varies, are shown in Figures 57, 58.

There is a single ellipsoidal wall of marginal stability in  $\mathcal{B}$ , passing through the two singular points. The region inside this wall (which we have just been discussing) is also called the “strong coupling” region, while the region outside is the weak coupling region.

Note that all of the WKB triangulations in this theory are just annuli traversed by two internal edges — exactly the prerequisite situation for our discussion of limit triangulations in Section 6.6.3. When  $u$  is in the strong coupling region the evolution with  $\vartheta$  is simple, and illustrated in Figure 58. On the other hand, in the weak coupling region we encounter a new feature, namely a BPS vectormultiplet. For an appropriate  $\vartheta_c$  a one-parameter family of closed WKB curves appears, corresponding to a single vectormultiplet of charge  $\gamma_1 + \gamma_2$ , as shown in Figure 59. Thus, if  $u$  is in the weak coupling region, as the phase of  $\vartheta$  varies,  $T_{\text{WKB}}(\vartheta, u)$  undergoes infinitely many elementary flips, corresponding to a spectrum of BPS



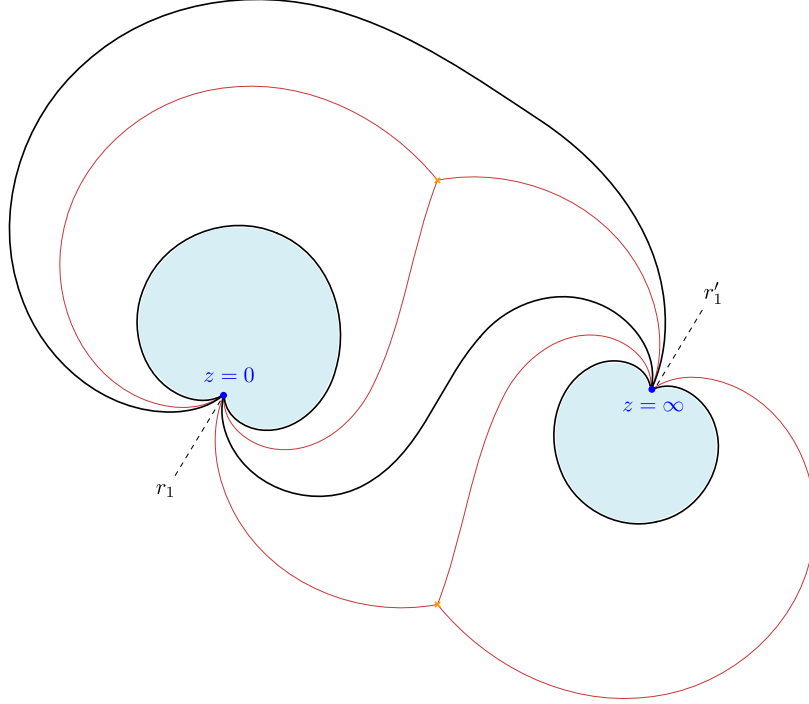


**Figure 57:** A generic  $T_{\text{WKB}}$  for the  $SU(2)$  theory with  $N_f = 0$ . For clarity  $z = \infty$  has been mapped to finite distance.

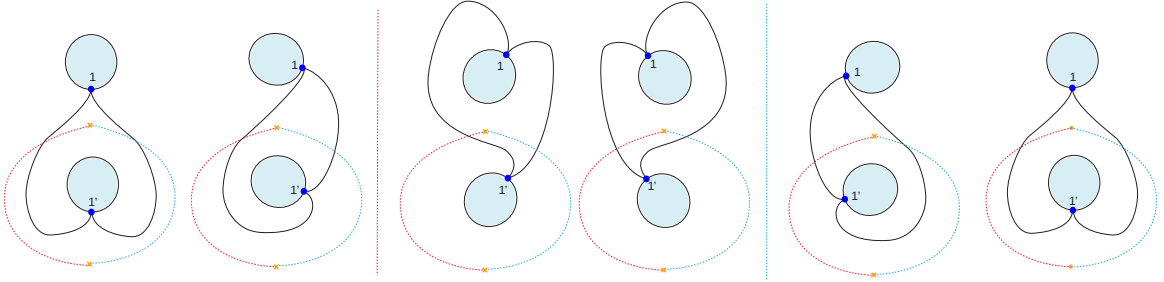


**Figure 58:** The evolution of  $T_{\text{WKB}}(\vartheta, u)$  for the  $SU(2)$  theory with  $N_f = 0$ , for  $u$  in the strong coupling region around  $u = 0$ . For clarity  $z = 0$  and  $z = \infty$  have been mapped to finite distance. There are two flips, corresponding to two BPS states  $\gamma_1, \gamma_2$  with  $\langle \gamma_1, \gamma_2 \rangle = 2$ . One finite WKB curve is the dotted red and the other is the dotted blue curve. The red (blue) dotted vertical line indicates the flips due to the existence of the red (blue) BPS state.

hypermultiplets with charges of the form  $(n+1)\gamma_1 + n\gamma_2$ , at BPS rays which accumulate at the phase of  $Z_{\gamma_1+\gamma_2}$ . At the critical phase for the vectormultiplet  $T_{\text{WKB}}$  transforms by a juggle. This is followed by another infinite sequence of flips, corresponding to a spectrum of BPS hypermultiplets, with charges of the form  $n\gamma_1 + (n+1)\gamma_2$ . So altogether we encounter the standard weak coupling BPS spectrum of the theory: a W-boson of electric charge  $\gamma_1 + \gamma_2$  and an infinite tower of dyons.

Comparing the spectrum on the two sides of the wall, we encounter the important

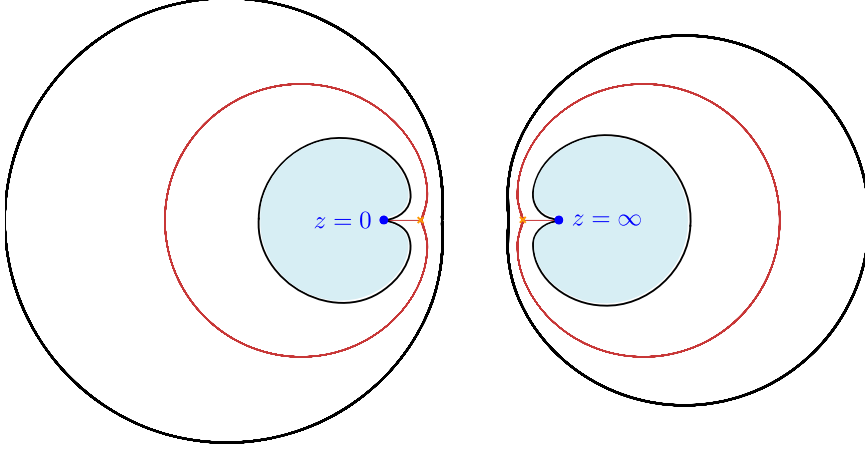


**Figure 59:** The limit WKB triangulation for the  $SU(2)$  theory with  $N_f = 0$ . For clarity  $z = \infty$  has been mapped to finite distance, and a few extra closed WKB curves are shown.

wall-crossing formula for charges with  $\langle \gamma_1, \gamma_2 \rangle = 2$ :

$$\mathcal{K}_{\gamma_1} \mathcal{K}_{\gamma_2} = \mathcal{K}_{\gamma_2} \mathcal{K}_{\gamma_1+2\gamma_2} \mathcal{K}_{2\gamma_1+3\gamma_2} \cdots \mathcal{K}_{\gamma_1+\gamma_2}^{-2} \cdots \mathcal{K}_{3\gamma_1+2\gamma_2} \mathcal{K}_{2\gamma_1+\gamma_2} \mathcal{K}_{\gamma_1}. \quad (10.2)$$

More precisely, this is the wall-crossing formula relevant for one of the two sections of the wall. For the other section, the relevant formula is

$$\mathcal{K}_{\gamma_2} \mathcal{K}_{-\gamma_1} = \mathcal{K}_{-\gamma_1} \mathcal{K}_{-2\gamma_1+\gamma_2} \mathcal{K}_{-3\gamma_1+2\gamma_2} \cdots \mathcal{K}_{-\gamma_1+\gamma_2}^{-2} \cdots \mathcal{K}_{-2\gamma_1+3\gamma_2} \mathcal{K}_{-\gamma_1+2\gamma_2} \mathcal{K}_{\gamma_2} \quad (10.3)$$

Again, the two spectra appearing on the right side are compatible with one another, once we take account of the expected monodromy around the singularities:

$$M_1 = (\gamma_1, \gamma_2) \rightarrow (\gamma_1, \gamma_2 - 2\gamma_1), \quad (10.4)$$

$$M_2 = (\gamma_1, \gamma_2) \rightarrow (\gamma_1 + 2\gamma_2, \gamma_2). \quad (10.5)$$

## 10.2 $N_f = 1$

If we add a single flavor to the  $SU(2)$  gauge theory, the quadratic differential is modified to

$$\lambda^2 = \left( \frac{\Lambda^2}{z^3} + \frac{3u}{z^2} + \frac{2\Lambda m}{z} + \Lambda^2 \right) (dz)^2. \quad (10.6)$$

Again, this may be easily derived using the methods of Section 3. The expansion around  $z = \infty$  now shows an irregular singularity with two WKB rays. The mass parameter  $m$  coincides with the residue at this singularity:

$$\lambda \sim \left( \Lambda + \frac{m}{z} + \cdots \right) dz. \quad (10.7)$$

There are three turning points. If we set  $m = 0$ , there are three singularities in  $\mathcal{B}$ , at  $u^3 = \frac{1}{4}\Lambda^6$ . At each singularity, a single BPS state becomes massless. In a “strong coupling” region around  $u = 0$ , meeting these three singularities, the BPS spectrum consists exactly of these three BPS states. They are realized as strings joining consecutive pairs of turning

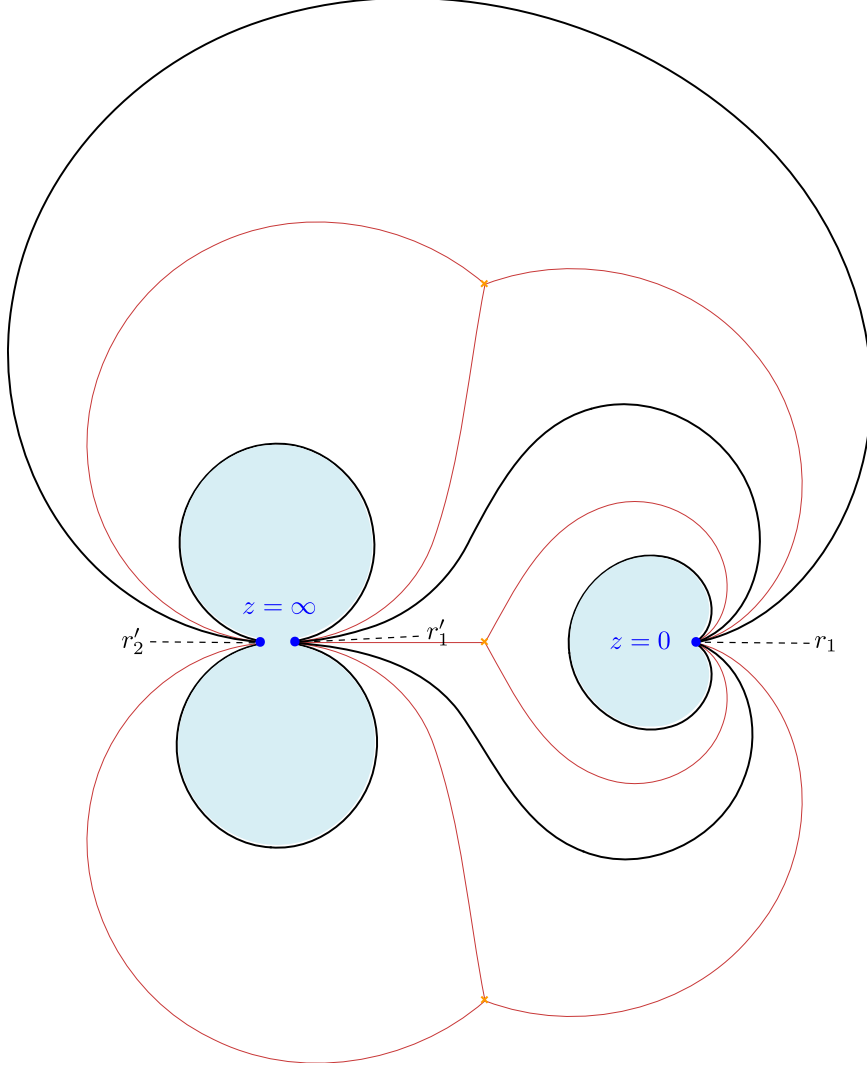


**Figure 60:**  $T_{\text{WKB}}$  for the  $SU(2)$  theory with  $N_f = 1$ . For clarity  $z = 0$  and  $z = \infty$  have been mapped to finite distance.

points clockwise around  $z = 0$ . Their charges  $\gamma_{1,2,3}$  are a basis of the charge lattice  $\hat{\Gamma}$ , satisfying  $\langle \gamma_1, \gamma_2 \rangle = \langle \gamma_2, \gamma_3 \rangle = \langle \gamma_3, \gamma_1 \rangle = 1$ . Furthermore,  $\sum \gamma_i$  can be wrapped around  $z = 0$ , and thus corresponds to a pure flavor charge.

At  $m = 0$ ,  $Z_{-\gamma_3} = Z_{\gamma_1 + \gamma_2}$ , and there is a single wall of marginal stability, where the central charges of the three BPS states align. This wall passes through the three singularities.

We now reverse the logic that we have been using in examining these examples. Thus far, we have been deducing the BPS spectra from the  $\vartheta$ -dependence of  $T_{\text{WKB}}$ , and then writing down the identities between products of symplectomorphisms which arise when we cross a wall. We will now instead use these identities to determine what the BPS spectra must be.

Consider for instance a section of the wall where  $Z_{\gamma_1}$ ,  $Z_{\gamma_2}$ ,  $Z_{-\gamma_3}$  are aligned. In the

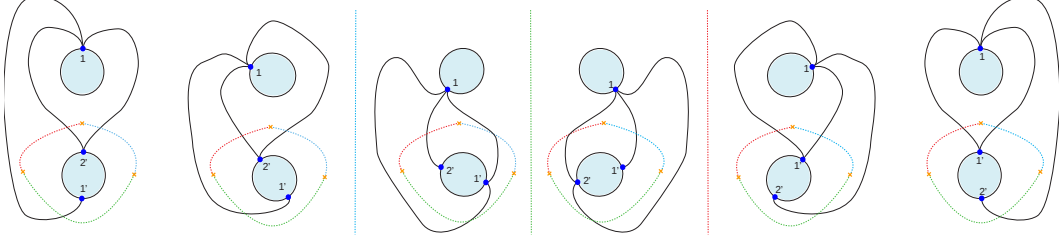


**Figure 61:** The evolution of  $T_{\text{WKB}}(\vartheta, u)$  with  $\vartheta$ , in the  $SU(2)$  theory with  $N_f = 1$ , for  $u$  in the strong coupling region around  $u = 0$ . For clarity  $z = \infty$  has been mapped to finite distance. There are three flips, corresponding to the three BPS states with charges  $\gamma_1, \gamma_2, -\gamma_3$ .

strong coupling region, the triangulation undergoes three flips as  $\vartheta$  crosses the corresponding phases, which combine to give the symplectomorphism  $\mathcal{K}_{\gamma_1} \mathcal{K}_{-\gamma_3} \mathcal{K}_{\gamma_2}$ . On the other side, the same symplectomorphism has to be decomposed into factors for which the phases are ordered in the opposite direction.

To find such a decomposition we can play around with the identities we already know. There is no problem bringing  $\mathcal{K}_{\gamma_1}$  to the right, by two applications of the pentagon identity

$$\mathcal{K}_{\gamma_1} \mathcal{K}_{-\gamma_3} \mathcal{K}_{\gamma_2} = \mathcal{K}_{-\gamma_3} \mathcal{K}_{\gamma_1 - \gamma_3} \mathcal{K}_{\gamma_2} \mathcal{K}_{\gamma_1 + \gamma_2} \mathcal{K}_{\gamma_1}. \quad (10.8)$$

However, the factors are still not properly ordered: we need to bring  $\mathcal{K}_{\gamma_2}$  to the left, across  $\mathcal{K}_{-\gamma_3} \mathcal{K}_{\gamma_1 - \gamma_3}$ . We have  $\langle \gamma_1 - \gamma_3, \gamma_2 \rangle = 2$ , so we need to use the identity (10.2) we encountered in the  $N_f = 0$  theory (with a change of basis), giving

$$\begin{aligned} & \mathcal{K}_{-\gamma_3} \mathcal{K}_{\gamma_1 - \gamma_3} \mathcal{K}_{\gamma_2} \mathcal{K}_{\gamma_1 + \gamma_2} \mathcal{K}_{\gamma_1} = \\ & \mathcal{K}_{-\gamma_3} \mathcal{K}_{\gamma_2} \mathcal{K}_{2\gamma_2 + \gamma_1 - \gamma_3} \mathcal{K}_{3\gamma_2 + 2\gamma_1 - 2\gamma_3} \cdots \mathcal{K}_{\gamma_1 - \gamma_3 + \gamma_2}^{-2} \cdots \mathcal{K}_{2\gamma_2 + 3\gamma_1 - 3\gamma_3} \mathcal{K}_{\gamma_2 + 2\gamma_1 - 2\gamma_3} \mathcal{K}_{\gamma_1 - \gamma_3} \mathcal{K}_{\gamma_1 + \gamma_2} \mathcal{K}_{\gamma_1}. \end{aligned} \quad (10.9)$$

We are almost done. The factors  $\mathcal{K}_{-\gamma_3}$  and  $\mathcal{K}_{\gamma_1 + \gamma_2}$  are associated to charges with  $Z_{-\gamma_3} = Z_{\gamma_1 + \gamma_2}$ , so in the properly reordered product they should be adjacent to the vectormultiplet of charge  $\gamma_1 - \gamma_3 + \gamma_2$ . To get them there we need to carry each through an infinite set of other factors; at each step we use the pentagon identity, and obtain the final result

$$\begin{aligned} & \mathcal{K}_{\gamma_1} \mathcal{K}_{-\gamma_3} \mathcal{K}_{\gamma_2} = \\ & \mathcal{K}_{\gamma_2} \mathcal{K}_{\gamma_2 - \gamma_3} \mathcal{K}_{2\gamma_2 + \gamma_1 - \gamma_3} \mathcal{K}_{2\gamma_2 + \gamma_1 - 2\gamma_3} \mathcal{K}_{3\gamma_2 + 2\gamma_1 - 2\gamma_3} \mathcal{K}_{3\gamma_2 + 2\gamma_1 - 3\gamma_3} \cdots \mathcal{K}_{-\gamma_3} \mathcal{K}_{\gamma_1 - \gamma_3 + \gamma_2}^{-2} \mathcal{K}_{\gamma_1 + \gamma_2} \cdots \\ & \cdots \mathcal{K}_{2\gamma_2 + 3\gamma_1 - 3\gamma_3} \mathcal{K}_{2\gamma_2 + 3\gamma_1 - 2\gamma_3} \mathcal{K}_{2\gamma_2 + 3\gamma_1 - 2\gamma_3} \mathcal{K}_{\gamma_2 + 2\gamma_1 - 2\gamma_3} \mathcal{K}_{2\gamma_1 + \gamma_2 - \gamma_3} \mathcal{K}_{\gamma_1 - \gamma_3} \mathcal{K}_{\gamma_1}. \end{aligned} \quad (10.10)$$

This indeed corresponds to the BPS spectrum in the weak coupling region outside the wall. Notice that the two “electric” hypermultiplets of charges  $-\gamma_3$  and  $\gamma_1 + \gamma_2$  are the basic matter particles in the Lagrangian of the  $SU(2)$  theory with  $N_f = 1$ , and they have the same gauge charge, half that of the W boson.

As we vary  $\vartheta$  in the weak coupling region,  $T_{\text{WKB}}$  undergoes an infinite sequence of flips and then a transformation similar to the “juggle” we described in Section 6.6.3 and encountered in the  $N_f = 0$  theory. However, it is not quite the same; in particular, in

the limiting triangulation one of the boundaries of the annulus has *two* vertices on it (coming from the two WKB rays entering the singularity at  $z = 0$ ). See Figure 62. This is a non-generic situation, which occurs here because we chose the special value  $m = 0$ . It is related to the fact that the coordinate transformation across the critical  $\vartheta$  must be  $\mathcal{K}_{-\gamma_3} \mathcal{K}_{\gamma_1-\gamma_3+\gamma_2}^{-2} \mathcal{K}_{\gamma_1+\gamma_2}$  corresponding to a vectormultiplet and two hypermultiplets, in contrast to the usual situation where we have only the vectormultiplet at the critical  $\vartheta$ .

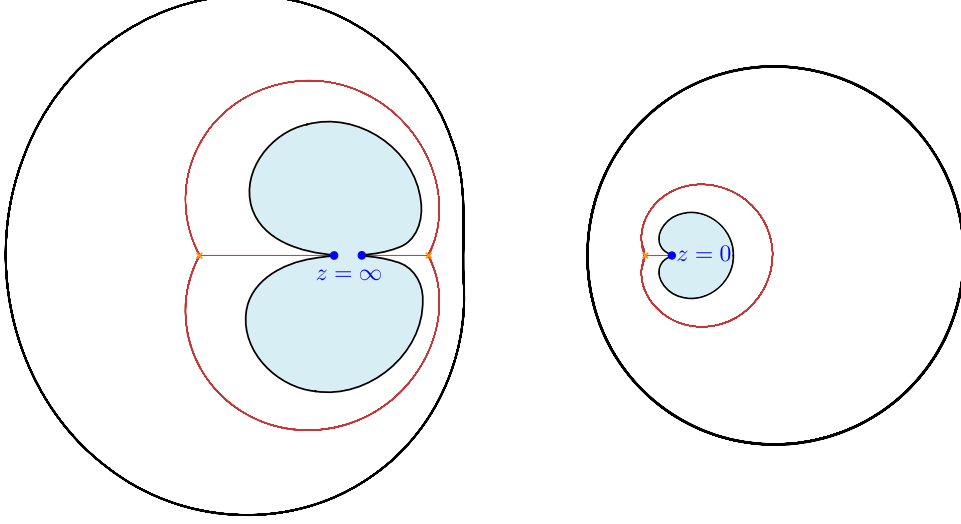


**Figure 62:** The limit  $T_{\text{WKB}}$  for the  $SU(2)$  theory with  $N_f = 1$  and  $m = 0$ . For clarity  $z = 0$  and  $z = \infty$  have been mapped to finite distance, and an extra closed WKB curve is shown.

As soon as we perturb  $m$  slightly away from zero, we reach a more conventional setup. As we move from the strong coupling region towards large  $u$ , the sequence of elementary operations we described, or some close analog, happens at a sequence of walls of marginal stability. At large but finite  $u$ , the central charges of the hypermultiplets associated with  $\mathcal{K}_{-\gamma_3}$  and  $\mathcal{K}_{\gamma_1+\gamma_2}$  are not exactly aligned with the central charge associated to  $\mathcal{K}_{\gamma_1-\gamma_3+\gamma_2}^{-2}$ . Hence in rearranging the product the two factors  $\mathcal{K}_{-\gamma_3}$  and  $\mathcal{K}_{\gamma_1+\gamma_2}$  should only be moved a finite number of steps. The “core” of the infinite product around  $\mathcal{K}_{\gamma_1-\gamma_3+\gamma_2}^{-2}$  then corresponds to the standard sequence of flips and juggles as in Section 6.6.3. The limit WKB triangulation is shown in Figure 63; now both boundaries of the annulus have only one vertex.

It is amusing to bring  $m$  close to the value  $\frac{3}{2}\Lambda$ , where two singularities in  $\mathcal{B}$  coalesce. We expect to see the  $N = 3$  theory from Section 9.4.4 emerge in a scaling region near the two singularities. Indeed, it is instructive to look at the shape of the WKB foliation (see Figure 64) in the scaling region, and see the pentagon appear near the region where the three turning points are converging.

### 10.3 $N_f = 2$ , first realization

Using the brane setup of Section 3, there are two ways to add a second flavor to the  $SU(2)$  gauge theory. Correspondingly, there are two distinct Hitchin systems, for which the metric on  $\mathcal{M}$  is expected to be the same. In this subsection we deal with the symmetric possibility,

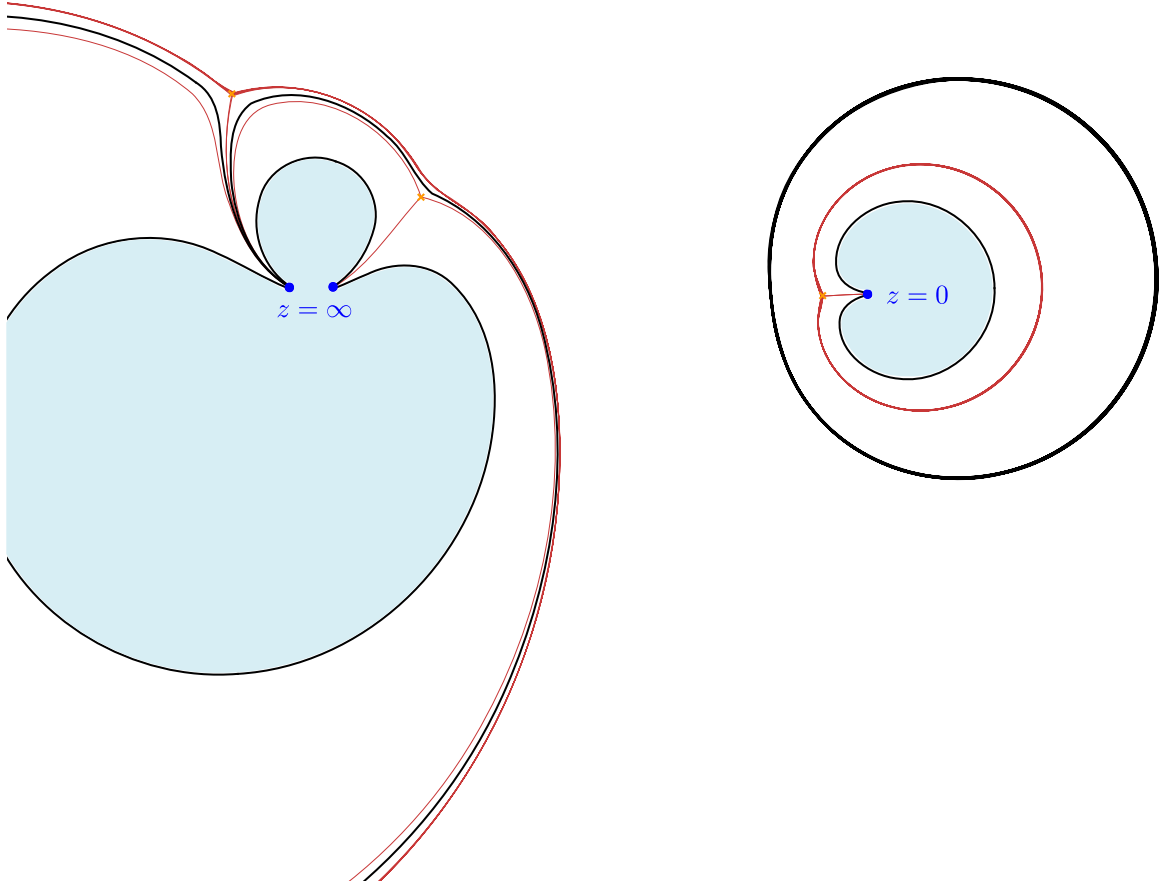


**Figure 63:** The limit  $T_{\text{WKB}}$  for the  $SU(2)$  theory with  $N_f = 1$  and  $m \neq 0$ . For clarity  $z = 0$  and  $z = \infty$  have been mapped to finite distance, and an extra closed WKB curve is shown.

where the quadratic differential is

$$\lambda^2 = \left( \frac{\Lambda^2}{z^4} + \frac{2\Lambda m_1}{z^3} + \frac{4u}{z^2} + \frac{2\Lambda m_2}{z} + \Lambda^2 \right) dz^2 \quad (10.11)$$

The expansion around either  $z = 0$  or  $z = \infty$  then shows an irregular singularity with two WKB rays. The two mass parameters  $m_{1,2}$  are the residues of the two poles.

There are four turning points, and four singularities in  $\mathcal{B}$ . The reader will probably guess that, once again, there will be a strong coupling region in  $\mathcal{B}$  where the BPS spectrum consists only of the four BPS particles which are massless at the four singularities.

If we set  $m_{1,2} = 0$ , a surprising simplification occurs. The Seiberg-Witten differential for the  $N_f = 2$  theory, and in fact the whole Hitchin system, can be mapped to those of the  $N_f = 0$  theory, by the simple coordinate transformation  $z^2 \rightarrow \hat{z}$ . This allows us to borrow much of the discussion from the  $N_f = 0$  case. Each turning point of the  $N_f = 0$  theory maps to two turning points of the  $N_f = 2$  theory. Each BPS hypermultiplet of the  $N_f = 0$  theory maps to a pair of BPS hypermultiplets in the  $N_f = 2$  theory. See Figure 65. This pair of hypermultiplets have the same gauge charges, but their flavor charges differ: the difference of the two corresponding paths can be deformed to a sum of paths around 0

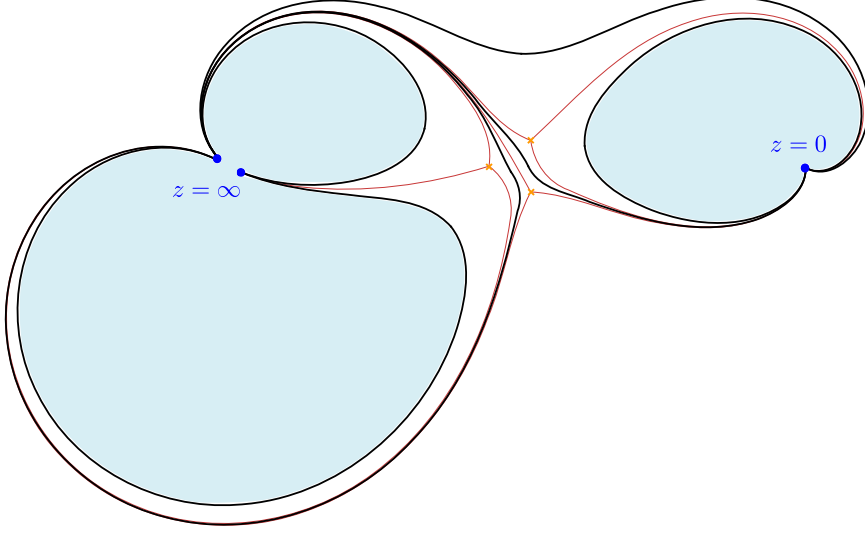


**Figure 64:** The WKB triangulation for the  $SU(2)$  theory with  $N_f = 1$ , with  $m$  adjusted near the scaling limit in which the  $N = 3$  theory from Section 9.4.4 emerges.

and infinity. We call the charges of one pair  $\gamma_1^{1,2}$ , and the other pair  $\gamma_2^{1,2}$ , with  $\langle \gamma_1^i, \gamma_2^j \rangle = 1$ . In addition  $\langle \gamma_1^i, \gamma_1^j \rangle = \langle \gamma_2^i, \gamma_2^j \rangle = 0$ . If we turn on masses then  $Z_{\gamma_1^1 - \gamma_1^2} = m_1 + m_2$ , while  $Z_{\gamma_2^1 - \gamma_2^2} = m_1 - m_2$ .

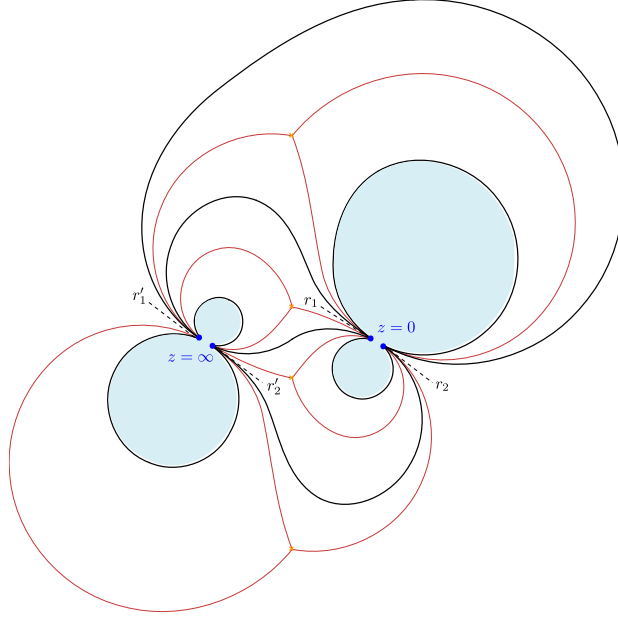


**Figure 65:** A typical WKB triangulation for the first realization of the  $SU(2)$  theory with  $N_f = 2$ ,  $m_1 = m_2 = 0$ . For clarity  $z = 0$  and  $z = \infty$  have been mapped to finite distance.

Following this reasoning we can guess the shape of the relevant wall-crossing formula — it should be a kind of doubling of the formula (10.2) for  $N_f = 0$ , of the form

$$\mathcal{K}_{\gamma_1^1} \mathcal{K}_{\gamma_1^2} \mathcal{K}_{\gamma_2^1} \mathcal{K}_{\gamma_2^2} = \mathcal{K}_{\gamma_2} \mathcal{K}_{\gamma_2} \mathcal{K}_{\gamma_1 + 2\gamma_2} \mathcal{K}_{\gamma_1 + 2\gamma_2} \cdots ??? \cdots \mathcal{K}_{2\gamma_1 + \gamma_2} \mathcal{K}_{2\gamma_1 + \gamma_2} \mathcal{K}_{\gamma_1} \mathcal{K}_{\gamma_1}. \quad (10.12)$$

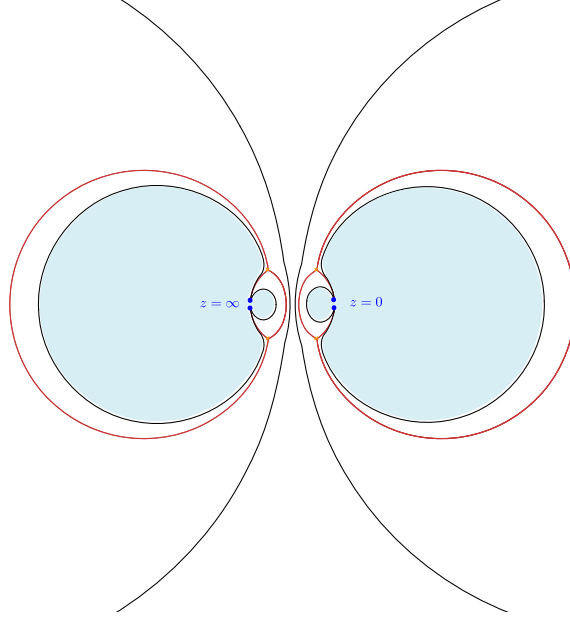


**Figure 66:** The limit WKB triangulation  $T_{\text{WKB}}(\vartheta_c)$  where a vectormultiplet appears, in the first realization of the  $SU(2)$  theory with  $N_f = 2$ ,  $m_1 = m_2 = 0$ . For clarity  $z = \infty$  has been mapped to finite distance, and we show two closed WKB curves among the 1-parameter family representing the vectormultiplet.

On the right side it is not obvious *a priori* which of the cycles  $\gamma_{1,2}^i$  each  $\gamma_{1,2}$  represents, though it may be determined from inspection of the flips in the WKB triangulation. Also, it is not obvious what should replace the juggle transformation, as we have two vertices on each of the circles surrounding the annular region — see Figure 66. We can of course simply play around with the wall-crossing formulae we already know to fully determine the right hand side. We begin by bringing  $\mathcal{K}_{\gamma_2^2}$  to the right, obtaining

$$\mathcal{K}_{\gamma_1^1} \mathcal{K}_{\gamma_1^2} \mathcal{K}_{\gamma_2^1} \mathcal{K}_{\gamma_2^2} = \mathcal{K}_{\gamma_1^1} \mathcal{K}_{\gamma_2^1} \mathcal{K}_{\gamma_2^1 + \gamma_1^2} \mathcal{K}_{\gamma_2^2} \mathcal{K}_{\gamma_2^2 + \gamma_1^2} \mathcal{K}_{\gamma_1^2}, \quad (10.13)$$

and then do the same for  $\mathcal{K}_{\gamma_1^2}$ , giving

$$\begin{aligned} \mathcal{K}_{\gamma_1^1} \mathcal{K}_{\gamma_2^1} \mathcal{K}_{\gamma_2^1 + \gamma_1^2} \mathcal{K}_{\gamma_2^2} \mathcal{K}_{\gamma_2^2 + \gamma_1^2} \mathcal{K}_{\gamma_1^2} = \\ \mathcal{K}_{\gamma_2^2} \mathcal{K}_{\gamma_2^2 + \gamma_1^1} \mathcal{K}_{\gamma_2^1 + \gamma_1^2} \mathcal{K}_{\gamma_2^1 + \gamma_1^2 + \gamma_1^1} \mathcal{K}_{\gamma_2^2} \mathcal{K}_{\gamma_2^2 + \gamma_1^1} \mathcal{K}_{\gamma_2^2 + \gamma_1^2} \mathcal{K}_{\gamma_2^2 + \gamma_1^2 + \gamma_1^1} \mathcal{K}_{\gamma_2^1} \mathcal{K}_{\gamma_1^1}. \end{aligned} \quad (10.14)$$

We still need to bring  $\mathcal{K}_{\gamma_2^2}$  to the left, but it will cross  $\mathcal{K}_{\gamma_2^1 + \gamma_1^2 + \gamma_1^1}$ , leading to an infinite product like those we encountered in the  $N_f = 0$  example:

$$\begin{aligned} \mathcal{K}_{\gamma_2^1} \mathcal{K}_{\gamma_2^1 + \gamma_1^1} \mathcal{K}_{\gamma_2^1 + \gamma_1^2} \mathcal{K}_{\gamma_2^1 + \gamma_1^2 + \gamma_1^1} \mathcal{K}_{\gamma_2^2} \mathcal{K}_{\gamma_2^2 + \gamma_1^1} \mathcal{K}_{\gamma_2^2 + \gamma_1^2} \mathcal{K}_{\gamma_2^2 + \gamma_1^2 + \gamma_1^1} \mathcal{K}_{\gamma_2^1} \mathcal{K}_{\gamma_1^1} = \\ \mathcal{K}_{\gamma_2^1} \mathcal{K}_{\gamma_2^1 + \gamma_1^1} \mathcal{K}_{\gamma_2^1 + \gamma_1^2} \mathcal{K}_{\gamma_2^2} \mathcal{K}_{\gamma_2^2 + 2\gamma_2^2 + \gamma_1^2 + \gamma_1^1} \cdots \mathcal{K}_{\gamma_2^1 + \gamma_2^2 + \gamma_1^2 + \gamma_1^1}^{-2} \cdots \\ \cdots \mathcal{K}_{2\gamma_2^1 + \gamma_2^2 + 2\gamma_1^2 + 2\gamma_1^1} \mathcal{K}_{\gamma_2^1 + \gamma_1^2 + \gamma_1^1} \mathcal{K}_{\gamma_2^2 + \gamma_1^1} \mathcal{K}_{\gamma_2^2 + \gamma_1^2} \mathcal{K}_{\gamma_2^2 + \gamma_1^2 + \gamma_1^1} \mathcal{K}_{\gamma_2^1} \mathcal{K}_{\gamma_1^1}. \end{aligned} \quad (10.15)$$

The factors  $\mathcal{K}_{\gamma_2^1 + \gamma_1^1} \mathcal{K}_{\gamma_2^1 + \gamma_1^2}$  and  $\mathcal{K}_{\gamma_2^2 + \gamma_1^1} \mathcal{K}_{\gamma_2^2 + \gamma_1^2}$  correspond to states with the same phase as the vector multiplet  $\mathcal{K}_{\gamma_2^1 + \gamma_2^2 + \gamma_1^2 + \gamma_1^1}^{-2}$ . Hence they need to be brought across the infinite



product, through a sequence of pentagon identities, giving the final result

$$\begin{aligned}
\mathcal{K}_{\gamma_1^1} \mathcal{K}_{\gamma_1^2} \mathcal{K}_{\gamma_2^1} \mathcal{K}_{\gamma_2^2} = & \\
& \mathcal{K}_{\gamma_2^1} \mathcal{K}_{\gamma_2^2} \mathcal{K}_{\gamma_1^1+\gamma_2^2+\gamma_2^1} \mathcal{K}_{\gamma_1^2+\gamma_2^2+\gamma_2^1} \mathcal{K}_{\gamma_1^2+\gamma_1^1+\gamma_2^2+2\gamma_2^1} \mathcal{K}_{\gamma_1^2+\gamma_1^1+\gamma_2^1+2\gamma_2^2} \cdots \\
& \cdots \mathcal{K}_{\gamma_2^1+\gamma_1^1} \mathcal{K}_{\gamma_2^1+\gamma_1^2} \mathcal{K}_{\gamma_2^1+\gamma_2^2+\gamma_1^1+\gamma_1^2}^{-2} \mathcal{K}_{\gamma_2^2+\gamma_1^1} \mathcal{K}_{\gamma_2^2+\gamma_1^2} \cdots \\
& \cdots \mathcal{K}_{\gamma_1^2+2\gamma_1^1+\gamma_2^2+\gamma_2^1} \mathcal{K}_{2\gamma_1^2+\gamma_1^1+\gamma_2^2+\gamma_2^1} \mathcal{K}_{\gamma_1^2+\gamma_1^1+\gamma_2^1} \mathcal{K}_{\gamma_1^2+\gamma_1^1+\gamma_2^2} \mathcal{K}_{\gamma_1^2} \mathcal{K}_{\gamma_1^1}. \quad (10.16)
\end{aligned}$$

As in the  $N_f = 1$  example, if we turn on  $m_{1,2} \neq 0$ , the single wall will fragment into several walls. By playing around with these parameters one can produce some entertaining results. For example, if we set  $m_1 = m_2 = 2\Lambda$ , we get a neat example,

$$\lambda^2 = \left( \frac{\Lambda^2(z+1)^4}{z^4} + \frac{16\tilde{u}}{z^2} \right) dz^2, \quad (10.17)$$

where three out of four singular points in  $\mathcal{B}$  coalesce at  $\tilde{u} = 0$ , and we can recover the  $N = 4$  Argyres-Douglas scaling limit. One of the four particles in the strong coupling region becomes very massive, and the other three coincide with the basic spectrum of the  $N = 4$  Argyres-Douglas theory.

#### 10.4 Intermission: non-abelian flavor symmetries and WKB triangulations

We noticed in Section 3.2.9 how the WKB flow lines behave when the mass parameter at a regular singularity  $\mathcal{P}$  goes to zero, and a non-abelian  $SU(2)$  flavor symmetry is restored. It is useful to consider the behavior of the whole WKB foliation in that limit. As  $m \rightarrow 0$ , a turning point  $\mathcal{T}$  moves toward  $\mathcal{P}$ . At generic  $\vartheta$ , one of the three separating WKB emerging from  $\mathcal{T}$  flows toward  $\mathcal{P}$ . The other two wrap around  $\mathcal{P}$  in opposite directions, and then flow away while remaining very close to each other, ending up at some other singularity. ( $T_{\text{WKB}}$  is thus degenerate, with a single edge coming out of  $\mathcal{P}$ .) As we vary  $\vartheta$ , we will occasionally meet pairs of BPS states with very close phases, when these two separatrices become finite WKB curves landing on another turning point  $\mathcal{T}'$ . The charges of these BPS states differ by (twice) a cycle wrapping around the singularity. In other words, these finite WKB curves represent a doublet of BPS particles with charges  $\gamma \pm \gamma_+$ , where  $\gamma_+$  is the flavor charge associated to the singularity  $\mathcal{P}$ .

For  $\vartheta$  in the narrow window between the phases of  $Z_{\gamma \pm \gamma_+}$ , these two separatrices pass on opposite sides of the turning point  $\mathcal{T}'$ , and go to different singularities. The corresponding transformations of the WKB triangulation are straightforward. The first BPS state induces a flip of the non-degenerate edge of the degenerate triangle associated to  $\mathcal{P}$ . Then two edges end on  $\mathcal{P}$ . The second BPS state induces a flip of the old edge ending on  $\mathcal{P}$ , so we get again a degenerate triangle.

#### 10.5 $N_f = 2$ , second realization

Next we consider with the asymmetric realization of the  $N_f = 2$  theory, where the irregular singularity at infinity is the same as the one in the  $N_f = 0$  theory, but the irregular

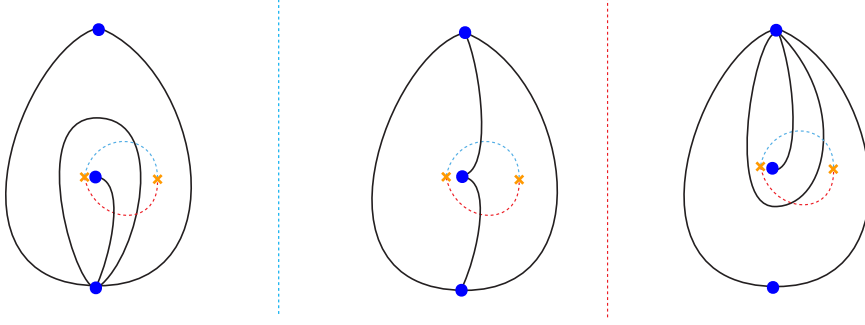


**Figure 67:** The two flips in  $T_{\text{WKB}}$  associated to a  $SU(2)$  flavor doublet of BPS hypermultiplets, for small  $SU(2)$  breaking mass.

singularity at  $z = 0$  is replaced by two regular singularities:

$$\lambda^2 = \frac{P_3(z)}{z^2(z-1)^2} = \left( \frac{m_+^2}{z^2} + \frac{m_-^2}{(z-1)^2} + \frac{\Lambda^2 + u}{2z} + \frac{\Lambda^2 - u}{2(z-1)} \right) dz^2 \quad (10.18)$$

Here the parameters  $u, \Lambda$  do not necessarily coincide with the ones in the previous subsection. The expansion around  $z = \infty$  shows an irregular singularity with a single WKB ray. There are three turning points. There are four singular points in  $\mathcal{B}$ .

For very small masses  $m_{\pm}$ , the typical  $T_{\text{WKB}}$  here has two degenerate triangles attached to the singularity at  $z = \infty$ . The strong-coupling spectrum just includes two pairs of BPS states, one for each singularity, as shown in Figure 68. Comparison with the previous

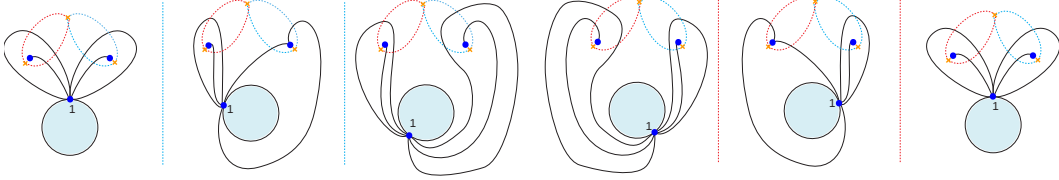


**Figure 68:** The evolution of the WKB triangulation for the second realization of the  $N_f = 2$  theory, in the strong coupling region around  $u = 0$ , for small  $m_{\pm}$ . For clarity  $z = \infty$  has been mapped to finite distance. There are two pairs of flips, corresponding to two BPS states with charges  $\gamma_1^i, \gamma_2^i$ , with  $\langle \gamma_1^i, \gamma_2^j \rangle = 1$ . Notice that the two middle pictures differ by a pop, which does not correspond to a BPS state.

section (or the analysis of Section 3) shows that  $m_{\pm} = m_1 \pm m_2$ . The weak-coupling spectrum manifests itself as a sequence of pairs of BPS states associated to either the singularity at  $z = 0$  or at  $z = 1$  (as described in the last section), which produces tightly wound degenerate triangles. For general  $m_{\pm}$ , less degenerate triangulations may occur, as in Figure 69.

It is not at all obvious that the two hyperkähler metrics corresponding to the two realizations of the  $N_f = 2$  theory are the same. Indeed, this is an example of the surprising isomorphism of Section 3.2.8. A proof that the two Hitchin systems for  $N_f = 2$  have the same hyperkähler metric goes as follows: the two systems have the same spectral curves (although they are embedded differently in  $T^*\mathbb{CP}^1$ ) and the same central charge functions.

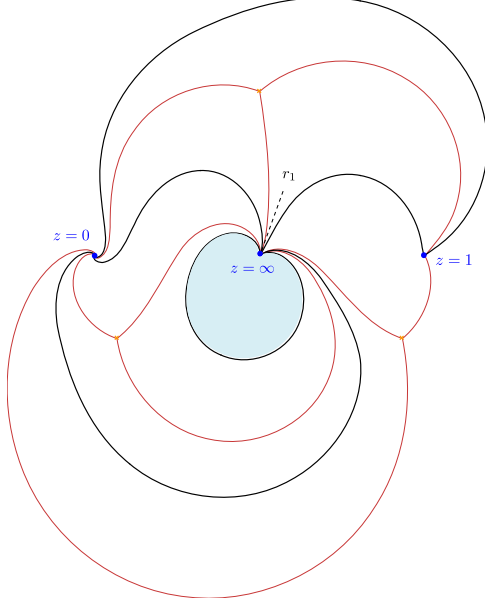


**Figure 69:** A typical WKB triangulation for the  $SU(2)$  theory with  $N_f = 2$ , second realization, with generic masses. For clarity  $z = \infty$  has been mapped to finite distance.

Now suppose we show (say, by explicit examination of  $T_{\text{WKB}}$ ) that the spectra of BPS states in the two systems coincide at some strong coupling point. Then the wall-crossing formula ensures that the spectra agree everywhere on  $\mathcal{B}$ , and moreover the functions  $\mathcal{X}_\gamma^\vartheta$  must also agree, as they are solutions of the same Riemann-Hilbert problem, with the same asymptotics. Hence the twistor spaces and the hyperkähler metrics for the two Hitchin systems must coincide.

### 10.6 $N_f = 3$

The  $SU(2)$  gauge theory with  $N_f = 3$  is associated to a  $SU(2)$  Hitchin system which is rather similar to the second realization of the  $N_f = 2$  theory. The quadratic differential is

$$\lambda^2 = \frac{P_4(z)}{z^2(z-1)^2} = \left( \frac{m_+^2}{z^2} + \frac{m_-^2}{(z-1)^2} + \frac{2\Lambda m + u}{2z} + \frac{2\Lambda m - u}{2(z-1)} + \Lambda^2 \right) dz^2 \quad (10.19)$$

The expansion around  $z = \infty$  shows an irregular singularity with two WKB rays. See Figure 70.

There are four turning points in the  $z$ -plane, and five singularities in  $\mathcal{B}$ . The three mass parameters  $m$ ,  $m_\pm$  appear on a different footing. (To treat them symmetrically we would have to realize the theory in terms of an  $SU(3)$  Hitchin system, which goes beyond the scope of this paper.)

For very small  $m$  and  $m_\pm$ , four of the singularities in  $\mathcal{B}$  come together near  $u = 0$ . The BPS particles which become massless at these four singularities have the same gauge charges, but different flavor charges. See Figure 71. We know that for small enough  $m_\pm$  a turning point will be close to each of the regular singularities, and BPS states will typically appear in doublets of the corresponding  $SU(2)_\pm$  subgroups of the  $SU(4)$  flavor

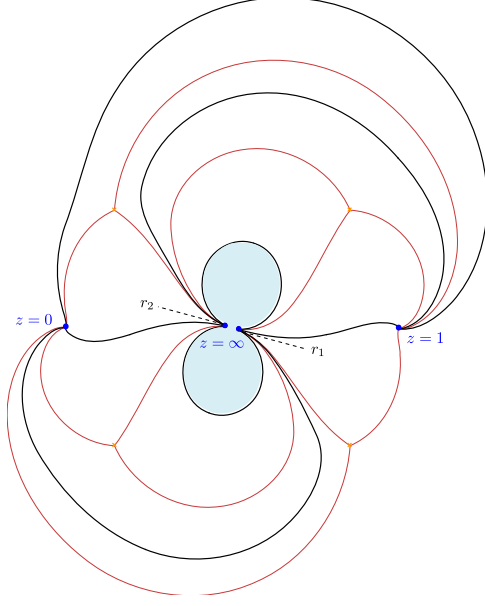


**Figure 70:** A typical WKB triangulation for the  $SU(2)$  theory with  $N_f = 3$ . For clarity  $z = \infty$  has been mapped to finite distance.

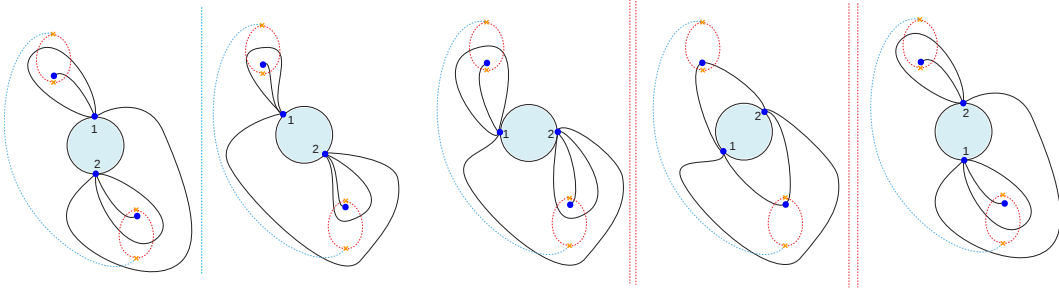


**Figure 71:** The evolution of  $T_{\text{WKB}}(\vartheta)$  in the  $N_f = 3$  theory, in the strong coupling region of  $\mathcal{B}$  around  $u = 0$ , for small  $m$  and  $m_{\pm}$ . For clarity  $z = \infty$  has been mapped to finite distance. As  $\vartheta$  varies there are five flips, corresponding to BPS states with charges  $\gamma_1^i, \gamma_2$  with  $\langle \gamma_1^i, \gamma_2 \rangle = 1$ . The second and third pictures differ by a pop, which does not correspond to a BPS state.

symmetry.  $m$  is the mass parameter for a remaining  $U(1) \in SU(4)$ . The four particles actually sit in a  $\mathbf{4}$  of  $SU(4)$  [84]. Indeed the  $\mathbf{4}$  decomposes as  $(\mathbf{2}, \mathbf{1})_{+1} \oplus (\mathbf{1}, \mathbf{2})_{-1}$  under  $SU(2) \times SU(2) \times U(1)$ . We see from Figure 71 that the two doublets indeed have charges which differ by the flavor charge at infinity.

There is a second singularity at  $u \sim \frac{\Lambda^2}{4}$ , where two turning points coalesce. All in all, there is a strong coupling region containing the interval  $0 < u < \frac{\Lambda^2}{4}$ , with a simple BPS spectrum: the quadruplet of particles of charge  $\gamma_1^i$  (all with the same gauge charge) and a single  $\gamma_2$  with  $\langle \gamma_1^i, \gamma_2 \rangle = 1$ . In addition  $\langle \gamma_1^i, \gamma_1^j \rangle = 0$  for all  $i, j$ . The wall-crossing formula then predicts the correct known spectrum in the weak coupling region, as we can see by a simple but tedious sequence of the identities we have used before. To write the final result

let  $\tilde{\gamma} = 2\gamma_2 + \gamma_1^1 + \gamma_1^2 + \gamma_1^3 + \gamma_1^4$ . Then:

$$\begin{aligned} \left( \prod_{i=1}^4 \mathcal{K}_{\gamma_1^i} \right) \mathcal{K}_{\gamma_2} &= \mathcal{K}_{\gamma_2} \left( \prod \mathcal{K}_{\gamma_2 + \gamma_1^i} \right) \mathcal{K}_{\gamma_2 + \tilde{\gamma}} \left( \prod \mathcal{K}_{\tilde{\gamma} - \gamma_1^i} \right) \cdots \\ &\cdots \mathcal{K}_{2\gamma_2 + \gamma_1^1 + \gamma_1^2 + \gamma_1^3 + \gamma_1^4} \left( \prod_{i < j} \mathcal{K}_{\gamma_2 + \gamma_1^i + \gamma_1^j} \right) \cdots \\ &\cdots \left( \prod \mathcal{K}_{\tilde{\gamma} - \gamma_2 - \gamma_1^i} \right) \mathcal{K}_{\tilde{\gamma} - \gamma_2} \left( \prod_{i=1}^4 \mathcal{K}_{\gamma_1^i} \right). \end{aligned} \quad (10.20)$$

### 10.7 $N_f = 4$ : The superconformal case

Finally, we have learned enough to discuss the  $N_f = 4$  theory properly. In this subsection we will only consider the “balanced” realization of the theory, with four regular singular points and four turning points on  $\mathbb{CP}^1$ . The Seiberg-Witten curve looks like

$$\lambda^2 = \frac{P_4(z)}{D_4(z)^2} (dz)^2 = \frac{P_4^0(z) + uD_4(z)}{D_4(z)^2} (dz)^2. \quad (10.21)$$

In the second equality we introduced a basepoint and defined a normalizable  $u$ -parameter. In addition to  $u$ , the theory has four mass parameters, and an exactly marginal gauge coupling. There are 6 singularities in the  $u$  plane  $\mathcal{B}$ .

If all the masses vanish (or if  $u$  is much larger than the masses) the WKB flows can become very intricate. In this regime the WKB flows determined by  $\lambda$  are well approximated by those for

$$\lambda_0 = \frac{dz}{\sqrt{D_4(z)}} = dv, \quad (10.22)$$

where  $v$  is a uniformizing coordinate on the elliptic curve  $y^2 = D_4(z)$ ; so these flows are just straight lines on a torus, of inclination determined by  $\vartheta$ . For any rational slope, we get closed WKB curves. In particular, there is an infinite spectrum of  $W$ -bosons forming an  $SL(2, \mathbb{Z})$  duality orbit.

At the same  $\vartheta$  where the  $W$ -bosons appear, eight hypermultiplets should also appear, in representations  $\mathbf{8}_v$ ,  $\mathbf{8}_s$  or  $\mathbf{8}_c$  of the  $Spin(8)$  flavor symmetry group. We can understand them as follows: since we are considering very small masses, each turning point is very close to one of the four regular singular points. BPS hypermultiplets joining two turning points thus arise in doublets of the two  $SU(2)$  flavor subgroups corresponding to the two endpoints. If we denote the four singular points as  $a, b, c, d$ , and the corresponding subgroups of  $Spin(8)$  as  $SU(2)_a, SU(2)_b, SU(2)_c, SU(2)_d$ , then we have the decompositions

$$\begin{aligned} \mathbf{8}_v &= (\mathbf{2}_a, \mathbf{2}_b, \mathbf{1}_c, \mathbf{1}_d) \oplus (\mathbf{1}_a, \mathbf{1}_b, \mathbf{2}_c, \mathbf{2}_d), \\ \mathbf{8}_s &= (\mathbf{2}_a, \mathbf{1}_b, \mathbf{2}_c, \mathbf{1}_d) \oplus (\mathbf{1}_a, \mathbf{2}_b, \mathbf{1}_c, \mathbf{2}_d), \\ \mathbf{8}_c &= (\mathbf{2}_a, \mathbf{1}_b, \mathbf{1}_c, \mathbf{2}_d) \oplus (\mathbf{1}_a, \mathbf{2}_b, \mathbf{2}_c, \mathbf{1}_d). \end{aligned} \quad (10.23)$$

Each closed WKB curve divides the four singular points into two pairs, either  $(ab, cd)$ ,  $(ac, bd)$ , or  $(ad, bc)$ . The corresponding pair of turning points, say  $(ab, cd)$ , supports the 8 BPS hypermultiplets in, say,  $\mathbf{8}_v$ .

As soon as we turn on finite mass parameters, the spectrum simplifies considerably. Each singularity becomes an attractor, preventing most of the closed WKB curves from appearing. Indeed, it is entertaining to introduce a different auxiliary torus by writing

$$\lambda = \frac{dz}{\sqrt{P_4(z)}} \frac{P_4(z)}{D_4(z)} = dv \frac{P_4(z)}{D_4(z)}, \quad (10.24)$$

where now  $dv = dz/\sqrt{P_4(z)}$  is a uniformizing parameter for the torus  $y^2 = P_4(z)$ . The WKB curves lift to flow lines for the meromorphic differential  $\lambda$  on this torus. Each zero of  $P_4$  becomes a double zero on the torus, and each zero of  $D_4$  lifts to a pair of poles. If the mass parameters are small, the pair of poles will be very close to the double zero. A local picture of the flow shows a localized disturbance, with a well-defined “absorption cross-section” for the flows. We can even compute that cross section. We integrate the local form of  $\lambda$ ,

$$w = \int \lambda \sim \int_{v=0}^v \frac{m(v')^2}{1 - (v')^2} dv' = -mv + \frac{m}{2} \log \frac{1+v}{1-v}. \quad (10.25)$$

Since  $-mv + \frac{m}{2} \log \frac{1+v}{1-v} \sim \frac{m}{3} v^3 + \dots$  there are six flows of  $\text{Im}(e^{-i\vartheta} w) = 0$  emerging from  $v = 0$ . The flows which asymptote to parallel lines have a spacing  $\pi \text{Re}(e^{-i\vartheta} m)$ . See Figure 72.

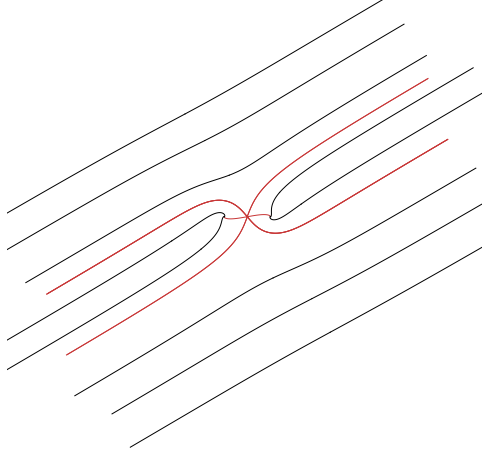


**Figure 72:** The local flow on the torus near a group of zeroes and poles of  $\lambda$ .

However small the mass parameter, the singularity will surely end up attracting any WKB curve which winds too many times around the torus, unless  $\vartheta$  is very close to the phase of the mass parameter. So unless the phases of all mass parameters are aligned, it appears that only a finite number of  $SL(2, \mathbb{Z})$  images of the W-boson will survive at finite  $u$ . Adjusting the mass parameters appropriately, it should even be possible to find a “strong coupling region” where no vectormultiplet BPS states survive. That would clearly be a good point from which to start our analysis.

With that in mind, let's consider the following symmetric choice of parameters:

$$\begin{aligned}\lambda^2 &= \frac{z^4 - u(z^4 - 1)}{(z^4 - 1)^2} = \\ &= \frac{1}{16(z-1)^2} - \frac{1}{16(z-i)^2} - \frac{1}{16(z+i)^2} + \frac{1}{16(z+1)^2} + \frac{1-4u}{16(z-1)} - \frac{i(4u-1)}{16(z-i)} + \frac{i(4u-1)}{16(z+i)} + \frac{4u-1}{16(z+1)}.\end{aligned}\tag{10.26}$$

We have adjusted the gauge coupling to  $\tau = i$ , which gives a useful discrete  $\mathbb{Z}_4$  symmetry to the problem. The singularities are  $z_a = 1$ ,  $z_b = i$ ,  $z_c = -1$ ,  $z_d = -i$ . The mass parameters turn out to be  $m_a = \frac{1}{4}z_a$ . Their sign is arbitrary: we used a convention such that  $\sum m_a = 0$  for this setup. An example of a WKB triangulation is shown in Figure 73.

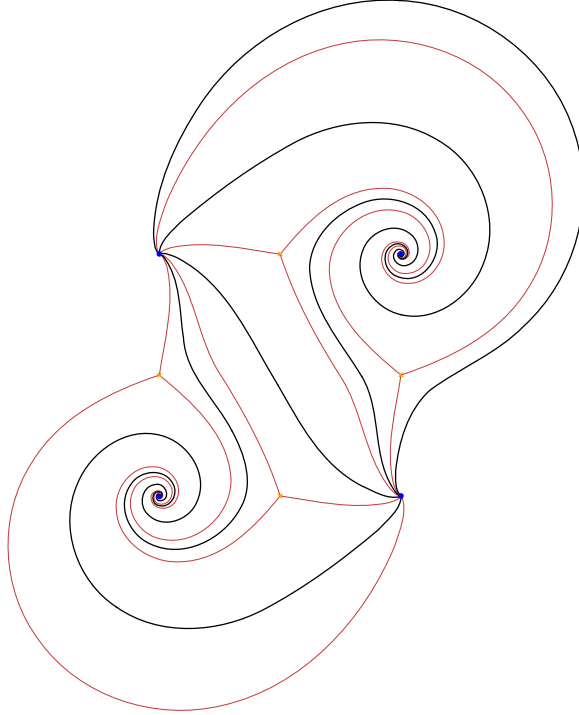


**Figure 73:** A typical WKB triangulation for the  $SU(2)$  theory with  $N_f = 4$ , at the special  $\mathbb{Z}_4$  symmetric point.

The  $\mathbb{Z}_4$  symmetry ensures that the six singularities in the  $u$  plane coalesce in two groups of three, giving two singular points of the  $N = 4$  type at  $u = 0, 1$ . As  $u$  approaches these two points, the turning points coalesce at  $z = 0$  or  $z = \infty$  respectively. We know that near each  $N = 4$  singularity there should be 6 light BPS particles, joining the turning points in all possible ways (passing either near  $z = 0$  or near  $z = \infty$ ). It is easy to see that on the segment  $0 < u < 1$  these two groups of 6 particles exhaust the BPS spectrum! This can be checked, say, at  $u = 1/2$ , and remains true on the whole segment because the phase of the central charges are actually constant there, so no wall-crossing may happen.

We expect to see an ellipsoidal “strong coupling” region where the spectrum consists of those 12 particles. We will need a convenient labeling of the charges for these BPS

particles. First of all, we can forget the flavor charges and project to a convenient  $\mathbb{Z}^2$  lattice of gauge charges, inspired by the labeling in the  $N = 4$  example. We will meet only charges

$$(0, 1), (1, 1), (1, 0), (1, -1). \quad (10.27)$$

Indeed, the turning points form a square; BPS strings joining opposite sides have the same gauge charge  $(0, 1)$  or  $(1, 0)$ , while the diagonals have gauge charge  $(1, 1)$  or  $(1, -1)$ .

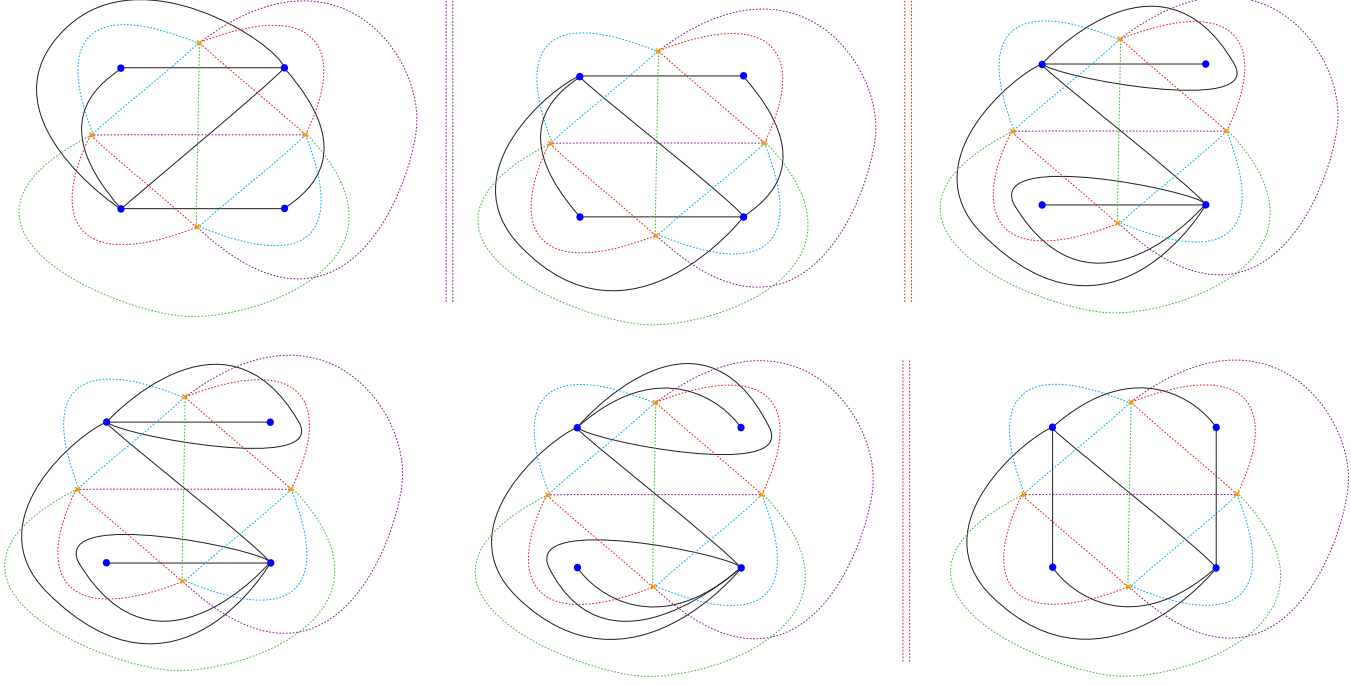


**Figure 74:** The evolution of the WKB triangulation for the  $SU(2)$  theory with  $N_f = 4$ , for the parameters specified in the text. We only show half of the overall evolution, i.e. six out of twelve flips. Because of the  $\mathbb{Z}_4$  symmetry of the problem, the second half of the sequence is identical to the first half, with pictures rotated by 90 degrees. We split the sequence further in two rows, the last triangulation in the first row coincides with the first in the second row. We see first a flip of the two diagonal edges, corresponding to the purple BPS states, then a flip of two side edges corresponding to two of the four red BPS states, then in the next row a pop of the northeast singularity and of the southwest one, followed by flips corresponding to the other two red BPS states. The other half of the evolution involves another flip of the diagonal edges due to the green BPS states, flips corresponding to two blue BPS states, a pop of the northwest and of the southeast singularities, and another flip from the other two blue BPS states.

In Figure 74 we show the evolution of  $T_{\text{WKB}}$ , from which we can read off the BPS particles at  $u = \frac{1}{2}$ . There are four particles of gauge charge  $(0, 1)$ , four of charge  $(1, 0)$ , two of charge  $(1, 1)$  and two of charge  $(1, -1)$ , with various combinations of flavor charges. Let us ignore the flavor charge information for the moment. The triangulations undergo a simple sequence of flips, which involves the required appearance of degenerate triangles for each regular singularity, at  $\vartheta = 0, \pi$  or  $\vartheta = \pm\pi/2$ .



Reading from the figure, the corresponding sequence of KS transformations is (suppressing flavor information, but showing a  $\pm$  sign distinguishing particles which become light at  $u = 0$  vs.  $u = 1$ ):

$$\mathcal{K}_{-1,1;+}\mathcal{K}_{1,-1;-}\mathcal{K}_{0,1;+}^2\mathcal{K}_{0,-1;-}^2\mathcal{K}_{1,1;+}\mathcal{K}_{-1,-1;-}\mathcal{K}_{1,0;+}^2\mathcal{K}_{-1,0;-}^2. \quad (10.28)$$

If we move to a region of large  $u$ , the phases of the charges, say,  $(1, 0; +)$  and  $(1, 0; -)$  will approach each other, as the flavor information becomes irrelevant. This will require a complete overhaul of the product of symplectomorphisms. A first step is the exchange of consecutive pairs of “side” and “diagonal” BPS states (now a  $*$  indicates a mixed flavor charge, with both  $+$  and  $-$  contributions):

$$\begin{aligned} (\mathcal{K}_{1,0;-}^2\mathcal{K}_{-1,1;+})(\mathcal{K}_{1,-1;-}\mathcal{K}_{0,1;+}^2)(\mathcal{K}_{0,-1;-}^2\mathcal{K}_{1,1;+})(\mathcal{K}_{-1,-1;-}\mathcal{K}_{1,0;+}^2) = \\ (\mathcal{K}_{-1,1;+}\mathcal{K}_{0,1;+}^2\mathcal{K}_{1,1;+}\mathcal{K}_{1,0;-}^2)(\mathcal{K}_{0,1;+}^2\mathcal{K}_{1,1;+}\mathcal{K}_{1,0;-}^2\mathcal{K}_{1,-1;-}) \\ (\mathcal{K}_{1,1;+}\mathcal{K}_{1,0;-}^2\mathcal{K}_{1,-1;-}\mathcal{K}_{0,-1;-}^2)(\mathcal{K}_{1,0;+}^2\mathcal{K}_{1,-1;-}\mathcal{K}_{0,-1;-}^2\mathcal{K}_{-1,-1;-}). \end{aligned} \quad (10.29)$$

We have applied the pentagon twice to each of the four pairs of transformations on the left. We already see something interesting: now there are 8 particles of gauge charge  $(1, 0)$ , 8 particles of gauge charge  $(0, 1)$ . Some of the octets of hypermultiplets of the very large  $u$  region are making their appearance. On the other hand we still see only 4 particles of charge  $(1, 1)$ .

The next steps towards the large  $u$  region generate vector multiplets: we recognize in pairs like  $\mathcal{K}_{1,0;-}^2\mathcal{K}_{0,1;+}^2$  the left hand side of the  $N_f = 2$  wall-crossing formula, and in pairs like  $\mathcal{K}_{1,-1;-}\mathcal{K}_{1,1;+}$  the left hand side of the  $N_f = 0$  wall crossing formula. The latter will give rise to a vectormultiplet of gauge charge  $(2, 0)$ , the former to a vectormultiplet of gauge charge  $(2, 2)$ , accompanied by 4 hypermultiplets of charge  $(1, 1)$ . These, together with the other 4 hypers already present at the previous step, form an octet.

From here on, the sequence of wall-crossings becomes increasingly intricate. As  $u$  grows, the phases of each member of the various octets move toward the phase of the corresponding W-boson. In the process one meets a recursive structure of wall-crossing formulae from the  $N_f = 0$  or  $N_f = 2$  theories; applying them repeatedly here gives rise to the infinitely dense structure of  $SL(2, \mathbb{Z})$  S-dual images of the W-bosons.

It is interesting to recover the flavor structure from our considerations here. Our special choice of masses breaks all  $SU(2)_{a,b,c,d}$  subgroups to their Cartan subgroups, but actually preserves some non-manifest part of  $SO(8)$ . In the three possible triality frames, the  $SO(8)$  Cartan generator has eigenvalues  $(m_a \pm m_c, m_b \pm m_d)$ ,  $(m_a \pm m_b, m_c \pm m_d)$ ,  $(m_a \pm m_d, m_c \pm m_b)$ . In the first frame, two eigenvalues are actually zero: a hidden  $SO(4) \sim SU(2)_L \times SU(2)_R$  is unbroken. This is essentially the reason for the reappearance here of the wall-crossing formulae from the  $N_f = 2$  example.  $\mathbf{8}_v$  contains a vector of this  $SO(4)$  and four singlets.  $\mathbf{8}_s$  and  $\mathbf{8}_c$  each contain two doublets  $\mathbf{2}_L$  and two doublets  $\mathbf{2}_R$ .

The wall-crossing we described is consistent with the idea that the original four particles of charge  $(1, 0)$  in the strong coupling region should be viewed as part of  $\mathbf{8}_s$ ; more precisely  $(1, 0; +)$  can be taken to be a doublet of  $SU(2)_L$  and  $(1, 0; -)$  a doublet of  $SU(2)_R$ . Similarly, the four particles of charge  $(0, 1)$  should be doublets of each kind in  $\mathbf{8}_c$ :  $(0, 1; +)$

can be taken to be a doublet of  $SU(2)_L$  and  $(0, 1; -)$  a doublet of  $SU(2)_R$ . The particles of charges  $(1, 1)$  (and similarly  $(1, -1)$ ) should be all singlets of  $8_v$ . Indeed it is easy to see that the first type of wall-crossing,

$$\mathcal{K}_{1,0;-}^2 \mathcal{K}_{-1,1;+} = \mathcal{K}_{-1,1;+} \mathcal{K}_{0,1;*}^2 \mathcal{K}_{1,1;*} \mathcal{K}_{1,0;-}^2, \quad (10.30)$$

produce the missing doublets in  $\mathbf{8}_s$  and  $\mathbf{8}_c$ , and the missing singlets of  $\mathbf{8}_v$ . The  $N_f = 2$  type wall-crossing of  $SU(2)_L$  doublets and  $SU(2)_R$  doublets like  $\mathcal{K}_{1,0;-}^2 \mathcal{K}_{0,1;+}^2$  produces the missing vectors in  $\mathbf{8}_v$ .

A simple way to describe the full charge lattice is the following. The six charges which become light at  $u \rightarrow 0$  (which we have labeled  $+$ ) satisfy the same linear relations as we found in the general  $N = 4$  analysis, and in particular span a three-dimensional lattice. The same is true of the six charges labeled  $-$ . The full charge lattice is the orthogonal sum of these two three-dimensional lattices.

In principle, one could determine the spectrum anywhere in parameter space from the strong coupling spectrum and the wall-crossing formula. In the next section we will propose a better method.

## 11. The spectrum generator

In this section, we give an algebraic method of determining the BPS spectrum of any theory related to an  $SU(2)$  Hitchin system.

Consider the evolution of the WKB triangulation  $T_{\text{WKB}}(\vartheta, \lambda^2)$  as  $\vartheta$  varies continuously through an arc of length  $\pi$ . As we saw in Section 6.6, generically there are three species of transformations of  $T_{\text{WKB}}$  which might occur at critical values  $\vartheta = \vartheta_c$ . Two of the three are flips and juggles, corresponding respectively to the BPS hypermultiplets and vectormultiplets we want to detect, with  $\arg -Z = \vartheta_c$ . As  $\vartheta$  varies we encounter exactly half of the BPS particles of the theory (given any BPS particle we encounter either the particle or its antiparticle). Each corresponds to a symplectomorphism acting on the coordinates  $\mathcal{X}_\gamma^\vartheta$ . The third possible transformation is a pop, which does not correspond to any of the BPS particles in which we are interested. Fortunately, these pops always occur within degenerate triangles. Thanks to the analysis of Section 7.6.3 these transformations actually give the trivial symplectomorphism, and hence can be ignored.

Composing all these symplectomorphisms in order, we arrive at a transformation  $\mathbf{S}$  relating  $\mathcal{X}^\vartheta$  and  $\mathcal{X}^{\vartheta+\pi}$ :

$$\mathbf{S} = \prod_{\gamma: \vartheta < \arg -Z_\gamma(u) < \vartheta + \pi}^{\curvearrowright} \mathcal{K}_\gamma^{\Omega(\gamma; u)}. \quad (11.1)$$

Here the product from left to right is taken in increasing order of  $\arg -Z_\gamma$ . This  $\mathbf{S}$  is a Stokes matrix for the Riemann-Hilbert problem of [1]. We will call it the *spectrum generator*.

Our trick is to notice that the technology of the previous sections provides a neat way of computing  $\mathbf{S}$  *without* following the continuous evolution of the triangulation. Once  $\mathbf{S}$  is known, the decomposition (11.1) uniquely determines the  $\Omega(\gamma; u)$ .

How will we compute  $\mathbf{S}$ ? Notice that the WKB foliations with phases  $\vartheta$  and  $\vartheta + \pi$  are identical. It follows that the undecorated WKB triangulations are also the same. What about the decorations? In the case of regular singularities, if we change  $\vartheta$  to  $\vartheta + \pi$ , it follows from Section 6.5 that the decoration switches from one monodromy eigenvector to the other — this is the transformation we called a pop. Similarly, it follows from the local analysis in Section 8 that the same conclusion holds for irregular singularities. So the decorated triangulation  $T_{\text{WKB}}(\vartheta + \pi)$  differs from  $T_{\text{WKB}}(\vartheta)$  by a pop transformation at every vertex — what we will refer to as an *omnipop*.

So to determine  $\mathbf{S}$  our job is to work out the explicit transformation corresponding to an omnipop.

### 11.1 Deriving the transformation under an omnipop

Given a vertex  $P$ , the decoration of  $T_{\text{WKB}}(\vartheta)$  provides a distinguished section (up to scale) near  $P$ . In the case of a regular singularity,  $P$  is the singular point, and for an irregular singular point,  $P$  is one of the distinguished points on the small circle surrounding the singularity. Choose a scale and let  $s_P$  be a distinguished section, while  $\tilde{s}_P$  is the new distinguished section resulting from a pop. Similarly, we write  $\mathcal{X}_{P_1 P_2}$  and  $\tilde{\mathcal{X}}_{P_1 P_2}$  for the original and new Fock-Goncharov coordinates at the edge  $E_{P_1 P_2}$  joining vertices  $P_1, P_2$  computed using the sections  $s_{P_i}$  and  $\tilde{s}_{P_i}$ , respectively.

It follows from the definitions in Section 7.1 that, for all  $E$ ,  $\gamma_E^{\vartheta+\pi} = -\gamma_E^\vartheta$ . Combining this with the definitions

$$\mathcal{X}_{\gamma_E^{\vartheta+\pi}}^{\vartheta+\pi} = \mathcal{X}_E^{T_{\text{WKB}}(\vartheta+\pi, \lambda^2)}, \quad \mathcal{X}_{\gamma_E^\vartheta}^\vartheta = \mathcal{X}_E^{T_{\text{WKB}}(\vartheta, \lambda^2)}, \quad (11.2)$$

we have

$$\mathcal{X}_\gamma^{\vartheta+\pi} = \mathcal{X}_\gamma^\vartheta \cdot \left( \mathcal{X}_E^{T_{\text{WKB}}(\vartheta, \lambda^2)} \tilde{\mathcal{X}}_E^{T_{\text{WKB}}(\vartheta, \lambda^2)} \right)^{-1} \quad (11.3)$$

for  $\gamma = \gamma_E^\vartheta$ . Therefore, we seek a simple formula for  $\mathcal{X}_E^T \tilde{\mathcal{X}}_E^T$  for a fixed decorated triangulation  $T$ . To ease the notation we will drop the superscript  $T$  in the computations that follow, but bear in mind that we are working within a fixed decorated triangulation.

For any edge  $PQ$  it will be convenient to define  $A_{PQ}$  by

$$A_{PQ} := -\frac{(s_Q \wedge \tilde{s}_P)(s_P \wedge \tilde{s}_Q)}{(s_P \wedge \tilde{s}_P)(s_Q \wedge \tilde{s}_Q)}. \quad (11.4)$$

Note that  $A_{PQ} = A_{QP}$ . This is a useful definition because one can easily show that<sup>41</sup>

$$1 + A_{PQ} = \frac{(s_P \wedge s_Q)(\tilde{s}_P \wedge \tilde{s}_Q)}{(\tilde{s}_P \wedge s_P)(\tilde{s}_Q \wedge s_Q)}, \quad (11.7)$$

---

<sup>41</sup>In order to obtain (11.7) from (11.4) we use the fact that in a two-dimensional vector space, for any three vectors  $v_1, v_2, v_3$ , we have

$$(v_1 \wedge v_2)v_3 + (v_3 \wedge v_1)v_2 + (v_2 \wedge v_3)v_1 = 0, \quad (11.5)$$

or equivalently, for any four vectors  $v_1, v_2, v_3, v_4$ , we have

$$(v_1 \wedge v_2)(v_3 \wedge v_4) + (v_3 \wedge v_1)(v_2 \wedge v_4) + (v_2 \wedge v_3)(v_1 \wedge v_4) = 0. \quad (11.6)$$

We will use this relation repeatedly in what follows.

and therefore, if  $E$  is the edge  $ac$  in the quadrilateral  $Q_E$  with vertices  $abcd$  in counter-clockwise order,

$$\tilde{\mathcal{X}}_E \mathcal{X}_E = \frac{(1 + A_{ab})(1 + A_{cd})}{(1 + A_{bc})(1 + A_{da})}. \quad (11.8)$$

Therefore we can solve our problem if we can express  $A_{ab}$  in terms of the coordinates  $\mathcal{X}_E^T$ .

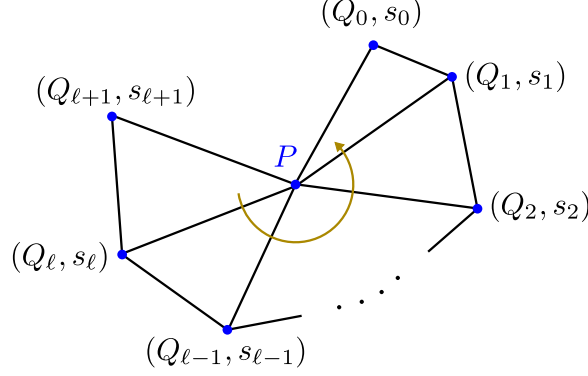


**Figure 75:** Partial star-shaped neighborhood of a vertex  $P$ , used in the computation of  $\Sigma(P; Q_{\ell+1} \rightarrow Q_0)$ . The brown arrow intersects the edges which occur in (11.9). The final edge intersected by the brown arrow only occurs in the final summand. The result (11.10) is expressed in terms of the decorations at  $P$  and  $Q_{\ell}$ , as well as at the bounding edges  $Q_0, Q_{\ell+1}$ , whose edges do not occur in the expression for  $\Sigma(P; Q_{\ell+1} \rightarrow Q_0)$ .

We begin with a key lemma. Consider a partial star-shaped neighborhood of a decorated point  $(P, s_P)$  with decorated vertices  $(Q_0, s_0), (Q_1, s_1), \dots, (Q_{\ell+1}, s_{\ell+1})$  in *clockwise* order, as in Figure 75. Denote the edge coordinates  $\mathcal{X}_{P, Q_j}$  simply by  $\mathcal{X}_{P, j}$ . We claim that the quantity

$$\Sigma(P; Q_{\ell+1} \rightarrow Q_0) := 1 + \mathcal{X}_{P, \ell} + \mathcal{X}_{P, \ell} \mathcal{X}_{P, \ell-1} + \dots + (\mathcal{X}_{P, \ell} \dots \mathcal{X}_{P, 1}) \quad (11.9)$$

can be written simply in terms of the sections  $s_P, s_0, s_{\ell}, s_{\ell+1}$ , which have been continued in a single-valued fashion in the simply connected region formed by the triangles. Indeed we have

$$\Sigma(P; Q_{\ell+1} \rightarrow Q_0) = \frac{(s_0 \wedge s_{\ell+1})(s_P \wedge s_{\ell})}{(s_{\ell+1} \wedge s_{\ell})(s_0 \wedge s_P)}. \quad (11.10)$$

To prove this, first check it for  $\ell = 1$ , using the identity (11.5). Then, for the inductive step note that if we add a further decorated vertex  $(Q_{\ell+2}, s_{\ell+2})$  then

$$\begin{aligned} \Sigma(P; Q_{\ell+2} \rightarrow Q_0) &= 1 + \Sigma(P; Q_{\ell+1} \rightarrow Q_0) \mathcal{X}_{P, \ell+1} \\ &= 1 - \frac{(s_0 \wedge s_{\ell+1})(s_P \wedge s_{\ell})}{(s_{\ell+1} \wedge s_{\ell})(s_0 \wedge s_P)} \frac{(s_P \wedge s_{\ell+2})(s_{\ell+1} \wedge s_{\ell})}{(s_{\ell+2} \wedge s_{\ell+1})(s_{\ell} \wedge s_P)} \\ &= 1 + \frac{(s_P \wedge s_{\ell+2})(s_0 \wedge s_{\ell+1})}{(s_{\ell+2} \wedge s_{\ell+1})(s_0 \wedge s_P)} \\ &= \frac{(s_0 \wedge s_P)(s_{\ell+2} \wedge s_{\ell+1}) + (s_0 \wedge s_{\ell+1})(s_P \wedge s_{\ell+2})}{(s_{\ell+2} \wedge s_{\ell+1})(s_0 \wedge s_P)} \\ &= \frac{(s_0 \wedge s_{\ell+2})(s_P \wedge s_{\ell+1})}{(s_{\ell+2} \wedge s_{\ell+1})(s_0 \wedge s_P)} \end{aligned} \quad (11.11)$$

where in the last line we have again used equation (11.5).

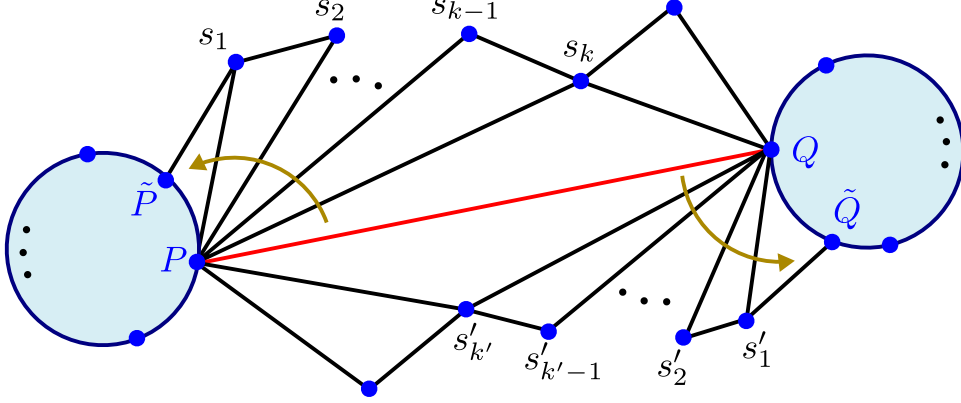


**Figure 76:** Configuration of edges involved in computing  $A_{PQ}$  when  $P, Q$  are both irregular singular points. The elementary pop transformations at  $P$  and  $Q$  associate the decorations at  $\tilde{P}, \tilde{Q}$  to the vertices  $P, Q$  respectively.

Now, to compute  $A_{PQ}$  we need to distinguish the cases where  $P, Q$  are regular or irregular singular points. Let us consider first the case where both  $P, Q$  are irregular singular points. Then we have the situation illustrated in Figure 76. Note that we have denoted  $\tilde{P}$  as the distinguished point from the WKB ray one step counterclockwise from  $P$ , so that for an elementary pop,  $\tilde{s}_P = s_{\tilde{P}}$ , and similarly for  $Q$ . Here we parallel-transport  $s_{\tilde{P}}$  along the edge going from  $P$  to  $\tilde{P}$ . Applying our lemma we have

$$\Sigma(P; Q \rightarrow \tilde{P}) = \frac{(\tilde{s}_P \wedge s_Q)(s_P \wedge s_k)}{(s_Q \wedge s_k)(\tilde{s}_P \wedge s_P)}, \quad (11.12)$$

$$\Sigma(Q; P \rightarrow \tilde{Q}) = \frac{(\tilde{s}_Q \wedge s_P)(s_Q \wedge s'_{k'})}{(s_P \wedge s'_{k'})(\tilde{s}_Q \wedge s_Q)}, \quad (11.13)$$

and by definition

$$\mathcal{X}_{PQ} = -\frac{(s_P \wedge s'_{k'})(s_Q \wedge s_k)}{(s'_{k'} \wedge s_Q)(s_k \wedge s_P)}. \quad (11.14)$$

Taking the product of these three expressions and cancelling factors we find:

$$\mathcal{X}_{PQ} \Sigma(P; Q \rightarrow \tilde{P}) \Sigma(Q; P \rightarrow \tilde{Q}) = -\frac{(\tilde{s}_P \wedge s_Q)(\tilde{s}_Q \wedge s_P)}{(\tilde{s}_P \wedge s_P)(\tilde{s}_Q \wedge s_Q)} = A_{PQ}. \quad (11.15)$$

This gives us the desired expression for  $A_{PQ}$  in terms of the coordinates  $\mathcal{X}_E^T$ . This expression even works if  $P, Q$  are consecutive points on the same boundary circle, since we defined  $\mathcal{X}_{PQ} = 0$  in that case.

Now let us consider the case where  $P$  is a regular singular point as shown in Figure 77. A new point arises in computing  $\Sigma(P; Q \rightarrow Q)$ : we must take into account the monodromy around the regular singular point. If  $M_P$  is the clockwise monodromy operator around  $P$ , we use expression (11.10) above with  $s_{\ell+1} = s_Q$  and  $s_0 = M^{-1}s_Q$ :

$$\Sigma(P; Q \rightarrow Q) = \frac{(s_P \wedge s_\ell)(M^{-1}s_Q \wedge s_Q)}{(s_Q \wedge s_\ell)(M^{-1}s_Q \wedge s_P)}. \quad (11.16)$$

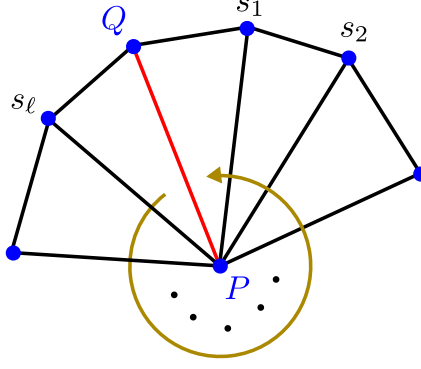


**Figure 77:** Configuration of edges involved in the computation of  $\Sigma(P; Q \rightarrow Q)$ , for  $P$  a regular singular point. Here one must take into account the monodromy around  $P$ , since in the inductive proof of (11.10) it is assumed that the  $s_i$  are single-valued in the region determined by the triangles. Thus, in the final inductive step one must move a cut.

This can be put in a more useful form by expanding  $s_Q$  in the basis  $s_P, \tilde{s}_P$ , where  $M s_P = \mu_P s_P$  and  $M \tilde{s}_P = \mu_P^{-1} \tilde{s}_P$ . Then we can expand  $s_Q = c_1 s_P + c_2 \tilde{s}_P$  and compute

$$M^{-1} s_Q \wedge s_Q = c_1 c_2 (\mu_P^{-1} - \mu_P) s_P \wedge \tilde{s}_P, \quad (11.17)$$

$$M^{-1} s_Q \wedge s_P = c_2 \mu_P \tilde{s}_P \wedge s_P. \quad (11.18)$$

Thus, using  $c_1 = (s_Q \wedge \tilde{s}_P) / (s_P \wedge \tilde{s}_P)$  we get

$$\Sigma(P; Q \rightarrow Q) = (1 - \mu_P^{-2}) \frac{(s_P \wedge s_\ell)(s_Q \wedge \tilde{s}_P)}{(s_Q \wedge s_\ell)(s_P \wedge \tilde{s}_P)}. \quad (11.19)$$

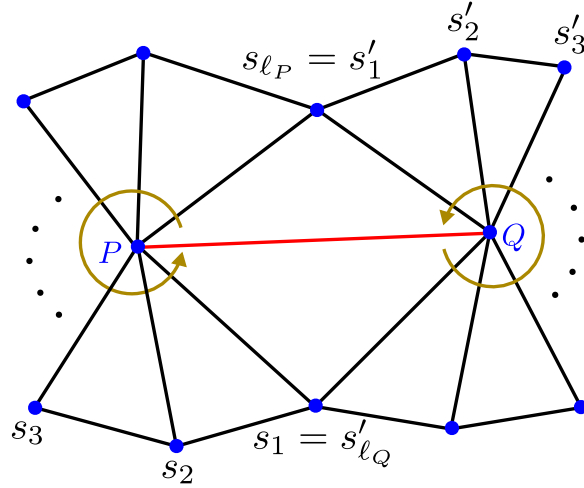


**Figure 78:** Configuration of edges involved in computing  $A_{PQ}$  when  $P, Q$  are both regular singular points.

Now, consider an edge between two regular singular points  $P$  and  $Q$  as in Figure 78. Using the result (11.19) for both  $P$  and  $Q$  we obtain

$$\mathcal{X}_{PQ} \Sigma(P; Q \rightarrow Q) \Sigma(Q; P \rightarrow P) = (1 - \mu_P^{-2})(1 - \mu_Q^{-2}) A_{PQ} \quad (11.20)$$

from which we obtain  $A_{PQ}$  in terms of the  $\mathcal{X}_E^T$ .

Finally, suppose  $P$  is an irregular singular point and  $Q$  is a regular singular point. Then similarly to the above we have

$$A_{PQ} = (1 - \mu_Q^{-2})^{-1} \mathcal{X}_{PQ} \Sigma(P; Q \rightarrow \tilde{P}) \Sigma(Q; P \rightarrow P). \quad (11.21)$$

Taken together, (11.3), (11.8), (11.15), (11.20), (11.21) completely solve the problem of determining the spectrum generator  $\mathbf{S}$  as an elementary symplectic transformation. In the following sections we will illustrate the kinds of formulae which appear in several examples.

Let us conclude with two remarks:

- The reader might be disturbed by the minus sign appearing in the final expression for  $A_{ab}$  in the case of a regular singular point. After all, any two triangulations should be connected by a sequence of flips, and the corresponding coordinate transformations only involve positive signs. Fortunately it is easy to rearrange the final formula (11.8) for the transformation of a cross-ratio in such a way that only positive signs appear. Indeed, in (11.8) each of the labels  $abcd$  appears once in the numerator and once in the denominator. Multiplying both numerator and denominator by  $(1 - \mu_a^2)(1 - \mu_b^2)(1 - \mu_c^2)(1 - \mu_d^2)$ , the factors in (11.8) can be combined into four blocks of the form

$$(1 - \mu_a^2)(1 - \mu_b^2)(1 + A_{ab}) = 1 - \mu_a^2 - \mu_b^2 + \mu_a^2 \mu_b^2 + \mathcal{X}_{a,b} \left( \sum_{i=0}^{k-1} \prod_{j=1}^i \mathcal{X}_{a,j} \right) \left( \sum_{i'=0}^{k'-1} \prod_{j'=1}^{i'} \mathcal{X}_{b,-j'} \right), \quad (11.22)$$

where there are  $k$  vertices in the star region around  $a$  and  $k'$  vertices in the star region around  $b$ . In this sum, the term with  $i = k - 1$ ,  $i' = 0$  equals  $\mu_a^2$ , and the term with  $i = 0$ ,  $i' = k' - 1$  equals  $\mu_b^2$ . These two terms then cancel the terms with negative signs. This cancellation is needed e.g. to show that the spectrum generators  $\mathbf{S}$  of the two realizations of the  $SU(2)$  theory with  $N_f = 2$  coincide, as one realization involves regular singularities (and hence negative signs can appear) while the other does not.

- In a region where  $|\mu_P| < 1$ , the expression (11.9) defining  $\Sigma(P; Q \rightarrow Q)$  can be rewritten in a suggestive form,

$$\frac{1}{(1 - \mu_P^2)} \Sigma(P; Q \rightarrow Q) = 1 + \sum_{i=1}^{\infty} \prod_{j=1}^i \mathcal{X}_{P,j}, \quad (11.23)$$

by expanding the denominator in a geometric series and remembering that  $\prod_{j=1}^k \mathcal{X}_{P,j} = \mu_P^2$ . (In this formula it is better to label the vertices in counterclockwise order.)

## 11.2 $N = 3$

We first consider the  $N = 3$  example discussed in Section 9.4.4. For notational simplicity we remove the  $\vartheta$ , and indicate  $\mathcal{X}^{\vartheta+\pi}$  as  $\tilde{\mathcal{X}}$ . We use the basis  $\gamma_1, \gamma_2$  of  $\hat{\Gamma}$  corresponding to

edges 13, 14 in Figure 79 with the orientation at  $\vartheta$  (as opposed to  $\vartheta + \pi$ ), in other words,  $\gamma_1 := \gamma_{13}^\vartheta$  and similarly for  $\gamma_2$ . Then from equation (11.3) and (11.8) we have

$$\tilde{\mathcal{X}}_{\gamma_1} = \mathcal{X}_{\gamma_1} \frac{(1 + A_{23})(1 + A_{41})}{(1 + A_{12})(1 + A_{34})}. \quad (11.24)$$

Now  $A_{12} = A_{23} = A_{34} = 0$ , while equation (11.15) simply gives  $A_{41} = \mathcal{X}_{\gamma_2}$ . Similarly,

$$\tilde{\mathcal{X}}_{\gamma_2} = \mathcal{X}_{\gamma_2} \frac{(1 + A_{34})(1 + A_{51})}{(1 + A_{13})(1 + A_{45})} \quad (11.25)$$

and  $A_{34} = A_{45} = A_{51} = 0$ , but, by equation (11.15)

$$A_{13} = \mathcal{X}_{\gamma_1}(1 + \mathcal{X}_{\gamma_2}). \quad (11.26)$$

So, altogether we obtain the transformation  $\mathbf{S}$ :

$$\tilde{\mathcal{X}}_{\gamma_1} = \mathcal{X}_{\gamma_1}(1 + \mathcal{X}_{\gamma_2}), \quad (11.27)$$

$$\tilde{\mathcal{X}}_{\gamma_2} = \mathcal{X}_{\gamma_2}(1 + \mathcal{X}_{\gamma_1} + \mathcal{X}_{\gamma_1}\mathcal{X}_{\gamma_2})^{-1}. \quad (11.28)$$

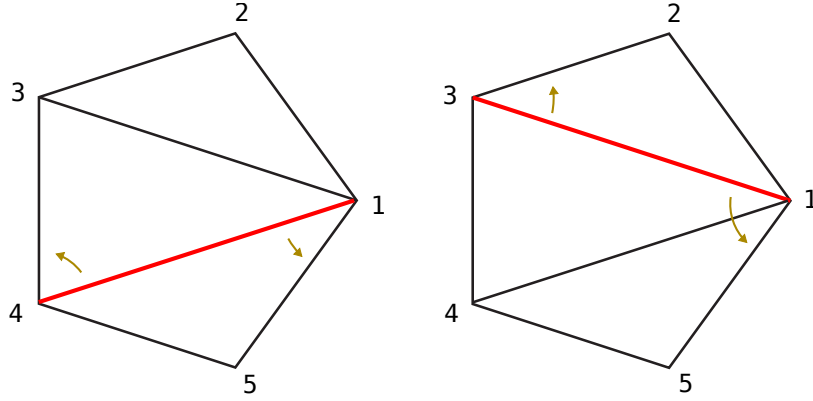


**Figure 79:** Diagram for computing the factors  $A_{ab}$  appearing in the spectrum generator of the  $N = 3$  theory. On the left is the example  $ab = 14$ , where we simply get  $A_{14} = \mathcal{X}_{\gamma_2}$  (since the brown arrows do not meet any edges). On the right is  $ab = 13$  where we get  $A_{13} = \mathcal{X}_{\gamma_1}(1 + \mathcal{X}_{\gamma_2})$ .

Above we promised that given  $\mathbf{S}$  one can recover the BPS spectrum. In this simple example that means recovering the decomposition  $\mathbf{S} = \mathcal{K}_{\gamma_1}\mathcal{K}_{\gamma_2}$  starting from (11.27), (11.28). The general algorithm for doing this was sketched in Section 2.3; let us see how it would work here. We are seeking a decomposition of the form

$$\mathbf{S} = \prod_{m,n \geq 0} \mathcal{K}_{m\gamma_1 + n\gamma_2}^{\Omega(m\gamma_1 + n\gamma_2; u)} \quad (11.29)$$

where the product is taken in increasing order of  $m/n$ , from 0 to  $\infty$ . First specialize to  $\mathcal{X}_{m\gamma_1 + n\gamma_2} = 0$  for all  $m + n \geq 2$ . After this specialization all  $\mathcal{K}_{m\gamma_1 + n\gamma_2}$  for  $m + n \geq 2$  become identity operators, so the decomposition reduces to

$$\mathbf{S} = \mathcal{K}_{\gamma_1}^{\Omega(\gamma_1; u)} \mathcal{K}_{\gamma_2}^{\Omega(\gamma_2; u)}. \quad (11.30)$$



The action of this operator is easily computed as

$$\tilde{\mathcal{X}}_{\gamma_1} = \mathcal{X}_{\gamma_1}(1 + \mathcal{X}_{\gamma_2})^{\Omega(\gamma_2; u)}, \quad (11.31)$$

$$\tilde{\mathcal{X}}_{\gamma_2} = \mathcal{X}_{\gamma_2}(1 + \mathcal{X}_{\gamma_1})^{-\Omega(\gamma_1; u)}. \quad (11.32)$$

Comparing this with the known action of  $\mathbf{S}$  by (11.27), (11.28) and recalling that we have set  $\mathcal{X}_{\gamma_1+\gamma_2} = 0$ , we see that the two are consistent only if  $\Omega(\gamma_1; u) = 1$  and  $\Omega(\gamma_2; u) = 1$ . We can now continue to the next order by specializing to  $\mathcal{X}_{m\gamma_1+n\gamma_2} = 0$  for all  $m+n \geq 3$ ; we would then have three new unknown  $\Omega$  appearing,

$$\mathbf{S} = \mathcal{K}_{\gamma_1} \mathcal{K}_{2\gamma_1}^{\Omega(2\gamma_1; u)} \mathcal{K}_{\gamma_1+\gamma_2}^{\Omega(\gamma_1+\gamma_2; u)} \mathcal{K}_{2\gamma_2}^{\Omega(2\gamma_2; u)} \mathcal{K}_{\gamma_2}. \quad (11.33)$$

Computing the action of this operator we find that it is consistent with (11.27), (11.28) only if all of these three unknown  $\Omega$  actually vanish. Similar computations to higher orders give the same result — all of the new  $\Omega$  which appear at each order turn out to vanish. This can be carried out as long as one has patience or computer time, but eventually one might be inspired to conjecture that in fact all of the higher  $\Omega$  vanish, i.e. that one has an exact identity  $\mathbf{S} = \mathcal{K}_{\gamma_1} \mathcal{K}_{\gamma_2}$ . Once conjectured this identity is of course easy to verify.

Note that had we sought a decomposition in the order of decreasing  $m/n$ , by the same algorithm we would have arrived at the formula  $\mathbf{S} = \mathcal{K}_{\gamma_2} \mathcal{K}_{\gamma_1+\gamma_2} \mathcal{K}_{\gamma_1}$ . The two different decompositions of course correspond to the two sides of the wall of marginal stability.

### 11.3 $N = 4$

Next we consider the  $N = 4$  example from Section 9.4.6. Let us focus on the triangulation of Figure 80 (a) and identify

$$\mathcal{X}_{\gamma_1} = \mathcal{X}_{14}, \quad \mathcal{X}_{\gamma_2} = \mathcal{X}_{15}, \quad \mathcal{X}_{\gamma_3} = \mathcal{X}_{13}. \quad (11.34)$$

Then (11.3) becomes

$$\tilde{\mathcal{X}}_{\gamma_1} = \mathcal{X}_{\gamma_1}(1 + A_{51})(1 + A_{13})^{-1}, \quad (11.35)$$

$$\tilde{\mathcal{X}}_{\gamma_2} = \mathcal{X}_{\gamma_2}(1 + A_{14})^{-1}, \quad (11.36)$$

$$\tilde{\mathcal{X}}_{\gamma_3} = \mathcal{X}_{\gamma_3}(1 + A_{14}). \quad (11.37)$$

Evaluating  $A_{13}, A_{15}, A_{14}$  using equation (11.15) and the identifications (11.34) we obtain:

$$\tilde{\mathcal{X}}_{\gamma_1} = \mathcal{X}_{\gamma_1}(1 + \mathcal{X}_{\gamma_2})(1 + \mathcal{X}_{\gamma_3} + \mathcal{X}_{\gamma_3}\mathcal{X}_{\gamma_1} + \mathcal{X}_{\gamma_3}\mathcal{X}_{\gamma_1}\mathcal{X}_{\gamma_2})^{-1}, \quad (11.38)$$

$$\tilde{\mathcal{X}}_{\gamma_2} = \mathcal{X}_{\gamma_2}(1 + \mathcal{X}_{\gamma_1} + \mathcal{X}_{\gamma_1}\mathcal{X}_{\gamma_2})^{-1}, \quad (11.39)$$

$$\tilde{\mathcal{X}}_{\gamma_3} = \mathcal{X}_{\gamma_3}(1 + \mathcal{X}_{\gamma_1} + \mathcal{X}_{\gamma_1}\mathcal{X}_{\gamma_2}). \quad (11.40)$$

This transformation indeed has the KS decomposition  $\mathbf{S} = \mathcal{K}_{\gamma_3} \mathcal{K}_{\gamma_1} \mathcal{K}_{\gamma_2}$  for an appropriate choice of  $(u, \vartheta)$ , agreeing with our expectations. Note that  $\mathcal{X}_{\gamma_1}$  comes from a quadrilateral with two internal edges, which correspond to the two multiplicative factors in (11.38).

Similarly, making the identifications

$$\mathcal{X}_{\gamma_1} = \mathcal{X}_{63}, \quad \mathcal{X}_{\gamma_2} = \mathcal{X}_{13}, \quad \mathcal{X}_{-\gamma_3} = \mathcal{X}_{46}, \quad (11.41)$$

appropriate to the triangulation in Figure 80 (b), we find that

$$\tilde{\mathcal{X}}_{\gamma_1} = \mathcal{X}_{\gamma_1}(1 + \mathcal{X}_{\gamma_2})(1 + \mathcal{X}_{-\gamma_3}), \quad (11.42)$$

$$\tilde{\mathcal{X}}_{\gamma_2} = \mathcal{X}_{\gamma_2} [1 + \mathcal{X}_{\gamma_1}(1 + \mathcal{X}_{\gamma_2})(1 + \mathcal{X}_{-\gamma_3})], \quad (11.43)$$

$$\tilde{\mathcal{X}}_{-\gamma_3} = \mathcal{X}_{-\gamma_3} [1 + \mathcal{X}_{\gamma_1}(1 + \mathcal{X}_{\gamma_2})(1 + \mathcal{X}_{-\gamma_3})]. \quad (11.44)$$

In this case  $\mathcal{X}_{\gamma_{2,3}}$  come from quadrilaterals which have the same single internal edge. Moving counterclockwise from that edge at either of its ends, we meet an internal edge, which contributes to the multiplicative factor in (11.43), (11.44).  $\mathcal{X}_{\gamma_1}$  comes from a quadrilateral with two internal edges, corresponding to the two factors in (11.42). The transformation (11.42)-(11.44) has the decomposition (for an appropriate value of  $(u, \vartheta)$ )  $\mathbf{S} = \mathcal{K}_{\gamma_1} \mathcal{K}_{\gamma_2} \mathcal{K}_{-\gamma_3}$ . Case (d) is similar and will be left to the reader.

Finally, consider the third type of triangulation of the hexagon, with a triangle of internal edges, as in Figure 80 (c):

$$\tilde{\mathcal{X}}_{-\gamma_1} = \mathcal{X}_{-\gamma_1}(1 + \mathcal{X}_{\gamma_1+\gamma_2} + \mathcal{X}_{\gamma_1+\gamma_2}\mathcal{X}_{-\gamma_1})^{-1}(1 + \mathcal{X}_{\gamma_3} + \mathcal{X}_{\gamma_3}\mathcal{X}_{\gamma_1+\gamma_2}), \quad (11.45)$$

$$\tilde{\mathcal{X}}_{\gamma_1+\gamma_2} = \mathcal{X}_{\gamma_1+\gamma_2}(1 + \mathcal{X}_{\gamma_3} + \mathcal{X}_{\gamma_3}\mathcal{X}_{\gamma_1+\gamma_2})^{-1}(1 + \mathcal{X}_{-\gamma_1} + \mathcal{X}_{-\gamma_1}\mathcal{X}_{\gamma_3}), \quad (11.46)$$

$$\tilde{\mathcal{X}}_{\gamma_3} = \mathcal{X}_{\gamma_3}(1 + \mathcal{X}_{-\gamma_1} + \mathcal{X}_{-\gamma_1}\mathcal{X}_{\gamma_3})^{-1}(1 + \mathcal{X}_{\gamma_1+\gamma_2} + \mathcal{X}_{\gamma_1+\gamma_2}\mathcal{X}_{-\gamma_1}). \quad (11.47)$$

The two factors in each transformation correspond to the fact that each quadrilateral has two internal edges. Here we find  $\mathbf{S} = \mathcal{K}_{-\gamma_1} \mathcal{K}_{\gamma_3} \mathcal{K}_{\gamma_2} \mathcal{K}_{\gamma_1+\gamma_2}$  (after some surprising simplifications).

#### 11.4 $SU(2)$ , $N_f = 0$

Now we turn to the  $SU(2)$  theory with  $N_f = 0$ . In Section 10.1 we explained that in the strong coupling region we have  $\mathbf{S} = \mathcal{K}_{\gamma_1} \mathcal{K}_{\gamma_2}$ , where  $\langle \gamma_1, \gamma_2 \rangle = 2$ . This transformation acts by

$$\tilde{\mathcal{X}}_{\gamma_1} = \mathcal{X}_{\gamma_1}(1 + \mathcal{X}_{\gamma_2})^2, \quad (11.48)$$

$$\tilde{\mathcal{X}}_{\gamma_2} = \mathcal{X}_{\gamma_2} [1 + \mathcal{X}_{\gamma_1}(1 + \mathcal{X}_{\gamma_2})^2]^{-2}. \quad (11.49)$$

This transformation can be obtained from  $T_{\text{WKB}}$  using the rules we have described. In particular, the fact that each quadrilateral in  $T_{\text{WKB}}$  has two coinciding internal edges leads to the overall powers of 2 in the multiplicative factors. See Figure 81.

#### 11.5 $SU(2)$ , $N_f = 1$

Next consider the  $SU(2)$  theory with  $N_f = 1$ , which we described in Section 10.2. Here at strong coupling we found that  $\mathbf{S} = \mathcal{K}_{\gamma_1} \mathcal{K}_{-\gamma_3} \mathcal{K}_{\gamma_2}$ , with  $\langle \gamma_1, \gamma_2 \rangle = \langle \gamma_2, \gamma_3 \rangle = \langle \gamma_3, \gamma_1 \rangle = 1$ . This transformation acts by

$$\tilde{\mathcal{X}}_{\gamma_1} = \mathcal{X}_{\gamma_1}(1 + \mathcal{X}_{\gamma_2})(1 + \mathcal{X}_{-\gamma_3} + \mathcal{X}_{-\gamma_3}\mathcal{X}_{\gamma_2}), \quad (11.50)$$

$$\tilde{\mathcal{X}}_{\gamma_2} = \mathcal{X}_{\gamma_2}(1 + \mathcal{X}_{-\gamma_3} + \mathcal{X}_{-\gamma_3}\mathcal{X}_{\gamma_2})^{-1} [1 + \mathcal{X}_{\gamma_1}(1 + \mathcal{X}_{\gamma_2})(1 + \mathcal{X}_{-\gamma_3} + \mathcal{X}_{-\gamma_3}\mathcal{X}_{\gamma_2})]^{-1}, \quad (11.51)$$

$$\tilde{\mathcal{X}}_{-\gamma_3} = \mathcal{X}_{-\gamma_3}(1 + \mathcal{X}_{\gamma_2}) [1 + \mathcal{X}_{\gamma_1}(1 + \mathcal{X}_{\gamma_2})(1 + \mathcal{X}_{-\gamma_3} + \mathcal{X}_{-\gamma_3}\mathcal{X}_{\gamma_2})]^{-1}. \quad (11.52)$$

Once again, it is straightforward to obtain these factors from the triangulation using our rules. See Figure 82.

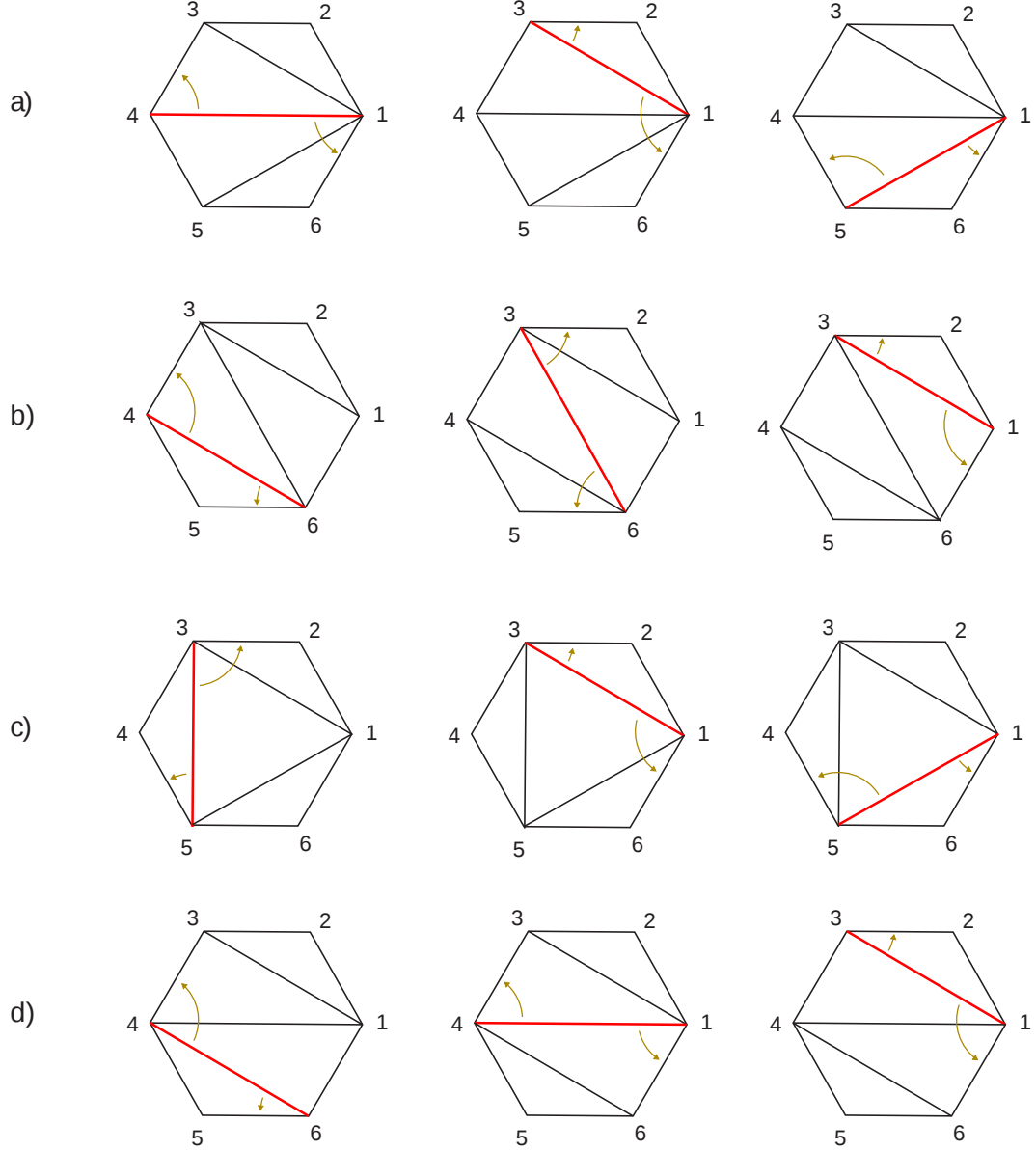


**Figure 80:** Diagrams for computing the factors  $A_{ab}$  appearing in the spectrum generator in the  $N = 4$  example. The four different triangulations we show occur as  $T_{\text{WKB}}(u, \vartheta)$  for different values of  $(u, \vartheta)$ . In a),  $ab = 14$  defines  $\gamma_1$ ,  $ab = 13$  defines  $\gamma_3$  and  $ab = 15$  defines  $\gamma_2$ . In b),  $ab = 63$  defines  $\gamma_1$ ,  $ab = 13$  defines  $\gamma_2$  and  $ab = 46$  defines  $-\gamma_3$ . In c),  $ab = 35$  defines  $-\gamma_1$ ,  $ab = 31$  defines  $\gamma_3$  and  $ab = 15$  defines  $\gamma_1 + \gamma_2$ . In d),  $ab = 46$ ,  $ab = 41$  and  $ab = 31$ .

### 11.6 $SU(2)$ , $N_f = 4$

As our final example, we describe the spectrum generator  $\mathbf{S}$  for the  $N_f = 4$  theory. We will consider a simple situation where  $T_{\text{WKB}}$  is the graph of a tetrahedron: we have six edges, labeled by all pairs  $ij$ ,  $i < j$ ,  $i, j = 1, \dots, 4$ , as in Figure 83. Applying our rules we have

$$\tilde{\mathcal{X}}_{12} = \mathcal{X}_{12} \frac{(1 + A_{13})(1 + A_{24})}{(1 + A_{23})(1 + A_{14})}, \quad (11.53)$$

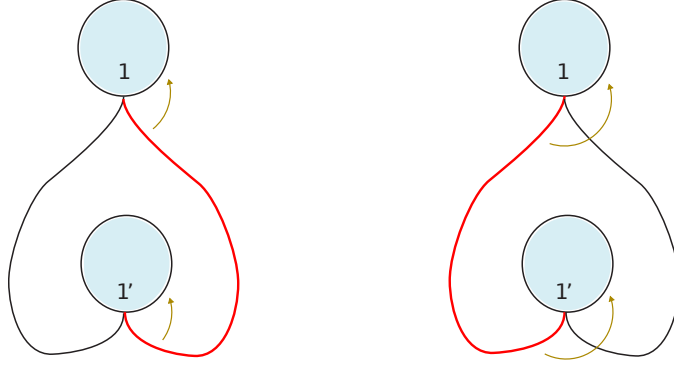


**Figure 81:** Diagram for computing the factors  $A_{ab}$  appearing in the spectrum generator of the  $SU(2)$  theory with  $N_f = 0$ .

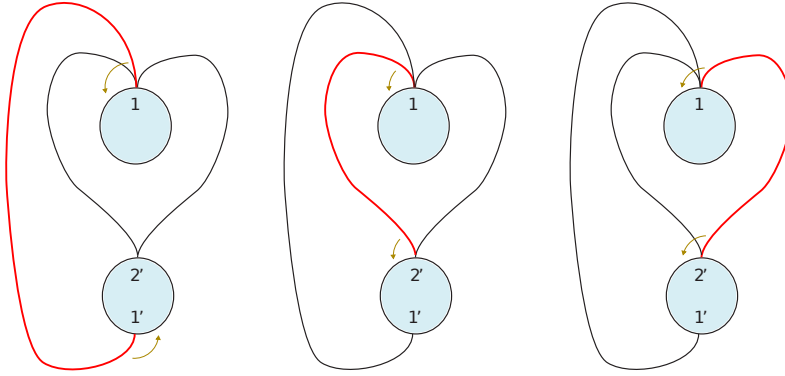


**Figure 82:** Diagram for computing the factors  $A_{ab}$  appearing in the spectrum generator of the  $N_f = 1$  theory.

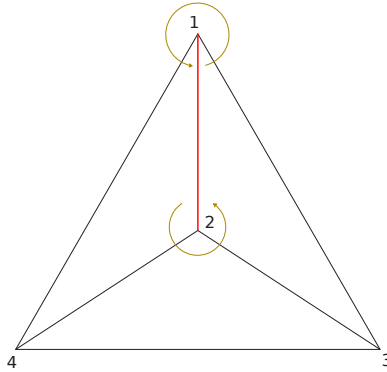


**Figure 83:** Diagram for computing the factor  $A_{12}$  appearing in the spectrum generator of the  $SU(2)$  theory with  $N_f = 4$ .

and 5 more transformations related to this by using tetrahedral symmetry. We can simplify the factors appearing in (11.53) slightly by multiplying numerator and denominator by  $(1 - \mu_1^2)(1 - \mu_2^2)(1 - \mu_3^2)(1 - \mu_4^2)$ . Then, for example, using  $\mu_2^2 = \mathcal{X}_{12}\mathcal{X}_{24}\mathcal{X}_{23}$  and  $\mu_3^2 =$

$\mathcal{X}_{34}\mathcal{X}_{23}\mathcal{X}_{13}$ , we obtain

$$(1 - \mu_2^2)(1 - \mu_3^2)(1 + A_{23}) = 1 + \mathcal{X}_{23} + \mathcal{X}_{12}\mathcal{X}_{23} + \mathcal{X}_{23}\mathcal{X}_{34} + \mathcal{X}_{12}\mathcal{X}_{13}\mathcal{X}_{23}\mathcal{X}_{34} + \mathcal{X}_{12}\mathcal{X}_{23}\mathcal{X}_{24}\mathcal{X}_{34} + \mathcal{X}_{12}\mathcal{X}_{13}\mathcal{X}_{23}\mathcal{X}_{24}\mathcal{X}_{34} + \mathcal{X}_{12}\mathcal{X}_{13}\mathcal{X}_{23}^2\mathcal{X}_{24}\mathcal{X}_{34}. \quad (11.54)$$

Based on the description of the spectrum which we gave in Section 10.7, we expect that the above transformation can be decomposed as

$$\mathcal{K}_{1,-1;-}\mathcal{K}_{0,1;+}^2\mathcal{K}_{0,-1;-}^2\mathcal{K}_{1,1;+}\mathcal{K}_{-1,-1;-}\mathcal{K}_{1,0;+}^2\mathcal{K}_{-1,0;-}^2\mathcal{K}_{1,-1;+}, \quad (11.55)$$

but we have not explicitly checked this.

## 12. Categorical matters

The mathematically oriented reader may wonder how closely the constructions in this paper can be related to the approach to Donaldson-Thomas invariants employed in [6]. In particular, in that approach the starting point is an appropriate category and a family of stability conditions thereon. How are these data realized in our examples? In this section we make a few observations which might help point the way. We are very rough and avoid several important issues, in particular the role of  $\mathbb{Z}$ -gradings in the story.

Let us begin with the case  $K = 2$  (on which we have been concentrating for the last few sections). By analogy to the Fukaya category of a Calabi-Yau threefold, we can then set up the basic story as follows. We have a Riemann surface  $C$  and a space  $\mathcal{B}$  of meromorphic quadratic differentials on  $C$ . Let  $\mathcal{B}' \subset \mathcal{B}$  be the regular locus, consisting of quadratic differentials with only *simple* zeroes. For any point  $u \in \mathcal{B}'$  we have a corresponding double covering  $\Sigma_u \rightarrow C$  equipped with a 1-form  $\lambda$ . In the usual discussion of stability conditions on the Fukaya category one considers a family of Calabi-Yau manifolds which are symplectically isomorphic and so can locally be identified with one fixed symplectic manifold. Similarly here, the various coverings  $\Sigma_u$ , when considered just as topological branched covers of  $C$ , can be identified with a single fixed  $\Sigma$ . Then:

- The objects of our category should be non-intersecting collections of oriented closed paths  $\gamma$  on  $\Sigma$  (or perhaps complexes of such collections of paths), which are anti-invariant under the exchange of the two sheets.
- The space of morphisms between two paths  $\gamma_1, \gamma_2$  should have a basis element for each point of  $\gamma_1 \cap \gamma_2$ .
- The K-theory class of a path  $\gamma$  should be its homology class.
- The space of stability conditions should be the universal cover  $\tilde{\mathcal{B}}$  of  $\mathcal{B}'$ .

Given a point of  $\tilde{\mathcal{B}}$  we can define the *phase function* on a path  $\gamma$  to be the phase of  $\lambda \cdot \partial_t$  where  $\partial_t$  is the positively oriented tangent vector. The stable objects in which we are ultimately interested are paths which have constant phase. This is an analogue of

the special Lagrangian condition which one imposes to define stable objects in the Fukaya category. The central charge function associated to a stability condition is the one we have been using throughout this paper,  $Z_\gamma = \frac{1}{\pi} \oint_\gamma \lambda$ .

If we have a pair of intersecting paths  $\gamma_1, \gamma_2$ , such that their phases near the intersection point obey  $\vartheta_2 < \vartheta_1 < \vartheta_2 + \pi$ , we can define a new path  $\gamma_1 \# \gamma_2$  by smoothing the intersection. We expect that a suitably general  $\gamma$  admits such a decomposition,

$$\gamma = \gamma_1 \# \cdots \# \gamma_n, \quad (12.1)$$

where the individual  $\gamma_i$  are stable, and the phases of the central charges of the constituents  $\gamma_i$  are monotonically decreasing. The existence and uniqueness of such decompositions is an essential prerequisite for the approach of [6] to the wall-crossing formula.

One approach to obtaining such decompositions has been described in [85] using a variant of mean curvature flow. The technology of this paper suggests a possible alternative. Namely, as we described in Section 6.3, for any phase  $\vartheta$  we have a corresponding decomposition of  $C$  into cells, bounded by the separating WKB curves. As we rotate  $\vartheta$  clockwise through generic values, these cells vary continuously, and we can likewise deform  $\gamma$  continuously so that its incidence relations with the separating WKB curves are unchanged. At some critical  $\vartheta = \vartheta_c$  where a BPS hypermultiplet appears, the topology of the cell decomposition changes: one of the cells collapses. This collapsing cell can “trap” a segment of  $\gamma$ , as indicated in Figure 84. This gives a natural splitting of  $\gamma$  into  $\gamma_1$  and  $\gamma'$ ,

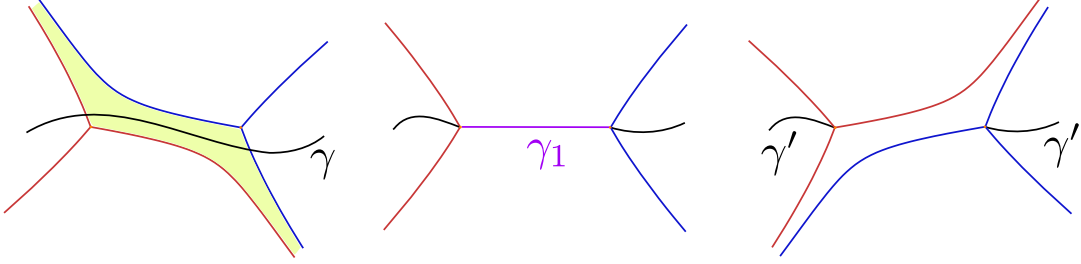


**Figure 84:** As  $\vartheta$  varies one of the cells defined by the WKB foliation (shaded) collapses, trapping a segment of the projection of  $\gamma$  to  $C$ . This gives a natural splitting of  $\gamma$  into  $\gamma_1$  and  $\gamma'$ .

where  $\gamma_1$  is the trapped segment (which is a stable object of phase  $\vartheta_c$ ) and  $\gamma'$  is the rest (perhaps disconnected). Continuing in this way  $\gamma'$  will be further decomposed into objects  $\gamma_i$ . Note that the  $\gamma_i$  naturally come out with their phases ordered, since we are rotating  $\vartheta$  in a definite direction! In this way we can determine geometrically a “Harder-Narasimhan filtration” of an unstable object.

As we remarked in Section 3.3, one actually expects that the theories we are considering can be realized directly via Type IIB string theory on an appropriate non-compact Calabi-Yau threefold. Presumably the category we are describing here should be identified with an appropriate version of the Fukaya category of that threefold.

Finally we note that all of these considerations should have a natural extension to the case  $K > 2$  where we have to consider not only BPS strings but also BPS string webs. The crucial question, of course, is to determine the structure which generalizes the

triangulations  $T_{\text{WKB}}(\vartheta, \lambda)$ , controls the WKB approximation, and encodes the spectrum generator for the theory. Since the first preprint version of this paper appeared, we have made some progress in this direction, to appear in [12].

### 13. $R \rightarrow \infty$ limit

As we reviewed in Section 2, the expectation from [1] is that as  $R \rightarrow \infty$  one should have

$$\mathcal{X}_\gamma^\vartheta \sim \exp(\pi R \zeta^{-1} Z_\gamma + i\theta_\gamma + \pi R \zeta \bar{Z}_\gamma) (1 + \mathcal{O}(e^{-\text{const.} R})) \quad (13.1)$$

so long as  $\zeta$  lies in the half-plane  $\mathbb{H}_\vartheta$  centered on  $e^{i\vartheta}$ . We would like to check that (13.1) indeed holds for the  $\mathcal{X}_\gamma^\vartheta$  we have defined.

We defined  $\mathcal{X}_\gamma^\vartheta$  as functions on the Hitchin moduli space  $\mathcal{M}$ , so in order even to make sense of the equation (13.1), we must make some identification between the moduli spaces  $\mathcal{M}$  for different  $R$ . For this we use the fact that  $\mathcal{M}$  can always be canonically identified with the ( $R$ -independent) moduli space of Higgs bundles, as remarked in Section 4.2.2. On this moduli space, moreover, there is a natural definition of the angular coordinates  $\theta_\gamma$  as we will see below.

Having made sense of (13.1), our strategy for proving it is to give an explicit but *approximate* description of the solution of Hitchin's equations corresponding to any fixed  $(u, \theta)$ . This approximate solution is very close to the true solution in the limit  $R \rightarrow \infty$ ; indeed, by studying linearized perturbations we will argue that it differs from the exact solution  $(A, \varphi)$  only by corrections which are exponentially suppressed as  $R \rightarrow \infty$ . On the other hand, the approximate solution is exactly diagonal along the edges of the WKB triangulation, and hence forms a very convenient starting point for a WKB analysis at large  $R$ . This WKB analysis then gives the desired (13.1).

In this section we will encounter a bit more of the fine structure of  $\mathcal{M}$  than we have seen in other parts of this paper — we have to pay a bit of attention to issues such as finite coverings depending on the precise choice of gauge group. The simplest version of the story arises if we take the gauge group to be  $PSU(2)$  rather than  $SU(2)$ , so for simplicity, we restrict to that case here. Related issues are discussed in the end of Appendix A.

#### 13.1 A parameterization of Higgs bundles

As mentioned above, to identify the moduli spaces  $\mathcal{M}$  at different values of  $R$ , it is convenient to use the Higgs bundle picture which is manifestly  $R$ -independent. We begin by giving a more explicit description of the gauge equivalence classes of Higgs bundles.

So suppose we have a Higgs bundle  $(V, \varphi, \bar{\partial})$ . As usual we write  $\text{Tr } \varphi^2 = 2\lambda^2$  and assume that  $\lambda^2$  has only simple zeroes.  $\lambda^2$  determines a point on the base  $\mathcal{B}$  of the Hitchin fibration. Now we want to parameterize the torus fiber.

Choose any spin structure  $K^{\frac{1}{2}}$  on  $C$ , and identify  $V$  with  $K^{-\frac{1}{2}} \oplus K^{\frac{1}{2}}$ . (The specific choice of spin structure here is irrelevant since different choices give the same  $PSL(2, \mathbb{C})$  bundle.) Then up to gauge equivalence we may take  $\varphi \in \text{End}(K^{-\frac{1}{2}} \oplus K^{\frac{1}{2}}) \otimes K$  of the form

$$\varphi = \begin{pmatrix} 0 & 1 \\ \lambda^2 & 0 \end{pmatrix}. \quad (13.2)$$

Having done so,  $\bar{\partial}\varphi = 0$  implies that  $\bar{\partial}$  differs from the standard holomorphic structure  $\bar{\partial}_0$  on  $K^{-\frac{1}{2}} \oplus K^{\frac{1}{2}}$  only by a matrix commuting with  $\varphi$ . A convenient way of writing this is

$$\bar{\partial} = \bar{\partial}_0 + \begin{pmatrix} 0 & \lambda^{-1} \\ \lambda & 0 \end{pmatrix} a^{0,1}, \quad (13.3)$$

where  $a^{0,1}$  is a  $(0,1)$ -form on the spectral curve  $\Sigma$ , which is odd under the exchange of the two sheets (so that  $\bar{\partial}$  is well defined).

Not all  $a^{0,1}$  give gauge inequivalent Higgs bundles: we should divide out by gauge transformations given by any section  $g_c$  of  $\text{End}(K^{-\frac{1}{2}} \oplus K^{\frac{1}{2}})$  which commutes with (13.2). Such a  $g_c$  can be written as

$$g_c = \exp \left[ i \begin{pmatrix} 0 & \lambda^{-1} \\ \lambda & 0 \end{pmatrix} f \right] \quad (13.4)$$

with  $f$  a complex-valued function on  $\Sigma$ , odd under exchanging sheets. While  $g_c$  must be single-valued,  $f$  need not be: upon going around a cycle  $\gamma \in H_1(\Sigma; \mathbb{Z})$  it may shift by

$$f \rightarrow f + 2\pi n_\gamma \quad (13.5)$$

for some  $n_\gamma \in \mathbb{Z}$ .<sup>42</sup> Such a gauge transformation shifts

$$a^{0,1} \rightarrow a^{0,1} + i\bar{\partial}f. \quad (13.6)$$

Using this freedom we can arrange that

$$da^{0,1} - \overline{da^{0,1}} = 0, \quad (13.7)$$

in other words,  $a^{0,1}$  is actually the  $(0,1)$  part of an imaginary *flat* 1-form

$$\tilde{a} = a^{0,1} - \overline{a^{0,1}}. \quad (13.8)$$

Even after fixing (13.7) there is still some gauge freedom left: if  $f$  is real then the gauge transformation (13.6) preserves (13.7), and transforms

$$\tilde{a} \rightarrow \tilde{a} + idf. \quad (13.9)$$

Hence the fiber of the Hitchin fibration is parameterized by the imaginary flat odd 1-forms  $\tilde{a}$  modulo this equivalence. More explicitly, we can give coordinates on the fiber as

$$\theta_\gamma := i \oint_\gamma \tilde{a} \quad (13.10)$$

for  $\gamma \in \hat{\Gamma}$ . A multivalued gauge transformation as in (13.5) shifts  $\theta_\gamma \rightarrow 2\pi n_\gamma + \theta_\gamma$ , so  $\theta_\gamma \in \mathbb{R}/2\pi\mathbb{Z}$ .

So we have obtained the angular coordinates  $\theta_\gamma$  on the fiber of the Hitchin fibration. We can also think of them in terms of  $\bar{\partial}$ -operators on a topologically trivial complex line bundle modulo complex abelian gauge transformations. If we were to consider all  $\bar{\partial}$ -operators then we would get  $\mathcal{A}^{0,1}/\mathcal{G}_c$ , which is just the Jacobian of the curve  $\Sigma$ . Since  $a^{0,1}$  is odd under deck transformations, we in fact get the Prym subvariety.

<sup>42</sup>There is a delicate point here. We actually consider Higgs bundles with structure group  $PSL(2, \mathbb{C})$ , so  $g_c$  need only be single-valued in that group. One might then have expected that  $n_\gamma$  should be allowed to be half-integer. Actually, requiring that  $g_c$  is well defined near the zeroes of  $\lambda$  turns out to imply that  $n_\gamma$  is an integer.



### 13.2 Reformulating Hitchin's equations

As we described in Section 4.2.2, to each of the Higgs bundles we have just described, there is a corresponding solution of Hitchin's equations [33, 86, 87, 55]. Although the Higgs bundle does not depend on  $R$ , its corresponding solution  $(A, \varphi)$  certainly does, and we are interested in studying its behavior in the  $R \rightarrow \infty$  limit.

The passage from the Higgs bundle  $(V, \varphi, \bar{\partial})$  to the desired  $(A, \varphi)$  proceeds as follows. First, the operator  $\bar{\partial}$  is identified with the  $(0, 1)$  part of  $d + A$ . Next, we fix a Hermitian metric on  $V$ , and then define the  $(1, 0)$  part of  $d + A$  to be minus the adjoint of  $\bar{\partial}$  in this metric, so that the full connection is unitary. We can then ask whether this connection, together with  $\varphi$ , gives a solution of Hitchin's equations or not. (They obviously solve  $\bar{\partial}_A \varphi = 0$ , so the real question is whether  $F + R^2[\varphi, \bar{\varphi}] = 0$ .) For some choice of metric on  $V$ , called the *harmonic metric*, this will indeed be the case.

A convenient way of specifying the harmonic metric is to give the change-of-basis matrix  $B$  between the basis we used in Section 13.1 and a unitary basis. It will be convenient to choose a patch  $U \subset C$ , with local coordinate  $z$ , and a trivialization  $(dz)^{\frac{1}{2}}$  of  $K^{\frac{1}{2}}$  over  $U$ . Then define  $p(z)$  by

$$\lambda^2 = p(z)(dz)^2 \quad (13.11)$$

and a (multivalued) function  $\eta$  by

$$\eta := \left( \frac{p}{\bar{p}} \right)^{1/8} = \frac{p^{1/4}}{|p|^{1/4}}. \quad (13.12)$$

Given a metric there is some freedom in the choice of unitary basis: we fix that freedom by requiring that in this basis  $\varphi$  should be purely off-diagonal and its upper right entry real. Then the most general possible change-of-basis matrix takes the form

$$B = \begin{pmatrix} |p|^{\frac{1}{4}} e^{h/2} & 0 \\ 0 & |p|^{-\frac{1}{4}} e^{-h/2} \end{pmatrix} \exp[\varphi f_c / p^{1/2}] \quad (13.13)$$

where  $h$  is a real-valued function on  $U$ . In the unitary basis one then gets

$$\varphi = \begin{pmatrix} 0 & |p|^{1/2} e^h \\ \frac{p}{|p|^{1/2}} e^{-h} & 0 \end{pmatrix} \quad (13.14)$$

and

$$A = a_{\bar{z}} d\bar{z} \begin{pmatrix} 0 & \bar{\eta}^2 e^h \\ \eta^2 e^{-h} & 0 \end{pmatrix} + a_z dz \begin{pmatrix} 0 & \bar{\eta}^2 e^{-h} \\ \eta^2 e^h & 0 \end{pmatrix} + b \sigma^3, \quad (13.15)$$

where  $a^{0,1} = a_{\bar{z}} d\bar{z}$ , we defined  $a_z := -(a_{\bar{z}})^*$ , and

$$b = (\partial - \bar{\partial}) \log \left( |p|^{\frac{1}{4}} e^{h/2} \right) = \frac{d\eta}{\eta} + \frac{1}{2} (\partial - \bar{\partial}) h. \quad (13.16)$$

Substitution into Hitchin's equations then requires that  $h$  and  $f_c$  satisfy

$$\partial_z \bar{\partial}_{\bar{z}} h - (|p| R^2 + |a_{\bar{z}} + \partial_{\bar{z}} f_c|^2) (e^{2h} - e^{-2h}) = 0, \quad (13.17)$$

$$e^{-h}\partial_z\left(e^{2h}(\partial_{\bar{z}}f_c+a_{\bar{z}})\right)+e^h\bar{\partial}_{\bar{z}}\left(e^{-2h}(\partial_z\bar{f}_c+(a_{\bar{z}})^*)\right)=0. \quad (13.18)$$

(Note that (13.18) is not equivalent to its complex conjugate.) As in the previous section, we partially fix the choice of  $a_{\bar{z}}$  by taking the corresponding imaginary one-form  $\tilde{a}$  to be flat. By a gauge transformation of  $\tilde{a}$  we can moreover take  $f_c$  to be real.<sup>43</sup>

### 13.3 The trivial solution

One obvious choice would be to take  $h = 0$ . In that case (13.17) is obviously solved, while (13.18) becomes

$$2\partial_z\partial_{\bar{z}}f_c+\partial_z a_{\bar{z}}+\bar{\partial}_{\bar{z}}a_{\bar{z}}^*=0, \quad (13.19)$$

which is also solved if we pick  $f_c = 0$ , since we have chosen  $\tilde{a}$  flat.

The only trouble with this solution is that it does not lead to a regular solution of Hitchin's equations. Indeed, with  $h = f_c = 0$ , our change-of-basis matrix  $B$  given in (13.13) becomes singular at the turning points, where  $p = 0$ . Requiring that  $B$  is regular imposes a boundary condition which will force  $h$  to have a singularity at each turning point.

In the next subsection we turn to the discussion of this honest regular solution of Hitchin's equations. We will argue that, if we fix a point  $\mathcal{P}$  which is not a turning point, then, for sufficiently large  $R$ ,  $h(\mathcal{P})$  and  $f_c(\mathcal{P})$  decay exponentially fast as  $R \rightarrow \infty$ . It follows that the “trivial” solution we considered here is actually exponentially close to the exact one.

### 13.4 The regular solution

For simplicity, we will first analyze the case  $\theta_\gamma = 0$ . In this case we can take  $\tilde{a} = 0$ , and clearly then  $f_c = 0$  will solve (13.18). This leads to an important simplification in (13.17): it becomes simply the equation of motion of the sinh-Gordon theory for a scalar field  $h$  on a surface with metric  $ds^2 = |p(z)||dz|^2$ ,

$$\partial_z\bar{\partial}_{\bar{z}}h-R^2|p|(e^{2h}-e^{-2h})=0. \quad (13.20)$$

Multiplying (13.20) by  $h$  and integrating shows that there are no nonsingular solutions with  $h \neq 0$  on any compact Riemann surface. This is just as well, since the only reason we want a solution with  $h \neq 0$  is to deal with our nontrivial boundary conditions, which we now describe.

First, as remarked above, near each zero  $z_a$  of  $p$ , the regularity of  $B$  requires

$$h \sim \log|z-z_a|^{-1/2}. \quad (13.21)$$

We should also discuss the behavior near the singular points  $\mathcal{P}_i \in C$ . Our boundary conditions on Hitchin's equations require that  $h \rightarrow 0$  there. It then follows from (13.16) that  $A \rightarrow \frac{d\eta}{\eta}\sigma^3$ . In particular, the boundary condition on  $A$  at  $\mathcal{P}_i$  can only be satisfied if  $m_i^{(3)} = 0$ . (This is what we expected: we have fixed all  $\theta_\gamma = 0$ , and  $m_i^{(3)} = \theta_\gamma$  for  $\gamma = C_i$ .)

---

<sup>43</sup>Below we will further partially fix  $\tilde{a}$  by taking it to vanish in some neighborhood of the turning points. In this case we cannot necessarily simultaneously take  $f_c$  to be real in this neighborhood. However, we can continue to take it to be real in some neighborhood away from the turning points.

We now argue using perturbation theory that solutions satisfying our boundary conditions exist.<sup>44</sup> Let  $h_{\text{ax}}$  be an approximate solution. The perturbative equation for the true solution  $h = h_{\text{ax}} + \delta h$  is

$$L(h_{\text{ax}})\delta h = E_0(h_{\text{ax}}) + \mathcal{I}(\delta h), \quad (13.22)$$

where  $L(h_{\text{ax}})$  is given by

$$L(h_{\text{ax}}) := \partial_z \bar{\partial}_{\bar{z}} - 4R^2 |p| \cosh(2h_{\text{ax}}), \quad (13.23)$$

the source term to begin the perturbation expansion is

$$E_0(h_{\text{ax}}) = -(\partial \bar{\partial} h_{\text{ax}} - 2R^2 |p| \sinh(2h_{\text{ax}})), \quad (13.24)$$

and  $\mathcal{I}$  are the interaction terms:

$$\mathcal{I} = 2R^2 |p| \left( \sinh(2h_{\text{ax}})(\cosh(2\delta h) - 1) + \cosh(2h_{\text{ax}})(\sinh(2\delta h) - 2\delta h) \right). \quad (13.25)$$

Let  $G(x, y)$  be the Green's function for the operator  $L(h_{\text{ax}})$ . Think of this as the operator in Euclidean space for a massive scalar field in two dimensions, with mass-squared  $4R^2 \cosh(h_{\text{ax}}) > 4R^2$ , on a surface with metric  $ds^2 = |p(z)||dz|^2$ . (Near the zeroes of  $p$  the Green's function reduces to that of a scalar field of mass-squared  $\text{const.} R^2$ .) Therefore, away from turning points, for  $x, y$  at fixed separation in the metric  $|p(z)||dz|^2$ , and as  $R \rightarrow \infty$ , we have

$$|G(x, y)| \sim e^{-2Rd(x, y)} \quad (13.26)$$

or even smaller (because the mass can get bigger), where  $d(x, y)$  is the geodesic distance from  $x$  to  $y$ . On the other hand, as  $d(x, y) \rightarrow 0$  the mass becomes irrelevant to the short-distance behavior and  $G(x, y) \sim -\frac{2}{\pi} \log |z(x) - z(y)|$ . We have

$$\delta h(x) = \int G(x, y) E_0(h_{\text{ax}}(y)) d^2 y \quad (13.27)$$

Now we construct a suitable  $h_{\text{ax}}$ . By a change of variable such that  $dw = 2R\sqrt{p(z)}dz$  we can bring the equation to the form

$$\partial_w \partial_{\bar{w}} h = \frac{1}{2} \sinh(2h). \quad (13.28)$$

In view of our boundary conditions it is natural to search for a solution which is radially symmetric in the  $w$ -coordinate around  $z_a$ . Thus, working in some neighborhood  $D_a = \{z : |z - z_a| = \rho_a\}$  we take  $w = \int_{z_a}^z 2R\sqrt{p(z)}dz$ . Of course,  $w$  is only locally well-defined, but in a suitable neighborhood  $D_a$  of  $z_a$  it will be undefined only up to a sign so that  $|w|$  is well-defined. It therefore makes sense to search for radially symmetric solutions  $h$  which are only functions of  $|w|$  in such a neighborhood. Letting  $x = 2|w|$ , the equation for  $h = \tilde{h}(x)$  reduces to

$$\left( \frac{d^2}{dx^2} + \frac{1}{x} \frac{d}{dx} \right) \tilde{h} = \frac{1}{2} \sinh(2\tilde{h}) \quad (13.29)$$

---

<sup>44</sup>Physically, it is obvious that they exist. These solutions are the semiclassical field configuration in the sinh-Gordon model in the presence of vertex operator sources at the points  $z = z_a$ .

This is the Painlevé III equation and has been well-studied in connection with correlation operators of spin and disorder operators in the massive Ising model. (See, for example [88].) It is known that if

$$\tilde{h}(x) = 2\sigma \log(8/x) - \log(\gamma(\frac{1}{2} - \sigma)) + \mathcal{O}(x^{2\pm 4\sigma}) \quad (13.30)$$

for  $x \rightarrow 0$  then

$$\tilde{h}(x) \rightarrow \frac{2 \sin(\pi\sigma)}{\pi} K_0(x) \quad (13.31)$$

for  $x \rightarrow \infty$  [69]. For our boundary conditions we take  $\sigma = 1/6$ . Let us denote the resulting solution, defined in  $D_a$  as  $h_P^{(a)}$ . Note that at any fixed value of  $z \in D_a$ , for  $R \rightarrow \infty$  we have  $h_P^{(a)} \sim \pi^{-1} K_0(\frac{8R}{3}|z|^{3/2}(1 + \dots))$  and this is exponentially small.

Now let  $C - \Pi_a D_a = \mathcal{F}$  be the complement of the regions near the turning points. We will refer to this as the “fatgraph region” because we regard it as a thickened version of a WKB triangulation. Choose

$$h_{\text{ax}} = \begin{cases} h_P^{(a)} & \text{in } D_a \\ 0 & \text{in } \mathcal{F} \end{cases} \quad (13.32)$$

This choice is convenient since the integral in (13.27) only receives support from the boundary  $\Pi \partial D_a$  of the fatgraph region.

The contribution of the boundary of a disk  $D_a$  to  $\delta h(x)$  can be written as:

$$-\frac{1}{4} \int_0^{2\pi} d\theta \left( \rho_a G(x, \rho_a e^{i\theta}) \partial_\rho h_P^{(a)} - \rho_a \left( \frac{\partial}{\partial \rho} G(x, \rho e^{i\theta}) \right) |_{\rho=\rho_a} h_P^{(a)} \right) \quad (13.33)$$

where we use coordinates  $z = z_a + \rho e^{i\theta}$ . In general, if  $x$  is distance  $\Delta$  away from  $\partial D_a$  in the metric  $|p(z)dz^2|$  then the difference  $|\delta h - h_{\text{ax}}|$  is – very roughly speaking – of order  $e^{-2R\Delta} e^{-\frac{8R}{3}\rho_a^{3/2}}$ , and so is exponentially smaller than  $h_P^{(a)}$  in the regions  $D_a$ .

The one place where this argument fails is when  $x \in \partial D_a$ . At short distances we may replace  $G(x, y) \sim -\text{const.} \log|x - y|$ . One finds that the corrections for  $x \in \partial D_a$  are therefore of order  $h_P^{(a)}$ , as is quite reasonable since the true solution will be  $\mathcal{C}^\infty$  and our initial approximation  $h_{\text{ax}}$  is discontinuous. So we expect the corrections to smooth out the discontinuity. Everywhere else the corrections are exponentially smaller than  $h_P^{(a)}$ .

Thus, we conclude that we have set up a good approximation scheme, and we have shown that we can consistently take  $h = h_{\text{ax}}$ .

Finally, let us consider the modifications to the above  $\theta_\gamma \neq 0$ . One can further partially fix the gauge freedom in the choice of flat gauge field  $\tilde{a}$  by choosing it to vanish near the turning points. Then, one can check that there exists a solution  $f_c$  to (13.18) which is smooth and consistent with our boundary condition on  $h$ . Thus, we can continue to take the same boundary conditions  $h \sim -\frac{1}{2} \log|z - z_a|$  in the neighborhood of the turning points. Away from turning points we construct solutions to the pair of equations (13.17), (13.18) as a perturbation series in both  $h$  and  $f_c$ . If  $h = 0$  we know that  $f_c$  is nonzero. If  $a = 0$  we also know that we can take  $f_c = 0$ . If  $a$  cannot be gauged to zero, because  $\theta_\gamma \neq 0$ , then we cannot set  $f_c = 0$ , but from the differential equation we learn that away

from turning points the derivatives of  $f_c$  are order  $h \times a$  or smaller. Therefore, we expect that  $f_c$  will be exponentially small for  $R \rightarrow \infty$  in the fatgraph region. Note that the presence of nonzero  $\tilde{a} + \bar{\partial}f_c - \partial\bar{f}_c$  simply increases the mass parameter in the Green's function and therefore increases the exponential suppression which makes  $h$  and therefore  $f_c$  small. It would be nice to do better here and really solve the connection problem for  $f_c$  connecting exponentially small solutions in the fatgraph region to appropriate solutions near the turning points.

### 13.5 The large $R$ limit of $\mathcal{X}_\gamma$

The upshot of the last section is that, along the edges of the WKB triangulation, the “trivial” solution described in Section 13.3 is equal to the exact solution of Hitchin's equations, up to corrections that are exponentially suppressed in  $R$ .

Now by using the  $SU(2)$  gauge transformation<sup>45</sup>

$$g = \frac{1}{\sqrt{2}} \begin{pmatrix} \bar{\eta} & -\bar{\eta} \\ \eta & \eta \end{pmatrix}, \quad (13.34)$$

we can bring this trivial solution to a diagonal gauge in which

$$\varphi = p^{1/2} \sigma^3, \quad (13.35)$$

$$A = (\tilde{a} + (\bar{\partial}f_c - \partial\bar{f}_c)) \sigma^3. \quad (13.36)$$

Then, by a computation very similar to that used in Section 7.4 above to compute the  $\zeta \rightarrow 0$  asymptotics of  $\mathcal{X}_\gamma$ , we find that

$$\mathcal{X}_\gamma^\vartheta = \mathcal{X}_\gamma^{\text{sf}} (1 + \mathcal{O}(e^{-cR})), \quad (13.37)$$

where

$$\mathcal{X}_\gamma^{\text{sf}} = \exp[\pi R \zeta^{-1} Z_\gamma + i\theta_\gamma + \pi R \zeta \overline{Z_\gamma}]. \quad (13.38)$$

We conjecture that the optimal value for the above constant  $c$  is given by the norm of the minimal period  $\pi \min_\gamma |Z_\gamma|$ . Indeed, it would be extremely interesting to compute these corrections! Comparison with equation (5.14) of [1] would allow one to extract the BPS degeneracies  $\Omega$ .

### 13.6 The real section

In the above discussion, the case where all  $\theta_\gamma = 0$ , so that we can take  $\tilde{a} = 0$  and  $f_c = 0$ , was particularly simple to analyze. There is also something else interesting about this locus.

Note that by a rigid gauge transformation of (13.14) taking  $(\sigma^1, \sigma^2, \sigma^3) \rightarrow (\sigma^1, \sigma^3, -\sigma^2)$  we can make  $\varphi$  a symmetric matrix, and  $A$  in (13.15) with  $a = 0$  becomes an antisymmetric real matrix. Therefore, if we choose  $\zeta$  to be a phase, then  $\mathcal{A}$  is traceless and real, that is, it

---

<sup>45</sup>This gauge transformation is actually multi-valued even when lifted to  $\Sigma$ ; note however that it would be single-valued on  $\Sigma$  when considered as an element of  $PSU(2)$ . As we noted at the beginning of this section, we are avoiding some subtleties by considering only gauge group  $PSU(2)$ .

is valued in  $sl(2, \mathbb{R})$ . From (6.10) it follows in particular that the monodromy eigenvalues  $\mu_i$  around each  $\mathcal{P}_i$  are real. Hence the monodromy matrix is hyperbolic, and we can choose our decorations (monodromy eigensections) to be real. It follows that the Fock-Goncharov coordinates  $\mathcal{X}_E^T$  are real on this locus. It defines a special “real section” of the Hitchin fibration. This real section has been discussed in [33, 89] and was also a very important ingredient in the considerations of [10].

### 13.7 Relation to Hitchin flows

We conclude this section by checking that the Hitchin flows in the holomorphic symplectic structure at  $\zeta = 0$  act by linear shifts of the  $\theta_\gamma$ .

From equation (4.10) and

$$\varpi_\zeta = -\frac{i}{2\zeta}\omega_+ + \omega_3 - \frac{i}{2}\zeta\omega_- \quad (13.39)$$

we learn that the holomorphic symplectic form in complex structure  $\zeta = 0$  is:

$$\omega_+ = 2iR \int \text{Tr}(\delta\varphi \wedge \delta A^{0,1}). \quad (13.40)$$

Now, using the Higgs bundle point of view, consider a linear flow holding  $\varphi$  fixed while

$$a^{0,1} \rightarrow a^{0,1} - it\omega_\gamma^{0,1} \quad (13.41)$$

Here  $\omega_\gamma$  is a real 1-form, Poincaré dual on  $\Sigma$  to  $\gamma$ , and odd under the deck transformation. This leads to a linear flow  $\theta_{\gamma'} \rightarrow \theta_{\gamma'} + t\langle \gamma', \gamma \rangle$ . Contracting this vector field with the (2, 0) form gives

$$\iota\left(\frac{\partial}{\partial t}\right)\omega_+ = \delta\left(4R \int_C \delta\lambda\omega_\gamma\right) = \delta(2\pi R Z_\gamma) \quad (13.42)$$

From this result we conclude that the symplectic form can be nicely written as

$$\omega_+ = -2\pi R \langle dZ, d\theta \rangle + \omega_+^{\text{horizontal}} \quad (13.43)$$

where  $\omega_+^{\text{horizontal}}$  has zero contraction with the vertical vectors of the Hitchin fibration.

Equation (13.43) is a nice check on our assertion about the  $R \rightarrow \infty$  asymptotics of the coordinates  $\mathcal{X}_\gamma$ . Indeed, if we take the large  $R$  limit of the symplectic form  $\varpi_\zeta := \frac{1}{2}\langle d\log \mathcal{X}, d\log \mathcal{X} \rangle$ <sup>46</sup> we get:

$$\varpi_\zeta \rightarrow \frac{1}{2}\langle \pi R \zeta^{-1} dZ + \pi R \zeta d\bar{Z} + id\theta, \pi R \zeta^{-1} dZ + \pi R \zeta d\bar{Z} + id\theta \rangle \quad (13.45)$$

We can extract the various powers of  $\zeta$ . The coefficient  $\langle dZ, dZ \rangle$  of the double pole vanishes because the  $dZ_\gamma$  are periods of holomorphic differentials.<sup>47</sup> The residue of the simple pole in  $\varpi_\zeta$  at  $\zeta = 0$  agrees with (13.43).

<sup>46</sup>The normalization of  $\varpi(\zeta)$  used in this paper differs from the choice made in [1]. Using equation 5.16 of [1] we find

$$\{\log \mathcal{X}_\gamma, \log \mathcal{X}_{\gamma'}\}_\zeta = 4\pi^2 R \langle \gamma, \gamma' \rangle \quad (13.44)$$

and therefore  $\varpi_\zeta^{\text{here}} = 4\pi^2 R \varpi_\zeta^{\text{there}}$ .

<sup>47</sup>Note that this would *not* happen if we allowed  $Z$  to vary arbitrarily in  $\text{Hom}(\hat{\Gamma}, \mathbb{C})$ , as one does in the theory of Bridgeland stability conditions [90]. The Coulomb branch  $\mathcal{B}$  is locally a Lagrangian subspace of an appropriate space of Bridgeland stability conditions.

The Hamiltonians  $Z_\gamma$  are closely related to the standard “Hitchin Hamiltonians”  $h_a$ . The latter are functions on  $\mathcal{B}$  defined by expanding the quadratic differential  $\text{Tr}\varphi^2$  as

$$\text{Tr}\varphi^2 = \sum h_a \beta_a, \quad (13.46)$$

where  $\beta_a$  are a basis of quadratic differentials with second order poles at  $\mathcal{P}_i$ . For the case of  $l$  regular singularities on  $\mathbb{CP}^1$ ,  $a = 1, \dots, 2l - 3$ . On the other hand, we can expand  $\lambda = \sum_{k=1}^{3l-6} Z_{\gamma_k} \alpha_k$ , where  $\alpha_k$  are meromorphic one-forms on  $\Sigma$  dual to a basis  $\gamma_k$  for  $\hat{\Gamma}$ , anti-invariant under the exchange of sheets,  $\sigma^*(\alpha_k) = -\alpha_k$ . Now,  $\lambda^2 = \frac{1}{2} \text{Tr}\varphi^2 = \sum_{k,j} Z_{\gamma_k} Z_{\gamma_j} \alpha_k \alpha_j$ . But  $\alpha_k \alpha_j$  are invariant under  $\sigma$  and hence can be expanded in the basis  $\beta_a$ . In this way we can write the standard Hamiltonians  $h_a$  as quadratic polynomials in the periods  $Z_{\gamma_k}$ .

#### 14. Comparison with [1]: differential equations and the Riemann-Hilbert problem

In this section we would like to compare the properties of the Darboux coordinates  $\mathcal{X}_\gamma^\theta$  constructed in this paper with the properties of the coordinates  $\mathcal{X}_\gamma^{\text{RH}}$  whose existence was established in [1].

One important property of the  $\mathcal{X}_\gamma^{\text{RH}}$  of [1] is that (letting  $\mathcal{X}$  stand for any of the  $\mathcal{X}_\gamma^{\text{RH}}$  or any function of them) they satisfy a set of differential equations of the form

$$\partial_{u^j} \mathcal{X} = \left( \frac{1}{\zeta} \mathcal{A}_{u^j}^{(-1)} + \mathcal{A}_{u^j}^{(0)} \right) \mathcal{X}, \quad (14.1)$$

$$\partial_{\bar{u}^j} \mathcal{X} = \left( \mathcal{A}_{\bar{u}^j}^{(0)} + \zeta \mathcal{A}_{\bar{u}^j}^{(1)} \right) \mathcal{X}, \quad (14.2)$$

$$\Lambda \partial_\Lambda \mathcal{X} = \left( \frac{1}{\zeta} \mathcal{A}_\Lambda^{(-1)} + \mathcal{A}_\Lambda^{(0)} \right) \mathcal{X}, \quad (14.3)$$

$$\bar{\Lambda} \partial_{\bar{\Lambda}} \mathcal{X} = \left( \mathcal{A}_{\bar{\Lambda}}^{(0)} + \zeta \mathcal{A}_{\bar{\Lambda}}^{(1)} \right) \mathcal{X}, \quad (14.4)$$

$$R \partial_R \mathcal{X} = \left( \frac{1}{\zeta} \mathcal{A}_R^{(-1)} + \mathcal{A}_R^{(0)} + \zeta \mathcal{A}_R^{(1)} \right) \mathcal{X}, \quad (14.5)$$

$$\zeta \partial_\zeta \mathcal{X} = \left( \frac{1}{\zeta} \mathcal{A}_\zeta^{(-1)} + \mathcal{A}_\zeta^{(0)} + \zeta \mathcal{A}_\zeta^{(1)} \right) \mathcal{X}. \quad (14.6)$$

On the right hand side of (14.1) we have introduced a connection  $\mathcal{A}$  on the space  $\mathcal{B} \times \mathbb{C}^\times \times \mathbb{R}_+$ . It is not to be confused with the  $\mathcal{A}$  on  $C$ , defined in (4.8)! The various pieces of the connection  $\mathcal{A}$  are complex vector fields on the torus fibers of  $\mathcal{M}$ , i.e. differential operators in some basis of angular coordinates  $\theta_a$ , evaluated at constant  $u, \bar{u}$ . On the right side we have also explicitly exhibited the  $\zeta$  dependence of the connection.

In writing these equations it is most natural to view the  $\mathcal{X}$  as functions not just on  $\mathcal{M}$ , but on an extended version of  $\mathcal{M}$ , where the parameters  $m_i, m_i^{(3)}$  determining the residues at the singularities  $\mathcal{P}_i$  are allowed to vary. The base  $\mathcal{B}$  is then extended to include  $m_i$  while the torus fiber is extended to include  $m_i^{(3)}$ .

Notice that if any set of coordinates satisfies these equations, then every other coordinate system related to it by a  $(R, \zeta)$ -independent coordinate transformation also satisfies

them. So in particular, if any set  $\mathcal{X}_\gamma^\vartheta$  satisfy them, or any  $\mathcal{X}_E^T$  for some triangulation does, then so do more conventional coordinates such as traces of monodromy matrices (as these are written as certain rational functions of the  $\mathcal{X}_E^T$  — see Appendix A).

One can obtain these differential equations simply from our asymptotic analysis. Here let us just discuss the most important example, the equation (14.6) controlling the  $\zeta$  dependence.<sup>48</sup> Consider a basis of coordinate functions  $\mathcal{X}_i$  and angles  $\theta_a$ , and define a vector field on the torus fiber by

$$\mathcal{A}_\zeta = \zeta \frac{\partial \mathcal{X}_i}{\partial \zeta} \left[ \frac{\partial \mathcal{X}_i}{\partial \theta_a} \right]^{-1} \frac{\partial}{\partial \theta_a}. \quad (14.7)$$

By the chain rule, this definition is clearly independent both of the specific parametrization of the torus fiber, and of the choice of coordinate system  $\mathcal{X}_i$ . The Jacobian  $\frac{\partial \mathcal{X}}{\partial \theta}$  is indeed invertible for a good coordinate system  $\mathcal{X}$ , as  $\mathcal{M}$  in any complex structure  $J^{(\zeta)}$  away from  $\zeta = 0, \infty$  is locally the complexification of the torus fiber. So we have more or less tautologically

$$\zeta \partial_\zeta \mathcal{X} = \mathcal{A}_\zeta \mathcal{X}. \quad (14.8)$$

Now depending on which properties of  $\mathcal{A}_\zeta$  have to be determined, different choices of coordinate system  $\mathcal{X}$  are appropriate. To show that  $\mathcal{A}_\zeta$  is holomorphic away from  $\zeta = 0, \infty$ , it is useful to use around each value of  $\zeta$  and point in  $\mathcal{M}$  some coordinate system which is good around that point. As long as the sections  $s_i, s_j$  given by the decoration do not coincide along some edge  $E_{ij}$  of  $T$ , the Fock-Goncharov coordinate system  $\mathcal{X}^T$  is fine; moreover, the traces of monodromy matrices around various cycles of  $C$  provide a perfectly sensible global choice of coordinates. To show that  $\mathcal{A}_\zeta$  has poles of order at most one at  $\zeta = 0, \infty$ , we consider the coordinate system  $\mathcal{X}^\vartheta$ , while letting  $\zeta$  approach 0 or  $\infty$  inside  $\mathbb{H}_\vartheta$ . Plugging the known asymptotics of  $\mathcal{X}^\vartheta$  into (14.7) then gives the desired information about  $\mathcal{A}_\zeta$ . So we obtain the desired (14.6).

The system of compatible differential equations (14.1)-(14.6) is quite powerful. In a finite-dimensional context where the operators  $\mathcal{A}$  are matrices instead of differential operators, such an equation would be directly equivalent to a Riemann-Hilbert problem. In our infinite-dimensional case, though, the differential equation (14.6) is not strong enough to guarantee that the solutions are holomorphic in  $\zeta$  away from  $\zeta = 0, \infty$ . (That is obvious from the fact that any rational function of some  $\mathcal{X}$  satisfying (14.1)-(14.6) also satisfies (14.1)-(14.6).)

For sufficiently large  $R$ , the error of the WKB analysis can be bounded with some work, so it should be possible to guarantee that the small flat section at one end of a WKB curve will never coincide with the small flat section at the other end, which means  $\mathcal{X}_\gamma^\vartheta$  will not have a pole in the neighborhood of the ray  $\zeta \in e^{i\vartheta} \mathbb{R}_+$ . For small  $R$ , though, we can see no clear way to rule out this possibility. Indeed, the WKB triangulation only carries information about the Higgs field  $\varphi$ : any constraint on the gauge connection  $A$  comes only very indirectly, from the solution of the Hitchin equations. It is conceivable

---

<sup>48</sup>If we view  $\mathcal{M}$  as the moduli space of Higgs bundles, extended by the parameters  $m_i$  and  $m_i^{(3)}$ , then this equation just represents the infinitesimal generator of the  $\mathbb{C}^\times$  action infinitesimally rescaling the Higgs field  $\varphi$ .



that nevertheless there is never a flat section  $s$  which is small at both ends of an edge in  $T_{\text{WKB}}$ , but we have not found any indications in favor of, or against, such a conjecture.

As a result, we can only assert with certainty that for sufficiently large  $R$  the coordinates  $\mathcal{X}_\gamma$ , and hence the metric on the Hitchin system moduli space, can be determined from the general Riemann-Hilbert problem formulated in [1], combined with the spectrum generator (Stokes matrix) computed here. It would be interesting to find out whether the Riemann-Hilbert problem simply fails to have a solution for small  $R$ , or if a solution exists, but gives the wrong metric. We hope to present some numerical tests in a future publication.

## Acknowledgements

We thank Aaron Bergman, Tom Bridgeland, Ron Donagi, David Dumas, Alexander Goncharov, Sergei Lukyanov, Sav Sethi, Ivan Smith, Yan Soibelman, Jörg Teschner, Valerio Toledano Laredo, Edward Witten, Xi Yin, and Sasha Zamolodchikov for helpful discussions and correspondence.

The work of GM is supported by the DOE under grant DE-FG02-96ER40949. We thank the KITP at UCSB for hospitality during the course of part of this work and therefore this research was supported in part by DARPA under Grant No. HR0011-09-1-0015 and by the National Science Foundation under Grant No. PHY05-51164. GM would like to thank the Galileo Galilei Institute and the Aspen Center for Physics for hospitality during the completion of this work. The work of AN is supported by the NSF under grant numbers PHY-0503584 and PHY-0804450. D.G. is supported in part by the DOE grant DE-FG02-90ER40542. D.G. is supported in part by the Roger Dashen membership in the Institute for Advanced Study.

## A. Expressing monodromy matrices in terms of Fock-Goncharov coordinates

In this appendix we give a simple argument that shows that the Fock-Goncharov coordinates  $\mathcal{X}_E^T$  really do provide a system of coordinates on a patch of  $\mathcal{M}$  defined by a decorated triangulation  $T$ . Of course, this result already appears in the work of Fock and Goncharov [10] (see Theorem 1.8 and Section 6.6 of that paper), as well as related literature on Teichmüller theory (see e.g. [91] and references therein), but for completeness, we give a proof here.

We would like to compute the monodromy matrix for a closed path  $P$  in  $C$ . If we can show that the traces of the powers of the monodromy matrix can be expressed in terms of  $\mathcal{X}_E^T$  then we are done, since those functions provide a complete set of gauge invariant functions on  $\mathcal{M}$ . It suffices to consider a simple closed curve with no self-intersections, and we restrict attention to this case.

Choosing a basepoint, the path  $P$  will begin in some triangle  $t_1$ , and pass through a number of triangles  $t_1, \dots, t_m$  in succession and then return to  $t_1$ . Associated to each triangle in this sequence we can consider three bases of flat sections, defined up to a common scale.

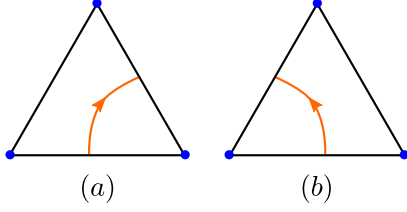


**Figure 85:** The right and left turns, given by simple matrices.

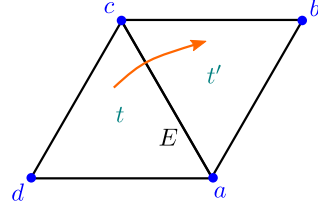


**Figure 86:** Passing through an edge  $E$  between triangles  $t$  and  $t'$ .

To define these, focus on one particular (oriented) triangle  $t \in T$  and label the vertices 1, 2, 3 in counterclockwise order around the boundary of  $t$ . Then to each edge  $E_{ij}$  of the triangle (where  $ij = 12, 23$  or  $31$ ) we associate an ordered basis of flat sections:

$$\mathcal{B}(E_{ij}, t) := (s_i(s_j \wedge s_k), s_j(s_k \wedge s_i)) \quad (\text{A.1})$$

Here we have used the decoration to choose  $s_i, s_j, s_k$  associated with each vertex, and  $i, j, k$  is in counterclockwise order. Of course, the decoration only defines each  $s_i$  up to scale, so we must make an *ad hoc* choice of three scales. Notice that different choices just change the basis  $\mathcal{B}(E_{ij}, t)$  by an overall scalar.

Now,  $s_i, s_j, s_k$  are initially defined in cut neighborhoods of the vertices  $i, j, k$ . They can be continued to be single-valued in the entire triangle  $t$ , and indeed can be continued into the next triangle  $t'$  met by the path  $P$  to be well-defined and single-valued in the larger region  $t \cup t'$  and so on, as long as the region remains simply connected. We will compute the monodromy matrix by computing the changes of basis from one such basis to another around the path  $P$ . There are two distinct kinds of change of basis we will need. If our path enters a triangle  $t$  through an edge  $E$  and leaves triangle  $t$  through edge  $E'$  then we will need the change of basis  $M_E^{E'}(t)$  computing the change of bases associated to the two edges within the triangle  $t$ . This is illustrated in Figure 85. On the other hand, if the path passes through an edge  $E$  from triangle  $t$  to triangle  $t'$  then we will need the change of basis  $M_t^{t'}(E)$  between the two different bases, as shown in Figure 86.

We first show how to compute  $M_E^{E'}(t)$ . Within a triangle  $t$  we have the simple relation

$$s_1(s_2 \wedge s_3) + s_2(s_3 \wedge s_1) + s_3(s_1 \wedge s_2) = 0 \quad (\text{A.2})$$

Using this relation it is then trivial to compute the change of basis

$$\mathcal{B}(E, t) = \mathcal{B}(E', t) M_E^{E'}(t) \quad (\text{A.3})$$

where

$$M_E^{E'}(t) = \begin{cases} \begin{pmatrix} 0 & -1 \\ 1 & -1 \end{pmatrix} & \langle E, E' \rangle = +1 \\ \begin{pmatrix} -1 & 1 \\ -1 & 0 \end{pmatrix} & \langle E, E' \rangle = -1 \end{cases} \quad (\text{A.4})$$

Note that  $\det M_E^{E'}(t) = 1$ , and that the case  $\langle E, E' \rangle = 1$  corresponds to a *right* turn, labeled a) in Figure 85. Note also that the right-turn matrix is the inverse of the left-turn.

On the other hand, if  $t \cup t'$  make a quadrilateral  $Q_E$  with vertices  $a, b, c, d$  in counter-clockwise order, (so  $t$  has vertices  $acd$  and  $t'$  has vertices  $abc$ , and  $E$  is the edge  $ac$ , as in Figure 86) then

$$\mathcal{B}(E, t') = \mathcal{B}(E, t) \begin{pmatrix} 0 & \frac{s_b \wedge s_c}{s_c \wedge s_d} \\ \frac{s_a \wedge s_b}{s_d \wedge s_a} & 0 \end{pmatrix} \quad (\text{A.5})$$

and hence

$$M_t^{t'}(E) = \frac{s_b \wedge s_c}{s_c \wedge s_d} \begin{pmatrix} 0 & 1 \\ -\mathcal{X}_E^T & 0 \end{pmatrix} \quad (\text{A.6})$$

In the argument below it will be useful to denote

$$\hat{M}_t^{t'}(E) := \begin{pmatrix} 0 & 1 \\ -\mathcal{X}_E^T & 0 \end{pmatrix} \quad (\text{A.7})$$

Note that  $\det \hat{M}_t^{t'}(E) = \mathcal{X}_E^T$ .

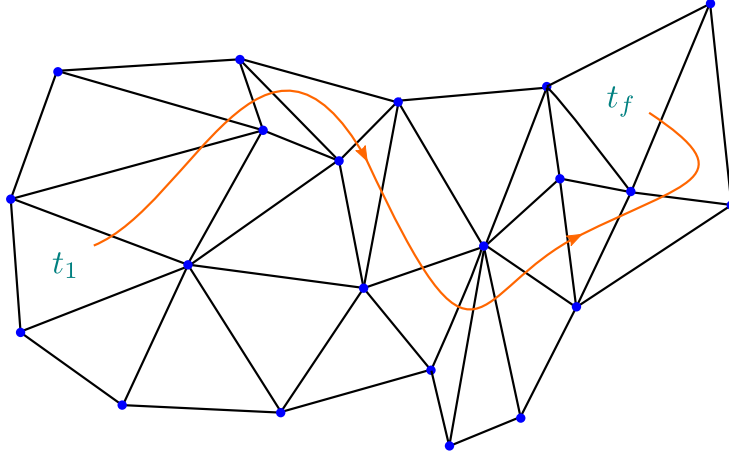


**Figure 87:** We compute the monodromy along the orange path by a series of basis changes within and between the successive triangles.

Now consider a path through several triangles as in Figure 87. After parallel transport of the basis  $\mathcal{B}(E_1, t_1)$  along an open path to a basis  $\tilde{\mathcal{B}}(E_1, t_1)$  which is single-valued throughout a simply connected region assembled by the successive triangles we have the relation in the final triangle  $t_f$  of the open path:

$$\mathcal{B}(E_f, t_f) = \tilde{\mathcal{B}}(E_1, t_1) M_{E_1}^{E_2}(t_1) M_{t_1}^{t_2}(E_2) M_{E_2}^{E_3}(t_2) \cdots M_{t_{f-1}}^{t_f}(E_f) \quad (\text{A.8})$$

Now suppose we close the path, taking  $t_f = t_1$  and  $E_f = E_1$ . Then  $\tilde{\mathcal{B}}(E_1, t_1) = \mathcal{B}(E_1, t_1) \cdot \mathcal{U}(P)$  where  $\mathcal{U}(P)$  is the monodromy matrix for the closed path  $P$  expressed in the basis  $\mathcal{B}(E_1, t_1)$ . Since this basis is well-defined up to scale and  $\mathcal{U}(P)$  changes by conjugation under any change of basis, it follows that  $\mathcal{U}(P)$  is a well-defined  $SL(2, \mathbb{C})$  matrix, independent of the choices of scale of  $s_i, s_j, s_k$  made for  $\mathcal{B}(E_1, t_1)$ . Therefore  $\mathcal{U}^{-1}$  is the above product of  $M$ -matrices. Now, because of the scalar prefactor  $\frac{s_b \wedge s_c}{s_c \wedge s_d}$  in equation (A.6) it is not obvious that the monodromy matrix  $\mathcal{U}(P)$  can be expressed in terms of the edge coordinates.

However, we can use the following trick. The matrix  $\mathcal{U}(P)^{-1}$ , is up to a scalar factor, the same as the product where we replace the factors  $M_t^{t'}(E)$  by  $\hat{M}_t^{t'}(E)$ . That is, we have

$$\mathcal{U}(P)^{-1} = \kappa M_{E_1}^{E_2}(t_1) \hat{M}_{t_1}^{t_2}(E_2) M_{E_2}^{E_3}(t_2) \cdots \hat{M}_{t_{f-1}}^{t_f}(E_f) \quad (\text{A.9})$$

for some scalar factor  $\kappa$ . We can determine  $\kappa^2$  by taking a determinant:

$$\kappa^{-2} = \mathcal{X}_{E_2}^T \cdots \mathcal{X}_{E_f}^T \quad (\text{A.10})$$

thus,  $\kappa$  involves a square-root of the product of  $\mathcal{X}_E^T$  along the edges met by the path  $P$ . In order to define this square root we may invoke a kind of nonabelian version of Stokes theorem: if  $C$  is a punctured  $\mathbb{CP}^1$  then the closed curve  $P$  bounds a region  $\mathcal{R}$ , and by a generalization of Section 5.2, we have

$$\mathcal{X}_{E_2}^T \cdots \mathcal{X}_{E_f}^T \prod_{E \in \text{Int}(\mathcal{R})} (\mathcal{X}_E^T)^2 = \prod_{v \in \text{Int}(\mathcal{R})} (\mu_v)^2. \quad (\text{A.11})$$

This formula allows us to choose the square root in a canonical way, namely

$$\kappa = (\mathcal{X}_{E_2}^T \cdots \mathcal{X}_{E_f}^T)^{-1/2} = \frac{\prod_{E \in \text{Int}(\mathcal{R})} \mathcal{X}_E^T}{\prod_{v \in \text{Int}(\mathcal{R})} \mu_v}. \quad (\text{A.12})$$

We conclude with several remarks:

1. In the above discussion we have assumed that all the triangles are nondegenerate. If there is a degenerate configuration such as shown in Figure 19 then we think of the edge  $E$  as being doubled. Thus, we choose decorations  $s_1$  at the central vertex and  $s_2$  at the outer vertex and use the triplet of sections  $s_1, Ms_2, s_2$  in the above construction, where  $M$  is the clockwise monodromy around the central vertex. In particular we regard  $E$  as having two “sides” with basis  $\mathcal{B}_{\text{left}} = \{s_1(Ms_2 \wedge s_2), Ms_2(s_2 \wedge s_1)\}$  on the left and  $\mathcal{B}_{\text{right}} = \{s_2(s_1 \wedge Ms_2), s_1(Ms_2 \wedge s_2)\}$  on the right. For a path that winds around avoiding the edge  $E$  we use an edge-to-edge transformation to relate these two bases. For a path that goes from left to right through the edge  $E$  we analytically continue  $\mathcal{B}_{\text{left}}$  through the edge with  $M^{-1}$  and obtain the change of basis

$$\mathcal{B}_{\text{right}} = \tilde{\mathcal{B}}_{\text{left}} \begin{pmatrix} 0 & \mu \\ -\mu^{-1} & 0 \end{pmatrix}. \quad (\text{A.13})$$

A similar remark applies to the outer degenerate triangle in Figure 20.

2. In generalizing this result to the case where  $C$  is a punctured surface of higher genus, we need to choose a system of square-roots  $(\mathcal{X}_{E_2}^T \cdots \mathcal{X}_{E_f}^T)^{-1/2}$ . It suffices to provide them for a basis of nonbounding cycles, and hence the set of such choices is a torsor for  $H_1(\tilde{C}, \mathbb{Z}_2)$ .
3. The monodromy matrix elements are evidently *polynomials* in the  $\mathcal{X}_E^T$  (divided by factors of  $\mu_v$ ), and in particular, the traces of the monodromy matrices for closed paths  $P$  can be written as

$$\text{Tr } \mathcal{U}(P) = \sum_{\gamma} a_{\gamma}(P) \mathcal{X}_{\gamma}. \quad (\text{A.14})$$

The geometrical coefficients  $a_\gamma(P)$  depend on the triangulation and in particular depend on  $\vartheta$ . Notice that the left-hand-side of (A.14) is independent of  $\vartheta$ , so that  $a_\gamma(P)$  and  $\mathcal{X}_\gamma^\vartheta$  must have compensating discontinuities. In the 5d Yang-Mills theory,  $\text{Tr } \mathcal{U}(P)$  is the vev of a supersymmetric Wilson line operator for  $\mathcal{A}$  along a path  $P$  in  $C$ . Clearly, it originates from a surface operator in the nonabelian six-dimensional  $(2,0)$  theory, wrapping a one-cycle in  $C$  times  $S_R^1$ . This represents a line operator in the ultraviolet four dimensional gauge theory. Depending on the cycle  $\gamma$ , this line operator can be a Wilson loop operator for the four dimensional gauge fields, an 't Hooft operator or a more general Wilson-'t Hooft operator. With this fact in mind, we interpret equation (A.14) as a relation between the line operators defined in the UV theory and their decomposition into a different basis of line operators which carry quantum numbers for the IR abelian theory. Indeed, the  $\mathcal{X}_\gamma$  are expectation values of line operators wrapped around  $S_R^1$ , defined in the IR four-dimensional  $\mathcal{N} = 2$  theory, (or equivalently, surface operators in the IR abelian  $(2,0)$  theory on  $\mathbb{R}^{1,2} \times S_R^1 \times \Sigma$ .)

There is a  $\zeta$ -dependent nilpotent supersymmetry operator  $Q_\zeta$  which annihilates these operators, and hence they are analogues of the supersymmetric 't Hooft-Wilson line operators similar to those discussed in [92, 93, 14]. With this interpretation, equation (A.14) encodes some interesting physics, which we hope to write about on another occasion.

4. There is a subtle point regarding the distinction between the moduli space of  $SL(2, \mathbb{C})$  and  $PSL(2, \mathbb{C})$  connections. In this paper we are considering connections on a trivialized  $SL(2, \mathbb{C})$  principal bundle over  $C$ , or on its quotient by the center, which is a trivialized  $PSL(2, \mathbb{C})$  bundle. There is a one-one correspondence between connections on these two bundles. However, there are  $PSL(2, \mathbb{C})$  gauge transformations which do not lift to  $SL(2, \mathbb{C})$  gauge transformations, so the moduli space of  $SL(2, \mathbb{C})$  connections is a discrete cover of the moduli space of  $PSL(2, \mathbb{C})$  connections. The  $\mathcal{X}_\gamma$  are defined on the quotient moduli space of  $PSL(2, \mathbb{C})$  connections, and can be pulled back to the moduli space of  $SL(2, \mathbb{C})$  connections. If we think of the moduli space as determined by specifying the monodromy eigenvalues  $\mu_i$  and not just  $\mu_i^2$ , then, when  $C = \mathbb{CP}^1$ , the  $\mathcal{X}_E^T$  uniquely determine a flat  $SL(2, \mathbb{C})$  connection modulo  $SL(2, \mathbb{C})$  gauge invariance. For  $C$  of higher genus, the  $\mathcal{X}_E^T$  do not quite separate points on the moduli space of  $SL(2, \mathbb{C})$  connections, even if we have specified the  $\mu_i$ : to determine the connection from the  $\mathcal{X}_E^T$ , we also need to specify the system of square roots  $(\mathcal{X}_{E_2}^T \cdots \mathcal{X}_{E_f}^T)^{-1/2}$ . The existence of these choices raises the question of what is the “correct” moduli space of the four dimensional gauge theory on  $\mathbb{R}^3 \times S^1$ . Should it be the moduli space of  $SL(2, \mathbb{C})$  connections, of  $PSL(2, \mathbb{C})$  connections or of some intermediate cover of the moduli space of  $PSL(2, \mathbb{C})$  connections? Interestingly, defining the appropriate four dimensional gauge theory also involves a discrete choice which might correspond to the above ambiguity. As described in [15], the appropriate four-dimensional gauge theories are generalized quivers of  $SU(2)$  gauge groups. A subgroup  $\mathcal{C}$  of the center of the gauge groups acts trivially on the matter fields, and there is a freedom to quotient the gauge group by any subgroup of  $\mathcal{C}$ . A

comparison with the well known case of the  $\mathcal{N} = 2^* SU(2)$  gauge theory, associated to the Hitchin equations on a once-punctured torus, should be sufficient to establish the full dictionary, but we will not pursue this matter further here.

## B. Computing the Hamiltonian flows

We begin with an auxiliary computation. Choose a path  $\gamma$ , parameterized as  $z(t)$ ,  $0 \leq t \leq 1$ . Define  $z_i = z(0)$  and  $z_j = z(1)$ . For the moment we take them to be regular points. Let  $s_i$  and  $s_j$  denote two flat sections along  $\gamma$ , with fixed boundary conditions  $s_i(t=0) = d_i$  and  $s_j(t=1) = d_j$ . Given these two sections we may consider the section  $s_i \wedge s_j$  of  $\wedge^2(V)$ . For convenience we also choose a flat section  $\epsilon$  of  $\wedge^2(V^*)$  (volume form); this may always be done since  $\mathcal{A}$  is  $sl(2)$ -valued. If we normalize by contracting with  $\epsilon$ , we can regard  $s_i \wedge s_j$  as a number, and we do this in what follows; in a local frame for  $V$ ,

$$s_i \wedge s_j = \epsilon_{ab} s_i^a(t) s_j^b(t). \quad (\text{B.1})$$

Since  $\epsilon$  and  $s_{i,j}$  are all flat,  $s_i \wedge s_j$  is independent of  $t$ . In what follows it is also convenient to use  $\epsilon$  to relate the section  $s_i^a$  of  $V$  to a dual section  $s_{ia}$  of  $V^*$ . In a local frame

$$s_{ia}(t) = \epsilon_{ab} s_i^b(t). \quad (\text{B.2})$$

Now define a function on the space  $\mathcal{N}$  of “all gauge fields” by

$$\mathcal{O}_{\gamma, d_i, d_j} := \log(s_i \wedge s_j). \quad (\text{B.3})$$

We want to compute  $\{\mathcal{O}_{\gamma, d_i, d_j}, \mathcal{A}_{\lambda b}^a(z)\}$ . We choose the sign of the Poisson bracket associated to (4.10) to be

$$\{\mathcal{O}, \mathcal{A}_{\lambda b}^a(z)\} = \epsilon_{\lambda\mu} \frac{\delta \mathcal{O}}{\delta \mathcal{A}_{\mu a}^b(z)}. \quad (\text{B.4})$$

Choose some  $t_*$  with  $z(t_*) \neq z$ , and evaluate  $\mathcal{O}_{\gamma, d_i, d_j}$  at this point; then (B.4) becomes

$$\{\mathcal{O}_{\gamma, d_i, d_j}, \mathcal{A}_{\lambda b}^a(z)\} = \frac{\epsilon_{\lambda\mu}}{s_i \wedge s_j} \epsilon_{a'b'} \left( \frac{\delta s_i^{a'}(t_*)}{\delta \mathcal{A}_{\mu a}^b(z)} s_j^{b'}(t_*) + s_i^{a'}(t_*) \frac{\delta s_j^{b'}(t_*)}{\delta \mathcal{A}_{\mu a}^b(z)} \right). \quad (\text{B.5})$$

To evaluate this we first introduce a bit of notation for the parallel transport: write  $\mathcal{A}(t) = \mathcal{A}_\mu(t) \dot{z}^\mu(t)$ , and let  $U(t_1, t_2)$  be the parallel-transport matrix from  $t_2$  to  $t_1$ , obeying

$$\frac{d}{dt_1} U(t_1, t_2) = -\mathcal{A}(t_1) U(t_1, t_2), \quad (\text{B.6})$$

$$\frac{d}{dt_2} U(t_1, t_2) = U(t_1, t_2) \mathcal{A}(t_2), \quad (\text{B.7})$$

and the boundary condition  $U(t, t) = \mathbf{1}$ . Then we have

$$\frac{\delta}{\delta \mathcal{A}_{\mu b}^a(z)} U(t_1, t_2)^c{}_d = \int_{t_1}^{t_2} dt \delta^{(2)}(z - z(t)) \dot{z}^\mu(t) U(t_1, t)^c{}_a U(t, t_2)^b{}_d. \quad (\text{B.8})$$

It follows that the variations of  $s_{i,j}$  with respect to  $\mathcal{A}$  are given by

$$\frac{\delta s_i^{a'}(t_*)}{\delta \mathcal{A}_{\mu a}^b(z)} = - \int_0^{t_*} dt \delta^{(2)}(z - z(t)) \dot{z}^\mu(t) \left[ U(t_*, t) a'_b s_i^a(t) - \frac{1}{2} \delta_b^a s_i^{a'}(t_*) \right], \quad (\text{B.9})$$

$$\frac{\delta s_j^{b'}(t_*)}{\delta \mathcal{A}_{\mu a}^b(z)} = \int_{t_*}^1 dt \delta^{(2)}(z - z(t)) \dot{z}^\mu(t) \left[ U(t_*, t) b'_b s_j^a(t) - \frac{1}{2} \delta_b^a s_j^{b'}(t_*) \right]. \quad (\text{B.10})$$

(The subtraction term arises because we are varying  $\mathcal{A}$  within the space of  $sl(2)$  connections, not  $gl(2)$  connections, so we should project out the trace.) Now using

$$s_i^a(t) s_{jb}(t) - \frac{1}{2} \delta_b^a s_i \wedge s_j = \frac{1}{2} (s_{ib} s_j^a + s_{jb} s_i^a)(t) \quad (\text{B.11})$$

(proven by contracting the dual index with a basis  $s_i^a, s_j^a$ ), we arrive at

$$\{\mathcal{O}_{\gamma, d_i, d_j}, \mathcal{A}_{\lambda b}^a(z)\} = \frac{1}{2} \epsilon_{\lambda \mu} \int_0^1 dt \delta^{(2)}(z - z(t)) \dot{z}^\mu(t) M(s_i, s_j)^a_b(t), \quad (\text{B.12})$$

where we defined the operator

$$M(s_i, s_j)^a_b(t) := \frac{s_{ib}(t) s_j^a(t) + s_{jb}(t) s_i^a(t)}{s_i \wedge s_j}. \quad (\text{B.13})$$

Now let us consider two paths. The first  $z_1(t) \in \gamma_1$  is a path from  $z_i$  to  $z_j$  such as we have been considering thus far. The second  $z_2(t) \in \gamma_2$  intersects  $\gamma_1$  transversally (or not at all). Now consider a vector  $v^a(t)$  parallel-transported along  $\gamma_2$ , with a fixed initial boundary condition. We want to compute  $\{\mathcal{O}_{\gamma_1, d_i, d_j}, v^a(t_*)\}$ , given by

$$\{\mathcal{O}_{\gamma_1, d_i, d_j}, v^a(t_*)\} = - \int_0^{t_*} dt \tilde{U}_b^a(t_*, t) \{\mathcal{O}_{\gamma_1, d_i, d_j}, \mathcal{A}(t)^b_c\} v^c(t), \quad (\text{B.14})$$

where  $\tilde{U}$  is the parallel transport along  $\gamma_2$ . Using (B.12) we find

$$\begin{aligned} & \{\mathcal{O}_{\gamma_1, d_i, d_j}, v^a(t_*)\} = \\ & \frac{1}{2} \int_0^1 dt_1 \int_0^{t_*} dt_2 \delta^{(2)}(z_2(t_2) - z_1(t_1)) \epsilon_{\lambda \mu} \dot{z}_2^\lambda(t_2) \dot{z}_1^\mu(t_1) \tilde{U}_b^a(t_*, t_2) M(s_i, s_j)^b_c(t_1) v^c(t_2). \end{aligned} \quad (\text{B.15})$$

Now note that

$$\delta^{(2)}(z_2(t_2) - z_1(t_1)) \epsilon_{\lambda \mu} \dot{z}_2^\lambda(t_2) \dot{z}_1^\mu(t_1) = -(\gamma_1 \cap \gamma_2) \delta(t_1 - t_1^{int}) \delta(t_2 - t_2^{int}) \quad (\text{B.16})$$

where  $t_i^{int}$  is the value of  $t$  at which the curves intersect, and  $\cap$  denotes the oriented intersection number. Thus we get

$$\{\mathcal{O}_{\gamma_1, d_i, d_j}, v(t_*)\} = \frac{1}{2} (\gamma_1 \cap \gamma_2) \left( \frac{s_i \wedge v}{s_i \wedge s_j} (t_2^{int}) s_j(t_*) + \frac{s_j \wedge v}{s_i \wedge s_j} (t_1^{int}) s_i(t_*) \right) \theta(t_* - t_2^{int}). \quad (\text{B.17})$$

where  $s_i, s_j$  have been parallel transported along  $\gamma_2$  from the intersection point to  $t_*$ .

Our goal in this Appendix was to describe the flow on  $\mathcal{M}$  generated by a function  $\log \mathcal{X}_E^T$ . To lift this function up to  $\mathcal{N}$  involves combining four functions  $\mathcal{O}_{\gamma, d_i, d_j}$  where we

identify  $\gamma$  successively with the four edges of the quadrilateral  $Q_E$ , and take  $d_i, d_j$  to agree with our choices of decoration at the vertices. Combining (B.17) for the four edges gives the flow we described in Section 5.4.

Strictly speaking we actually have to regularize by deforming the quadrilateral slightly, pushing its vertices away from the singular points, and then take a limit where the vertices approach the singular points. The regularized functions  $\mathcal{O}_{\gamma, d_i, d_j}$  are not gauge invariant (because  $d_{i,j}$  are not), but their combination does become gauge invariant in the limit: recall that the gauge group  $\mathcal{G}$  only includes transformations which at the singularities are restricted to the maximal torus  $\mathbb{C}^\times \subset SL(2, \mathbb{C})$ ; this group preserves  $d_{i,j}$  up to overall rescaling, and that overall rescaling cancels out when we sum over the four edges.

### C. WKB error analysis

In this Appendix we consider the propagation of the exponentially growing flat sections along a WKB curve. Our goal is to see that the  $\zeta \rightarrow 0$  asymptotics of this propagation are just obtained by integrating the eigenvalue  $\lambda$  of the Higgs field  $\varphi$ .

More precisely: choose a gauge in which  $\varphi$  is diagonal,

$$\varphi = \begin{pmatrix} \lambda & 0 \\ 0 & -\lambda \end{pmatrix}. \quad (\text{C.1})$$

Then let  $z(t)$  be a WKB curve with phase  $\vartheta$ , and let  $\zeta \in \mathbb{H}_\vartheta$ , so that  $\text{Re} \lambda_z z'(t)/\zeta < 0$ . Let  $s$  be a flat section with

$$s(z(0)) = \begin{pmatrix} 1 \\ 0 \end{pmatrix}. \quad (\text{C.2})$$

The statement of the WKB approximation is that as  $\zeta \rightarrow 0$  we have

$$s(z(t)) \sim c(t) \begin{pmatrix} e^{-\frac{R}{\zeta} \int_{z(0)}^{z(t)} \lambda} \\ 0 \end{pmatrix}, \quad (\text{C.3})$$

for some function  $c(t)$  independent of  $\zeta$ .

To prove (C.3), begin by defining the WKB remainder  $\psi$  by

$$\psi(z) = s(z) \exp \left( \frac{R}{\zeta} \int_{z(0)}^z \lambda \right). \quad (\text{C.4})$$

The flatness equations  $(d + \mathcal{A})s = 0$  become

$$(\partial_{\bar{z}} + A_{\bar{z}} + R\zeta \bar{\varphi}_{\bar{z}})\psi = 0, \quad (\text{C.5})$$

$$(\partial_z + A_z + \frac{R}{\zeta}(\varphi_z - \lambda_z \mathbf{1}))\psi = 0. \quad (\text{C.6})$$

So along the curve  $z(t)$  the evolution of  $\psi$  is

$$\left( \frac{d}{dt} + B(t) \right) \psi(z(t)) = 0 \quad (\text{C.7})$$



where

$$B(t) = \frac{R}{\zeta} z' \begin{pmatrix} 0 & 0 \\ 0 & -2\lambda_z \end{pmatrix} + z' A_z + \bar{z}' (A_{\bar{z}} + R\zeta \bar{\varphi}_{\bar{z}}). \quad (\text{C.8})$$

The desired (C.3) is equivalent to saying that  $\lim_{\zeta \rightarrow 0} \psi$  exists and moreover its second component vanishes. Why should this be so? The intuition is that the only term in  $B(t)$  that is not finite as  $\zeta \rightarrow 0$  is the term  $-2Rz'\lambda_z/\zeta$  in the bottom right corner, and the only effect of this term will be to introduce a factor like  $e^{-\#/\zeta}$  (with  $\text{Re}\# > 0$ ) in the second component of  $\psi$ , which thus vanishes as  $\zeta \rightarrow 0$ .

To justify this intuition, let  $B_0(t) = g(t)B(t)g^{-1}(t)$  be the diagonalization of  $B(t)$ . We would like to show that

$$\lim_{\zeta \rightarrow 0} \left\| \text{Pexp} \int_0^t B(t) - \text{Pexp} \int_0^t B_0(t) \right\| = 0. \quad (\text{C.9})$$

Having established (C.9) we may use  $B_0$  instead of  $B$  to evaluate the parallel transport of  $\psi$  in the  $\zeta \rightarrow 0$  limit; that would prove the desired (C.3).

A direct computation, using only the fact that  $B(t)$  is a  $2 \times 2$  matrix for which the real part of the bottom right entry approaches  $-\infty$  while all others remain finite, shows that  $\exp B_0(t)$  is bounded as  $\zeta \rightarrow 0$  and that we can choose  $g(t)$  such that  $g(t) \rightarrow \mathbf{1}$  as  $\zeta \rightarrow 0$ . From these two facts (C.9) follows. To see this, we first break the interval into small pieces over which  $B$  is slowly varying, to reduce to the case where  $B$  is  $t$ -independent. In that case (C.9) reduces to

$$\lim_{\zeta \rightarrow 0} \|e^{tB} - e^{tB_0}\| = 0. \quad (\text{C.10})$$

But this follows from  $B = gB_0g^{-1}$ ,  $\lim_{\zeta \rightarrow 0} g = \mathbf{1}$ , and the existence of  $\lim_{\zeta \rightarrow 0} e^{tB_0}$ .<sup>49</sup> This finishes the proof of (C.9) and hence of (C.3).

More precisely, we have shown (C.3) in the case where the WKB curve begins at a regular point. For our application we need to consider the case where the WKB curve begins at a singularity, located at say  $z(0)$ . In that case we clearly cannot hope for (C.3) to hold on the nose since  $\int_{z(0)}^{z(t)} \lambda$  diverges. Instead choose some other function  $I(z)$ , defined on a neighborhood of the WKB curve (excluding the singularity), with  $dI = \lambda$ . Then an argument similar to the above shows there is a flat section  $s$  which as  $\zeta \rightarrow 0$  behaves as

$$s(z(t)) \sim \begin{pmatrix} c(t)e^{-\frac{R}{\zeta}I(z(t))} \\ 0 \end{pmatrix}. \quad (\text{C.11})$$

Moreover, one can take  $s$  to be the small flat section associated to the WKB curve  $z(t)$  and singularity  $z(0)$ .

## D. Holomorphic coordinates on multi-center Taub-NUT

We begin with the Gibbons-Hawking ansatz. The Taub-NUT space  $TN$  has a map  $\pi : TN \rightarrow \mathbb{R}^3$ , with generic fiber a circle, and metric

$$ds^2 = V^{-1}\Theta^2 + V(d\vec{r})^2, \quad (\text{D.1})$$

---

<sup>49</sup>This is the moment where we use the fact that, as  $\zeta \rightarrow 0$ , the real part of the bottom right entry of  $B(t)$  approaches  $-\infty$  rather than  $+\infty$ .

with  $d\Theta = \pi^*(\ast dV)$ . The globally well-defined one-form  $\Theta$  is normalized by  $\pi_*\Theta = 4\pi$ .

The Taub-NUT centers are at  $\vec{r}_a$  and

$$V = 1 + \sum_a \frac{1}{|\vec{r} - \vec{r}_a|}. \quad (\text{D.2})$$

Let  $z = x^1 + ix^2$ . Holomorphic functions in one complex structure are annihilated by

$$\partial_{\bar{z}} - \Theta_{\bar{z}} \partial_{\psi} \quad (\text{D.3})$$

$$\partial_3 + (iV - \Theta_3) \partial_{\psi} \quad (\text{D.4})$$

where  $\partial_{\psi}$  is the globally well-defined vector field generating rotations in the fiber, normalized to  $\langle \Theta, \partial_{\psi} \rangle = 1$ .

To write the holomorphic coordinates it is useful to cover the manifold by patches. Introduce angular coordinates  $(\theta_a, \phi_a)$  associated with each center. We will define patches  $\mathcal{U}_{\epsilon}$  where  $\epsilon$  is a vector with one component for each center and  $\epsilon_a = \pm 1$ . We let  $\mathcal{U}_{\epsilon}$  be the set of  $\vec{r}$ ,  $\vec{r} \neq \vec{r}_a$  so that  $\theta_a \neq \frac{1}{2}(1 - \epsilon_a)\pi$ . Over each patch we can define a fiber coordinate  $\psi_{\epsilon}$  of period  $4\pi$  so that

$$\Theta = d\psi_{\epsilon} + A_{\epsilon} \quad (\text{D.5})$$

$$A_{\epsilon} = \sum_a \epsilon_a (1 + \epsilon_a \cos \theta_a) d\phi_a \quad (\text{D.6})$$

Since  $\Theta$  is globally well-defined one reads off the transition functions for  $\psi_{\epsilon}$ . Now, it is convenient to define:

$$R_{a,\pm} := |\vec{r} - \vec{r}_a| \pm (x_3 - x_{3,a}) \quad (\text{D.7})$$

Note that  $R_{a,+}R_{a,-} = |z - z_a|^2$ . It is straightforward to verify that

$$\tilde{U}_{\epsilon} = \prod_{\epsilon_a=+1} (R_{a,-})^{-1/2} \prod_{\epsilon_a=-1} (R_{a,+})^{1/2} e^{\frac{1}{2}(i\psi_{\epsilon} + x_3)} \quad (\text{D.8})$$

is annihilated by the antiholomorphic vector fields. Holomorphy is preserved if we multiply (D.8) by  $\prod_{\epsilon_a=+1} (z - z_a)$ , and we do this to define

$$U_{\epsilon} = \prod_a (R_{a,+})^{1/2} \prod_{\epsilon_a=+1} \frac{z - z_a}{|z - z_a|} e^{\frac{1}{2}(i\psi_{\epsilon} + x_3)} \quad (\text{D.9})$$

One verifies that  $U_{\epsilon}$  is in fact independent of  $\epsilon$ , i.e., it is *globally well-defined*. As we have said, it is holomorphic on  $TN$ . Its divisor is a disjoint union of holomorphic disks which project to the lines  $\theta_a = \pi$ . We henceforth drop the subscript  $\epsilon$  and simply write  $U$ . Any global holomorphic function on  $TN$  with winding number 1 around the fibers must be a polynomial in  $z$  times  $U$ .

Now, one may also check that

$$W = \prod_a (z - z_a) / U \quad (\text{D.10})$$

is globally well-defined and holomorphic. Its divisor is a union of holomorphic disks projecting to the lines  $\theta_a = 0$ . One can write explicitly

$$W = \prod_a (R_{a,-})^{1/2} \prod_{\epsilon_a = -1} \frac{z - z_a}{|z - z_a|} e^{-\frac{1}{2}(i\psi_\epsilon + x_3)}. \quad (\text{D.11})$$

In Section 3.2 we consider the limit  $x_{3,a} \rightarrow \pm\infty$  at fixed  $\vec{r}$ . Suppose we take  $x_{3,a} \rightarrow +\infty$  for  $a \in \mathcal{R}$  and  $x_{3,a} \rightarrow -\infty$  for  $a \in \mathcal{L}$ . Then  $\vec{r}$  is in the patch with  $\epsilon_a = +1$  for  $a \in \mathcal{R}$  and  $\epsilon_a = -1$  for  $a \in \mathcal{L}$ . One finds that

$$\tilde{U}_\epsilon \rightarrow \prod_{a \in \mathcal{R}} (2x_{3,a})^{-1/2} \prod_{a \in \mathcal{L}} (2|x_{3,a}|)^{+1/2} e^{\frac{1}{2}(i\psi + x_3)} \quad (\text{D.12})$$

Therefore, to have a good limit, we normalize  $U$  so that

$$U = \prod_{a \in \mathcal{R}} (z - z_a) \prod_{a \in \mathcal{R}} \left( \frac{2x_{3,a}}{R_{a,-}} \right)^{1/2} \prod_{a \in \mathcal{L}} \left( \frac{R_{a,+}}{2|x_{3,a}|} \right)^{1/2} e^{\frac{1}{2}(i\psi_\epsilon + x_3)} \quad (\text{D.13})$$

in this distinguished coordinate patch.

Now, we can apply this to the discussion in Section 3.2.5. We identify the cylindrical coordinate  $t = e^{-\frac{1}{2}(i\psi_\epsilon + x_3)}$ , and  $z$  is identified with  $v$ , while  $x^3$  is identified with  $x^6$ . Therefore, in the limit we have

$$U \rightarrow t^{-1} \prod_{a \in \mathcal{R}} (v - v_a), \quad (\text{D.14})$$

$$W \rightarrow t \prod_{a \in \mathcal{L}} (v - v_a), \quad (\text{D.15})$$

in terms of the natural holomorphic coordinates  $(t, v)$  on  $T^*\mathbb{C}^\times$ .

## E. Configurations of integers with nonpositive second discrete derivative

We summarize here some simple observations about the collections of integers  $\{k_\alpha\}$ ,  $0 \leq \alpha \leq n+1$ , which arise in the D4/NS5-brane configurations of Section 3.2. According to (3.42) these configurations obey

$$-2k_\alpha + k_{\alpha+1} + k_{\alpha-1} + d_\alpha \leq 0, \quad 1 \leq \alpha \leq n. \quad (\text{E.1})$$

Since  $d_\alpha \geq 0$ , (E.1) implies that if we think of  $k_\alpha$  as a function of  $\alpha$ , its second discrete derivative is nonpositive, i.e. its graph is convex.

There are three basic cases to be distinguished. The first case is  $k_1 - k_0 > 0$ . Then the  $k_\alpha$  are strictly increasing for  $0 \leq \alpha \leq \alpha_-$ , attain a maximal value  $K$  for  $\alpha_- \leq \alpha \leq \alpha_+$ , and are strictly decreasing for  $\alpha \geq \alpha_+$ . See Figure 88. If  $k_1 - k_0 = 0$  then we have a similar behavior except that  $\alpha_- = 0$ , shown in Figure 89. Finally, if  $k_1 - k_0 < 0$  then we have  $\alpha_- = \alpha_+ = 0$ , as in Figure 90.

There is also an important special case where the second discrete derivative vanishes,  $-2k_\alpha + k_{\alpha+1} + k_{\alpha-1} = 0$  for  $1 \leq \alpha \leq n$ . In this case the graph is just a line, i.e.

$$k_\alpha = k_0 + \alpha r, \quad 0 \leq \alpha \leq n+1. \quad (\text{E.2})$$

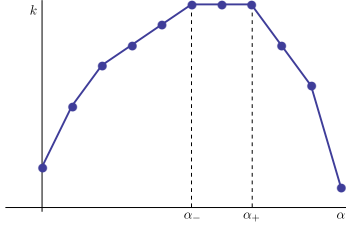


**Figure 88:** The typical profile of a set of integers  $k_\alpha$  with  $2k_\alpha - k_{\alpha-1} - k_{\alpha+1} \geq 0$  when  $k_1 - k_0 > 0$ .

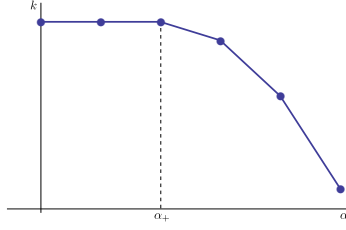


**Figure 89:** The typical profile of a set of integers  $k_\alpha$  with  $2k_\alpha - k_{\alpha-1} - k_{\alpha+1} \geq 0$  when  $k_1 - k_0 = 0$ .

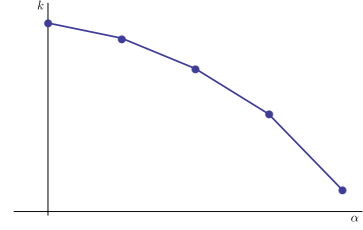


**Figure 90:** The typical profile of a set of integers  $k_\alpha$  with  $2k_\alpha - k_{\alpha-1} - k_{\alpha+1} \geq 0$  when  $k_1 - k_0 < 0$ .

## References

- [1] D. Gaiotto, G. W. Moore, and A. Neitzke, “Four-dimensional wall-crossing via three-dimensional field theory,” [0807.4723](#).
- [2] E. Witten, “Solutions of four-dimensional field theories via M-theory,” *Nucl. Phys.* **B500** (1997) 3–42, [hep-th/9703166](#).
- [3] A. Klemm, W. Lerche, P. Mayr, C. Vafa, and N. P. Warner, “Self-Dual Strings and N=2 Supersymmetric Field Theory,” *Nucl. Phys.* **B477** (1996) 746–766, [hep-th/9604034](#).
- [4] P. Boalch, “Irregular connections and Kac-Moody root systems,” [0806.1050](#).
- [5] A. Strominger, “Open  $p$ -branes,” *Phys. Lett.* **B383** (1996) 44–47, [hep-th/9512059](#).
- [6] M. Kontsevich and Y. Soibelman, “Stability structures, motivic Donaldson-Thomas invariants and cluster transformations,” [0811.2435](#).
- [7] N. A. Nekrasov and S. L. Shatashvili, “Quantum integrability and supersymmetric vacua,” [0901.4748](#).
- [8] P. Dorey and R. Tateo, “On the relation between Stokes multipliers and the T-Q systems of conformal field theory,” *Nucl. Phys.* **B563** (1999) 573–602, [hep-th/9906219](#).
- [9] P. Dorey and R. Tateo, “Excited states by analytic continuation of TBA equations,” *Nucl. Phys.* **B482** (1996) 639–659, [hep-th/9607167](#).
- [10] V. Fock and A. Goncharov, “Moduli spaces of local systems and higher Teichmüller theory,” *Publ. Math. Inst. Hautes Études Sci.* (2006), no. 103, 1–211, [math/0311149](#).
- [11] L. F. Alday and J. Maldacena, “Null polygonal Wilson loops and minimal surfaces in Anti-de-Sitter space,” [0904.0663](#).
- [12] D. Gaiotto, G. W. Moore, and A. Neitzke, “Spectral networks.” In preparation.
- [13] D. Gaiotto, G. W. Moore, and A. Neitzke, “Spin lifts and spectral networks.” In preparation.
- [14] A. Kapustin and E. Witten, “Electric-magnetic duality and the geometric Langlands program,” [hep-th/0604151](#).
- [15] D. Gaiotto, “N=2 dualities,” [0904.2715](#).
- [16] S. Cecotti and C. Vafa, “On classification of  $\mathcal{N} = 2$  supersymmetric theories,” *Commun. Math. Phys.* **158** (1993) 569–644, [hep-th/9211097](#).

- [17] F. Denef and G. W. Moore, “Split states, entropy enigmas, holes and halos,” [hep-th/0702146](#).
- [18] F. Denef, “Supergravity flows and D-brane stability,” *JHEP* **08** (2000) 050, [hep-th/0005049](#).
- [19] E. Witten, “Some comments on string dynamics,” [hep-th/9507121](#).
- [20] E. Witten, “Five-branes and M-theory on an orbifold,” *Nucl. Phys.* **B463** (1996) 383–397, [hep-th/9512219](#).
- [21] N. Seiberg and E. Witten, “Comments on String Dynamics in Six Dimensions,” *Nucl. Phys.* **B471** (1996) 121–134, [hep-th/9603003](#).
- [22] N. Seiberg, “Notes on theories with 16 supercharges,” *Nucl. Phys. Proc. Suppl.* **67** (1998) 158–171, [hep-th/9705117](#).
- [23] N. Seiberg, “New theories in six dimensions and matrix description of M-theory on  $T^5$  and  $T^5/\mathbb{Z}_2$ ,” *Phys. Lett.* **B408** (1997) 98–104, [hep-th/9705221](#).
- [24] O. Aharony, M. Berkooz, and N. Seiberg, “Light-cone description of (2,0) superconformal theories in six dimensions,” *Adv. Theor. Math. Phys.* **2** (1998) 119–153, [hep-th/9712117](#).
- [25] J. Bhattacharya, S. Bhattacharyya, S. Minwalla, and S. Raju, “Indices for Superconformal Field Theories in 3,5 and 6 Dimensions,” *JHEP* **02** (2008) 064, [0801.1435](#).
- [26] K.-M. Lee and H.-U. Yee, “BPS string webs in the 6-dim (2,0) theories,” *JHEP* **03** (2007) 057, [hep-th/0606150](#).
- [27] A. Sen, “String network,” *JHEP* **03** (1998) 005, [hep-th/9711130](#).
- [28] O. Aharony, A. Hanany, and B. Kol, “Webs of (p,q) 5-branes, five dimensional field theories and grid diagrams,” *JHEP* **01** (1998) 002, [hep-th/9710116](#).
- [29] K. Dasgupta and S. Mukhi, “BPS nature of 3-string junctions,” *Phys. Lett.* **B423** (1998) 261–264, [hep-th/9711094](#).
- [30] E. Witten, “Topological Quantum Field Theory,” *Commun. Math. Phys.* **117** (1988) 353.
- [31] A. Brandhuber and S. Stieberger, “Self-dual strings and stability of BPS states in  $N = 2$   $SU(2)$  gauge theories,” *Nucl. Phys.* **B488** (1997) 199–222, [hep-th/9610053](#).
- [32] A. Mikhailov, “BPS states and minimal surfaces,” *Nucl. Phys.* **B533** (1998) 243–274, [hep-th/9708068](#).
- [33] N. J. Hitchin, “The self-duality equations on a Riemann surface,” *Proc. London Math. Soc.* (3) **55** (1987), no. 1, 59–126.
- [34] S. A. Cherkis and A. Kapustin, “Singular monopoles and supersymmetric gauge theories in three dimensions,” *Nucl. Phys.* **B525** (1998) 215–234, [hep-th/9711145](#).
- [35] S. Gukov and A. Kapustin, “New  $N = 2$  superconformal field theories from M/F theory orbifolds,” *Nucl. Phys.* **B545** (1999) 283–308, [hep-th/9808175](#).
- [36] A. Kapustin, “Solution of  $N = 2$  gauge theories via compactification to three dimensions,” *Nucl. Phys.* **B534** (1998) 531–545, [hep-th/9804069](#).
- [37] S. A. Cherkis and A. Kapustin, “Nahm transform for periodic monopoles and  $N = 2$  super Yang-Mills theory,” *Commun. Math. Phys.* **218** (2001) 333–371, [hep-th/0006050](#).

- [38] A. Gorsky, I. Krichever, A. Marshakov, A. Mironov, and A. Morozov, “Integrability and Seiberg-Witten exact solution,” *Phys. Lett.* **B355** (1995) 466–474, [hep-th/9505035](#).
- [39] E. J. Martinec and N. P. Warner, “Integrable systems and supersymmetric gauge theory,” *Nucl. Phys.* **B459** (1996) 97–112, [hep-th/9509161](#).
- [40] R. Y. Donagi and E. Witten, “Supersymmetric Yang-Mills theory and integrable systems,” *Nucl. Phys.* **B460** (1996) 299–334, [hep-th/9510101](#).
- [41] H. Itoyama and A. Morozov, “Integrability and Seiberg-Witten theory: Curves and periods,” *Nucl. Phys.* **B477** (1996) 855–877, [hep-th/9511126](#).
- [42] N. Seiberg and E. Witten, “Gauge dynamics and compactification to three dimensions,” [hep-th/9607163](#).
- [43] S. Gukov and E. Witten, “Gauge theory, ramification, and the geometric Langlands program,” [hep-th/0612073](#).
- [44] E. Frenkel and E. Witten, “Geometric Endoscopy and Mirror Symmetry,” [0710.5939](#).
- [45] J. A. Harvey, G. W. Moore, and A. Strominger, “Reducing S duality to T duality,” *Phys. Rev.* **D52** (1995) 7161–7167, [hep-th/9501022](#).
- [46] M. Bershadsky, A. Johansen, V. Sadov, and C. Vafa, “Topological reduction of 4-d SYM to 2-d sigma models,” *Nucl. Phys.* **B448** (1995) 166–186, [hep-th/9501096](#).
- [47] E. Witten, “Gauge theory and wild ramification,” [0710.0631](#).
- [48] A. Fayyazuddin and M. Spalinski, “The Seiberg-Witten differential from M-theory,” *Nucl. Phys.* **B508** (1997) 219–228, [hep-th/9706087](#).
- [49] M. Henningson and P. Yi, “Four-dimensional BPS-spectra via M-theory,” *Phys. Rev.* **D57** (1998) 1291–1298, [hep-th/9707251](#).
- [50] P. C. Argyres, M. R. Plesser, and A. D. Shapere, “The Coulomb phase of  $\mathcal{N} = 2$  supersymmetric QCD,” *Phys. Rev. Lett.* **75** (1995) 1699–1702, [hep-th/9505100](#).
- [51] A. Hanany and E. Witten, “Type IIB superstrings, BPS monopoles, and three-dimensional gauge dynamics,” *Nucl. Phys.* **B492** (1997) 152–190, [hep-th/9611230](#).
- [52] S. Katz, P. Mayr, and C. Vafa, “Mirror symmetry and exact solution of 4D  $\mathcal{N} = 2$  gauge theories. I,” *Adv. Theor. Math. Phys.* **1** (1998) 53–114, [hep-th/9706110](#).
- [53] H. Konno, “Construction of the moduli space of stable parabolic Higgs bundles on a Riemann surface,” *J. Math. Soc. Japan* **45** (1993), no. 2, 253–276.
- [54] H. Nakajima, “Hyper-Kähler structures on moduli spaces of parabolic Higgs bundles on Riemann surfaces,” in *Moduli of vector bundles (Sanda, 1994; Kyoto, 1994)*, vol. 179 of *Lecture Notes in Pure and Appl. Math.*, pp. 199–208. Dekker, New York, 1996.
- [55] O. Biquard and P. Boalch, “Wild nonabelian Hodge theory on curves,” [math/0111098](#).
- [56] N. J. Hitchin, A. Karlhede, U. Lindstrom, and M. Roček, “Hyperkähler metrics and supersymmetry,” *Commun. Math. Phys.* **108** (1987) 535.
- [57] C. Simpson, “Harmonic bundles on noncompact curves,” *J. Amer. Math. Soc.* **3** (1990) 713–770.
- [58] A. Kapustin and S. Sethi, “The Higgs branch of impurity theories,” *Adv. Theor. Math. Phys.* **2** (1998) 571–591, [hep-th/9804027](#).

- [59] S. Gukov and E. Witten, “Rigid Surface Operators,” [0804.1561](#).
- [60] K. Strebel, *Quadratic differentials*, vol. 5 of *Ergebnisse der Mathematik und ihrer Grenzgebiete (3) [Results in Mathematics and Related Areas (3)]*. Springer-Verlag, Berlin, 1984.
- [61] B. Keller, “Cluster algebras, quiver representations and triangulated categories,” [0807.1960](#).
- [62] D. Gaiotto, G. W. Moore, and A. Neitzke, “Framed BPS States,” [1006.0146](#).
- [63] S. Cecotti, A. Neitzke, and C. Vafa, “R-Twisting and 4d/2d Correspondences,” [1006.3435](#).
- [64] S. Cecotti and C. Vafa, “Classification of complete  $N=2$  supersymmetric theories in 4 dimensions,” [1103.5832](#).
- [65] P. Boalch, “Symplectic manifolds and isomonodromic deformations,” *Adv. Math.* **163** (2001), no. 2, 137–205.
- [66] P. C. Argyres and M. R. Douglas, “New phenomena in  $SU(3)$  supersymmetric gauge theory,” *Nucl. Phys.* **B448** (1995) 93–126, [hep-th/9505062](#).
- [67] P. C. Argyres, M. Ronen Plesser, N. Seiberg, and E. Witten, “New  $N=2$  Superconformal Field Theories in Four Dimensions,” *Nucl. Phys.* **B461** (1996) 71–84, [hep-th/9511154](#).
- [68] A. D. Shapere and C. Vafa, “BPS structure of Argyres-Douglas superconformal theories,” [hep-th/9910182](#).
- [69] B. M. McCoy, C. A. Tracy, and T. T. Wu, “Painleve Functions of the Third Kind,” *J. Math. Phys.* **18** (1977) 1058.
- [70] H. Ooguri and C. Vafa, “Summing up D-instantons,” *Phys. Rev. Lett.* **77** (1996) 3296–3298, [hep-th/9608079](#).
- [71] N. Seiberg and S. H. Shenker, “Hypermultiplet moduli space and string compactification to three dimensions,” *Phys. Lett.* **B388** (1996) 521–523, [hep-th/9608086](#).
- [72] J. D. Stasheff, “Homotopy associativity of  $H$ -spaces. I, II,” *Trans. Amer. Math. Soc.* **108** (1963), 275–292; *ibid.* **108** (1963) 293–312.
- [73] C. Lee, “The associahedron and triangulations of the  $n$ -gon,” *Europ. J. Combin.* **10** (1989) 551–560.
- [74] S. L. Devadoss and R. C. Read, “Cellular structures determined by polygons and trees,” *Ann. Comb.* **5** (2001), no. 1, 71–98, [math/0008145](#).
- [75] S. MacLane, ed., *Coherence in categories*. Lecture Notes in Mathematics, Vol. 281. Springer-Verlag, Berlin, 1972.
- [76] A. Bilal and F. Ferrari, “Curves of Marginal Stability and Weak and Strong-Coupling BPS Spectra in  $N = 2$  Supersymmetric QCD,” *Nucl. Phys.* **B480** (1996) 589–622, [hep-th/9605101](#).
- [77] A. Bilal and F. Ferrari, “The Strong-Coupling Spectrum of the Seiberg-Witten Theory,” *Nucl. Phys.* **B469** (1996) 387–402, [hep-th/9602082](#).
- [78] F. Ferrari, “The dyon spectra of finite gauge theories,” *Nucl. Phys.* **B501** (1997) 53–96, [hep-th/9702166](#).
- [79] T. Banks, M. R. Douglas, and N. Seiberg, “Probing F-theory with branes,” *Phys. Lett.* **B387** (1996) 278–281, [hep-th/9605199](#).



- [80] M. R. Douglas, D. A. Lowe, and J. H. Schwarz, “Probing F-theory with multiple branes,” *Phys. Lett.* **B394** (1997) 297–301, [hep-th/9612062](#).
- [81] M. R. Gaberdiel, T. Hauer, and B. Zwiebach, “Open string-string junction transitions,” *Nucl. Phys.* **B525** (1998) 117–145, [hep-th/9801205](#).
- [82] A. Mikhailov, N. Nekrasov, and S. Sethi, “Geometric realizations of BPS states in  $N = 2$  theories,” *Nucl. Phys.* **B531** (1998) 345–362, [hep-th/9803142](#).
- [83] O. DeWolfe, T. Hauer, A. Iqbal, and B. Zwiebach, “Constraints on the BPS spectrum of  $N = 2$ ,  $D = 4$  theories with A-D-E flavor symmetry,” *Nucl. Phys.* **B534** (1998) 261–274, [hep-th/9805220](#).
- [84] N. Seiberg and E. Witten, “Monopoles, duality and chiral symmetry breaking in  $N=2$  supersymmetric QCD,” *Nucl. Phys.* **B431** (1994) 484–550, [hep-th/9408099](#).
- [85] R. Thomas and S.-T. Yau, “Special Lagrangians, stable bundles and mean curvature flow,” [math/0104197](#).
- [86] K. Corlette, “Flat  $G$ -bundles with canonical metrics,” *J. Differential Geom.* **28** (1988), no. 3, 361–382.
- [87] C. T. Simpson, “Harmonic bundles on noncompact curves,” *J. Amer. Math. Soc.* **3** (1990), no. 3, 713–770.
- [88] V. Fateev, D. Fradkin, S. L. Lukyanov, A. B. Zamolodchikov, and A. B. Zamolodchikov, “Expectation values of descendent fields in the sine-Gordon model,” *Nucl. Phys.* **B540** (1999) 587–609, [hep-th/9807236](#).
- [89] N. J. Hitchin, “Lie groups and Teichmüller space,” *Topology* **31** (1992), no. 3, 449–473.
- [90] T. Bridgeland, “Stability conditions on triangulated categories,” [math.AG/0212237](#).
- [91] L. Chekhov and R. C. Penner, “On quantizing Teichmüller and Thurston theories,” [math/0403247](#).
- [92] J. M. Maldacena, “Wilson loops in large  $N$  field theories,” *Phys. Rev. Lett.* **80** (1998) 4859–4862, [hep-th/9803002](#).
- [93] S.-J. Rey and J.-T. Yee, “Macroscopic strings as heavy quarks in large  $N$  gauge theory and anti-de Sitter supergravity,” *Eur. Phys. J.* **C22** (2001) 379–394, [hep-th/9803001](#).